POLITECNICO DI TORINO

Ph.D. Course in Electrical Engineering – XXVI cycle

Ph.D. Dissertation

Economy of grid-connected photovoltaic systems and comparison of irradiance/electric power predictions vs. experimental results

Valeria Concetta Cocina

Supervisor
Prof. Filippo Spertino

Ph.D. Course Co-ordinator
Prof. Mario Chiampi

March 2014

Contents

Abstract

This thesis is focused on various aspects concerning the Distributed Generation (DG) from Renewable Energy Sources (RES) and in particular from PhotoVoltaics (PV).

The PV generation strongly depends on weather conditions (irradiance and temperature), therefore the solar irradiance forecast is very important for grid-connected PV systems. The PV power injected into the grid is concentrated during sunlight hours, in which the maximum peak load demand occurs and, as a consequence, an impact on the electrical system occurs.

The task of the Transmission System Operator (TSO) is to ensure a constant balance between supply and consumption within the grid. Therefore, the presence of strong fluctuations of the solar radiation requires additional regulatory actions and compensation, through the use of short-term power backup, causing an increase in network costs.

Thus, the solar irradiance forecast is necessary for an accurate evaluation of the PV power from PV systems, for the management of electrical grids in order to minimize the costs of energy imbalance and for the decisions concerning the energy market.

This thesis essentially consists of two parts. In the first part, the profitability of investments in the rooftop grid-connected PV systems subjected to incentive and the grid-parity analysis in the two main European PV markets (Italy and Germany) are presented. In the second part, in order to minimize the costs of energy imbalance in the Italian electricity market, the comparison of irradiance and electric power predictions with respect to the experimental results of grid-connected PV systems is presented.

In the first part of the thesis, a deep study of the aspects on the PV installation performance, on the cumulative installed capacity in recent years and on the incentive policy, underlining, in particular, the differences between the two main European PV markets (Italy and Germany) is carried out.

Then, the feed-in tariffs, the authorization procedures, the procedures for the connection to the network and the technical barriers for the installation of PV systems in the rooftop of buildings for both Italy and Germany are analyzed.

Subsequently, the economic analysis of PV rooftop systems has been carried out, in order to identify the profit indicators, such as Net Present Value (*NPV*) and Internal Rate of Return (*IRR*) for particular case studies, different according to the type of the PV plant, the site of installation and the beginning of operation.

Through this analysis, it was possible to quantify the differences in terms of economics performance over the past seven years (from 2006 to 2013) between the different types of PV installations on rooftop, highlighting much higher profits in Italy than in Germany, causing the so-called “gold rush” effect.

Further analysis dealt with the “self-sustaining” policy of the PV market in Italy and Germany, in which the costs for the construction of facilities make the investment attractive in absence of incentive for the achievement of the so-called “grid-parity”, that occurs when the electricity produced by the PV system and the traditional energy drawn from the power grid have the same price. In particular, the analysis was performed for particular case studies (dwelling houses, common users of apartment-blocks and tertiary-sector users), including the PV penetration study and hidden costs in the energy bill.

In the second part of the thesis, the aspects related to the prediction of solar irradiance and AC power profiles of real grid-connected PV systems in operation in the South of Italy have been analyzed.

Each PV system, under study, is equipped with: one pyranometer and two reference solar cells for measuring the horizontal global irradiance, two reference solar cells for the tilted global irradiance, and one thermo-hygrometer for measuring ambient temperature, relative humidity and wind speed.

In order to improve the PV power injection into the grid, it is important to measure, as correctly as possible, the global solar radiation in short term on annual basis from these solar cells on the horizontal and tilted plane. For this reason, the validation of global irradiance data from solar cells on the horizontal and tilted plane, through the comparison with the pyranometer uncertainty, taken as reference, has been carried out.

Then, through the solar irradiance forecasts data of 3-day ahead on the horizontal plane, at the same latitude and longitude of the PV plants, given us by a weather forecast provider, it has been possible to make a comparison with the measured data.

Moreover, a method to classify each hour of a day in three categories (variable, cloudy, or clear) has been implemented. In this way, it has been possible to understand if there is a correlation between the solar irradiance from measured data and from forecasts.

A special focus has been on the prediction of the so-called “broken clouds” phenomenon, in which the sky is mainly clear, but the passage of clouds affects the irradiance evolution. Therefore, in order to estimate the number of occurrence of “broken clouds” in a day, a specific threshold value has been considered. With the perspective of the day-ahead market, the “broken clouds” analysis has been performed for the 15-min averaged values.

In order to determine the accuracy between the predicted and measured data, the error estimation measurement has been carried out through the use of statistical methods. The indicators used in this evaluation are the Mean Absolute Error (*MAE*) and the Mean Bias Error (*MBE*).

Then, in order to link the solar irradiance and cell temperature data with the AC power delivered to the grid, a dedicated PV conversion model has been defined. For the definition of the PV conversion model, many loss factors that influence the PV system behavior, have been taken into account. These losses are mainly due to: dirt in the PV modules; reflection of the PV module glass, thermal losses with respect to STC; electrical mismatch losses; DC-cable losses; MPPT and DC−AC conversion losses.

Finally, the error parameters between the power measured by the meters and the AC power calculated from the model have been determined with respect to the real grid-connected PV systems.

Acknowledgment

I would first like to thank my supervisor, Professor Ing. Filippo Spertino, for his continuous guidance throughout the period of my PhD studies, whose interest, expertise, and guidance was essential in directing and completing this work.

I would like to express my gratitude to Professor Ing. Paolo Di Leo and Professor Ing. Gianfranco Chicco, for their support and constant guide.

For their sympathy, help and support during these years, many thanks to all the Professors, technical and administrative staff of the Energy Department.

For the inestimable contribution, many thanks to my family and to Maurizio who have always believed in me, sustaining and encouraging me in all the phases of my personal and professional life.

List of papers

- Cocina V., Di Leo P., Spertino F., "Economic analysis of investment in the rooftop photovoltaic systems: A long-term research in the two main markets". Renewable and Sustainable Energy Reviews, Vol 28, Dec 2013, pp. 531-540, ISSN1364-0321, http://dx.doi.org/10.1016/j.rser.2013.08.024.
- Cocina V., Di Leo P., Spertino F., "Which are the constraints limiting the PV grid-parity in the main European markets?", Solar Energy Journal, Elsevier, Nov 2013, accepted.
- Cocina V., Di Leo P., Spertino F., Tina G. M., "Storage sizing procedure and experimental verification of stand-alone photovoltaic systems". IEEE Conference ENERGYCON 2012, Firenze (Italy), Sep 2012, doi: 10.1109/EnergyCon.2012.6348199.
- Cocina V., Di Leo P., Spertino F., "Accurate measurements of solar irradiance for evaluation of photovoltaic power profiles". IEEE Conference POWERTECH 2013, Grenoble (France), Jun 2013, doi: 10.1109/PTC.2013.6652475.
- Cocina V., Di Leo P., Spertino F., Ciocia A., "New Concept for PV Grid Parity in Typical Case Studies: Hidden Costs Included". 28th EUPVSEC European Photovoltaic Solar Energy Conference and Exhibition – Paris (France), Oct 2013.
- Chicco G., Cocina V., Mazza A., Spertino F., "Data Pre-Processing and Representation for Energy Calculations in Net Metering Conditions", IEEE Conference ENERGYCON 2014, Dubrovnik (Croatia), May 2014, submitted and accepted.
- Chicco G., Cocina V., Di Leo P., Spertino F., "Weather forecast-based power predictions and experimental results from photovoltaic systems". IEEE Conference SPEEDAM 2014, Ischia (Italy), Jun 2014, submitted and accepted.
- Chicco G., Cocina V., Spertino F., "Characterization of solar irradiance profiles for photovoltaic system studies through data rescaling in time and amplitude", UPEC 2014 - International Universities' Power Engineering Conference, Cluj-Napoca (Romania), Sep 2014, submitted.
- Cocina V., Spertino F., book chapter: "Il Generatore Fotovoaltaico: Mismatch e Risultati della simulazione con le configurazioni di ombratura considerate". Impianti fotovoltaici: guida pratica / Monopoli M., Comitato Elettrotecnico Italiano (CEI) Ed. Milano, Nov 2012, ISBN 9788843200924, pp. 26-56.

Nomenclature

Symbol	Description
a	solar height
A	apparent solar constant
α_S	share of energy sold to the grid
β	tilt angle
B	coefficient of atmospheric extinction
C	coefficient of diffuse irradiance
C_F	fixed costs
CF_k	cash flow (at k-th year)
C_I	installation cost
c_I	specific installation cost
c_L	linear loss coefficient
C_{OM}	yearly Operation and Maintenance cost
c_{OM}	O&M cost expressed as a percentage of the specific installation cost
CRF	Capital Recovery Factor
c_S	square loss coefficient

δ	solar declination angle
$\Delta Gpyr$	absolute uncertainty of the pyranometer
ΔG_{21}	deviations of 2-day ahead prediction with respect to the 1-day ahead prediction
ΔG_{31}	deviations of 3-day ahead prediction with respect to the 1-day ahead prediction
Δ_0	deviation amplitude
ε	estimation error
E_{g_inj}	share of PV energy production delivered to the grid
ε_h	relative uncertainty for the irradiation H_h
η_{MPPT}	efficiency of the tracker
E_{s_cons}	amount of PV energy production self-consumed by the PV system's owner
ε_t	relative uncertainty of the "time" quantity
$\underline{E}_{Th}$	voltage source
$\underline{Z}_{Th}$ t	equivalent impedance
$\underline{E}_T$	e.m.f. of secondary windings of the distribution transformer
φ	azimuth angle
f	inflation rate
f_{elec}	national inflation rate of the electricity
F_{sc}	sky-surface view factor
g	day of the year
G_{a_rain}	solar cell irradiation in a clear-sky days after rain
G_{bn}	beam normal irradiance

G_{b_rain}	solar cell irradiation in a clear-sky days before rain
G_{dh}	horizontal diffuse irradiance
G_{fore}	1-day ahead forecast irradiance
G_{hcell}	horizontal global irradiance from solar cells
G_{lim}	irradiance limit below which the output is vanishing
G_{max_PVGIS}	maximum clear-sky irradiance value on a fixed plane from PVGIS
G_{meas}	measured irradiance
G_{pyr}	horizontal global irradiance from pyranometer
G_{sc}	solar constant
G_{tcell}	tilted global irradiance from solar cells
γ_{th}	thermal coefficient of maximum power of the modules
G_{th}	total horizontal irradiance
g_{tot}	total number of days in the year
G_0	extra-atmospheric total solar irradiance
h	hour of the day
i	basic interest rate
i^*	real interest rate
i^*_{feed}	real interest rates for the feed-in tariff
i^*_{OM}	real interest rates for the O&M costs
i^*_{ose}	real interest rates for the on-site-exchange
IRR	Internal Rate of Return

k_d	fraction of the hourly diffuse irradiation on a horizontal plane
k_E	ratio between the PV energy production and the energy consumption
k_s	solar height at the sunset and at the sunrise
k_t	hourly clearness index
k_{tf}	hourly clearness index value of forecasts
l_{cable}	DC-cable losses
l_{dirt}	losses for soiling and dirt
l_{mis}	electrical mismatch losses
l_{refl}	losses due to reflection of the PV module glass
l_{th}	thermal losses
MAE	mean absolute error
MARR	Minimum Attractive Rate of Return
MBE	mean bias error
$\mu_{PV\text{-}trnsf}$	of the distribution-transformer
$\mu_{PV\text{-}load}$	power rating of the peak load
nRMSE	normalized root mean square error
NOCT	Normal Operating Cell Temperature
NPV	Net Present Value
ϖ_0	deviation phase
ρ	albedo
P_{AC}	AC power

P_{DC}	DC power
P_{fore}	delivered power to the grid
p_{inj}	unitary price paid to the PV owner per kWh injected into the grid
P_{L}	load profile
P_{Lmin}	minimum peak
P_{Lmax}	maximum peak
P_{meas}	power from the energy meters of the PV plant
P_{mpp}	available power at maximum power point
p_{PV}	energy cost used for net metering in Germany
p_{PV}^{*}	energy cost used for energy sold to the grid in Italy
P_{PVlim}	PV power profile limit
P_{PVm}	peak power at STC
P_{PVrev}	reverse flow of PV power profile
P_{PVr}	total rated power of the PV array
PR	Performance Ratio
P_{rated}	rated power
ψ	hour angle
P_{0}	no-load power losses along the operation
θ	angle between the solar beam and the direction orthogonal to the tilt plane
$RMSE$	root mean square error
RH	relative humidity

R_{PV}	yearly revenues
s_{bill}	cost in €/kWh saved from the utility bill
s_{PV}	energy cost used for self-consumption in Italy
STDERR	standard deviation of errors
T_{amb}	ambient temperature
T_C	cell temperature
v_w	wind speed
WACC	Weighted Average Cost of Capital
ξ	latitude
Y_r	reference yield
Y_f	final yield
ζ	longitude
z	zenith angle
$\underline{Z}_{grid}$	equivalent impedance
$\underline{Z}_{LVl}$, $\underline{Z}_{LVl2}$	impedance of the distribution lines
$\underline{Z}_L$, $\underline{Z}_{L2}$	impedance of the loads supplied by the lines
$\underline{Z}_{MVg}$	primary grid impedance
$\underline{Z}_{scT}$	short circuit impedance of the distribution transformer

Chapter 1

Economic analysis of investment in the rooftop photovoltaic systems in the two main markets

Introduction

In the past the installation cost of PV systems was so high that no economic convenience appeared, with respect to the bill paid to the utilities for the grid electricity. That was the reason, for which the stand alone PV systems were the unique applications of this technology in zones where the network was not available as in mountains, islands or rural sites.

The increasing costs of fossil fuels, due to the impressive usage around the world, and the consequent concerns on climate change (greenhouse gases, global warming) have pushed the national Governments towards a major employment of RES, according to several protocols as e.g. the Kyoto one. Especially in Europe, in the last years, a policy for RES deployment, based on incentive in terms of feed-in tariffs, has been implemented.

These tariffs have produced, for the owners of PV systems, such revenues that also the grid connected PV plants have become viable from the economic point of view. Obviously, the money for the incentive is a burden for the community, but, if the mechanism is well done, it can generate many advantages like reduction of installation cost due to economies of scale, clean electricity production, job creation, technological innovation and safe investments.

In fact, the main target should be to create a self-sustaining market based on two factors: firstly, the economies of scale [1] i.e., the decrements in cost per unit, that PV companies achieve (about -20 %), as the size of the facilities and the usage levels of other inputs increase; secondly, the cost of electricity from fossil fuels which is continuously increasing. After the start-up period, the feed-in tariff should be progressively reduced, in such a way as to reduce the burden on the electricity bill and to hold an attractive performance of the PV investments.

Nowadays, Germany and Italy are the main markets in the world for PV installations: in Germany the feed-in tariff is in operation since 2000 with about 30 GW_p of installed power and in Italy since 2005 with about 17 GW_p, after many adjustments.

In this chapter, a long-term research on the investments in regards to PV plants of active users charged by the retail electricity price with different size and location, roof mounted, in Germany and Italy, according to the variable conditions of the incentives (2006 − 2012) is provided. Such a study permits to determine the particular economic revenues during the time evolution among the various types of PV systems, emphasizing the efficiency of the incentive policies in the two major markets. At this aim, the installation costs of the PV plants, according to size, location and begin of life, have been defined by suitable assumptions; then, the performance indicators in terms of Net Present Value (*NPV*) and Internal Rate of Return (*IRR*) have been computed.

1.1. The Worldwide PV Market

Globally, the volume of new PV capacities world-wide rose from 16.6 − 20.2 GW_p in 2010 to 24.1 – 27.6 GW_p in 2011 and 37.7 GW_p in 2012 considering a remarkable difference between the installed power and the grid-connected power (typical delay of some months in Italy). The number of markets reaching more than 1 GW_p of additional capacity during 2011 rose from 3 to 6 [2].

The European share in the global PV arena still remains predominant with more than 75 % of all new capacity in 2011. The two biggest markets, Italy and Germany, account for nearly 60 % of global market growth during 2010 [3].

The growth rate of PV during 2011 reached almost 70 %, with growing contributions from Southern European countries, over 60 GW_p of PV systems were installed at the end of 2011. In Italy and France, specific regulations created strong installation growth in 2010; however, the grid connection was to be counted only in 2011. This effect has included between 3 and 5 GW_p of installations made in 2010 with grid connection taking place in 2011.

During 2012, a 20 % increase of the grid-connected capacity occurred, in comparison to 2011.Overall, at the end of 2012 it has been reached 101 GW_p of cumulative installed capacity, value equal to 2.3 times compared to that recorded at the end of 2010.

Table 1.1 shows the top markets world-wide, both in terms of grid-connected capacity during 2012, 2011 and 2010 and cumulative installed capacity at the end of 2011 and 2012. It is interesting to note that China, at first place of PV module manufacturers in the world, is becoming an important market in the PV installation.

Table 1.1 − The installed and grid-connected capacity in 2010, 2011 and 2012 (source: IEA)

Country	2010 grid-connected capacity (MW)	2010 installed capacity (MW)	2011 grid-connected capacity (MW)	2011 installed capacity (MW)	2011 cumulative installed capacity (MW)	2012 grid-connected capacity (MW)	2012 cumulative installed capacity (MW)
Italy	2321	5900	9000	5500	12500	3480	16280
Germany	7406	7406	7500	7500	24700	7600	32278
China	520	520	2000	2000	2900	3500	7000
USA	887	887	1600	1600	4200	3200	7583
France	716	716	1500	1500	2500	1200	4200
Japan	986.8	986.8	1100	1100	4700	2000	6914
Total in the world	16629	20208	27700	24200	67350	33700	101000

The growth of the PV market is based on the increasing oil prices and consequent air pollution, on the requirement of environmentally friendly energy generation, and is sustained by the support of the environmentally-conscious public incentives, direct subsidies and Research and Development (R&D) support. Without such support, the industry could not grow to levels that would enable the reduction of the price of electricity generated from photovoltaics to the levels of conventional energy generation [4]. Due to the increasing market volume, performance and reliability of PV systems have become key issues for minimizing business risks and increasing market actors' trust. A more accurate yield prognosis and information on operational availability of PV systems are crucial for investment decisions and market growth. In this context, performance and yield data, reliability statistics and empirical values concerning maintenance are by far more relevant today than in the past.

As previously mentioned, Europe remains the geographic area leader for PV installations. During 2010 Germany represented the most important country in the PV market with around 7.4 GW_p of installed new PV plants, while in 2011 Italy with around 9 GW_p of grid-connected new PV plants had the primacy. Spain, major player in 2008, has installed in the last years only around 400 MW_p per year. The reason is in the incentive policy change, with the introduction of a too low threshold for installations and significant cuts in tariffs.

The main novelties of 2010 are in France and Czech Republic. As per France, the installed power during 2011 was around 1.5 GW_p, a very big increase compared to the previous year. Regarding Czech Republic, where the PV market is in the large part constituted by small and medium-sized plants (4.2 MW_p is the size of the largest PV plant built in 2010), the power installed in 2010 was 1360 MW_p, which has permitted to reach USA in the cumulative installed power, however the installation in 2011 has gone down below 1,000 MW_p.

In addition, new European countries are entering in the PV market, for example Greece installed in 2010 around 150 MW_p and in 2011 around 350 MW_p, or Israel and Turkey had "strong" introduction of a new system of incentives in 2010. In Israel PV power of about 50 MW_p has been installed, but it is expected to reach in 2015 the target of 300 MW_p. In Turkey, despite the power installed in 2010 does not reach 10 MW_p, it is expected for 2015 a huge potential market [5].

1.2. PV Market and Industry in Italy

The PV progress in Italy is impressive, particularly in 2010 when the so-called "Salva Alcoa" Decree has been implemented. In this Decree, the incentive rates, provided in 2010 by the "Nuovo Conto Energia" feed-in tariff, are recognized in all PV systems that have concluded the installation of mounting structure and electrical installation by December 2010 have concluded and the connection to the grid by June 2011 have obtained.

As per new installations, the year by year growth was +382 % in 2008, +112 % in 2009 and +192 % in 2010. In 2010 about 138900 new PV plants (2.1 GW of total PV power) started into operation, and other 55000 PV plants (3.95 GW of total PV power) are completed (Fig. 1.1). The total PV power installed approximately in 210000 plants in operation at the end of 2010 was 3276 MW, more than 64 times the value in 2007 [5].

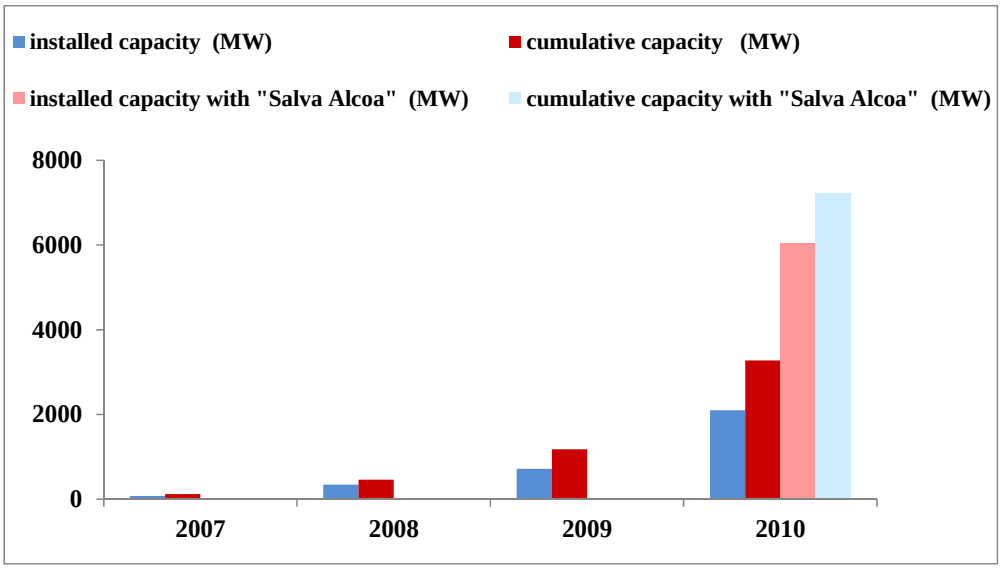

Fig. 1.1 − The development of new installations and total PV power since 2007 in Italy.

As shown in Fig. 1.2, the residential systems (1 − 20 kW) decreased from 44.5 % in 2007 to 19.4 % in 2010. If in 2007 PV market was based on private customers who opted for the electrical system integration exploiting the space on their roof, in 2010 this phenomenon was in minority. The typical residential system customer is changed, both in terms of technologies knowledge and available implementation alternatives, and in terms of “contractual power” for installers, thanks to the “buying-groups” that install PV systems of large dimensions.

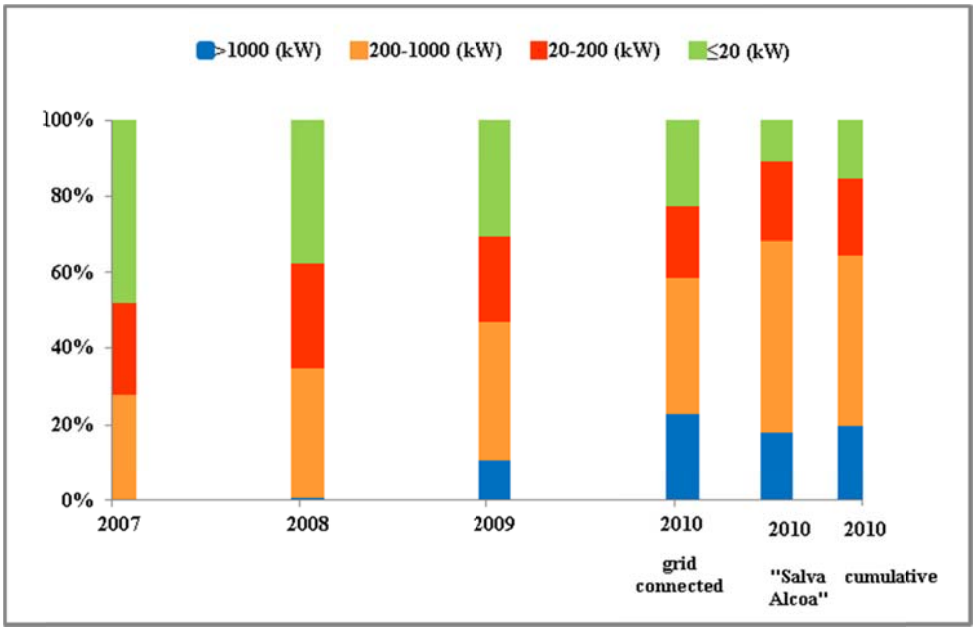

Fig. 1.2 − The sizing segmentation of PV market in Italy since 2007.

In Table 1.2 is shown the current number of installed PV plants and the installed capacity in Italy provided by the GSE (Italian feed-in tariff Operator). More than 90 % of capacity is covered by high size plant even if the most number of installed PV plant is the within the 20 kW power range. Moreover, the middle size power covers less than 3 % of the total number and less than 4 % of the total capacity.

Considering Italian Regions, the major player for installed capacity is Puglia, in the south of Italy, with 2200 MW, characterized by huge amount of radiation and low regulation barriers. In the north of Italy an important role is played by the most industrialized regions, Lombardia with 1332 MW, Emilia Romagna with 1273 MW, Veneto with 1167 MW and Piemonte with 1077 MW. As per Sicily, in the south of Italy, characterized by the highest irradiation in Italy, although a large number of PV plants (around 20000), the installed capacity, due to the excessive bureaucratization, is relatively low (only 865 MW).

Regarding the Italian PV sector, 800 is the number of business companies operating in 2010, to which several thousand local operators are added that takes care of the residential and commercial installation sand 430 bank sand financial institutions active in the facilities financing [5]. In 2010 an increasing of Italian companies in the PV industry takes place (Fig. 1.3).

Table 1.2 − Number of installed PV plant and cumulative capacity according to the PV power range.

Cumulative values	Number of installed PV plants	Cumulative installed capacity [MW]
All PV plants	333189	12855
< 20 kW	292492	1749
From 20 to 50 kW	11847	468
> 50 kW	28850	10637

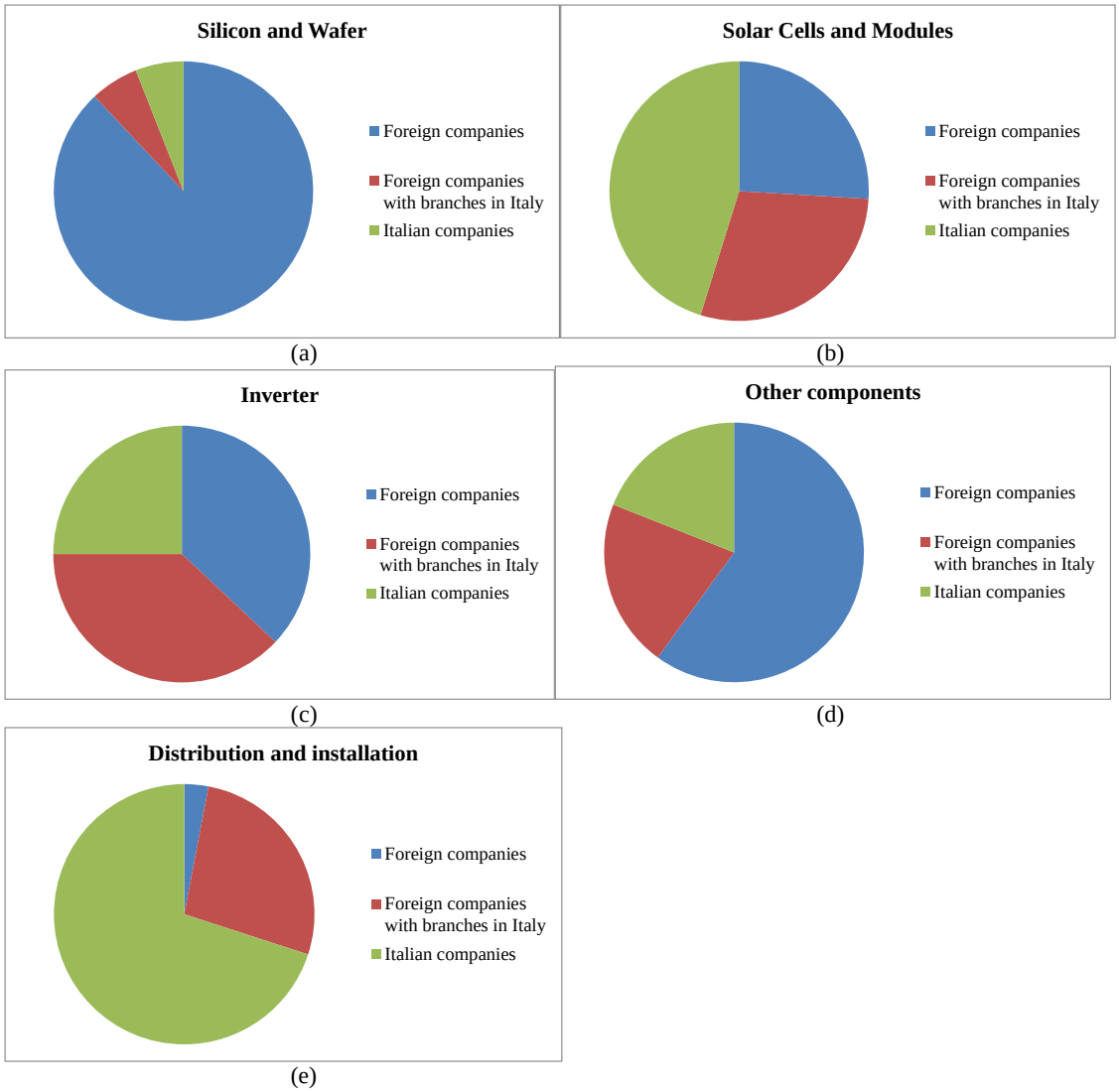

Fig. 1.3 − (a) Silicon and Wafer industry; (b) Solar Cells and Modules industry; (c) Inverter industry, (d) Other components industry; (e) Distribution and installation industry.

The production of silicon and wafers is relatively marginal: in 2010, in addition to an US multinational corporation that has two branches in Italy (one in the northwest of Italy for the production of wafers and the other one in the northeast of Italy for the production of solar grade silicon), an Italian company joins in the PV market. In the production of solar cells and modules, Italian companies represent the majority share and also foreign companies that have a branch in Italy are grown (Table 1.3).

Table 1.3 − Solar cells and modules companies.

Value Chain	Company	Capacity 2009 [MWp]	Capacity 2010 [MWp]	Production 2010 [MWp]
Fully Integrated (Cell/Module)	Solsonica	25/50	35/70	35/64
	Helios Technology	60/55	60/55	n/a
	Xgroup	90/30	90/55	55/55
	EniPower	30/30	30/30	1/10
Module	MIX Group	60	90	48
	Solarday	60	90	42
	Renergies (gruppo Afin)	30	40	37
	Brandoni Solare	20	40	28
	Vipiemme Solar	20	25	21

Even in the production of inverters, a US multinational corporation with a branch in Italy in addition to the other Italian companies represent one of the majority share of the market (Table 1.4). The main inverter manufacturing companies in the world belong to Germany (approximately 70 % of installed capacity in 2010), USA (approximately >10 % of installed capacity in 2010) and Austria (approximately 10 % of installed capacity in 2010).

Distribution and installation are Italian companies activities, although in recent years there was a considerable number of foreign companies. Almost all Italian companies are involved in distribution and installation of PV components.

Table 1.4 – Inverters companies.

Component	Company	Capacity 2010 [MWp]	Production 2010 [MWp]
Inverters	Power-One Italy	3000	2600
	Elettronica Santerno	1400	880
	Siel	400	380
	Aros Technology (Riello Elettronica)	310	310
	Answer Drives	200	195
	Astrid Energy Enterprises	190	185
	Italcoel	110	33
	Fimer	240	n/a

1.3. Feed-In Tariff Policy and Bureaucratic Barriers

1.3.1. The Italian situation

GSE ("Gestore Servizi Energetici") is the Italian Energy Services Operator for the approval of incentives for the electricity production from renewable sources and receives the energy delivered to the grid by the so-called "Scambio sul Posto", i.e., on-site exchange [6]. The owners of solar PV systems can use the incentives and/or services described in the following list.

- The "Conto Energia" (CE, photovoltaic-electricity bill) is the incentive mechanism of production from solar photovoltaic energy. The incentive is paid according to the electricity production, since the grid-connection date of the PV plant for a period of twenty years. The rate is constant throughout the incentive period. The highest rate is approved for small domestic plants in building integration; on the other hand, the lowest rates are recognized to the large plants not architecturally integrated.

1. The first phase of CE program (issued in late 2005) was completed during 2009. In this context 5,733 plants have been installed, corresponding to a total power around 164 MW_p. At this stage it was necessary to send the design documents to GSE for obtaining the assignment of the tariff before the installation.
2. The second phase of CE program started in 2007, when the first phase was still in force, and was completed at the end of 2010. During this period, it resulted in setting into operation about 125,000 plants corresponding to a total power of 2,736 MW_p. From this stage on, it was possible to install the PV plant and only after to send the final documents for the tariff assignment. Taking into account both the first and second phase, the installed PV power at the end of December 2010 was over 2.9 GW_p without the contribution of the so-called "Salva Alcoa" Decree. The feed-in tariffs were constant for 2007 − 2008 and only a -2 % decay per year (period 2009 − 2010).
3. In July 2010, a new edition of CE decree was established for the third phase At this stage the maximum power, that could have the feed-in tariff updated every quarter year,

was limited to 3500 MW_p and a premium is given for PV plants with predictable power profiles.

4. Furthermore, after a huge peak in PV installations, a fourth phase of CE decree, established in May 2011, was in force with an economic cap within 6 and 7 billion Euros for all the PV systems subject to incentive. Here, it is possible to distinguish between small and large grid-connected Photovoltaic (PV) Systems. *Small grid-connected PV* are: Building Integrated Photovoltaic System (BIPV) with peak power up to 1,000 kW_p, other photovoltaic systems at ground level with peak power up to 200 kW_p operating under on-site exchange, and systems of whatever power in buildings and areas whose owner is a public administration (Municipalities, Provinces, Ministries, schools). These PV systems receive automatically the feed-in tariff according to the power levels. All other PV systems, not covered by this definition, are called *Large grid-connected PV systems* [7] and need the positive check of GSE after the registration in a suitable logbook.

5. Finally, a fifth phase of CE is in force up to now, since August 2012, when the threshold of 6 billion Euros has been reached and the maximum cap has been fixed to 6.7 billion Euros. In this current mechanism the incentive is different because the PV energy is divided in two parts, one is the amount which is sold to the grid and the other one is the self-consumed that produces the maximum profit because it receives a premium tariff besides the saving in the utility bill.

- "Ritiro Dedicato" (Dedicated Delivery) is a GSE service in force, a simple way to place the electricity generated and fed into the grid on the electricity market through the GSE. PV systems have access to this service through the GSE for the delivery of all energy into the grid. The GSE recognizes to the producer of the PV plant a electricity price in €/kWh variable in the range 0.07−0.105.
- "Scambio sul Posto" (on site) is a mechanism operated by the GSE since January 2009 for PV plants powered by renewable energies with power up to 200 kW_p. It permits to give an economic value to the energy fed into the grid, according to an economic compensation principle with the energy value paid from the grid.

An additional amount in the feed-in tariff will be paid whenever the PV system is combined with energy saving techniques.

Differently from Germany, one of the main hindered problems for a more virtuous development of the Italian PV market in recent years has definitely been the excessive bureaucratization of the necessary authorization practices for the installation, the starting of the production and the promoting of a new facility.

The PV progress in Italy is impressive, particularly in 2010 when the so-called "Salva Alcoa" Decree has been implemented. In this Decree, the incentive rates, provided in 2010 by the 2nd "Conto Energia" feed-in tariff, are generously recognized in all PV systems, in which the installations of mounting structure and electrical components have concluded by December 2010 and the connection to the grid has performed by June 2011.

As per the new installations, the year by year growth was +382 % in 2008, +112 % in 2009 and +192 % in 2010. In this year about 138,900 new PV plants (2.1 GW_p of total PV power) started into operation, and other 55,000 PV plants (3.95 GW_p globally) have been completed. The total installed PV power, approximately shared in 210,000 plants in operation at the end of 2010, was 3276 MW_p, more than 64 times the value in 2007 [5].

As shown in Table 1.5, the residential systems (1 − 20 kW_p) decreased from 44.5 % in 2007 to 19.4 % in 2010. If in 2007 PV market was based on private customers who opted for the electrical system integration exploiting the space on their roof, in 2010 this phenomenon was in minority. The typical residential system customer is changed, both in terms of technologies knowledge and available implementation alternatives, and in terms of "contractual power" for installers, thanks to the "buying-groups" that install multiple PV systems with large size.

In Table 1.5 is reported the current number of installed PV plants and the installed capacity in Italy provided by the GSE in 2011. More than 90 % of capacity is covered

by high size plant, even if the most number of installed PV plants is within the 20 kW_p power range. Moreover, the middle size power covers less than 3 % of the total number and less than 4 % of the total capacity. Table 1.6 provides the tariff rates valid up to August 2012 when the 5th CE has changed newly the amounts.

Table 1.5 − Number of installed PV plants and cumulative capacity according to the PV power range in 2011 in Italy (source: GSE).

Cumulative values	Number of installed PV plants	Cumulative installed capacity [MW]
All PV plants	333189	12855
< 20 kW	292492	1749
From 20 to 50 kW	11847	468
> 50 kW	28850	10637

Table 1.6 − Italian PV feed-in tariff for the first and second half of 2012 (source: [8]).

Power Range [kW]	First half of 2012 [€/kWh]	Second half of 2012 [€/kWh]
1≤P≤3	0.274	0.252
3<P ≤20	0.247	0.227
20<P ≤200	0.233	0.214
200<P ≤1000	0.224	0.202
1000<P ≤5000	0.182	0.164
P>5000	0.171	0.154

To obtain the incentive, the responsible person for PV system must submit relevant documents to the GSE, such as detailed drawings concerning electrical scheme with main devices (PV modules and their connections, grid-connected inverters, cables, protections and energy counters, etc.) and photos showing components and their locations in the plants. Moreover, as per the authorization, it must be submitted one of the following titles:

- the exclusive license ("Autorizzazione Unica" − AU) referred to the Article 12 of Legislative Decree n. 387/2003: the procedure lasts at least 6 months and requires a joint agreement from many public agencies);

- the Start Activity Document ("Denuncia di Inizio Attività" − DIA), according to the President of the Republic Decree n. 380 of 2001, if applicable, or the simplified habilitation declaration, according to the Legislative Decree n. 28/2011;
- the hard copy of free-construction document ("comunicazione di attività in edilizia libera"), referred to guidelines adopted pursuant to the Legislative Decree n. 387/2003 (the most simple and quickest procedure);
- the Start Activity Notice ("Comunicazione di Inizio Attività" − CIA) or the Start Activity Certificate ("Segnalazione Certificata di Inizio Attività" – SCIA), of the Ministerial Decree, n. 122/2010.

1.3.2. The German situation

The rapid increase of PV market in Germany began in 90's decade with the so-called "Thousand Roofs Programme", showing that the grid coupled feed-in from many small PV systems was technically possible [9]. The "Thousand Roofs Programme" sent a positive signal to the PV industry and provided an important impulse for the further development of the technology. It was aimed specifically at house owners and hence for the first time included private households in electricity generation; so these people became power producers.

After this, the Renewable Energy Sources Act ("Erneuerbare-Energien-Gesetz" − EEG) in 2000 provided a reliable and long-term framework for PV and made solar electricity generation economically interesting. In terms of achieving expansion targets for renewable energies in the electricity sector, the EEG is actually the most effective funding instrument at the German government's disposal [10]. It determines the procedure of grid access for renewable energies and guarantees favourable feed-in tariffs.

The purpose of this Act is to facilitate a reliable development of energy supply, particularly for the sake of protecting the climate and the environment, to reduce the

costs of energy supply to the national economy, also by incorporating external long-term effects, to preserve fossil fuels [11]. The Act aims to increase the share of renewable energy sources in electricity supply to at least 30 % by 2020 and to continuously increase that share thereafter.

The Act regulates: the priority connection to the grid for electricity supply of installations generating electricity from renewable energy sources within the Germany territory, including its exclusive economic zone; the priority purchase, transmission, distribution and payment for such electricity by the grid system operations, and the nationwide equalization scheme for the quantity of electricity purchased.

For PV, the feed-in tariff depends on the system size and whether the system is ground mounted or attached to a building [12]. Since 2009, there is also a tariff for self-consumed power. The rates are guaranteed for an operation period of 20 years. Initially, a steady yearly reduction of the PV tariffs was foreseen. On the background of a constantly rising number of installations, a mechanism was introduced to adapt the EEG tariff to the market growth. Under this scheme, the reductions are increased or decreased if the market deviates from a predefined corridor.

For 2009 this corridor was defined to be between 1,000 MW_p and 1,500 MW_p, which was significantly exceeded as the market reached 3,800 MW_p. For 2010 to 2012, a new corridor between 2,500 and 3,500 MW_p was defined. Furthermore, for 2010 two additional reduction steps were agreed to adapt the tariff to the system price level. With around 7,000 MW_p installed in 2010 the new corridor was surpassed again considerably. Beside the EEG support for the development of PV installations, the decrease of system prices continues which makes PV systems economically more and more attractive.

In addition to the EEG, PV receives support from other sources: local fiscal authorities provide tax credits for PV investments; the state owned bank (KfW– Bankengruppe) and other banks (e.g., UmweltBank and SwkBank) provides loans for individuals as well as for local authorities. Since at the beginning of 2009 the owners of new PV

systems are legally obliged to register their systems at the German Federal Network Agency, which showed in 2011 an additional capacity of 7.4 GW_p and in total around 24.7 GW_p connected to the German grid.

As a consequence, Germany produced 12 TWh of PV−electricity in 2010, which were roughly 2 % of the national consumption. All renewable energies together have a share of 16.8 % of the domestic energy supply. At the same time, the German National Renewable Energy Action Plan includes a target of a 38.6 % share of renewable energies in the electricity sector for 2020.

For PV, the scenario assumes a future development of annually 3,500 MW_p from 2012 to 2020. This leads to an installed capacity of almost 52 GW_p in 2020 and a resulting electricity production of around 8% of the overall consumption.

In the debate over the second EEG revision in 2008, the rising remuneration payments drew intensive criticism as per their effectiveness. The growing demand for solar systems had been the reason that module prices did not drop proportionally with manufacturing costs. Solar companies thus made very high profits at this time.

The new version of the Renewable Energy Sources Act, which came into force in 2009, therefore established a steeper digression of feed-in tariffs, increasing the rate of reduction from 5 % annually to 8 or 10 %.

System prices dropped further, by about 30 % in 2009, even though the number of installed solar power systems grew considerably and more strongly than expected. Finally, the debate over support for solar power and changes in the feed-in tariffs illustrates the excellent development which Photovoltaics has undergone in recent years [9]. For typical home roof systems up to 30 kW_p of capacity, feed-in tariffs of December 2011 is 24,43 ct€/kWh, as shown in Table 1.7. The costs of PV systems will drop still further in future. Solar PV power in Germany will reach the so-called grid parity from the active-user viewpoint, i.e. equal retail price as household power, as soon as in three years with a very high probability. That will be a watershed for investments

in Photovoltaics, the self-produced power will be cheaper than what the power company can provide.

Table 1.7 − PV feed-in tariff of the EEG from 2010 in Germany

Date of commissionig	< 30 kW_p	up to 100 kW_p	up to 1 MW_p	> 1MW_p
01.01.2010- 30.06.2010	39,14	37,23	35,23	29,37
01.07.2010 - 31.09.2010	34,05	32,39	30,65	25,55
01.10.2010 - 31.12.2010	33,03	31,42	29,73	24,79
01.01.2011 - 30.06.2011	28,74	27,33	25,86	21,56
01.07.2011 - 31.12.2011	24,43	23,23	21,98	18,33
2012 (-15%)	20,77	19,75	18,68	15,58

1.3.2.1. PV Industry in Germany

During the year 2010 in Germany a lot of companies opened new production facilities or expanded their production [12]. Table 1.8(a) shows the production capacity and the total number of employees in major German companies of crystalline silicon, wafer, cell, module and fully integrated production for 2010, on the contrary Table 1.8(b) shows the thin film production companies.

Due to the well-developed PV industry, all components for an entire PV system are available in Germany as shown in Table 1.9.

Table 1.10(a) shows the leading manufacturers of materials for PV modules produced in Germany, while Table 1.10(b) shows the leading manufacturers of PV system components.

Table 1.8 − Production capacity and number of employees in German companies: (a) crystalline silicon, wafer, cell, module and fully integrated production; (b) thin film production.

Value Chain	Company	Capacity 2010 [MWp]	n° of employees
Silicon	Wacker chemie	33,000t	1766
	PV Crystalox Solar Silicon	1,800t	115
Wafer	SCHOTT Solar Wafer	500	400
	PV Crystalox	400	145
Cell	Q-Cells	500	1300
	SCHOTT Solar	305	520
	ITS Innotech Solar	135	36
	Sunways	116	350
	Solland Solar Cells	110	275
Module	CENTROSOLAR	350	700
	Aleo solar (Bosch)	280	801
	SOLON	251	470
	SOLARWATT	240	470
	Solar-Fabrik	210	350
	Scheuten Solar technology	200	270
	Heckert Solar	180	205
	ALGATEC Solar	130	233
Fully Integrated (Wafer/Cell/Module)	SolarWorld	1000/250/550	990
	Bosch Solar Energy	400/550/150	2500
	Conergy	200/250/250	750
	Sovello	180/180/180	1250

(a)

Value Chain	Company	Capacity 2010 [MWp]	n° of employees
a-Si a-Si/µc-Si	Schüco TF	110	150
CIS	Solibro (Q-Cells)	135	500
CIGS	AVANCIS	120	223
CIGSSe	Nanosolar	120	77
CdTe	First Solar	447	600
GaAs	Azur Space Solar Power	250	135

(b)

Table 1.9 − Leading PV equipment suppliers produced in Germany.

Equipment	Company	n° of employees
Silicon	Centrotherm SiTec	150
Ingot/Wafer	ALD Vacuum Technologies	365
	Centrotherm SiTec	150
	KUKA Systems	1200
	RENA	1150
Cell	Centrotherm Photovoltaics group	1500
- Turnkey Lines	Roth & Rau	500
Cell - Thermal Equipment	Rehm Thermal Systems	170
Cell - West Chemistry	RENA	1150
Cell	Centrotherm Photovoltaics group	1500
- Anti-reflective	Roth & Rau	500
coating	VON ARDENNE Anlagentechnik	570
Module	Centrotherm Photovoltaics group	1500
- Turnkey Lines	KUKA Systems	1200
Thin Film - Turnkey Lines	Centrotherm Photovoltaics group	1370
Thin Film	Grenzebach	1500
- Vacuum Deposition	KUKA Systems	1200
Laser Processing	RENA	1150
	Manz Automation	400
	Rofin	1600

Table 1.10 − Major companies and number of employees of materials for: (a) PV modules; (b) PV systems components.

Material	Company	n° of employees
Frontsheets	Wacker Chemie AG	10000
Tapes/Adhesives/Sealants	Wacker Chemie AG	10000
Junction Boxes	Phoenix Contact Deutschland GmbH	8400
	Tyco Electronics GmbH	1950
	Weidmüller Interface GmbH & Co. KG	1800

(a)

Component	Company	Capacity 2010 [MWp]	n° of employees
Inverters	Bonfiglioli Vectron	n/a	80
	Diehl AKO	700	140
	KAKO new energy	1200	350
	REFU Elektronik	n/a	170
	SMA Solar technology	10000	4000
	Steca Elektronik	40	510
Cables	Lumberg Connect		1000
	Multi-Contact		120
	Tyco Electronics		1950
Connectors	Multi-Contact		120
	U.I.Lapp GmbH		800
	Wieland Electric		1000

(b)

1.4. Economic Analysis of a PV Rooftop System

In recent years, a progressive price decrease of components for PV installations (modules, inverters) has occurred. In order to reduce the burden of the incentive rate on the national budget and maintain the investment attractive for investors, a progressive tariff decline is also occurred [13].

This section provides an economic analysis method of investments in PV systems installed on the roof, considering current incentive policies, and apply it to some

significant case studies in the European Countries in which PV market is currently the most prosperous: Germany and Italy. This analysis highlights the current convenience margin of the PV investments.

The most important cost items for a PV plant are: the PV module costs (40 – 55 % of total amount), the inverter/cable/protection costs (10 %), the building-integration costs (10 – 15 %), the installation costs (10 – 15 %), the design/bureaucratic-document costs (5 – 10 %). Usually, the support structure of PV modules influence only for a little, without a complete building integration. As per installation costs a continuous decline occurs. Concerning the PV modules, a reduction from 3200 €/kW_p of 2009 to 1200 €/kW_p of 2011 occurs for crystalline silicon; while regarding the thin film technology, the costs are reduced from 2200 €/kW_p of 2009 to 1000 €/kW_p of 2011 [14]. Nowadays, these figures are within 500-1000 €/kW_p for the technologies available in market.

1.4.1. Investment Assessment in PV systems by *NPV* and *IRR*

In order to determine the convenience of an investment, as for example the electricity production, with respect to other investments, a conventional method implies the assessment of the *NPV* and the *IRR* during the PV plant life [15].

The parameters which influence the yearly *NPV* calculation [16], [17] are:

- the installation cost C_I in €/y [18], [19], [20], [21], [22], [23];
- the rated power P_{PVr} in kW_p of the PV system;
- the yearly Revenues, R_{PV} in €/y, are calculated as:

$$R_{PV,k} = E_{AC} \cdot p_{PV} + E_{g\_inj} \cdot p_{inj} + E_{s\_cons} \cdot s_{bill} \quad (1.1)$$

where:

E_{AC}: PV energy production in kWh;

p_{PV} : feed-in tariff unitary price in €/kWh;

E_{g_inj}: share of PV energy production delivered to the grid (different according to residential, commercial and industrial loads) in kWh;

$p_{inj:}$ unitary price in € paid to the PV owner per kWh injected into the grid;

E_{s_cons}: amount of PV energy production self-consumed by the PV system's owner (different according to residential, commercial and industrial loads) in kWh;

s_{bill}: cost in €/kWh saved from the utility bill;

- the yearly Operation and Maintenance (O&M) cost C_{OM} in €/y;
- the real interest rate i^*.

According to the following formula, the real interest rate i^*takes into account the effect of the inflation rate f that reduces the basic interest rate i, if the feed-in tariff is updated through the inflation rate

$$i^* = \frac{i - f}{1 + f} \cong i - f \quad \text{when } f << 1 \tag{1.2}$$

In fact, the present value of a future cash flow CF_k (at k-th year) that includes inflation rate is equivalent to a present value weighted by i^*, according to:

$$\frac{CF_k \cdot (1+f)^k}{(1+i)^k} \approx \frac{CF_k}{(1+i^*)^k} \tag{1.3}$$

The cash flows at k-th year is composed of multiple items in terms of both revenues and costs, characterized by different real interest rates: the situation is different between Germany and Italy. In particular, in Germany the real interest rates are two: one for the feed-in tariff, $i^*_{feed} = i$,, not updated [24], [25] according to the national inflation rate (determined by multiple goods and services), f, the other for the O&M costs, i^*_{OM}, that includes the national inflation rate [26],calculated as a mean value in the last ten years according to equation (1.2):

$$i^*_{OM} = i - f \tag{1.4}$$

On the other hand, in Italy the real interest rates are three: the first two items are the same (feed-in tariff not updated according to the inflation [24]), the additional item, that deals with the on-site-exchange, i^*_{ose}, is defined by the national inflation rate of the electricity as a single good, f_{elec}, [27], [28], [29], [30], according to equation (1.2):

$$i^*_{ose} = i - f_{elec} \tag{1.5}$$

Many papers present suitable formulas for the economic analysis of investment in renewable energy installations [31], [32], [33], [34]. Here the discussion starts from equation (1.1), in order to define basically *NPV* as a mathematical series after *N* years of operation. In our case, the *NPV* after 25 years of guaranteed energy production (20 years of feed-in tariff in Germany and Italy and 25 years of on-site exchange in Italy), is defined as:

$$NPV = -C_I + \sum_{k=1}^{N}\left[\frac{\left(E_{AC}\cdot p_{PV}\right)}{\left(1+i\right)^k} + \frac{\left(E_{g\_inj}\cdot p_{inj} + E_{s\_cons}\cdot s_{bill}\right)}{\left(1+i^*_{ose}\right)^k} - \frac{C_{OM,k}}{\left(1+i^*_{OM}\right)^k}\right] \tag{1.6}$$

As previously mentioned, it is possible to evaluate the investment through economic indicators, such as the net present value and the internal rate of return.

- *NPV* of a time series of cash flows is defined as the sum of the present values of the individual cash flows of the same entity. The interest rate takes into account the alternative uses of capital, or the minimum return that an investment must generate in order to equalize an investment of equal duration and risk on the financial market. Therefore, *NPV* takes into account the lacking revenues arising from the alternative use of money. If an investment is associated with a positive *NPV*, it is not only convenient from the economic and financial point of view but can be also more convenient than other investments with similar characteristics. A negative *NPV* means the investment return is less than the alternative one.
- The interest rate of the cash flows of an investment is equal to the Weighted Average Cost of Capital (*WACC*). *WACC* is calculated considering only objective parameters,

such as the rate of return without risk (long-term government bonds, e.g. German "bund"), or the Market Premium between the return of a portfolio of stock titles and the return rate without risk.

- *IRR* is a financial viability indicator and represents the yield of an investment. *IRR* is an annual compound rate of the real return of investment. In general, an investment should be pursued when *IRR* is greater than the Minimum Attractive Rate of Return (*MARR*), which coincides with the normal rate of return for an investor or a company. Mathematically, *IRR* is defined as the interest rate that makes the *NPV* of a series of cash flows equal to zero. According to this criterion, an investment is desirable when *IRR* is greater than another reference rate (for example, *WACC*).

Based on these considerations, a possible analysis of economic investment for PV systems on rooftop in Italy and Germany is made, considering both the various rules of feed-in tariffs and the current installation costs. Obviously, this analysis should take into account the geographical location of the PV system or the predicted productivity.

Actually, in the economic analysis of a grid-connected PV system, it is necessary to calculate, with adequate accuracy, the yearly electricity production at the AC terminals (E_{AC}). Therefore, the following formula can be used [35]:

$$E_{AC} = P_{PVm} \cdot N_m \cdot Y_r \cdot PR \tag{1.7}$$

where:

$P_{PVm} \cdot N_m$ is the total rated power of the PV array P_{PVr}, constituted by N_m equal modules with individual rated or peak power (i.e., in the maximum power point) P_{PVm} at the Standard Test Conditions (*STC*, irradiance G_{STC} = 1 kW/m^2, cell temperature T_{STC} = 25 °C), declared by the manufacturer;

Y_r is the reference yield, i.e. the ratio $H_g(\beta,\gamma)/G_{\mathrm{STC}}$, in other words the ideal number of equivalent hours per year (peak solar hours); it is worth noting that the global irradiation

$H_g(\beta,\gamma)$ is strongly dependent on the site with variations around the average value of ±20 % in Italy and ±10 % in Germany, in kWh/m^2, corresponding to the optimal tilt angle β with azimuth angle $\gamma = 0°$ (South orientation);

PR is the Performance Ratio, i.e., the recommended parameter for comparing the PV systems. In case of building integration, *PR* is 2 − 5 % lower (with crystalline silicon) for higher thermal loading consequent to less air circulation. Usual values are in the range 0.65-0.85 pu.

Finally, the yearly energy production of a PV plant characterized by P_{PVr} can be written:

$$E_{AC} = P_{PVr} \cdot Y_f \tag{1.8}$$

in which the final yield is $Y_f = Y_r \cdot PR$, i.e. the ratio of the energy production to the installed PV power (in kWh/kW$_p$).

Therefore, it is possible to calculate the revenues from electricity according to the productivity of the PV system and the feed-in tariff p_{PV} by the German and Italian formulas, respectively:

$$R_{PV} = P_{PVr} \cdot Y_f \cdot p_{PV} \quad \text{and} \quad R_{PV} = P_{PVr} \cdot Y_f \cdot p_{PV} + P_{PVr} \cdot Y_f \cdot p_{inj} \cdot \alpha_S + P_{PVr} \cdot Y_f \cdot s_{bill} \cdot (1-\alpha_S) \tag{1.9}$$

where, as a first approximation, the share of energy sold to the grid $\alpha_S = 0.7$ for loads <= 20kWp and $\alpha_S = 0.3$ for loads > 20kWp, whereas the remainder (1-α_S) is the saved energy. In the Italian formula the price paid to the PV owner per kWh injected into the grid p_{inj} is curtailed through a taxation [36], that is typically assumed equal to 20 % [37].

Due to purposes of comparison between PV systems of different size, the *NPV* equation can be divided by the rated power P_{PVr} to obtain *npv* in €/kW$_p$. If we introduce the Capital Recovery Factor (*CRF*, defined in [32]), each term of the summation, except the installation cost, is divided by its *CRF*:

$$npv = NPV / P_{PVr} = -c_I + \left(p_{PV} \cdot Y_f\right) \cdot \left(1 - \left(1+i\right)^{-N}\right) / i + \left(p_{inj} \cdot Y_f \cdot \alpha_S + s_{bill} \cdot Y_f \cdot \left(1-\alpha_S\right)\right) \cdot \left(1 - \left(1+i^*_{ose}\right)^{-N}\right) / i^*_{ose} - c_{OM} \cdot \left(1 - \left(1+i^*_{OM}\right)^{-N}\right) / i^*_{OM} \quad (1.10)$$

where

$c_I = C_I / P_{PVr}$ is the specific installation cost in €/kW$_p$;

$c_{OM} = c_I \cdot C_{OM} / C_I$ is the O&M cost expressed as a percentage of the specific installation cost.

In conclusion, the ratio of the *npv* to the specific installation cost permits the definition of a normalized index of profitability npv_{pu} in per unit, as displayed in the following case studies.

1.4.2. Case Studies in Italy and Germany

Generally speaking, the production of goods or services follows the experience curve (or learning curve). Each time cumulative volume doubles, value added costs (including manufacturing, marketing, distribution, etc.) fall by a constant percentage [1], [38].

With reference to the cumulative installation volume of grid-connected PV power in Italy and Germany (more than 50 % of the world PV market), the experience curve of the global installation cost and the same curve of the main item, i.e., the PV module cost, are shown in Fig. 1.4 on the basis of statistical data [18], [19], [20], [21], [22], [23].

It is worth noting that every doubling in the market volume corresponds to about -19 % reduction in the installation cost and about -25 % reduction in the PV module cost.

Thus, in long run (6 years) the percentage of the PV module cost decreases with respect to the installation cost from 75 % down to 40 %.

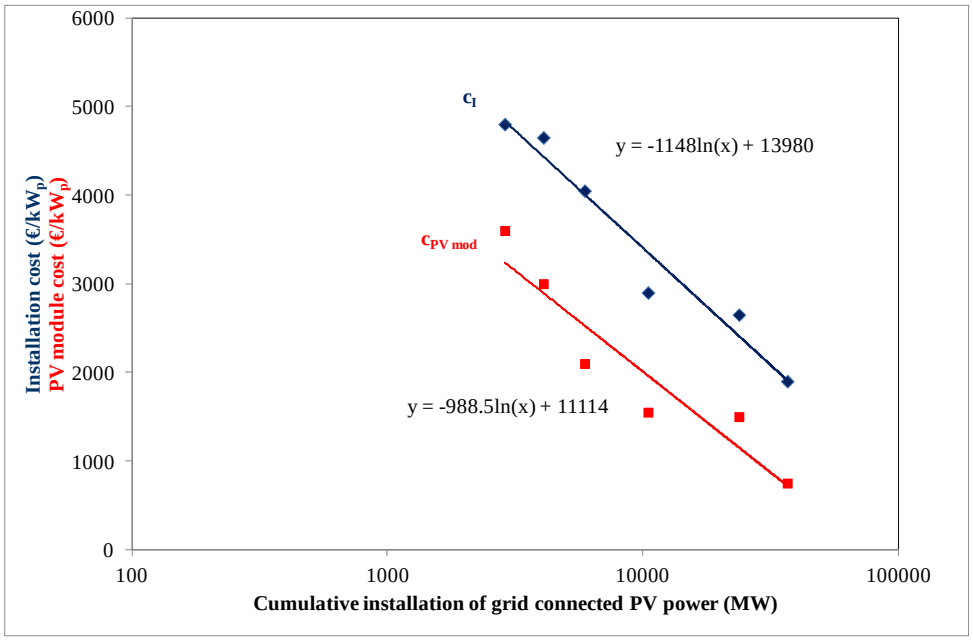

Fig. 1.4 − Experience curves of installation cost and PV module cost vs. the installation volume of PV power (2006-2011).

Now, it is possible to analyze each PV investment, referring to Central Italy and Central Germany: in this case the final yield per year from PVGIS (Photovoltaic Geographical Information System) website from European Commission JRC is roughly 1250 kWh/kW_p for Italy and 875 kWh/kW_p for Germany in 2006. Due to the continuous improvement in the design methodology, installation techniques, efficiency and availability of commercial inverters, it is supposed an increment of 1 % per year in the yearly productivity.

About the possible PV investments in the economic analysis during seven years (since 2006 to 2012), four types of PV systems installed on rooftop for energy saving are considered, by assuming money paid by the owners and typical O&M costs [39], [40]:

1. *residential*, small size of 3 kW_p for Italy and 6 kW_p for Germany (due to major consumption typical at German latitudes with less sunlight hours), in which the investor

is a family for satisfying the consumption of a dwelling house (O&M yearly cost = 1 % of the total investment);
2. *commercial A*, size of 20 kW_p, typical for small business, in which the investor is a owner of a shop or a laboratory (O&M yearly cost = 1 % of the total investment);
3. *commercial B*, size of 200 kW_p, typical for medium-large business, in which the investor is a company (O&M yearly cost = 1.5 % of the total investment, higher than the previous cases due to the advisable periodic cleaning);
4. *industrial*, size of 1 MW_p, typical for industrial business, in which the investor is a company (O&M yearly cost = 1.5 % of the total investment, higher than the previous cases due to the advisable periodic cleaning).

The incentive rates differ according to the current feed-in tariff (e.g. in Italy five different frameworks in the examined period) and the PV system size. The choice of the interest rate, derived from a financial investment with the same duration and risk of the PV installation in the considered Country, is influenced by the different investors (i = 4 %, f = 2 %, f_{elec} = 2.2 %, for residential and commercial A investors, i = 7 %, f = 2 %, f_{elec} = 7.3 %, for commercial B and industrial investors in Italy) and takes into account the different economic situation ([41] in which a 2 %-spread is given in average) of Italy vs. Germany, where the interest rates are assumed 2 % and 5 %, respectively, whereas the inflation f = 1.7 %.

The case-study results are shown in terms of time evolution of three quantities: the total specific installation cost c_I, the feed-in tariff p_{PV} according to the year and the *npv* in per unit or in percent with respect to the installation cost. The uncertainty bars in the *npv* index puts in evidence the difference due to the role of the site in the reference yield, according to the Northern Italy or Germany (lower) or to the Southern Italy or Germany (higher) installation. Moreover, in a single diagram the *IRR* trends are simultaneously displayed for all the case studies.

With reference to Italy, starting from the 1st phase of the CE, a forecasting analysis for 2013, with respect to the new feed-in tariff (i.e. the 5th CE) is represented. The

forecasting analysis is examined in two limit conditions, defined when the self-consumed energy is 100 % (best case, complete saving) and when zero self-consumption (worst case) occurs.

For the residential investor (Fig. 1.5), the *npv* performance follows the reduction of the installation cost and the feed-in tariff in the period 2006 − 2007, while it is constant (≈ 0.5 pu) in the period 2007 − 2008. From2008 to 2010a sharp increase occurs in the *npv* (up to 1.3 pu), due to the strong reduction of the installation cost and almost constant feed-in tariff (2nd CE from 2007 to 2010). The 3rd CE permits still a low increment in *npv* (1.5 pu), but, after this, the *npv* trend is declining down to 0.3-1.1 pu with the 4th – 5th CEs, according to the share between the PV energy sold to the grid and the PV energy self-consumed.

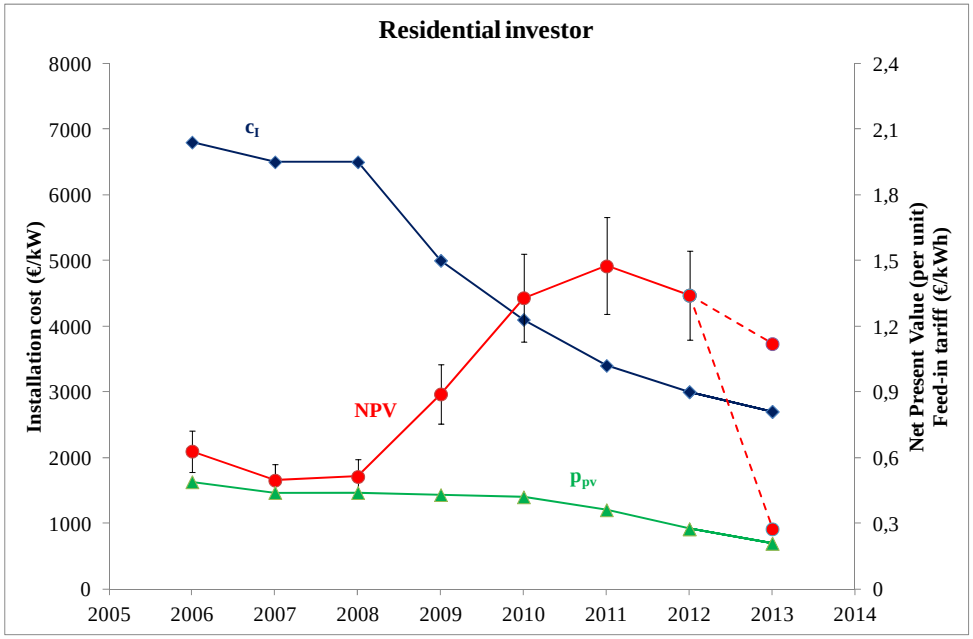

Fig. 1.5 − The time evolution of the three quantities in the economic analysis for 3 kWp system in Italy.

In case of the 20 kW_p investor (Fig. 1.6) a sensible reduction of the *npv* trend is noted in the period 2006 − 2007 when the installation cost is almost constant. Then, in 2008 − 2010 interval the situation is similar to the previous case, even if the *npv* for 20 kW_p investor is quite higher (≈1.66 pu) than *npv* in the residential case. The major increase of the *npv* trend is in the period 2009 − 2010 when a noticeable reduction of the

installation cost occurs. With the 3rd CE the trend of *npv* can no longer increase and the last two programs determine the decrements in 2012 and 2013 down to ≈ 0.47 − 1.49 pu.

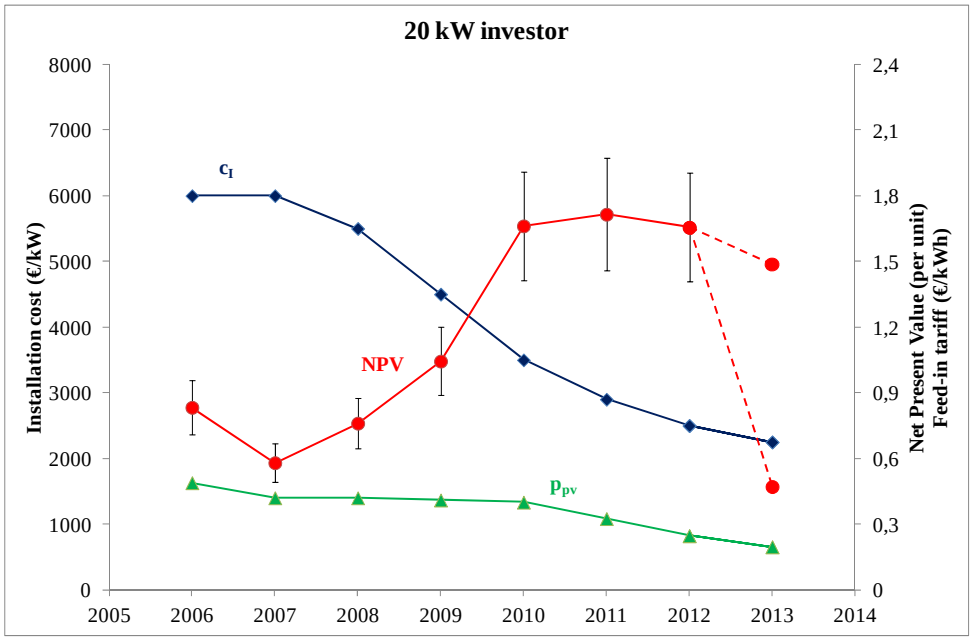

Fig. 1.6 − The time evolution of the three quantities in the economic analysis for 20 kWp system in Italy.

Considering the 200 kW_p investor (Fig. 1.7), in the period 2006 − 2007 a low reduction of the *npv* trend is observed, due to an almost constant trend of the installation cost and a low reduction in the feed-in tariff. Two increments of the *npv* trend are observed: the first in the period 2008 − 2009 and the second, which is the major, in the period 2010 − 2011 when a strong reduction of the installation cost occurs. The peak of *npv* happens with 3rd CE (≈ 2.2 pu) and then it deviates in the range 0.2 − 2.4 pu with 4th – 5th CEs.

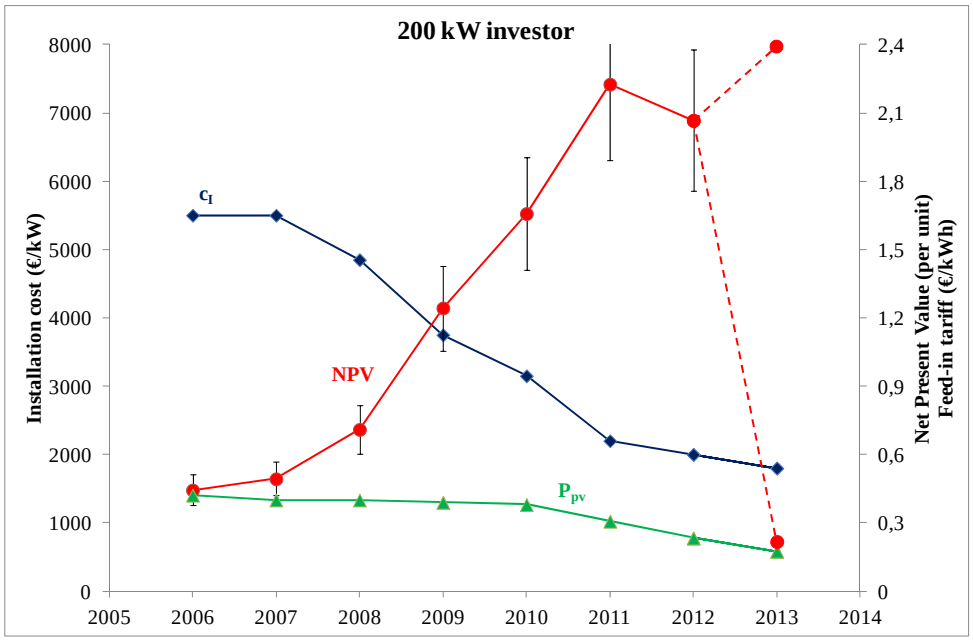

Fig.1.7 − The time evolution of the three quantities in the economic analysis for 200 kWp system in Italy.

In regards to the industrial investor (Fig. 1.8), due to an almost constant trend of the installation cost in the period 2006 − 2007 but a low decrease of feed-in tariff, a low reduction of the *npv* trend is observed. Moreover, as the case of the 200 kW_p investor, two increases of the *npv* trend are observed: the first in the period 2008 − 2009 which is the higher (from 0.7 to 1.5 pu) for a strong reduction of the installation cost, and the second in the period 2010 − 2011 (from 1.6 to 2.2 pu). In this case, with the 5th CE, the *npv* values drop to 0.1 − 1.5 pu, i.e., the minimum value for all the 4 investments.

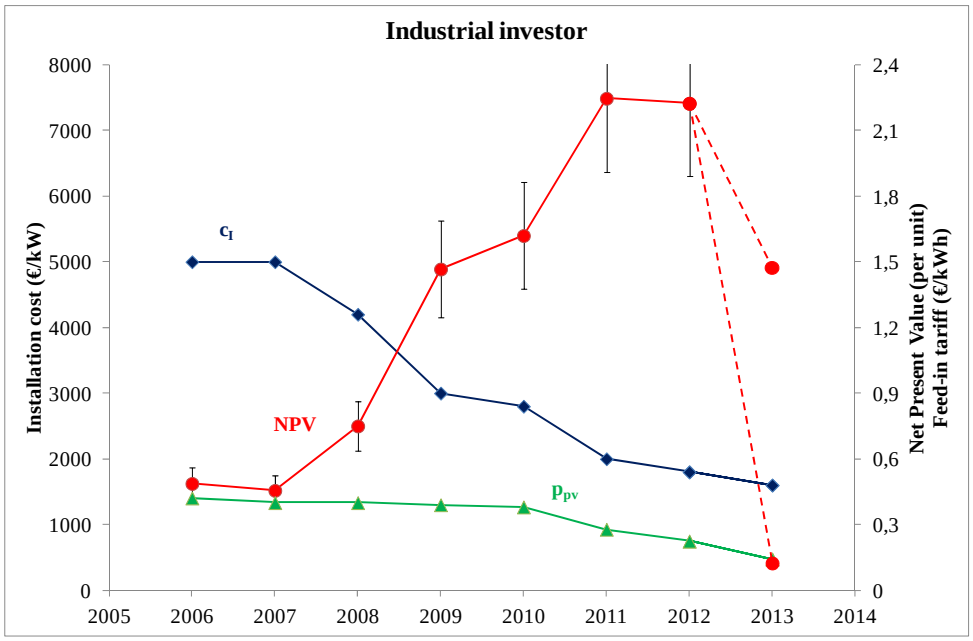

Fig. 1.8 − The time evolution of the three quantities in the economic analysis for 1 MWp system in Italy.

It is noteworthy that, in all the examined PV investments, the period 2009 − 2010 has permitted the highest growth, whereas in 2011 − 2012achange in the *NPV* trend occurs from positive to negative.

Concerning the 2013 predictions about the residential and the commercial investors, the 5th CE permits still profitable *NPV* indices, if the self-consumption is maximized.

Fig. 1.9 shows the evolution of *IRR* index for all the investors: the two higher power sizes exhibit sensible gains in the interval 2009 − 2012, whereas in 2013 the values will go back to 2008 levels.

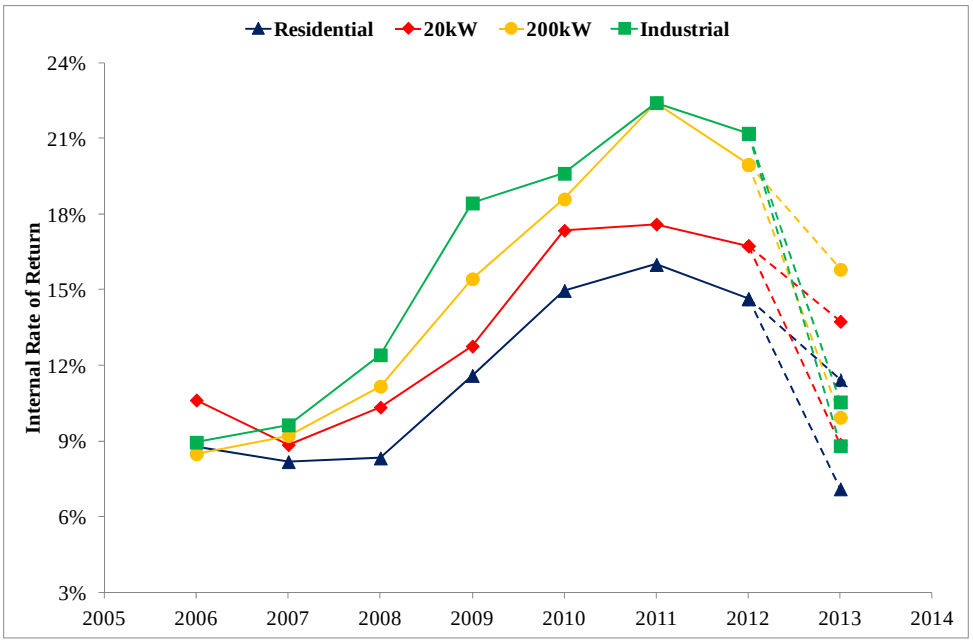

Fig. 1.9 − The time evolution of IRR for all the four PV systems in Italy.

With reference to Germany, Figures 1.10, 1.11, 1.12, 1.13 show the economic indicators c_I, p_{PV} and *npv* in Germany. The evolution of *NPV* is similar couple by couple, i.e. the residential and 20 kW_p investors have always positive values, usually higher than 0.3 pu, while the 200 kW_p and 1 MW_p investors exhibit $NPV > 0$ only since 2009 and 2008, respectively, with increasing trend in the last years. In particular, the 20 kW_p investment is the most profitable, the *npv* values are almost constant with a sensible increment in 2010 − 2012. Then, Fig. 1.14 shows the *IRR* graph, in which from 2006 to 2009 the indicators are superimposed for all the investors, whereas in the range 2010 − 2012 the medium size PV systems give the best economic gains.

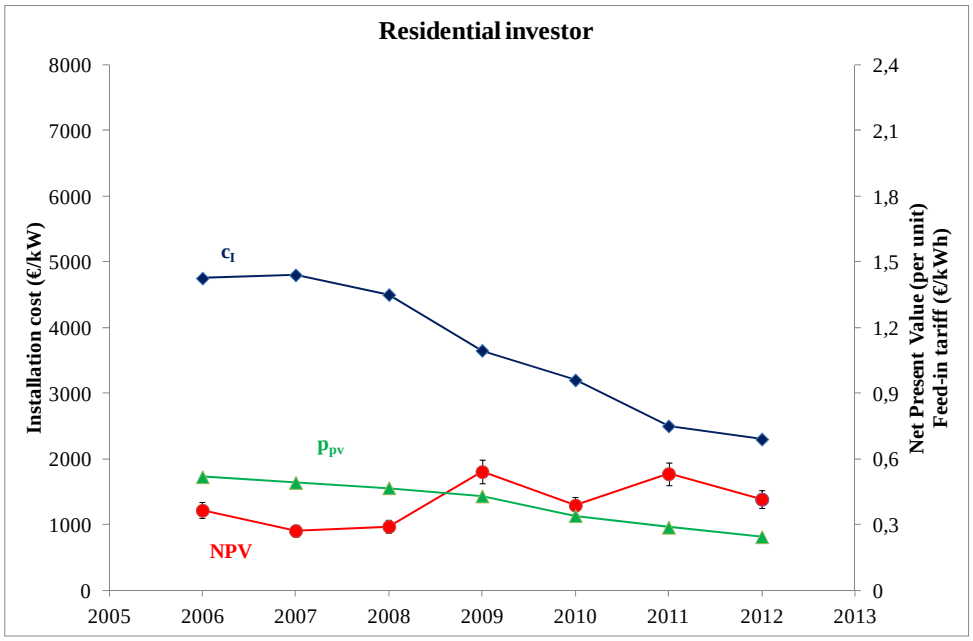

Fig. 1.10 − The time evolution of the three quantities in the economic analysis for 3 kWp system in Germany.

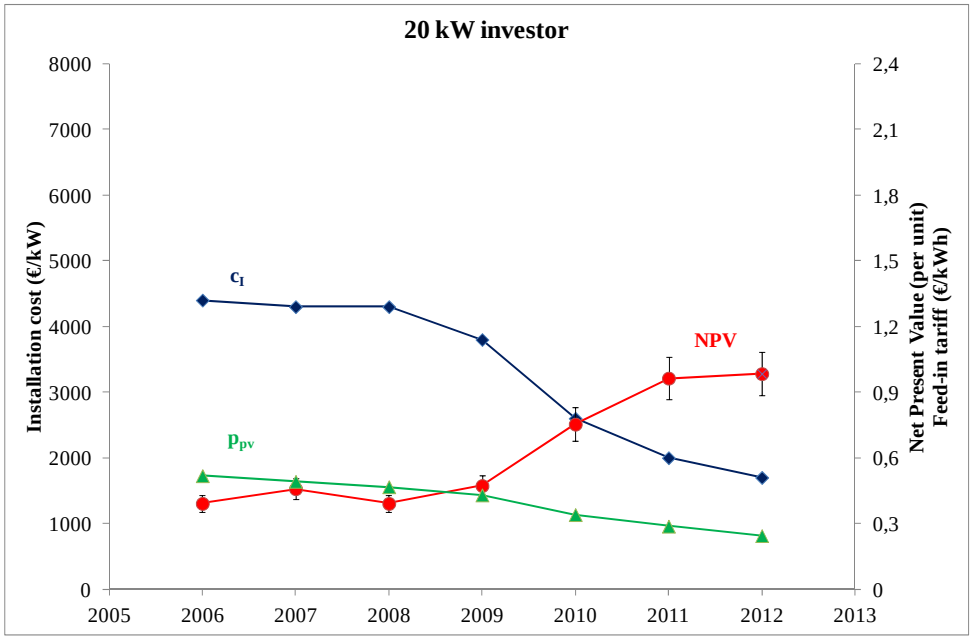

Fig. 1.11 − The time evolution of the three quantities in the economic analysis for 20 kWp system in Germany.

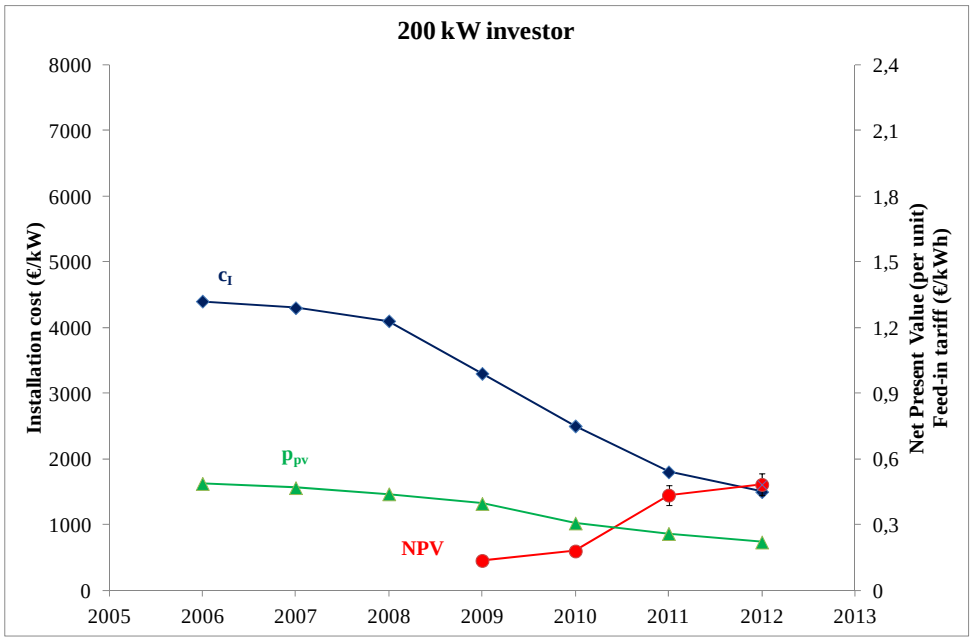

Fig. 1.12 − The time evolution of the three quantities in the economic analysis for 200 kWp system in Germany.

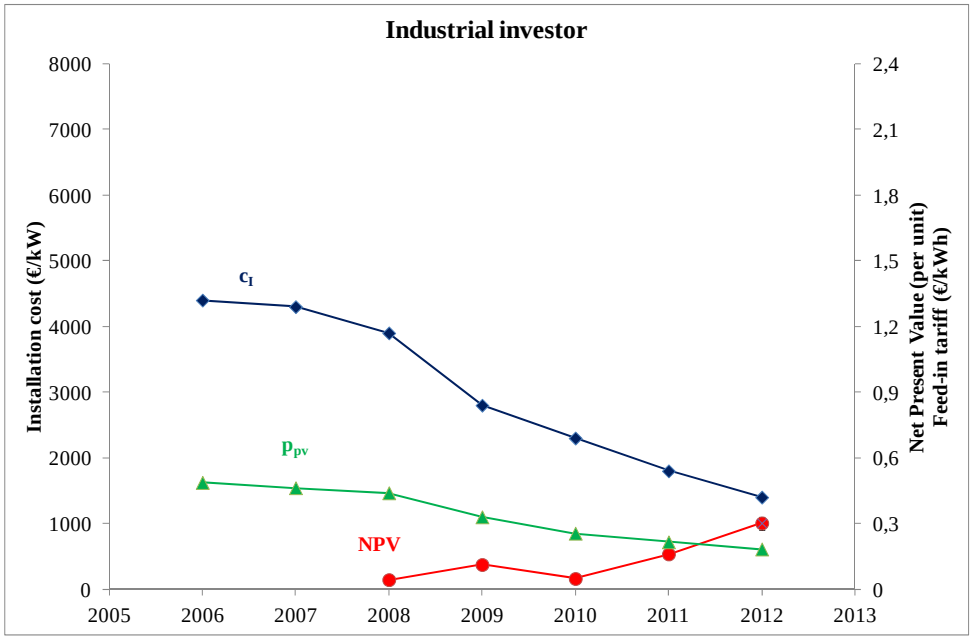

Fig. 1.13 − The time evolution of the three quantities in the economic analysis for 1 MWp system in Germany.

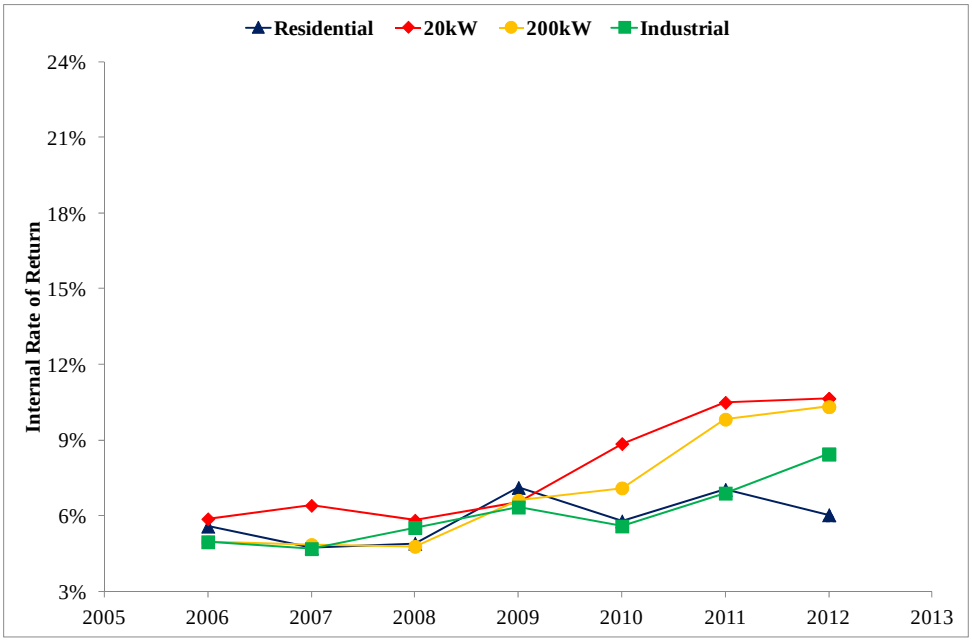

Fig. 1.14 − The time evolution of IRR for all the four PV systems in Germany.

Tables 1.11 and 1.12 shows the economic-analysis results, after 25 years of each considered type (1−4), in which:

- *npv* (pu) is the *NPV* in per unit with respect to the initial cost of the investment;
- *Z-NPV-P* (Zero NPV Period) is the number of years when *NPV* without loan become zero.

Table 1.11 − Economic analysis results after 20 years of four Italian PV systems in 2012

Type	*npv* (pu)	*IRR*	Z-NPV-P Years
1	1,34	14,6%	8
2	1,66	16,7%	7
3	2,07	20,0%	6
4	2,22	21,2%	6

Table 1.12 − Economic analysis results after 20 years of the four German PV systemsin 2012

Type	*npv* (pu)	*IRR*	Z-NPV-P Years
1	0,42	6,0%	13
2	0,98	10,6%	9
3	0,48	10,3%	11
4	0,3	8,4%	13

The Italian market ensures till 2012 major profit margins: the *npv* indexes are always higher than 100 % with peak up to 250 % with the industrial investor; the *IRR* parameters are always higher than 10 %. In Italian market the political incentive preserve large sizes of PV systems, in which the *npv* exceeds 200 % and the Zero NPV Period goes down to 6 years, whereas in Germany the feed-in tariff pushes the development of medium size PV plants. This is due to the great Italian productivity and the incentive mechanism has not yet reached the same maturity as in Germany. Comparing Table 1.11 and Table 1.12, for current year, there is a considerable convenience of PV market in Italy (with the 4th CE) for investors of the PV sector.

An economic analysis should take into account a possible funding body (i.e., a bank). The financial indicators to evaluate the investment should be compared in cases where the initial capital for the installation of the PV system belongs to the investor or it is anticipated by the lender, according to the current conditions of major Italian and German banking groups. Therefore, the financing terms vary depending on the PV plant size and private or company investors: a strong difference in the economic conditions between Germany and Italy occurs. The investment up to 100,000 € can be totally loaned with interest rate of 6 – 8 % in Italy and 2 – 3 % in Germany. On the other hand, above this threshold, the investment is partially loaned (70 – 80 %) with interest rate around 10 % in Italy and 4 % in Germany with typical duration of 10 − 15 years [42], [43], [44], [45].

If we analyzed the results, the financing of investment would involve interesting *NPV* achievements, for a zero initial capital (small plants) or minimum (20 – 30 % of total).

In particular, *IRR* without loan would be lower than the same with loan, corresponding to minimum risk. Infact, *IRR* is not appropriate to measure the actual convenience of an investment, because it does not consider the comparison among the investment cases in terms of *NPV*, but it considers only the percentage efficiency. Hence, a little investment with a very high *IRR* can have a lower *NPV* than a great investment with lower *IRR*. In other cases, when the investment does not provide negative cash flows, *IRR* cannot be calculated. Finally, if the own capital is invested, even if with a lower *IRR*, a *npv* higher than the unity without any risk is obtained. Thus, the cases with loan are not presented in this context.

1.5. Summary

From statistical information in terms of learning curves the incentive policies bring to noticeable installation volume increments and cost decrements in the two main PV markets. The analysis presented in this work highlights the 2006 − 2012 profit margins of four different investments in rooftop PV systems, in which the 2012 economic situation is, by far, more profitable in Italy with *npv* > 200 % of the installation cost after 20 years and *IRR* > 20 % in the industrial PV system with respect to the best German PV system, characterized by *npv* > 1 pu and *IRR* ≈ 10 %.

The maturity of German feed-in tariff is substantially reached in the last seven years, because the *NPV* and *IRR* parameters are subject to limited fluctuations, thanks to timely legislator regulations after the decline of the installation costs, whereas in Italy the situation in the studied period is affected by a stop-and-go mode. Here, the political intervention was so slow that the incentive rates had a little decay in 2007 − 2010, when the worldwide economies of scale in PV modules achieved an impressive decrement in the global costs and the national huge irradiation permitted booming production revenues. Consequently, the exaggerate profits, particularly in the PV systems belonging to the megawatt size, have almost saturated the global funds in the Italian electricity bill.

Concerning the near future, two joint reasons create concern in Italy: with the new feed-in tariff the 2013 economic indicators will drop close to the German levels, i.e., *npv* in the range 0.3 − 1.2 pu and *IRR* in the range 6 – 15 %; then, the rapid penetration of DG, as the PV systems, will require new grid-interface protections and new functionalities for the inverters in order to improve the network stability in case of unpredictable perturbations. Less problems are foreseen in Germany in these directions.

Finally, the long-term and sustainable development of PV systems, already in grid parity in Southern Italy, will be concentrated in the residential and commercial sizes, where the energy saving is substantial and the grid connection is already available and poorly influenced by the intrinsic variations of the PV power profiles.

Chapter 2

Photovoltaic grid-parity in the main European markets

Introduction

Roughly speaking, the grid-parity concept [46], [47] deals with the economic conditions which make the PV electricity as convenient as the electricity produced by the conventional centralised power stations (wholesale cost [48]) or delivered by the distribution system operators (retail cost [49]), thanks to the possibility to install PV plants near the consumers.

The Levelized Cost of Electricity (LCOE) is a life-cycle cost concept which seeks to account for all physical assets and resources required to deliver one unit of electricity output [50], [51]. Installation cost of PV systems, their operation and maintenance costs, prices of electricity injection into the grid are items involved in the LCOE assessment.

Obviously, the economic conditions depend on technical parameters as the reference yield, the performance ratio and the final yield of the PV systems, but now the impressive deployment of PV installations in Europe (as, for example, in the two main PV markets Germany and Italy) induces some technical barriers [52], [53], [54], [55] both at transmission level (e.g., the possibility of replacing substantial amount of generation from fossil fuels with intermittent sources as solar PV/wind power systems

in the national consumption profile) and at distribution level (e.g., the possibility of inverting the behaviour of passive lines with risk of overvoltage and in general voltage rise for the grid transformers).

Usually, the cost of electricity from utility grid is referred to the consumption in terms of €/kWh, but for deeper insight the cost consists of three contributions, the variable cost function of the consumed energy (generation, transmission, distribution, taxes, incentives for renewable energies, etc.) and two fixed costs, one depending on the delivery/exchange contract, the other depending on the available power.

Therefore, the transmission/distribution limits and the fixed costs must be taken into account in the grid-parity analysis with respect to the photovoltaic systems.

This chapter is devoted to the comprehensive study of the conditions, both technical and economic, needed for the true achievement of grid parity in regards to the photovoltaic electricity. The PV systems under study are those on the rooftop, i.e., close to the users, belonging to residential and tertiary sectors, and thus the reference cost is the retail electricity price. The chapter starts from the technical barriers (at distribution levels), then it examines the hidden costs within the electricity bill, prior to present the financial analysis of investment, based on the PV installation cost and the solar irradiation, which permit to achieve the full competitiveness with the retail electricity cost.

2.1. Technical barriers in the development of PV rooftop systems

2.1.1. Theoretical background

In the past, most of the distribution networks at high, medium and low voltage level, was designed in order to operate in radial configuration with a single source [56].

With this kind of network, the power flow is from the substation to the loads in every point of the grid. On the other hand, in presence of DG as the one from PV systems, i.e., when the network has multiple sources, it is possible to have power flow in reverse direction, from DG units to the substations. In this case, it is possible to define power penetration as the percentage of DG power referred to the rated power of the distribution transformer. The reverse power flow is the main problem that makes the integration of DG units not easy: the distribution limit (bottleneck) is prevailing on the transmission limit that is not considered in this work. Obviously, a grid-connected PV system increases the voltage in its point of common coupling (PCC).

The grid behaviour is assumed as that of a Thévenin generator, in which the voltage source $\underline{E}_{Th}$ and the equivalent impedance $\underline{Z}_{Th}$ take into account different contributions:

- the e.m.f. of secondary windings of the distribution transformer $\underline{E}_{T}$;
- the primary grid impedance $\underline{Z}_{MVg}$ (in other terms the short circuit power of the grid in that point) and the short circuit impedance of the distribution transformer $\underline{Z}_{scT}$;
- the impedances of the distribution lines $\underline{Z}_{LVl}$ (by neglecting the capacitive parameters if they are below a given limit) $\underline{Z}_{LVl2}$;
- the corresponding impedances $\underline{Z}_{L}$ of the loads supplied by these lines (however, many times, it is not possible to define a constant impedance when the loads are non-linear as occurs for power electronics, discharge lamps, electro-magnetic machines in no-load condition,…).

Fig. 2.1 shows an example with two lines and two loads. The value of the equivalent impedance named as $\underline{Z}_{grid}$, seen by the DG unit, depends on the PCC: if it is at the beginning of the lines, near the transformer, as in case (a), the voltage drop and power losses of the lines are not influenced; the situation changes if it is at the end, near the loads, as in case (b) with the line which supplies the load $\underline{Z}_{L2}$. Usually, as a first approximation, the impedance of the loads are considered infinite in the calculation of $\underline{Z}_{grid}$ and so in the case (a) it results:

$$\underline{Z}_{grid} = \underline{Z}_{MVg} + \underline{Z}_{scT} \tag{2.1}$$

while in the case (b) it results:

$$\underline{Z}_{grid} = \underline{Z}_{MVg} + \underline{Z}_{scT} + \underline{Z}_{LVl2} \tag{2.2}$$

In the latter case, the value of $\underline{Z}_{grid}$ could be so high that the PV power capacity should be reduced, in order to satisfy the constraints for transformer and lines of the network in terms of power losses, voltage variation, unbalance, harmonics and so on.

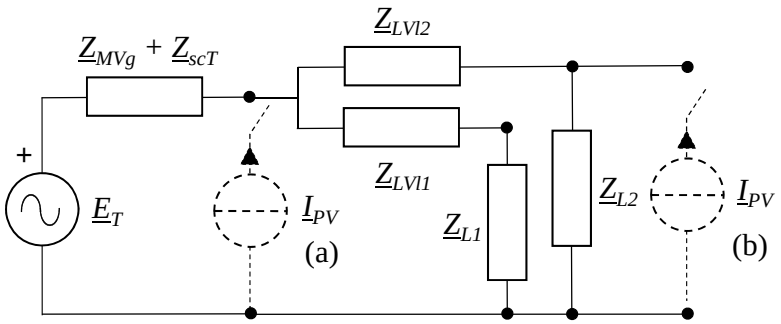

Fig. 2.1 − PCC at the beginning or at the end of the LV lines.

2.1.2. Application to residential and tertiary-sector users

From this simple case it is clear that every distribution grid must be examined in order to assess the maximum penetration of PV generation. In this work two real case studies are presented, in which the typical users are different, in one case they are residential users and in the other one they belong mainly to the tertiary sector. These case studies deal with a big city, in which the commercial users are concentrated in downtown and the residential users are concentrated in outskirts: thus, the grid is particularly strong compared with rural areas. In a national energy balance, e.g. from Eurostat database [57], the residential loads account for 20-30 % of the total consumption, as well as the tertiary-sector loads; hence, these two types of loads cover above 50 % of grid electricity. The corresponding load profiles depend on the actions of

the people, in other words with residential loads people stay at home in the first part of the morning and in the final part of the evening, while around the noon the consumption is relatively low. Contrary, with the tertiary sector the consumption is concentrated in the central part of the day (the usual 8-hour work period plus lunch), that permits a better matching with the PV power profile.

In details, the starting data for the PV penetration study include (Table 2.1(a) and 2.1(b)):

- the power rating of the distribution transformer, equipped with no-load tap changer, and the short circuit parameters (voltage in percent corresponding to the rated current, power losses in percent);
- the section and length of the cables with the corresponding current rating (ampacity);
- the weekly monitoring of the three-phase currents and active power, since the power factor is always higher than 0.9.

From these well-known parameters one can calculate the grid impedance, with the abovementioned approximation, for the two application cases.

Concerning the residential users, the grid impedance of each line is within $35 - 41$ mΩ, the resistive component is within $18 - 22$ mΩ, whereas the inductive component is $30 - 34$ mΩ. In this situation it is not advisable to use the ampacity of every distribution line, owing to both the consequent transformer overload and the excessive voltage drops (> 4 % of the rated value). Actually, the weekly monitoring puts into evidence that the loading in the three distribution lines is generally weak (up to $35 - 50$ % of the ampacity), as well as the voltage drops (≈ 1.9 %).

Table 2.1 − The main specifications of MV-LV distribution systems of:

(a) residential users

Transformer 22 kV / 0.4 kV		
Power rating	***V_{SC} %***	***P_{SC} %***
400 kVA	**6**	**1.2**

LV Lines		
Section	***Length***	***Ampacity***
150 mm^2	**116 m**	**357 A**
150 mm^2	**105 m**	**357 A**
120 mm^2	**70 m**	**310 A**

(b) tertiary sector users

Transformer 22 kV / 0.4 kV		
Power rating	***V_{SC} %***	***P_{SC} %***
400 kVA	**6**	**1.2**

LV Lines		
Section	***Length***	***Ampacity***
150 mm^2	**97 m**	**357 A**
150 mm^2	**85 m**	**357 A**
120 mm^2	**64 m**	**310 A**

Concerning the tertiary sector users, the transformer has the same size, the distribution lines have the same section but different lengths and thus the grid impedances are in the range 34 − 38 mΩ, the resistive component is within 17 − 20 mΩ, whereas the inductive component is 30 − 33 mΩ. Similar remarks can be done as in the previous case, even if the loading and voltage drops are generally higher (up to 60 % of the ampacity and 2.1 %, respectively).

For PV penetration study, by assuming a pessimistic guess (rule of thumb), one can consider the month with maximum irradiation in clear-sky day, in which also the commercial/residential loads are particularly huge, due to the air cooling demand: the summer solstice, obviously, occurs in June at North latitudes with peak irradiance G_p = 960 W/m^2 in Turin, Italy. Then, it is possible to simulate the connection of rooftop PV systems by a simplified model [58] which involves the direct proportionality with the solar irradiance without the various sources of losses (unitary performance ratio). Certainly, the rated power (named “watt-peak” at Standard Test Conditions) of a PV device, measured when it is subject to irradiance G_{STC} = 1000 W/m^2 and temperature T_{STC} = 25 °C, is needed for the simulation. For what concerns the power factor of a PV inverter, the reactive power at the output is negligible.

On the basis of this information about MV−LV distribution, Figures 2.2, 2.3, 2.4 show the experimental comparison among residential/tertiary users in work days and holidays. In particular, within the week of monitoring, for the residential-users in Fig.

2.2 it has been selected the day with both the maximum peak P_{Lmax} = 261 kW occurring in the evening, and the minimum peak P_{Lmin} considering only the sunlight hours (from 9 a.m. to 5 p.m.), due to the practical similarity of the profiles day by day. Then, in the tertiary-sector loads the day with maximum power load (Fig. 2.3 with P_{Lmax} = 304 kW) and the day with minimum power during the weekend (Fig. 2.4) are examined for including the best and the worst cases.

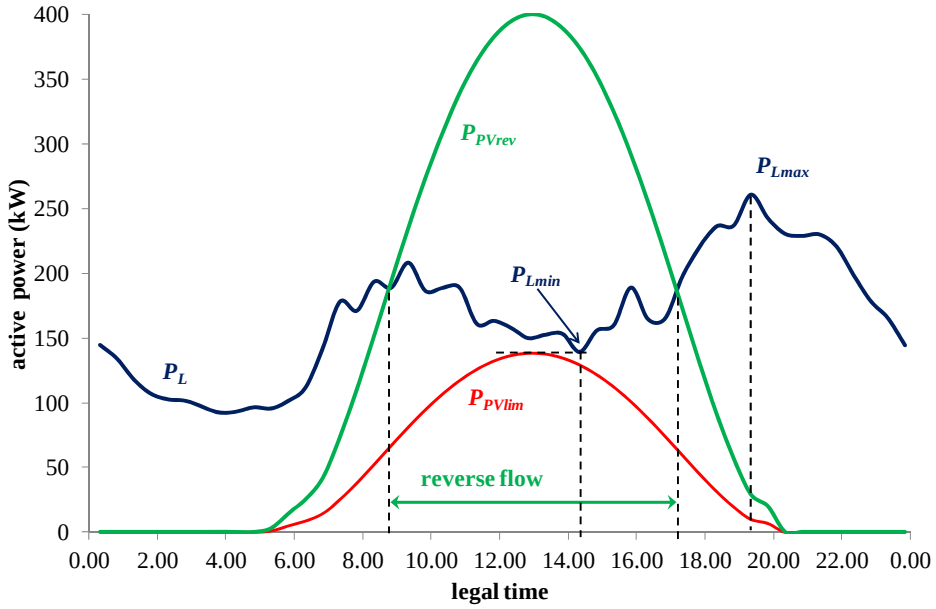

Fig. 2.2 − The daily profile of residential loads and two possible PV profiles.

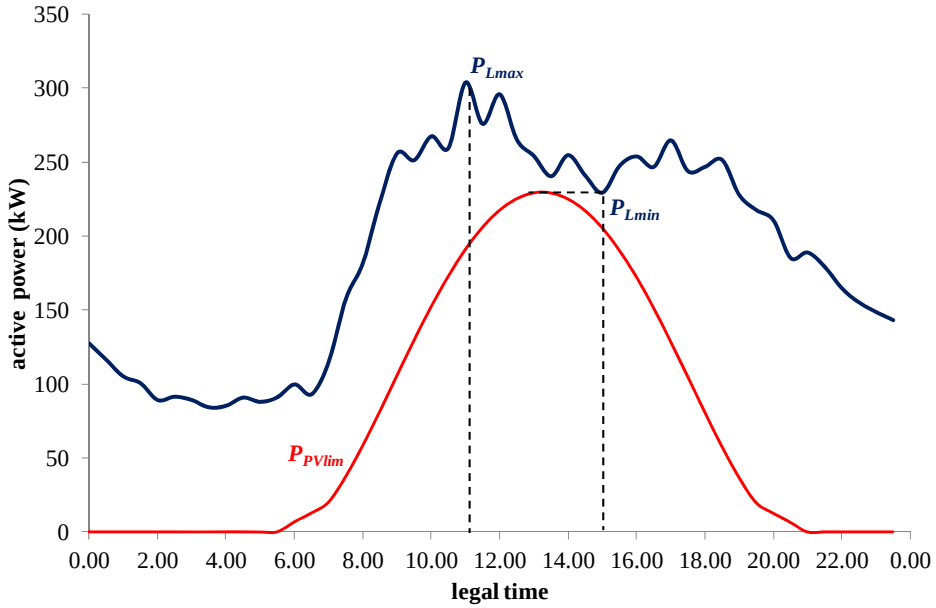

Fig. 2.3 − The work-day profile of tertiary loads and the limit PV profile.

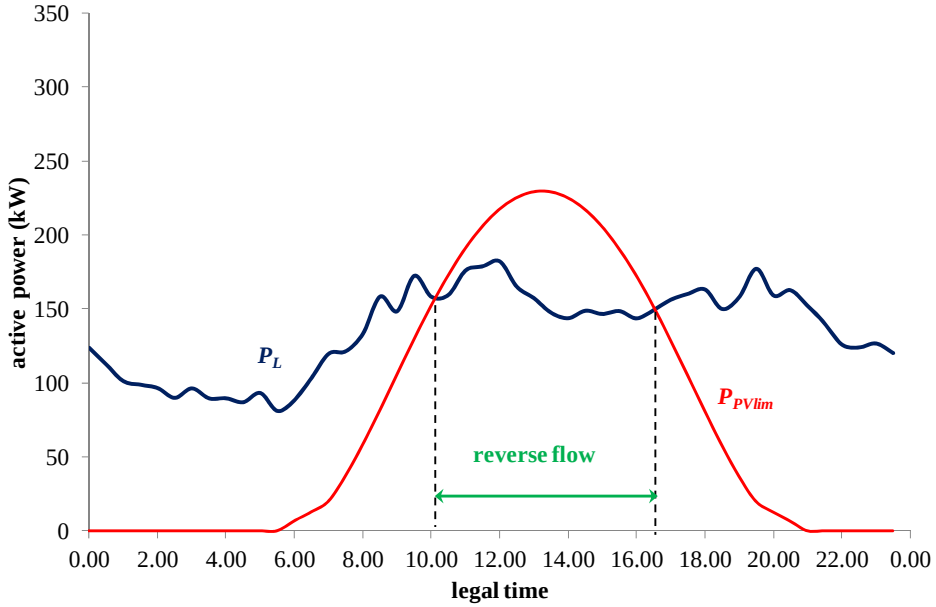

Fig. 2.4 − The Saturday profile of tertiary loads and the limit PV profile with reverse flow.

After that, it is possible to simulate the connection of rooftop PV systems (25° tilt angle towards South) at the end of the distribution lines.

Both for residential and tertiary sector loads, the condition for maximum penetration can be stated in such a way as to limit the PV power profile P_{PVlim} below the load profile P_L in every sunlight situation (P_{Lmin} = 139 kW for residential loads and P_{Lmin} = 229 kW for tertiary-sector users). As per the red PV profile, corresponding to a peak power of 145 kW_p, in Fig. 2.2 no reversal of the power flow, in order to avoid possible unpredicted reduction of the load. Likewise, Fig. 2.3 shows the generated power of 240-kW_p photovoltaic systems without reverse injection into the grid.

Therefore, the estimations of PV penetration, for all the two types of users, are rounded with pessimistic assumption, due to the possibility to increment the peak power taking into account the actual losses (I-V mismatch due to manufacturing tolerance, dirt, over-temperatures with respect to 25 °C, inverter efficiency, etc.) and non-optimal sun exposition.

Otherwise, if at the higher voltage level (MV or HV) of the distribution transformer the control is able to manage (e.g., by on-load tap-changer or, more recently, “electronic transformer”) the reverse power flows, it is feasible to load the distribution lines with negative active power (i.e., from the end to the start of the lines by means of PV generation) and with absorbed reactive power that counteracts the tendency to voltage rise (in the same way as the inductive behaviour of the loads).

In this case, in Fig. 2.2 a power rating of 420 kW_p, higher than the size of the transformer, generates the green curve P_{PVrev}, in which the reverse flow is limited to the interval between 9 a.m. and 5 p.m.

With reference to the tertiary loads in June, since the work days give much higher consumption (Monday-Friday in Fig. 2.3 with peak load P_{Lmax} = 304 kW), in the weekend a reverse flow, due to 240-kW_p photovoltaic systems, occurs in the interval 10 a.m. – 4:30 p.m., without causing voltage-rise problems (Fig. 2.4).

The most important results in these different situations (no reverse flow for residential users and reverse flow limited to the weekend period for tertiary-sector users) are expressed in terms of the following factors:

- the peak power of the PV systems as a percentage of the power rating of the distribution-transformer $\mu_{PV\text{-}trnsf}$ or of the peak load $\mu_{PV\text{-}load}$: $\mu_{PV\text{-}trnsf}$ = 36 % and $\mu_{PV\text{-}load}$ = 56 % for residential users, $\mu_{PV\text{-}trnsf}$ = 60 % and $\mu_{PV\text{-}load}$ = 79 % for tertiary users, respectively;
- the ratio $\kappa_E = E_{PV}/E_{load}$ defined as the PV energy production to the energy consumption: κ_E = 28 % without reverse flow for residential users, κ_E = 41 % in the work days and κ_E = 57 % in the weekend for tertiary users, respectively.

To know more in depth the PV penetration parameters, other consumption profiles of residential and tertiary sector users, with similar supply conditions defined in Table 2.1(a) and 2.1(b), have been measured. Applying the previous procedure to calculate the PV peak powers through the maximum and minimum load powers, one is able to provide the readers a range of the factors $\mu_{PV\text{-}trnsf}$, $\mu_{PV\text{-}load}$ and κ_E. In particular, two additional profiles of residential users (Fig. 2.5) and four additional profiles of tertiary-sector users (Fig. 2.6) are presented. About the residential users, the ranges are $\mu_{PV\text{-}trnsf}$ = 30 – 36 %, $\mu_{PV\text{-}load}$ = 56 – 73 %, and κ_E = 28 – 31 %, whereas, for the tertiary sector users in the work days, the ranges are $\mu_{PV\text{-}trnsf}$ = 19 – 60 %, $\mu_{PV\text{-}load}$ = 69 – 79 %, and κ_E = 41 – 48 %.

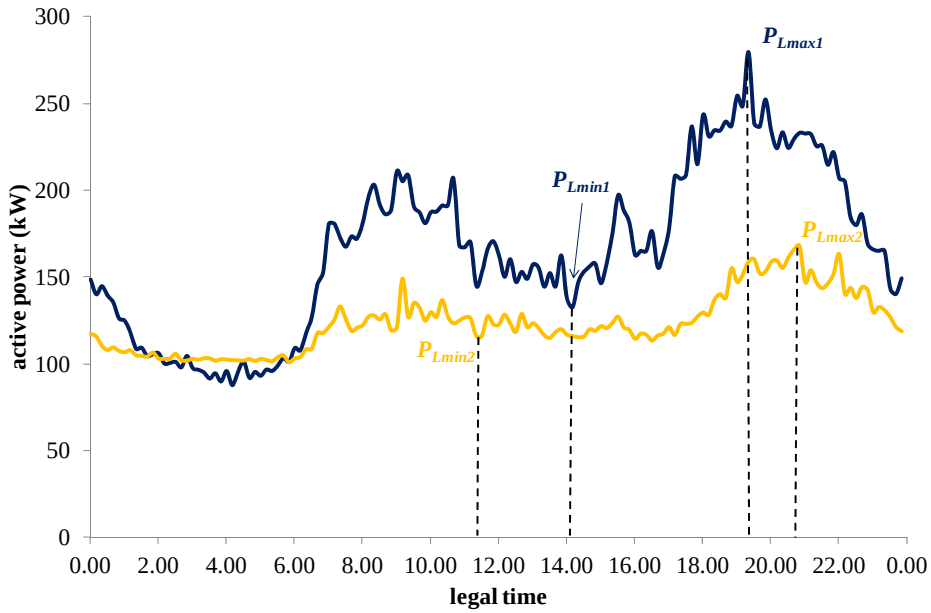

Fig. 2.5 −Two additional residential profiles with in evidence maximum and minimum peak powers.

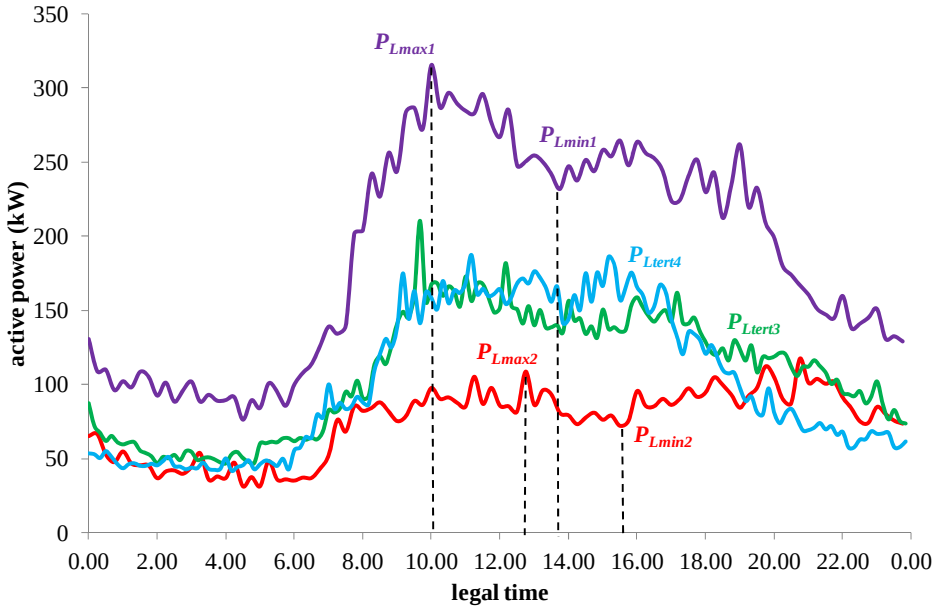

Fig. 2.6 − Four additional tertiary-sector profiles.

Finally, these PV penetration results are achievable without any upgrading of the distribution systems. Hence, the further analysis in the following sections is valid under the assumption that the future PV installations in grid parity do not approach the abovementioned limits, otherwise it is clear that the electricity tariff will increase, due to the investments in the upgrading of the distribution system.

In fact, the PV penetration levels can be boosted, whenever the distribution system operator installs new distribution lines and/or transformers. In addition, storage systems of both the PV systems and the distribution system operator can provide further increment in PV penetration levels.

2.1.3. The structure of the electricity bill

Within the framework [59], [60], [61], [62], [63] of either the net-metering (Germany) or the on-site exchange (Italy with different prices between the electricity sold to the grid and the electricity purchased by the utilities), three case studies about dwelling houses, common usages of apartment blocks and tertiary-sector consumers are studied in special detail.

As previously said, the tariff can have three contributions on yearly basis: the contract cost in €/customer, the power cost in €/kW and the consumption cost in €/kWh are distinguished in Italy. Otherwise, the fixed cost is independent from the available power, as occurs in Germany.

These fixed costs, for a given voltage level (low LV – medium MV - high HV) and type of connection (single-phase and three-phase), are mainly expressed according to:

1. the delivery contract before the PV system connection or the exchange contract after it between the utility and the customer, that include administrative costs and the metering service (€/customer);

2. the available power that includes the investments in the construction of centralized power stations, power transformers, transmission/distribution lines, made by the electricity companies (€/kW).
The tariff for the single residential households, the common loads of apartment-blocks (e.g., lift, night-lamps, auxiliary pumps, electric gates, surveillance devices, etc.) and the MV industrial/tertiary-sector customers (with contract power up to 200 kW) are different.

For the residential customers about the dwelling house, the total consumption in kWh is subdivided into 4 ranges: 0−1800; 1801−2640; 2641−4400; >4400. The consumption cost increases from the first to the fourth range and the amounts, corresponding to the third and the fourth, are much greater than the first two ranges. In this case the fixed costs are kept low, because electricity is assumed as a primary welfare.

For the common loads of the apartment-blocks (usually three-phase), the fixed costs (i.e., contract and power items) are much greater than the corresponding costs for residential, whereas the consumption cost is similar to the second range of residential cost without subdivision into ranges.

For the industrial/tertiary-sector customers, which need to install their own MV/LV transformation system, the fixed costs are only slightly lower than the previous LV level, even if the supply is performed at MV level. The working hours, mainly during the sunlight ones, determine the peak-load hours in which the consumption cost is maximum, then the night-hours and holidays define the off-peak periods with minimum consumption cost. Finally, in the mid-level hours the consumption cost is intermediate among the two mentioned costs.

The case studies in the successive section are based on actual electricity bills from Italy and Germany, the two main PV markets in the period 2010 − 2012.

The first case study (*dwelling house*) is characterized by these data:

- yearly consumption of 4500 kWh with 3-kW available power from the utility (Italy);
- fixed costs C_F = 92 € (Italy) and C_F = 85 € (Germany);
- energy cost, i.e. money saving s_{PV} = 0.182 €/kWh (Italy), and amounts sold to the grid p_{PV}^* = 0.128 €/kWh (on-site exchange in Italy) or p_{PV} = 0.26 €/kWh (mean tariff, applied in Germany for typical consumption of 4 persons and used for net metering).

The second case study (*common loads of apartment-block*) is characterized by these data:

- yearly consumption of 6000 kWh with 10-kW available power from the utility (Italy);
- fixed costs C_F = 609 € (Italy, with huge impact in the consequent results) and C_F = 85 € (Germany);
- energy cost, i.e. money saving, s_{PV} = 0.195 €/kWh (Italy), and amounts sold to the grid p_{PV}^* = 0.128 €/kWh (on-site exchange in Italy) or p_{PV} = 0.26 €/kWh (used for net metering in Germany).

The third case study (*tertiary-sector loads*) is characterized by these data:

- yearly consumption of 330,000 kWh with 200-kW available power from the utility (Italy);
- fixed costs C_F= 4538 € (Italy) and C_F = 164 € (Germany);
- energy cost, i.e. money saving, s_{PV} = 0.208 €/kWh (Italy), and amounts sold to the grid p_{PV}^* = 0.11 €/kWh (on-site exchange in Italy) or p_{PV} = 0.196 €/kWh (used for net metering in Germany).

2.2. PV grid parity in three case studies

2.2.1. Methodology

Generally speaking, the production of goods or services follows the experience curve (or learning curve). Each time cumulative volume doubles, value added costs (including manufacturing, marketing, distribution, etc.) fall by a constant percentage. It is worth noting that every doubling in the market volume corresponds to about -19 % reduction in the installation cost and about -25 % reduction in the PV module cost [64], [65]. In the further case studies, the specific installation costs c_I are considered within the range 1400-2500 €/kW_p [66].

As already seen in chapter 1, for the determination of the cost effectiveness of an investment, as for example the electricity production, with respect to other investments, a conventional method implies the assessment of the *NPV* during the PV plant life (25 years with guaranteed performance).

In this case, the parameters which influence the yearly *NPV* calculation are:

- the installation cost C_I in €/y, assuming that the capital is totally paid by the investor (100 % equity);
- the rated power P_{PVr} in kW_p of the PV system (declared by the manufacturer);
- the yearly Revenues, R_{PV} in €/y, calculated as either the product of PV energy production E_{AC} with the electricity price p_{PV} (net-metering in Germany) or the sum of two contributions (on-site exchange in Italy), in which the first one is the product of the energy delivered to the grid (different according to residential/tertiary-sector loads) with the corresponding price p^*_{PV}; the second one is the product of the self-consumed energy (different according to residential/tertiary-sector loads) with the money saving s_{PV} (cost avoided from the utility bill);
- the yearly Operation and Maintenance cost C_{OM} in €/y;

- the fixed costs C_F *in*€/y;
- the real interest rate i^*.

Actually, the real interest rate i^* takes into account the effect of the inflation rate f (according to the inflation rate of electricity production, 1 – 2 % in Germany and 2 – 6 % in Italy, mainly based on fossil fuels) that reduces the basic interest rate i. Due to the different economic situations between the two Countries as shown in [67], the interest rates are i =3 – 6 % in Germany and i =4 – 10 % in Italy. Thus, the corresponding real interest rates are calculated by the known formula, eq. (1.2).

The interest rate is equal to the rate of return on the capital with low risk [68] (long-term government bonds, e.g. German "bund" or Italian "BTP").
Therefore, it is possible to define the *NPV* after N years of cash flows, in our case after 25 years of operation, as:

$$NPV = -C_I + \sum_{k=1}^{N} \left(R_{PV,k} - C_{OM,k} - C_F\right) \Big/ \left(1+i^*\right)^k \tag{2.3}$$

Assuming the revenues, the O&M and fixed costs constant, the previous formula can be rewritten as:

$$NPV = -C_I + (R_{PV} - C_{OM} - C_F) \sum_{k=1}^{N} 1 \Big/ \left(1+i^*\right)^k \tag{2.4}$$

If the well-known summation (the reciprocal of the capital recovery factor) is replaced, *NPV* equation becomes:

$$NPV = -C_I + \left(R_{PV} - C_{OM} - C_F\right) \cdot \left(1 - \left(1+i^*\right)^{-N}\right) \Big/ i^* \tag{2.5}$$

In the economic analysis of a grid-connected PV system, it is required to calculate the yearly electricity production at the AC terminals (E_{AC}). Therefore, according to [69], as previously seen in chapter 1, the used expression for E_{AC} is the eq. (1.8).

By the final yield Y_f, it is possible to calculate the required peak power, in such a way as to compensate for the yearly consumption in the different case studies.

Actually, it is possible to calculate the revenues from electricity according to the productivity of the PV system and the net-metering or the on-site exchange mechanisms:

$$R_{PV} = P_{PVr} \cdot Y_f \cdot p_{PV} \quad \text{or} \quad R_{PV} = P_{PVr} \cdot Y_f \cdot p^*_{PV} \cdot \alpha_S + P_{PVr} \cdot Y_f \cdot s_{PV} \cdot (1 - \alpha_S) \tag{2.6}$$

where, as a first approximation, the share of sold energy $\alpha_S = 0.7$ with residential loads and $\alpha_S = 0.3$ with tertiary sector loads.

For comparison between PV systems of different size, the *NPV* equation can be divided by the rated power P_{PVr} in the net-metering case for the sake of simplicity [70]

$$NPV/P_{PVr} = -c_I + \left(p_{PV} \cdot Y_f - c_{OM} - C_F/P_{PVr}\right) \cdot \left(1 - \left(1 + i^*\right)^{-N}\right) / i^* \tag{2.7}$$

where:

$c_I = C_I / P_{PVr}$ is the specific installation cost in €/kW$_p$;

$c_{OM} = c_I \cdot C_{OM} / C_I$ is the O&M cost expressed as a percentage (1 %) of the specific installation cost, essentially for the cleaning of PV modules, replace of inverters and energy monitoring cost [71],[72].

2.2.2 Simulation results

Global irradiation data are available on the PVGIS website [73]. Average values of 10 years are considered accurate and representative. Table 2.2 and Table 2.3 report the energy assessment parameters of the twenty German/Italian major cities with the peak powers for all the three case studies A, B and C (tilt angles of 35°/25°).

The trend of *NPV*, as a function of the installation cost, is linear with negative slope; each line is shifted towards the bottom by increasing the real interest rate. The intercept of *NPV* with the horizontal axis represents the starting condition of cost effectiveness for a PV system in grid parity. The overall results from Matlab® software are presented only for two cities, the best and the worst ones, Düsseldorf and Munich in Germany, Trento and Palermo in Italy, chosen with the purpose of covering different weather conditions.

Table 2.2 − Parameters for energy assessment (PVGIS site) for the major German cities.

German major cities	Y_r **(h/y)**	***PR*** **(%)**	Y_f **(h/y)**	P_{PVr} ***(A)*** ***(kW)***	P_{PVr} ***(B)*** ***(kW)***	P_{PVr} ***(C)*** ***(kW)***
Berlin	1150	78.1	891	5.1	6.7	370
Bremen	1100	78.2	857	5.3	7	385
Dorthmund	1090	78.1	847	5.3	7.1	390
Dresden	1130	78.6	882	5.1	6.8	374
Düsseldorf	1090	78	846	5.3	7.1	390
Erfurt	1130	78.5	887	5.1	6.8	372
Essen	1090	78	848	5.3	7.1	389
Frankfurt	1150	78.2	894	5	6.7	369
Hamburg	1100	78.4	861	5.2	7	383
Hannover	1090	78.5	852	5.3	7	387
Kiel	1130	78.1	879	5.1	6.8	375
Köln	1090	78.1	849	5.3	7.1	389
Leipzig	1120	78.5	877	5.1	6.8	376
Magdeburg	1100	78.4	858	5.2	7	385
Mainz	1160	78.1	899	5	6.7	367
München	1310	78.7	1030	4.4	5.8	320
Saarbrücken	1200	78	929	4.8	6.5	355
Schwerin	1130	78.5	886	5.1	6.8	372
Stuttgart	1220	78.2	948	4.7	6.3	348
Wiesbaden	1150	78.2	895	5	6.7	369

Table 2.3 − Energy assessment (PVGIS site) for the major Italian cities.

Italian major cities	Y_r **(h/y)**	***PR*** **(%)**	Y_f **(h/y)**	P_{PVr} ***(A)*** ***(kW)***	P_{PVr} ***(B)*** ***(kW)***	P_{PVr} ***(C)*** ***(kW)***
Ancona	1640	76.4	1250	3.6	4.8	264
Aosta	1580	76.9	1210	3.7	5	273
Bari	1800	75.5	1350	3.3	4.4	244
Bologna	1420	76.6	1090	4.1	5.5	303
Cagliari	1830	75.8	1380	3.3	4.3	239
Campobasso	1690	76.9	1300	3.5	4.6	254
Catanzaro	1730	76.1	1310	3.4	4.6	252
Firenze	1530	76.4	1130	4	5.3	292
Genova	1540	76.5	1170	3.8	5.1	282
L'Aquila	1620	77.4	1250	3.6	4.8	264
Milano	1450	77.5	1120	4	5.4	295
Napoli	1680	75.6	1260	3.6	4.8	262
Palermo	1860	75.9	1410	3.2	4.3	234
Perugia	1590	76.3	1210	3.7	5	273
Potenza	1780	76.4	1350	3.3	4.4	244
Roma	1660	76.4	1260	3.6	4.8	262
Torino	1540	77.7	1190	3.8	5	277
Trento	1370	77.2	1050	4.3	5.7	314
Trieste	1440	77	1100	4.1	5.5	300
Venezia	1440	76.6	1100	4.1	5.5	300

Basically, we can claim that the geographic location has a strong impact in grid-parity fulfilment and thus the ranking of all the cities is ordered according to Southern zone (first positions), Central zone (intermediate positions) and Northern zone (last positions).

However, there are significant exceptions as, for example, Berlin and Aosta, in which Northern sites exhibit energy production similar to Central zone of Germany and Italy, respectively. Other particularities involve: Munich and Stuttgart, in which the Eastern city gives greater yields than the Western city, even if the latitudes are very close; Aosta and Trento, in which the first one (Western city) behaves much better than the other at nearly the same latitude.

Moreover, two cities, Palermo and Cagliari, located in islands (Sicily and Sardinia, respectively) reach the first places in PV productivities. Then, the relative deviations of the German cities in the performance (≈ ±10 % of the average value) are reduced with respect to the deviations of the Italian cities (≈ ±15 %).

Fig. 2.7 shows the outputs for a "dwelling-house" (case A), in which with a real interest rates of 2 % the limit for installation cost in grid parity is achieved in Germany, because the 2012 cost is within 2000 – 2400 €/kW_p [66].

On the other hand, in Fig. 2.8 the corresponding limit for grid parity in Italy is almost reached, since the 2012 cost is 2500 – 2800 €/kW_p [66], indicating that the grid parity is near to be achieved also in Northern Italy. Reference [74] provides similar results for this case study.

Fig. 2.9 shows the same results for the common loads of "apartment-block" (case B), in which only the German cities provide the grid-parity conditions with real interest rate of 3 % and 2012 installation cost in the range 1800 – 2200 €/kW_p [66].

Finally, Fig. 2.10 and Fig. 2.11 are related to the "tertiary sector" (case C), in which the grid parity conditions with a real interest rate of 4 % are fulfilled, due to the 2012 installation cost is comprised in the range 1400 – 1500 €/kW_p in Germany and in the range 1500 – 1700 €/kW_p in Italy [66].

The fulfilment of the grid parity is highlighted in Table 2.2 and Table 2.3, where the PV rated power for each case and each city is written in green colour, otherwise the same power is written in red colour. In conclusion, the PV systems which cannot achieve the grid parity are uniquely in Italy and are dwelling houses in Northern zone and all the common loads of apartment blocks.

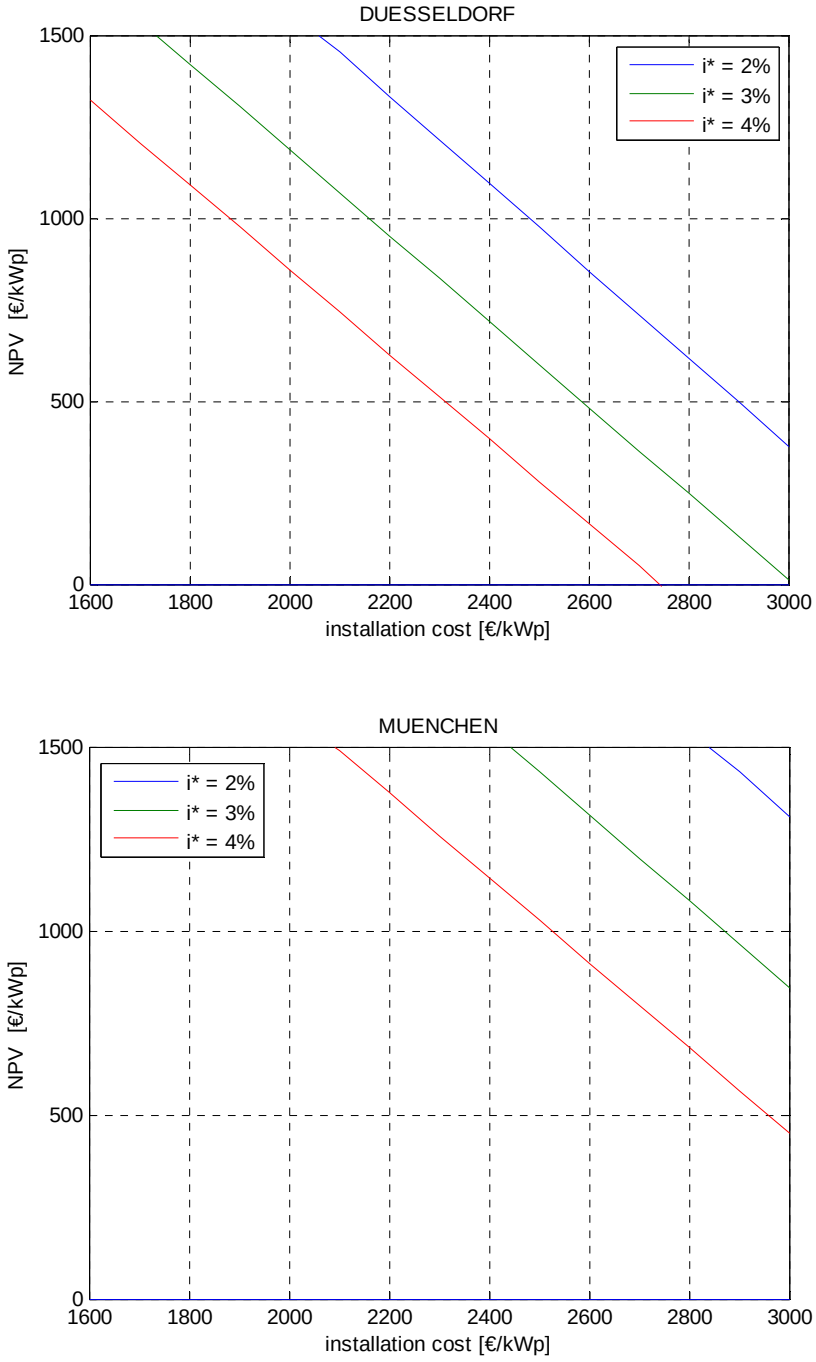

Fig. 2.7 − PV grid parity conditions for dwelling house in Düsseldorf and München (Germany).

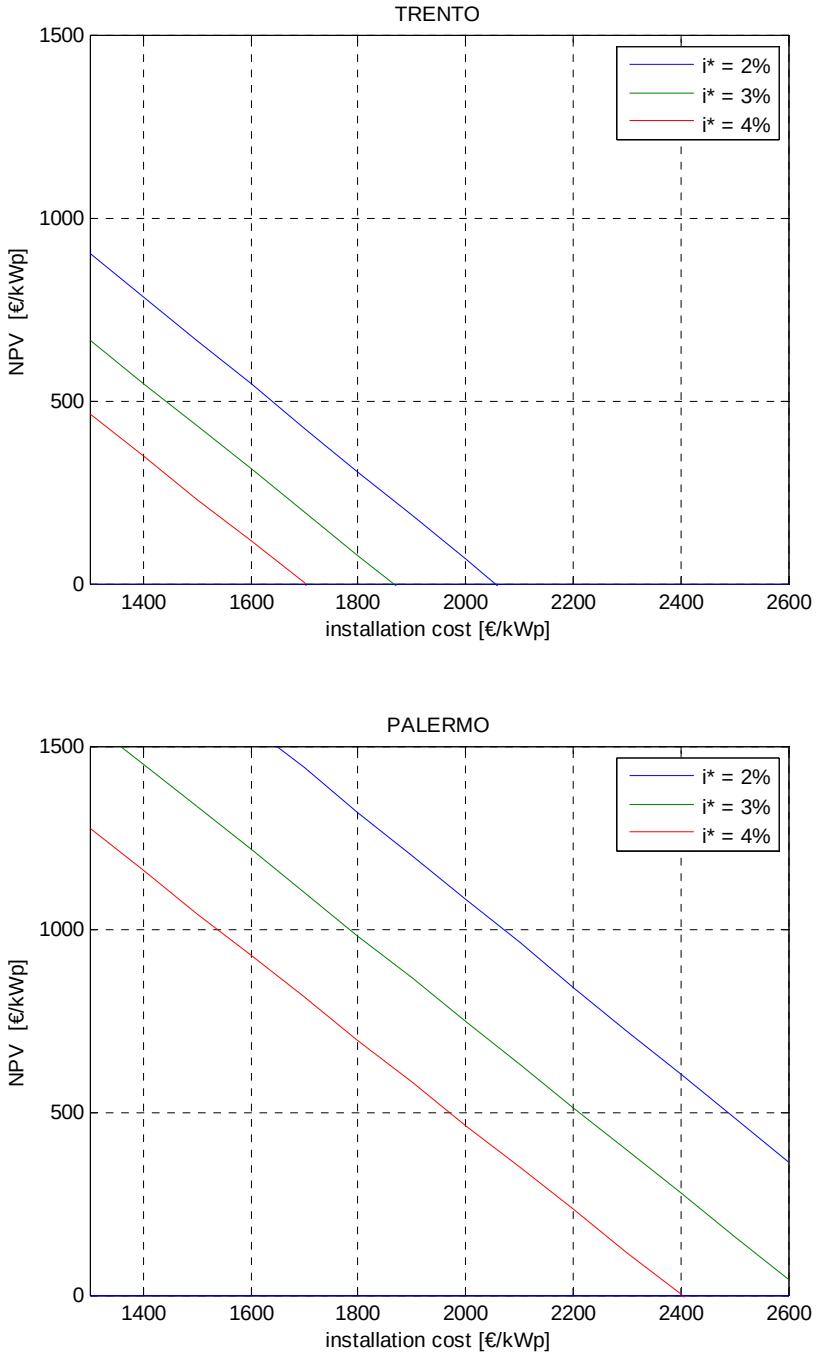

Fig. 2.8 − PV grid parity conditions for dwelling house in Trento and Palermo (Italy).

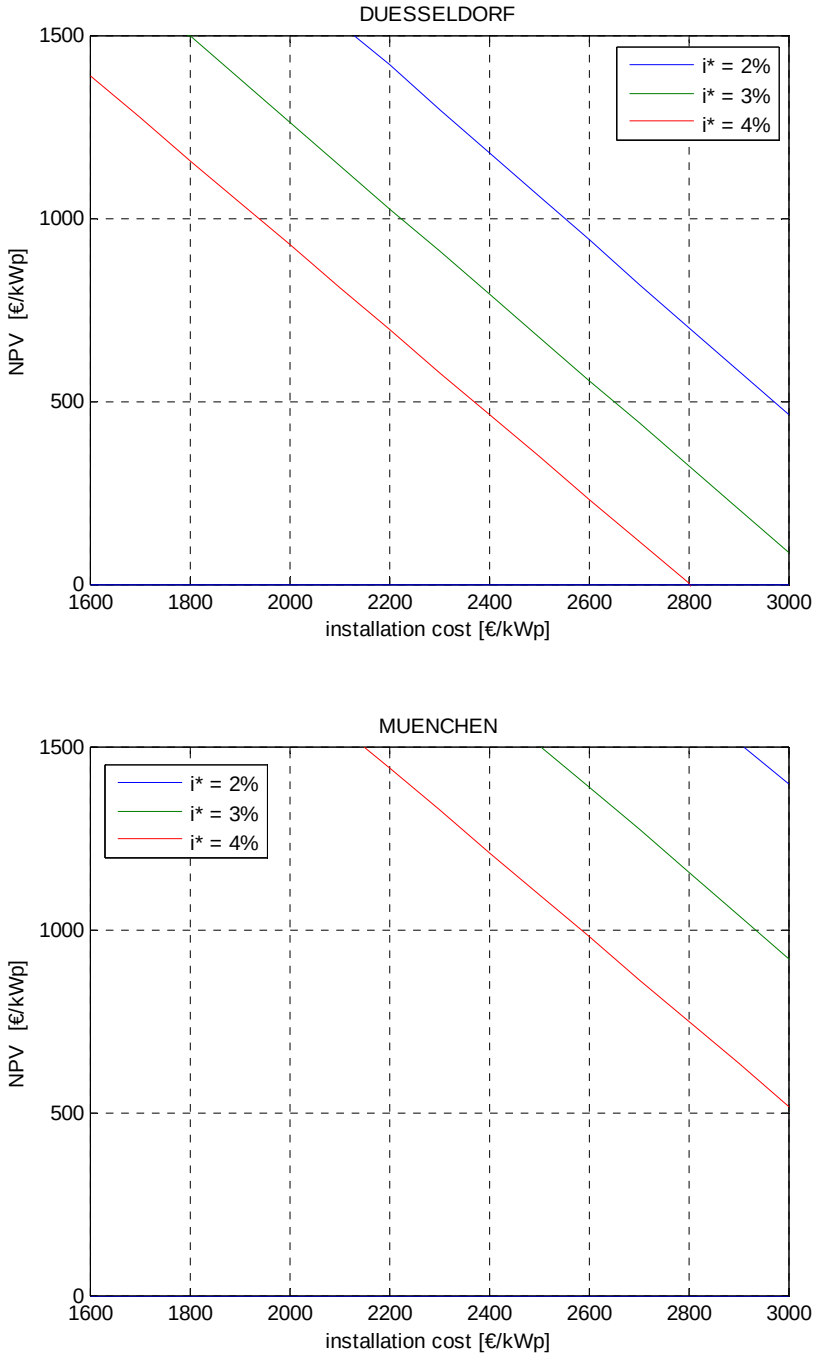

Fig. 2.9 − PV grid parity conditions for common loads of apartment-block in Düsseldorf and München (Germany).

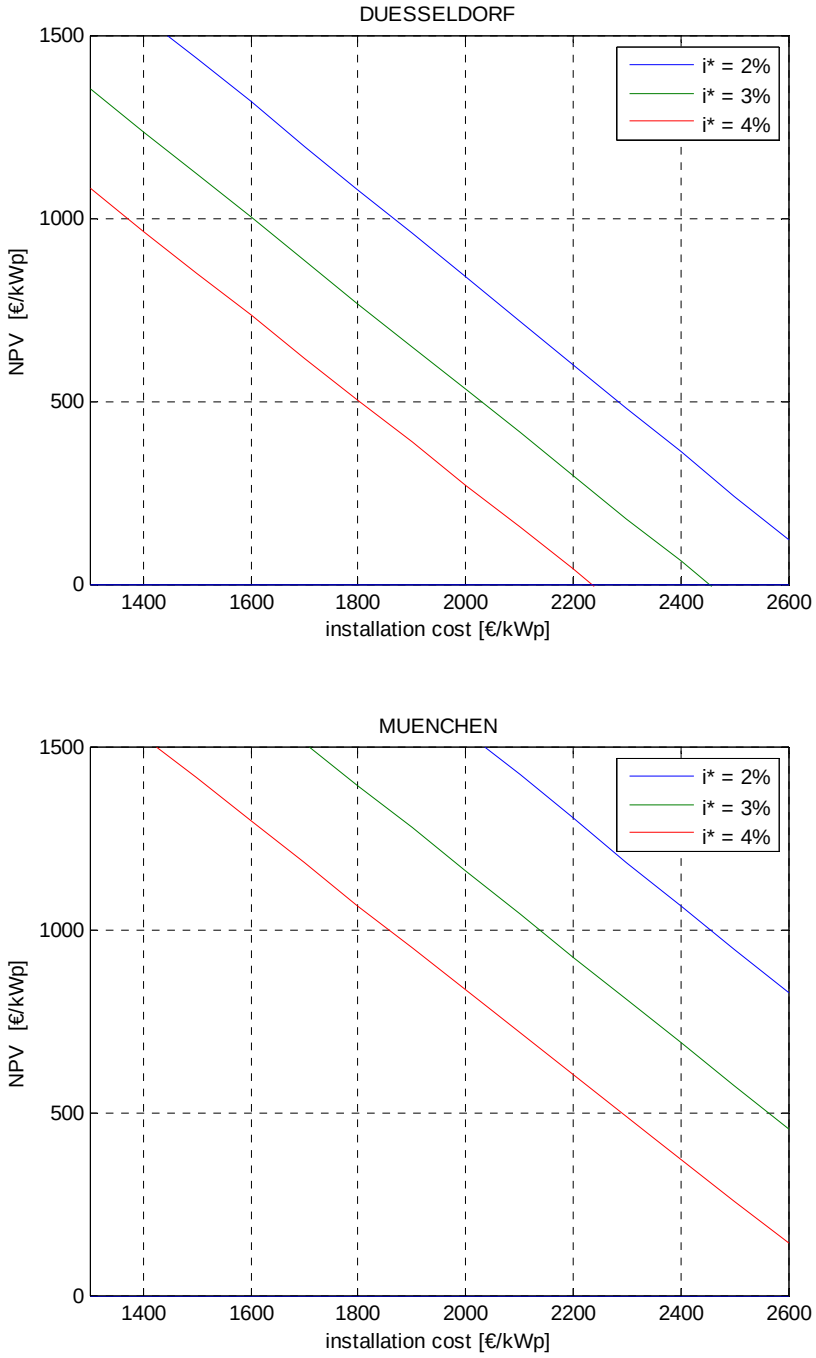

Fig. 2.10 − PV grid parity conditions for tertiary-sector loads in Düsseldorf and Munich (Germany).

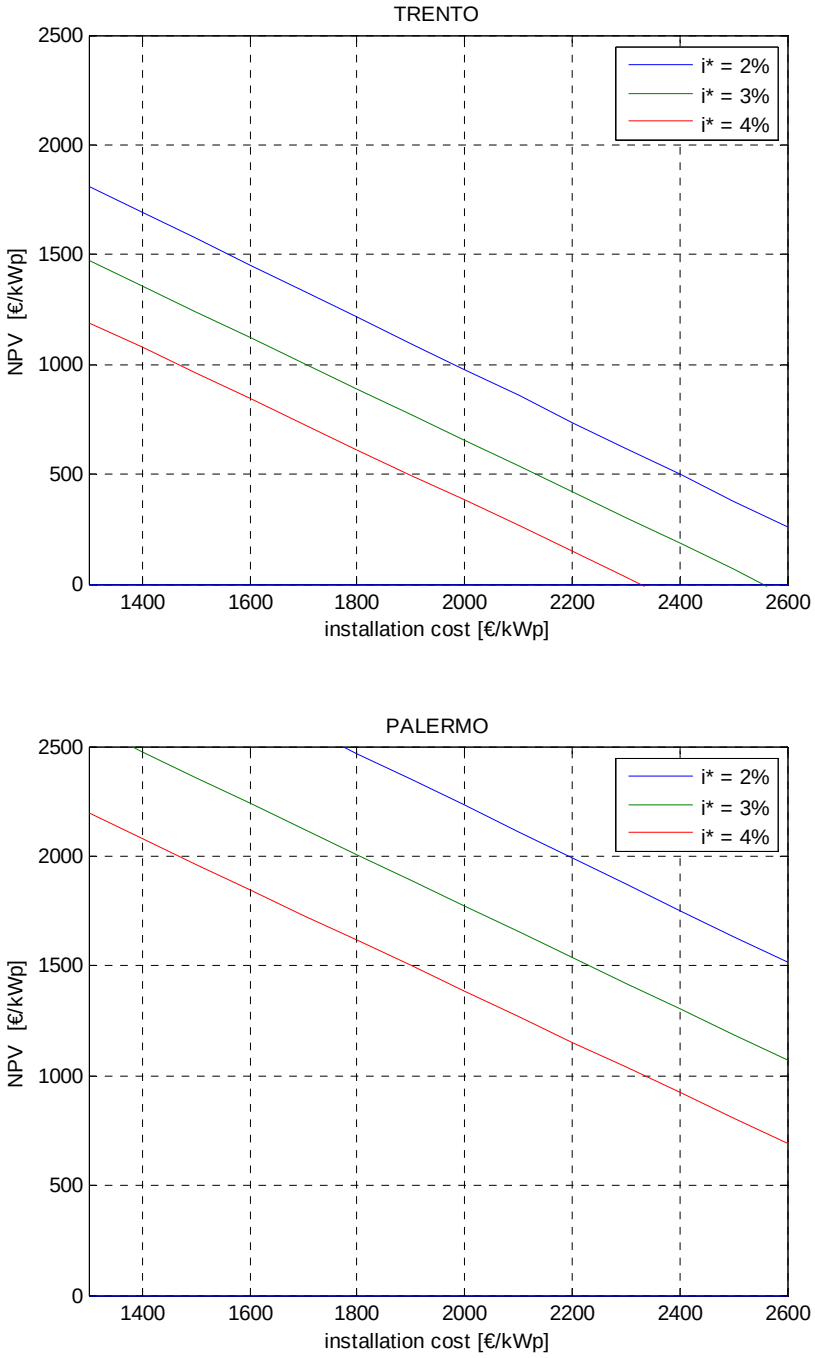

Fig. 2.11 − PV grid parity conditions for tertiary-sector loads in Trento and Palermo (Italy).

2.3. Summary

In this chapter a new concept of photovoltaic grid parity is presented, with reference to three typical case studies, by including the distribution-network limits and the fixed costs of the electricity bills.

In regards to the residential/tertiary sector loads, real cases from medium-voltage distribution systems are described, in which the ratio of the admissible PV peak power to the peak load reaches 73 % for residential users and 79 % for tertiary-sector users, whereas the corresponding energy ratio goes up to 31 % for residential users and 48 % for tertiary-users in work days without reversal of the power flow.

The electricity bills have been deeply analysed for dwelling houses, common loads of apartment blocks and tertiary-sector users: in Germany the fixed costs are generally negligible, whereas in Italy the “available power” item charges a heavy fee for the common loads of apartment blocks.

Therefore, the grid parity problem is analysed as an investment in which the net present value is the tool for proving the cost effectiveness or not of the installation of a photovoltaic plant.

The main results, shown in the maximum spread of irradiation depending on the installation-sites, take into account the different economic situation in the Countries by the interest rates of 3 – 6 % in Germany and 4 – 10 % in Italy. In details, the grid parity for dwelling houses is reached in Germany and Central/Southern Italy, whereas it is almost achieved in Northern Italy. For the common users in apartment-blocks the grid parity is reached in Germany, while it is unrealistic to be reached in Italy with the current economic/regulatory situation. Finally, for the tertiary-sector users the grid parity is reached in Germany and in Italy.

Chapter 3

Accurate measurements of solar irradiance

Introduction

The operation of grid-connected PV systems is characterized by several uncertainties due to the irradiance variations, the number of currently operating units, the points where these units are sited, the power rating and the injection of harmonic currents. Models have been developed for the calculation of power flows, harmonics and voltages in the feeders [75]-[78]. A PV array can be modeled as an irradiance-driven current generator, with a proper Maximum Power Point (MPP) tracking algorithm; it is connected to the network via a PV inverter.

Other models have been successfully used to determine the power output series of a PV plant of any size using only irradiance measurements. From the operator viewpoint, this can be a powerful tool to study the integration of PV plants in the power network, providing artificial power output series for the grid operator in his simulation software. Maximum power fluctuation is needed to establish the maximum permitted PV penetration rate at a particular grid. As expected, due to the big surface covered by a PV plant in comparison with the discrete character of a irradiance sensor, the power curve is significantly smoother than the irradiance curve [79]. Moreover, a wavelet variability

model (WVM) for simulating PV power output, given time series of single irradiance sensor using spatio-temporal correlations, is described in [80].

The acceptable penetration level of PV systems is under investigation, especially today when e.g. about 30 GW_p in Germany and 16 GW_p in Italy have been connected to the grid (PV power rating corresponding to 1000 W/m^2 and 25 °C, i.e., Standard Test Conditions, STC). In order to enhance the penetration of the intermittent PV power into the network, it is important to measure as correctly as possible the solar irradiance both by pyranometers, which exhibit relative uncertainties of 1 % − 2 %, and by reference solar cells with higher uncertainties around 2.5 % − 5 %. These two types of instrument have intrinsically low accuracy for different reasons:

- the pyranometer, based on the Seebeck effect (thermocouple), with wide (≈0.3 − 3 μm) and constant spectral response in function of the wavelength, has low sensitivity (a few $\mu V/W \cdot m^{-2}$) and requires an electronic amplifier with consequent repetitive calibration and maintenance;
- the reference solar cell in crystalline silicon has narrow (≈ 0.3 − 1.1 μm) and variable spectral response and sensitive to deviations from the STC solar spectrum, but have the same spectral response of the PV modules with higher sensitivity (tens of $mA/W \cdot m^{-2}$).

Another difference concerns the response time that is 5 − 20 s for the pyranometer and less than 1 ms for the reference solar cells. The directional error, i.e., linked to the angle of the solar beam with respect to the vector normal to the surface, is typically lower for pyranometer than for reference solar cell.

From the previous considerations it can be understood the interest for an experimental campaign for comparing the outdoor performance of different irradiance-meters.

In this chapter it is presented a comprehensive study of sensors placed both in horizontal position and in tilted one. In particular, five meteorological stations have been installed in different location in South of Italy. The checking of the measurement uncertainty has been carried out for guaranteeing the reliability of the results. The study includes various

types of days from the clear sky to the completely cloudy sky, focusing on the peak values and their variations. The impact of the tilt angle is also evaluated on daily, monthly and yearly basis.

3.1. The meteorological stations

With the goal to represent the zone of Italy characterized by the highest PV penetration, each out of the five identical meteorological stations, located at latitudes within 39° − 41°N (Fig. 3.1), has been equipped with:

- 1 pyranometer (ISO Secondary Standard) and 2 reference solar cells in crystalline silicon for measuring the horizontal global irradiance G_{pyr} and G_{hcell};
- 2 reference solar cells in crystalline silicon for the tilted global irradiance G_{tcell};
- 1 thermo-hygrometer for the other physical quantities (T_{amb} and RH) except for the atmospheric pressure.

Fig. 3.1 − The five meteorological stations located at latitudes within 39° − 41°N.

The main specifications of the pyranometers are:

- spectral range from 0.285 μm to 2.8 μm;
- sensitivity 7 − 14 μV/W·m^{-2};
- response time ≤ 5 s;
- zero offset < 10 W/m^2;
- directional error (up to 80° with 1000 W/m² beam) < 10 W/m^2.

The calibration procedure, carried out by the manufacturer, can be performed by comparison with a Primary Standard subject to the actual solar spectrum or by a sun-simulator.

The tilt angle of the solar cells is 30°, with South orientation, for optimizing the solar energy capture. The time step for all the stored parameters is 1 min, value useful for the electricity market, in which supply and demand are matched, every 15 min, according to the updates of bids and offers.

The absolute uncertainty of the pyranometer ($\Delta G_{pyr} \approx 10 - 20$ W/m^2) is the starting point for the computation of the corresponding uncertainties [81] for the daily/monthly irradiations in kWh·m^{-2}.

The formula of propagation of relative uncertainty ε_{Hh} for the irradiation H_h is the following with k index of the measurements during the sunlight period:

$$\varepsilon_{Hh} = \varepsilon_t + \sum_k \left(G_{hk} \cdot \varepsilon_{Ghk}\right) \Big/ \sum_k G_{hk} \tag{3.1}$$

in which the relative uncertainty of the "time" quantity ε_t is considered negligible with respect to the relative uncertainty ε_{Ghk} of the "irradiance" quantity G_{hk}.

Hence, the expression is coincident with the weighted average of the relative uncertainties ε_{Ghk} by the irradiance values. Typical values of uncertainties are ± 250 Wh/m^2 on daily basis and ± 7.5 kWh/m^2 on monthly basis in spring/summer period.

Furthermore, these values are the threshold within which the measurements of the solar cells must be included for having the label of “acceptable values”. The recorded measurements are extended to 1 year, from January 2012 to December 2012. The missing values in the five stations are limited to a few days. Tables of event have been compiled for 12-month period, in which the lack of data lasts for 1 day and a half at maximum; the regular data are obviously recorded. Finally, it can be stated that the availability of the two stations is at least 99 %.

3.2. Quasi-instantaneous quantities during a single day

Starting from the summer period, it is possible to note in Fig. 3.2 the different behavior of the horizontal irradiances G_{pyr}, G_{hcell} vs. the tilted one G_{tcell}. in a *clear-sky* day. Actually, in July in the morning till 11 a.m. and in the afternoon after 3 p.m., G_{pyr} is higher than G_{tcell}, whereas only in 4 hours the tilted plane collects more solar radiation than the horizontal plane. In particular, at midday the sun-height is ≈ 70° and it is reasonable that the direct beam is closer to the normal in case of tilted plane (≈ 1000 W/m^2) than in case of horizontal plane (≈ 960 W/m^2). About the ambient temperature T_{amb} and the relative humidity *RH*, they have a “complementary” behavior in clear-sky conditions. When T_{amb} achieves peak values around 35 °C in the interval 2 − 5 p.m., *RH* decreases down to the minimum values around 30 %. On the other hand, the peak values of *RH* at sunrise (≈ 6 a.m.) and at midnight (≈ 80 %) are corresponding to the minimum values of T_{amb} (≈ 20°C).

The days with “broken clouds” exhibit a special behavior, in which the sky is mainly clear, but the passage of clouds affects the irradiance evolution. When the obstruction of the clouds occurs, the irradiance is attenuated, but when the clouds are around the Sun, the beam irradiance is amplified and so the peak values can rise up to 1200 W/m^2 (Fig. 3.3). This situation corresponds to 20 % more irradiance than STC. Furthermore, steep *G*

variations are recorded up to 700 W/m^2 in 15 min. Finally, another remark can be done about *RH* that holds continuously values close to 100 % in the night period.

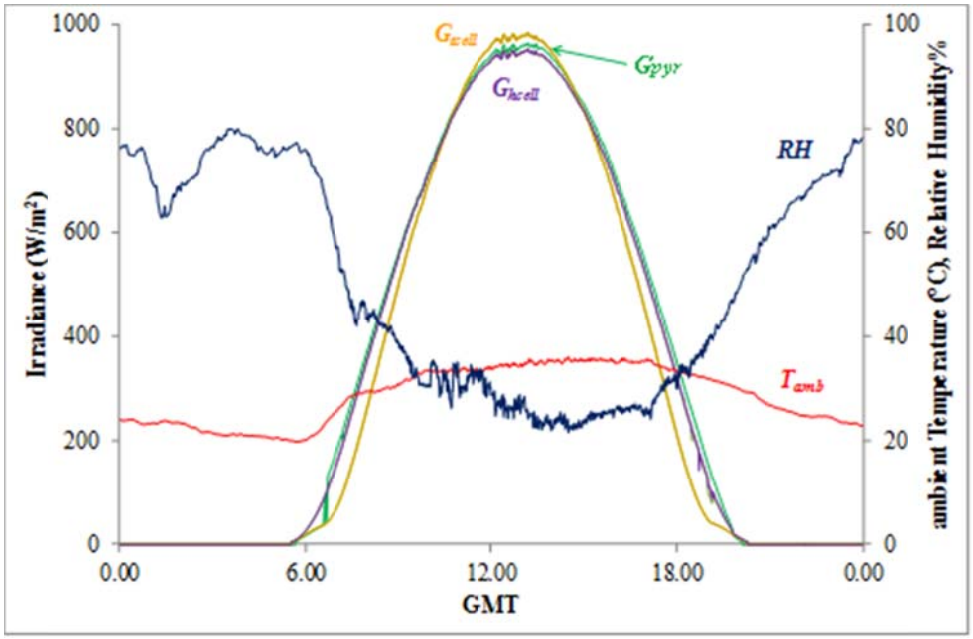

Fig. 3.2 − Daily evolution of the measured quantities in a clear day of July.

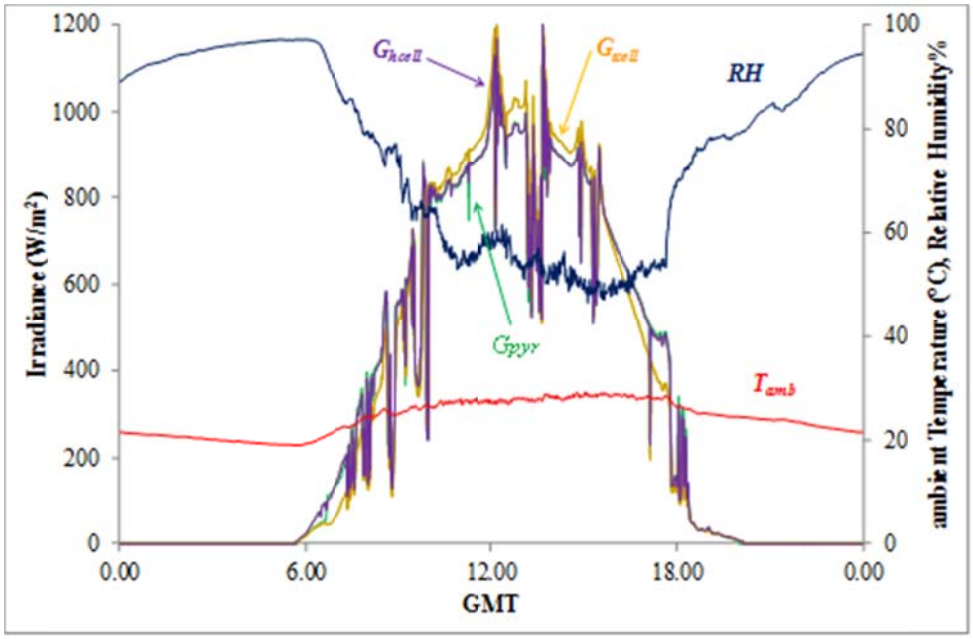

Fig. 3.3 − Daily evolution in a “broken clouds” day of July.

The analysis of days with completely cloudy sky is very difficult in summer, since many times, e.g. in July, there are not situations in which the only diffuse irradiance is present. If one considers the winter data in clear sky days, the more evident result is the impressive increment in the irradiance on the tilt angle with respect to the horizontal irradiance. Indeed, the peak value of G_{tcell} exceeds by far 800 W/m^2, while the corresponding G_{pyr} is less than 500 W/m^2 (Fig. 3.4). With low sun heights it is possible to have shade on the sensors, as in case of the morning at 7:30 − 8:00 a.m.. Moreover, the discussion about *RH* brings to higher impact than in the summer, since there are more than 12 h with *RH* > 80 %; then, the minimum value is, however, about 45 %.

Also in this season, the “broken clouds” phenomenon produces peak values of irradiance very close to 1000 W/m^2 or, in other words, it overcomes by far (≈ 20 %) the values with clear sky condition.

In winter it is easier the analysis of days with completely cloudy sky, even if the types of diffuse radiation are many, since the color is variable from blue to grey. In fact, Fig. 3.5 shows an example, in which the irradiance evolution is always below 100 W/m^2 and no practical difference happens between horizontal and tilt quantities. Furthermore, the ambient temperature is subject to little variations (about 8 °C) and the relative humidity is above 70 % along nearly 20 hours.

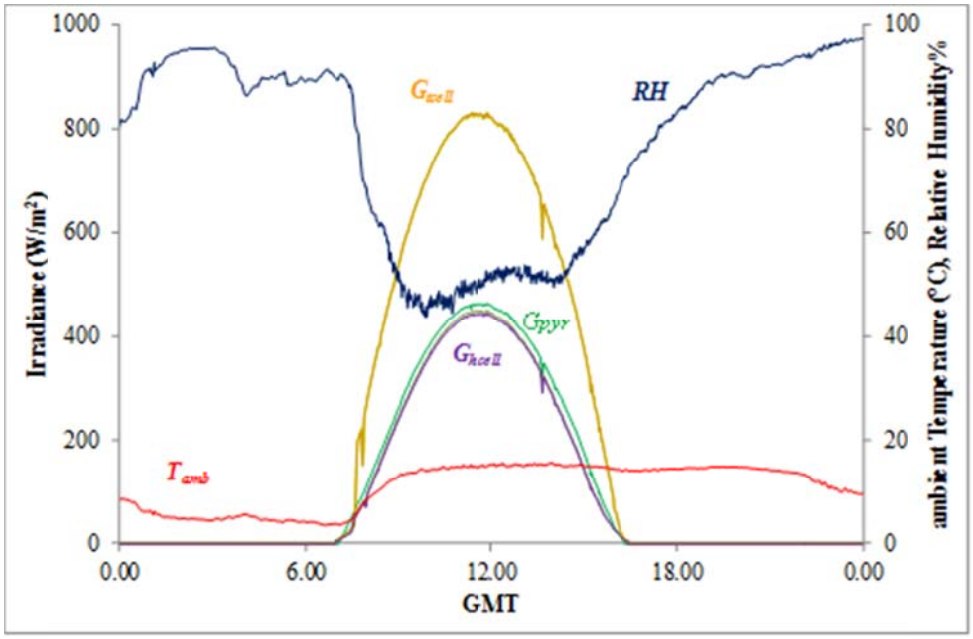

Fig. 3.4 − Daily evolution in a clear day of December.

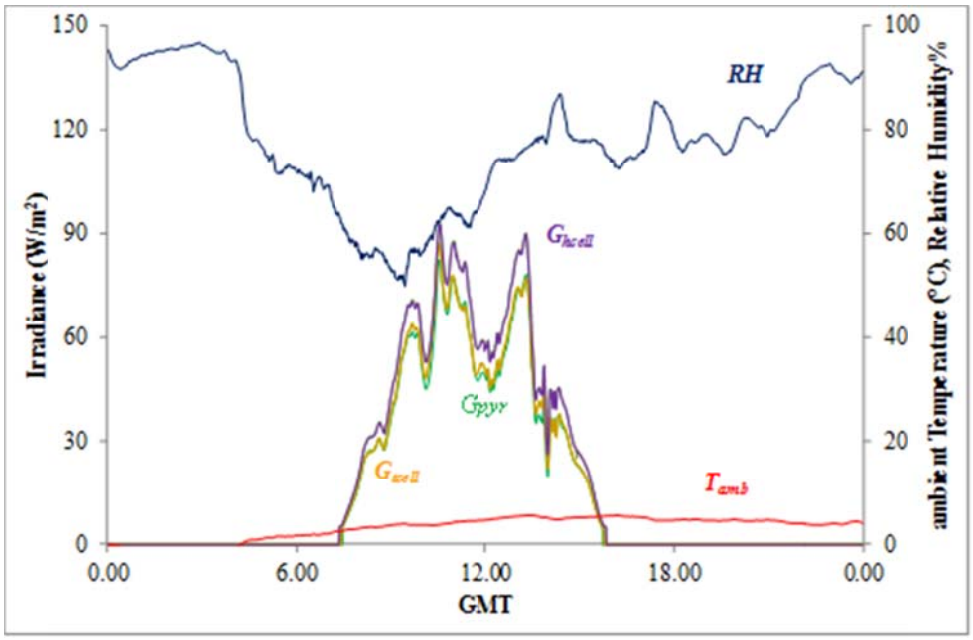

Fig. 3.5 − Daily evolution in a cloudy day of December.

3.3. Monthly quantities for a whole year

After the study of the daily evolution of the quantities, the monthly and yearly behavior are here summarized.

Firstly, it is needed to note that the measurements of the solar cells are generally within the measurement uncertainty of the pyranometer in spring-summer period. In particular, the values from the solar cells are slightly lower than those from the pyranometer. In winter, in some conditions, the deviations of solar-cell sensors exceed the uncertainty of pyranometer with sensors placed on the horizontal plane, due to the great directional errors of solar cells when the angles between the sun beam and the normal to the surface are higher than 60°. On the other hand, the deviations of solar-cell sensors are within the pyranometer uncertainty, when the sensors are installed on the tilted plane.

Table 3.1(a) and Table 3.1(b) report, from January 2012 to December 2012, the percent deviations of the horizontal solar cell 1 and horizontal solar cell 2 respectively, vs. the pyranometer for the five meteorological stations. From these table, it is worth noted that in the month of August, the minimum deviations for the horizontal solar cell 2, within ±12 % (but less than percent in some months), is achieved by the stations “Gi”. The station “Ma” achieves the minimum deviations within $\pm 5 - 6$ % both for the horizontal solar cells 1 and 2.

Table 3.2(a) and 3.2(b) show, in the same interval, the percent deviations of the tilted solar cell 1 and tilted solar cell 2 respectively, vs. the pyranometer for the same stations. Here, the minimum deviations, within ±9 %, are achieved by the station “Ma”. In this case the pyranometer measurements are corrected by a suitable procedure which takes into account many quantities as, for example, the extra-terrestrial horizontal irradiation and the clearness index [82], [83].

Table 3.1− (a) Monthly deviation of the horizontal solar cell 1 vs. pyranometer (year 2012).

Stat.s	Jan	Feb	Mar	Apr	May	Jun	Jul	Aug	Sep	Oct	Nov	Dec
Ga1	-9.8	-3.8	-4.8	-2.6	-2.7	-2.8	-2.5	-3.6	-4.6	-5.9	-8.3	-11.5
Ga2	-5.2	-0.7	-1.8	-0.9	-1.3	-1.8	-1.3	-2.2	-2.1	-2.2	-2.8	-4.8
Ru	-9.1	-4.1	-4.5	-2.5	-2.3	-2.2	-2.5	-3.5	-3.6	-5.1	-6.3	-9.5
Gi	-4.1	-0.1	-0.7	0.4	0.0	-1.0	-0.8	-1.7	-1.1	-1.0	-0.8	-4.1
Ma	-3.5	0.3	-0.6	0.4	-0.2	-0.9	-1.1	5.6	0.3	-0.8	-1.1	-3.5

Table 3.1 − (b) Monthly deviation of the horizontal solar cell 2 vs. pyranometer (year 2012).

Stat.s	Jan	Feb	Mar	Apr	May	Jun	Jul	Aug	Sep	Oct	Nov	Dec
Ga1	-8.8	-7.4	-5.3	-2.5	-1.5	-3.0	-2.2	-3.2	-4.5	-6.3	-7.5	-8.5
Ga2	-5.1	-1.1	-2.4	-1.2	-2.2	-3.3	-2.0	-3.3	-3.5	-2.5	-3.3	-4.9
Ru	-9.2	-4.1	-6.0	-2.8	-3.2	-3.1	-3.5	-3.9	-4.3	-5.5	-6.5	-9.9
Gi	-3.6	-0.4	-1.3	-0.1	-1.0	-2.1	-2.6	-11.9	-1.1	-1.0	-0.8	-5.0
Ma	-4.6	-0.4	-1.6	-0.2	-1.1	-1.5	-1.2	5.0	-0.5	-1.8	-2.3	-4.8

Table 3.2 – (a) Monthly deviation of the tilted solar cell 1 vs. pyranometer (year 2012).

Stat.s	Jan	Feb	Mar	Apr	May	Jun	Jul	Aug	Sep	Oct	Nov	Dec
Ga1	0.1	-2.3	-2.5	-0.3	-0.8	-2.0	-0.7	-0.1	-0.4	-1.3	-0.6	-1.6
Ga2	-0.4	-2.8	-2.0	0.8	0.6	-0.3	1.1	1.2	0.2	-0.9	-0.8	-1.4
Ru	1.8	-1.1	-0.8	1.6	1.5	0.2	0.4	0.7	0.8	-1.3	-0.8	-8.6
Gi	2.2	2.2	-0.4	0.4	1.9	1.4	2.1	3.2	2.1	2.6	1.2	1.7
Ma	-0.3	0.0	-1.6	3.0	1.3	0.6	2.7	9.5	2.5	0.5	1.5	-0.4

Table 3.2 – (b) Monthly deviation of the tilted solar cell 2 vs. pyranometer (year 2012).

Stat.s	Jan	Feb	Mar	Apr	May	Jun	Jul	Aug	Sep	Oct	Nov	Dec
Ga1	0.0	-2.8	-2.9	-0.4	-0.9	-1.9	-0.2	0.3	-0.7	-1.5	-2.0	-3.0
Ga2	-0.3	-3.1	-2.8	0.2	-0.3	-1.7	0.0	0.6	-0.4	-2.0	-1.7	-2.3
Ru	0.9	-1.8	-1.8	1.1	0.7	-0.2	0.0	0.4	0.2	-1.3	-0.7	-9.2
Gi	2.1	2.1	-0.7	0.1	0.9	0.5	0.4	2.3	1.9	2.5	1.2	1.5
Ma	-0.3	-0.1	-1.9	2.8	0.8	0.1	2.3	9.1	2.2	0.6	1.5	-0.4

The linearity and the correlation between pyranometers and solar cells are evident, as shown in Fig. 3.6(a) and 3.6(b) for the site “Gi”, Fig. 3.7(a) and 3.7(b) for the site “Ma”, Fig. 3.8(a) and 3.8(b) for the site “Ga1”, Fig. 3.9(a) and 3.9(b) for the site “Ga2”, Fig. 3.10(a) and 3.10(b) for the site “Ru”.

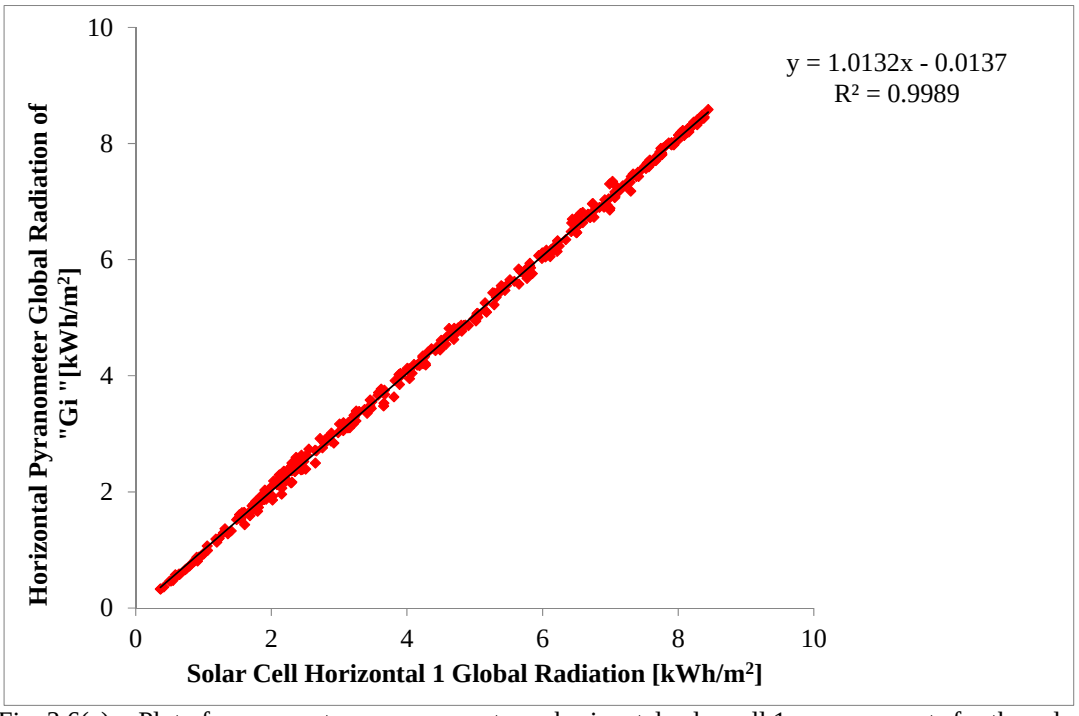

Fig. 3.6(a) − Plot of pyranometer measurements vs. horizontal solar cell 1 measurements for the solar station “Gi”.

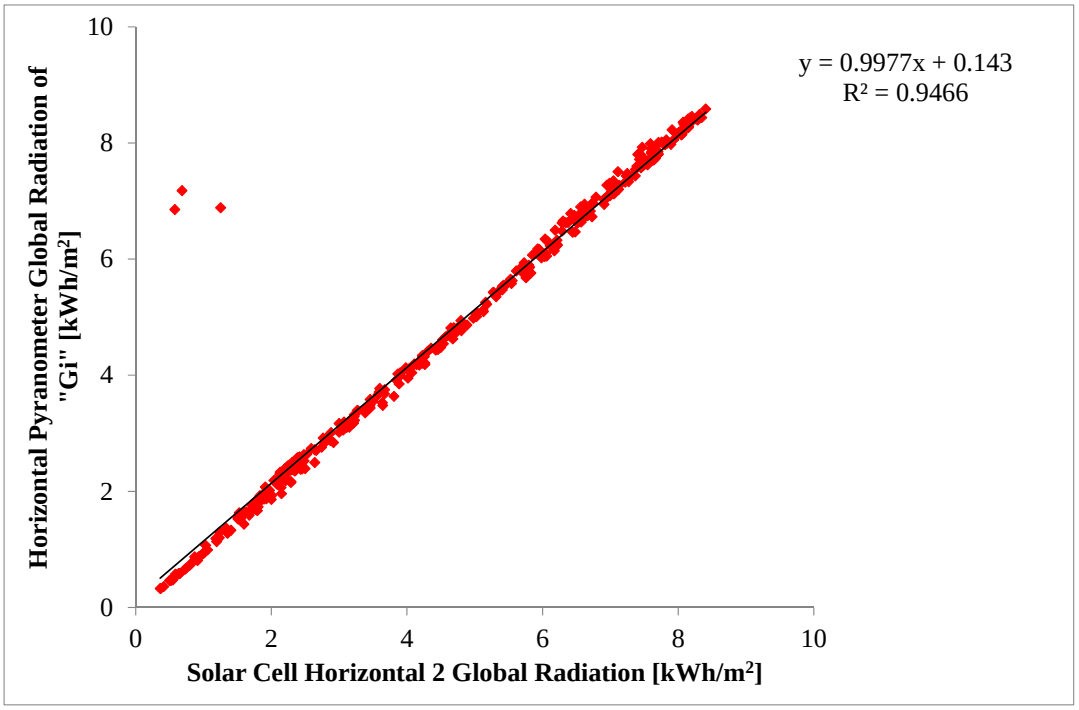

Fig. 3.6(b) − Plot of pyranometer measurements vs. horizontal solar cell 2 measurements for the solar station “Gi”.

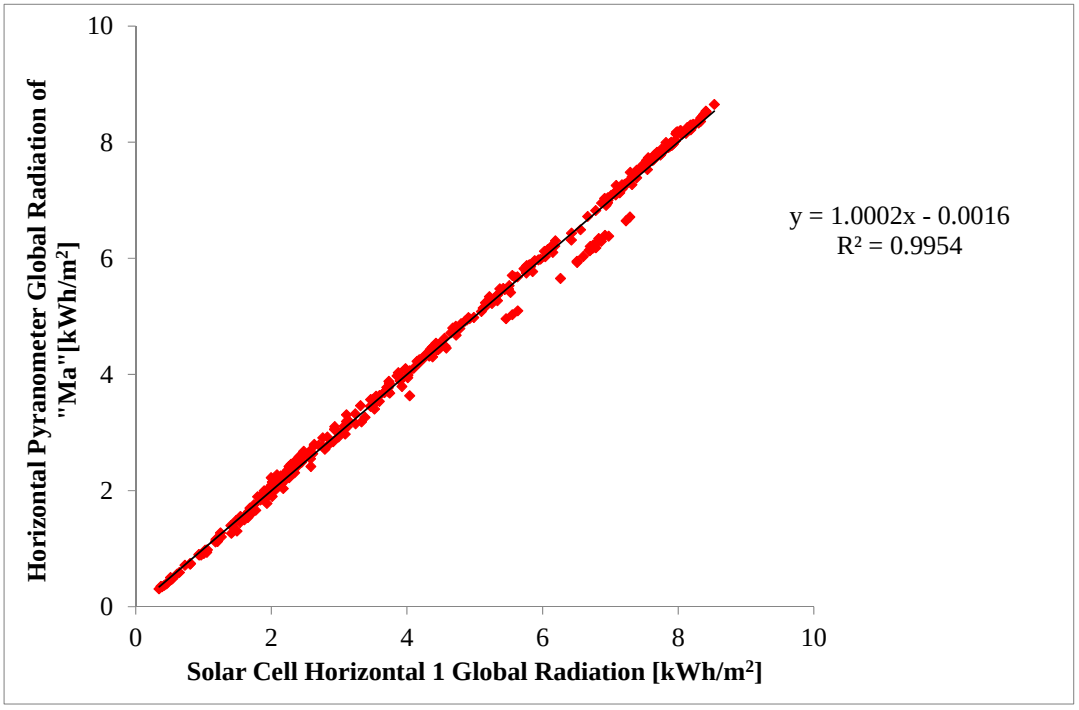

Fig. 3.7(a) − Plot of pyranometer measurements vs. horizontal solar cell 1 measurements for the solar station “Ma”.

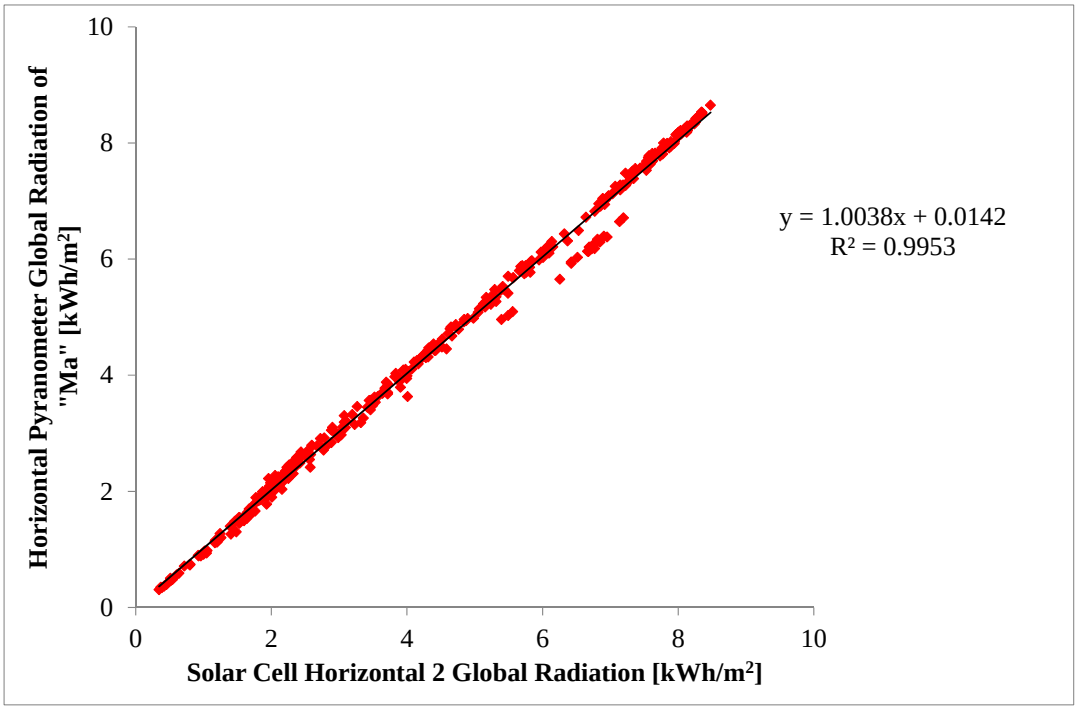

Fig. 3.7(b) − Plot of pyranometer measurements vs. horizontal solar cell 2 measurements for the solar station “Ma”.

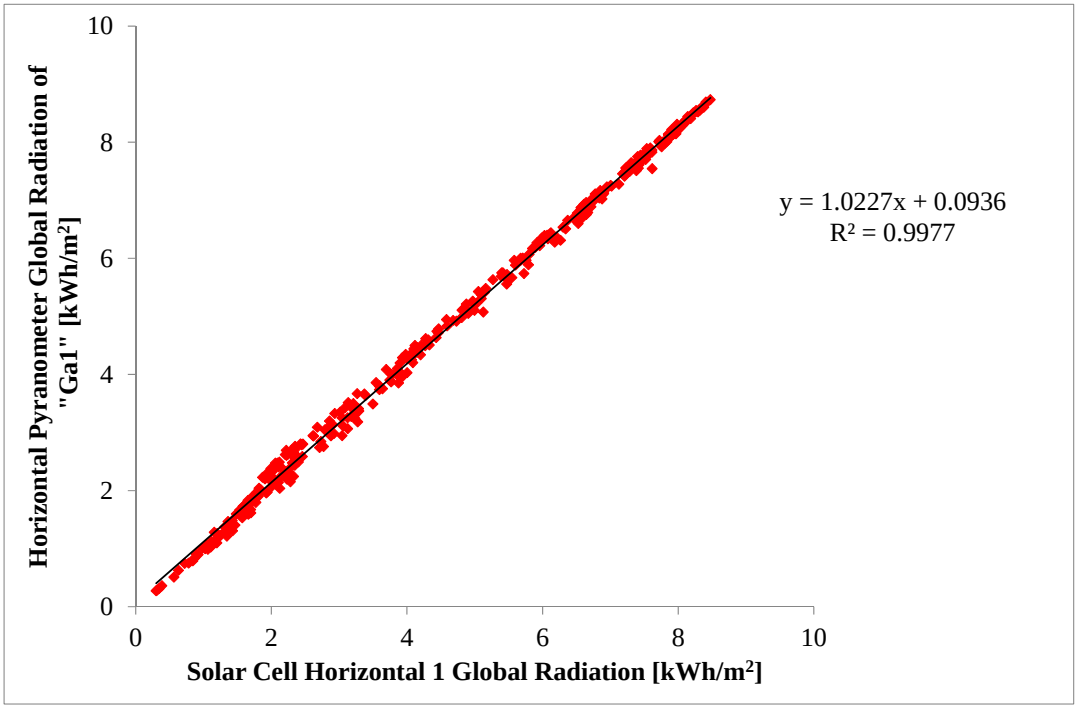

Fig. 3.8(a) − Plot of pyranometer measurements vs. horizontal solar cell 1 measurements for the solar station “Ga1”.

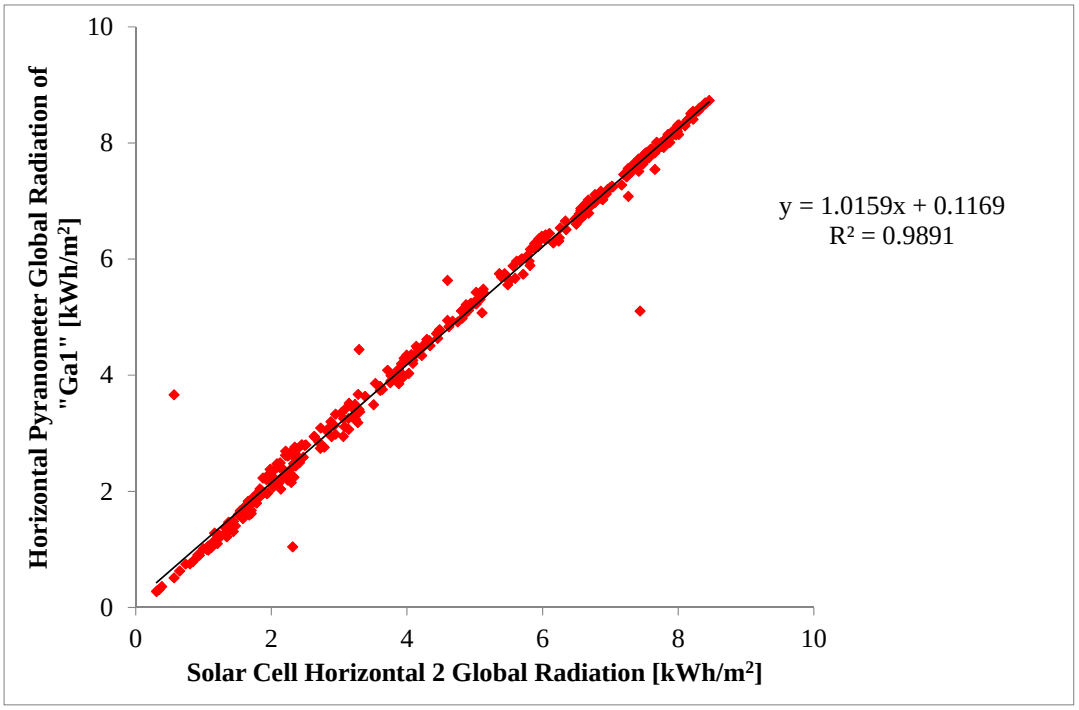

Fig. 3.8(b) − Plot of pyranometer measurements vs. horizontal solar cell 2 measurements for the solar station “Ga1”.

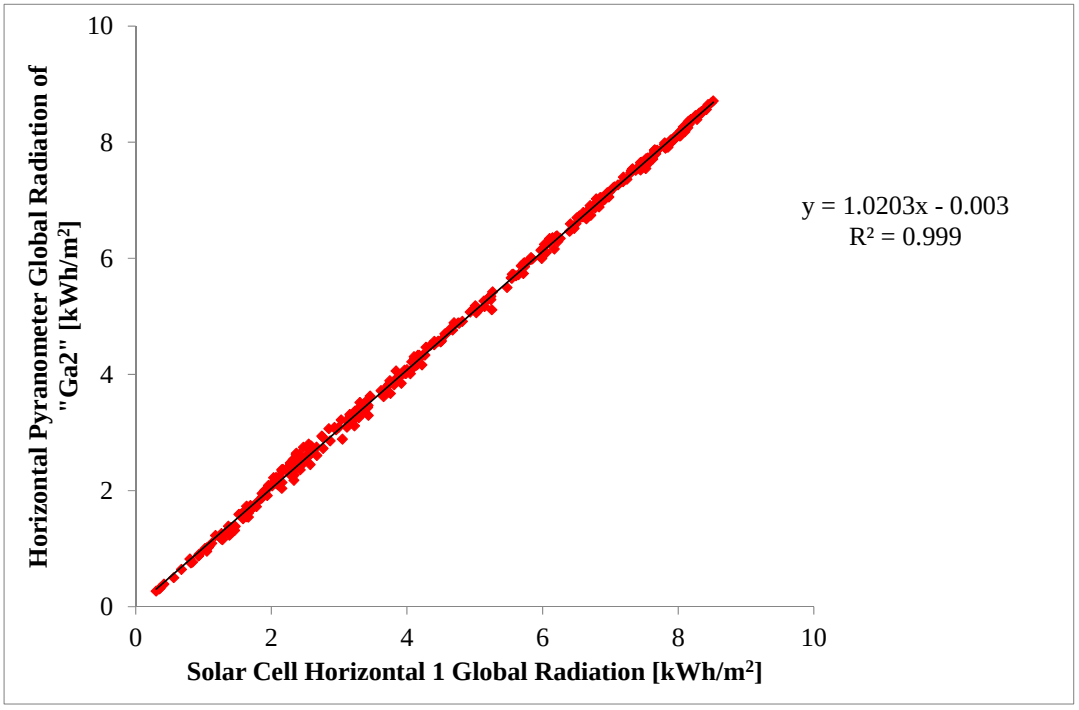

Fig. 3.9(a) − Plot of pyranometer measurements vs. horizontal solar cell 1 measurements for the solar station “Ga2”.

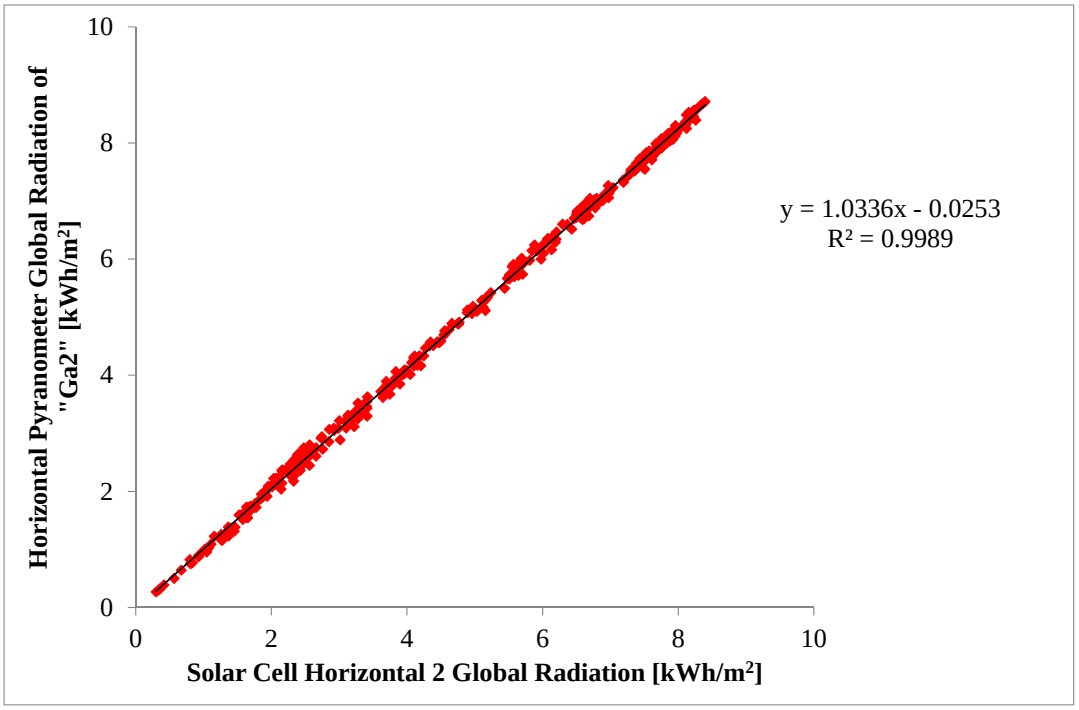

Fig. 3.9(b) − Plot of pyranometer measurements vs. horizontal solar cell 2 measurements for the solar station “Ga2”.

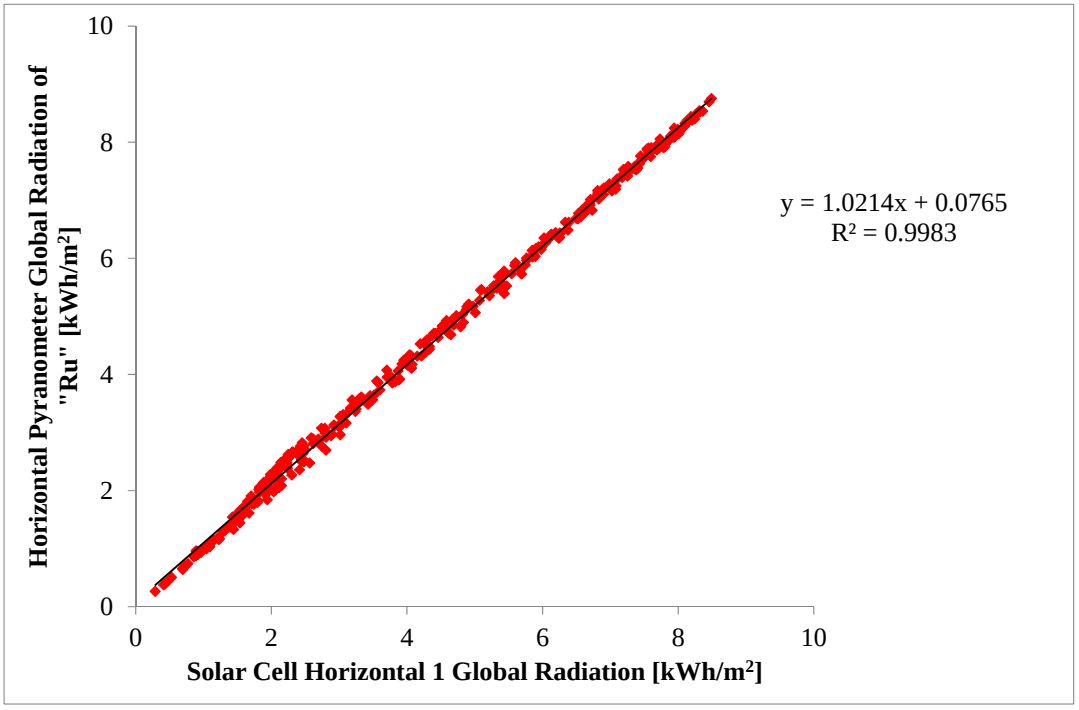

Fig. 3.10(a) − Plot of pyranometer measurements vs. horizontal solar cell 1 measurements for the solar station “Ru”.

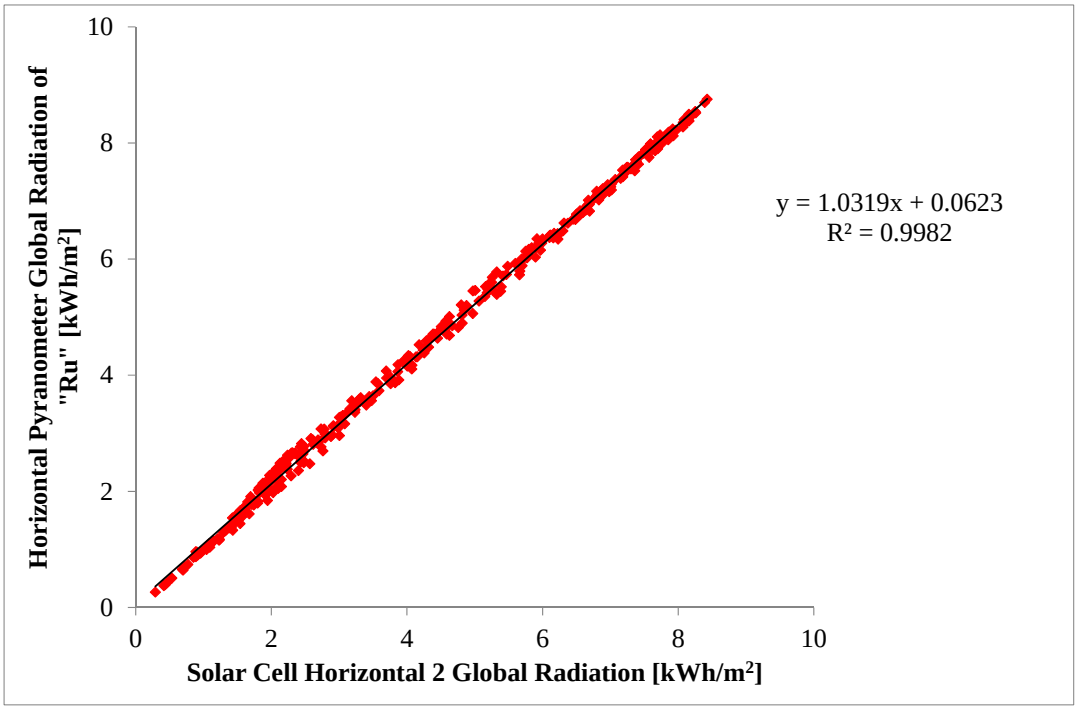

Fig. 3.10(b) − Plot of pyranometer measurements vs. horizontal solar cell 2 measurements for the solar station “Ru”.

It is interesting to know which months for the tilt irradiation are more favorable than for the horizontal irradiation. The answer is the period from September to April, whereas the horizontal irradiation is higher in the period from May to July.

The transition among the two irradiation occurs in August (Table 3.3(a) for the site "Gi", Table 3.3(b) for the site "Ma", Table 3.3(c) for the site "Ga1", Table 3.3(d) for the site "Ga2" and Table 3.3(e) for the site "Ru"). Obviously, these statements are valid for the latitudes under study, i.e. in the range 39° − 41° N, in which the majority of PV systems is connected to the public network in Italy.

Table 3.3(a) − Monthly values of irradiation in the station "Gi".

Months	**H_h pyr. (kWh/m^2)**	**H_t sol.1 (kWh/m^2)**	**H_h sol.1 (kWh/m^2)**	**H_t sol.2 (kWh/m^2)**	**H_h sol.2 (kWh/m^2)**
Jan	67	112	64	112	64
Feb	65	88	65	88	65
Mar	137	170	137	169	136
Apr	147	156	147	156	146
May	197	192	197	190	195
Jun	238	221	236	219	233
Jul	229	218	227	214	223
Aug	209	221	205	219	184
Sep	146	173	145	173	144
Oct	108	151	106	151	106
Nov	57	86	57	86	57
Dec	57	100	55	99	55
Year 2012	1657	1888	1640	1877	1608

Table 3.3(b) − Monthly values of irradiation in the station “Ma”.

Months	H_h pyr. (kWh/m^2)	H_t sol.1 (kWh/m^2)	H_h sol.1 (kWh/m^2)	H_t sol.2 (kWh/m^2)	H_h sol.2 (kWh/m^2)
Jan	69	113	66	113	65
Feb	67	90	68	90	67
Mar	143	175	142	174	141
Apr	153	163	153	163	152
May	206	200	205	199	204
Jun	243	222	240	221	239
Jul	238	225	235	224	235
Aug	199	222	210	221	209
Sep	147	176	148	175	147
Oct	114	158	113	158	112
Nov	61	93	60	93	59
Dec	55	92	53	92	53
Year 2012	1694	1927	1694	1922	1682

Table 3.3(c) − Monthly values of irradiation in the station “Ga1”.

Months	H_h pyr. (kWh/m^2)	H_t sol.1 (kWh/m^2)	H_h sol.1 (kWh/m^2)	H_t sol.2 (kWh/m^2)	H_h sol.2 (kWh/m^2)
Jan	67	104	60	104	61
Feb	70	88	67	88	64
Mar	147	176	140	175	139
Apr	154	163	150	162	150
May	210	203	204	203	207
Jun	244	224	237	224	237
Jul	238	226	232	227	232
Aug	213	220	205	221	206
Sep	155	179	148	179	148
Oct	111	145	104	144	104
Nov	65	94	59	92	60
Dec	57	88	50	87	52
Year 2012	1730	1909	1658	1906	1661

Table 3.3(d) − Monthly values of irradiation in the station “Ga2”.

Months	H_h pyr. (kWh/m^2)	H_t sol.1 (kWh/m^2)	H_h sol.1 (kWh/m^2)	H_t sol.2 (kWh/m^2)	H_h sol.2 (kWh/m^2)
Jan	66	107	63	108	63
Feb	70	91	69	91	69
Mar	146	179	144	178	143
Apr	154	163	152	162	152
May	210	202	207	200	205
Jun	243	220	238	217	235
Jul	237	223	234	221	233
Aug	212	219	208	218	205
Sep	154	180	151	179	149
Oct	110	149	108	148	107
Nov	64	97	62	96	62
Dec	56	92	53	92	53
Year 2012	1723	1924	1690	1908	1676

Table 3.3(e) − Monthly values of irradiation in the station “Ru”.

Months	H_h pyr. (kWh/m^2)	H_t sol.1 (kWh/m^2)	H_h sol.1 (kWh/m^2)	H_t sol.2 (kWh/m^2)	H_h sol.2 (kWh/m^2)
Jan	67	112	61	111	61
Feb	70	92	67	92	67
Mar	147	182	140	180	138
Apr	152	162	148	161	148
May	206	200	201	198	200
Jun	243	221	237	220	235
Jul	235	219	229	218	227
Aug	212	217	204	217	204
Sep	152	178	146	177	145
Oct	111	149	105	149	105
Nov	64	96	60	96	60
Dec	56	91	50	91	50
Year 2012	1714	1919	1651	1910	1639

A topic concerning the energy production of PV systems is the variation of the global irradiation among sites located within a range of a few hundreds of kilometers: four sites with flat terrain, 20 − 70 km away from each other, exhibit monthly and yearly deviations within ± 2 %. With greater distance (≈ 150 km) for the last station the variation can arrive at -7 %.

Further noticeable problem is the variation minute by minute of the irradiance (i.e., the derivative or in practice the incremental ratio): this parameter assumes reduced values when the weather is sunny or completely cloudy, but it requires a careful monitoring in broken-cloud conditions.

If we consider a single location with huge derivative, this variation is higher than the variation of the average of the locations together considered. In other words, the increase

of the number of locations, with the corresponding increment of the covered surface, has a “smoothing effect” on the combined PV energy production.

An example is shown in Fig. 3.11 with the 15-min irradiances in three sites (black, green and orange colors), 150 km away from each other, and their average values (red color). The smoothing effect provides strong reductions in positive and negative derivatives: the positive derivative has a percent reduction within - 44 % − - 78 % vs. each site, whereas the negative derivative has a reduction of -37 % − -57 %.

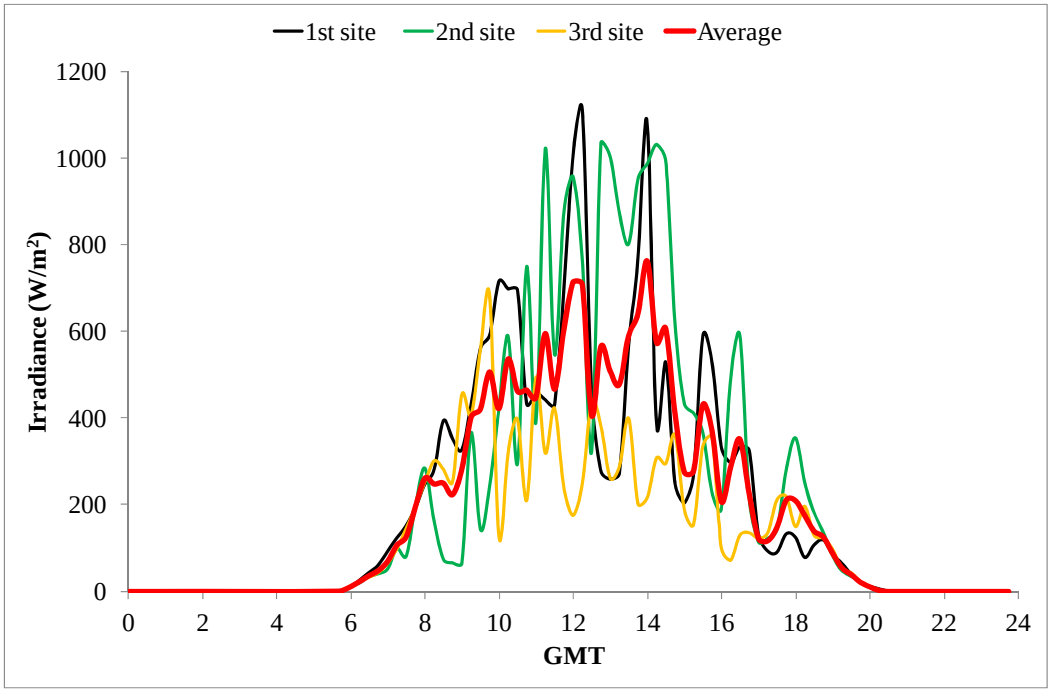

Fig. 3.11 − Smoothing effect in the irradiances of 3 sites due to the average values.

3.4. A comparison with simulated clear sky/cloudy sky days

The experimental results for the horizontal and tilt irradiances in case of clear sky and completely cloudy sky conditions suggest the search of models to simulate these practical evolutions.

A possible solution is the employment of the PVGIS online software [73] in the tool "Daily irradiance", which provides computed values G_{hSIM} every 15 min. In a clear day of July the G_{hMEAS} deviations are quite low (around 20 W/m^2) and within the measurement uncertainty, as it is possible to see in Fig. 3.12 for the horizontal irradiance.

Moreover, in PVGIS the diffuse contribution is corresponding to the blue color of the sky, thus, in case of complete covering from grey clouds, the actual irradiance values are lower than the simulated values.

In Fig. 3.13 the two types of days (blue sky vs. grey sky) with prevailing diffuse radiation are compared with the PVGIS simulation of cloudy-sky day. With grey clouds (on 21st Dec) the deviations between measurements (G_h) and simulation (G_{dSIM}) are noticeable both in percent (> 50 %) and in physical units (> 60 W/m^2), instead of mainly blue-sky conditions (on 26th Dec).

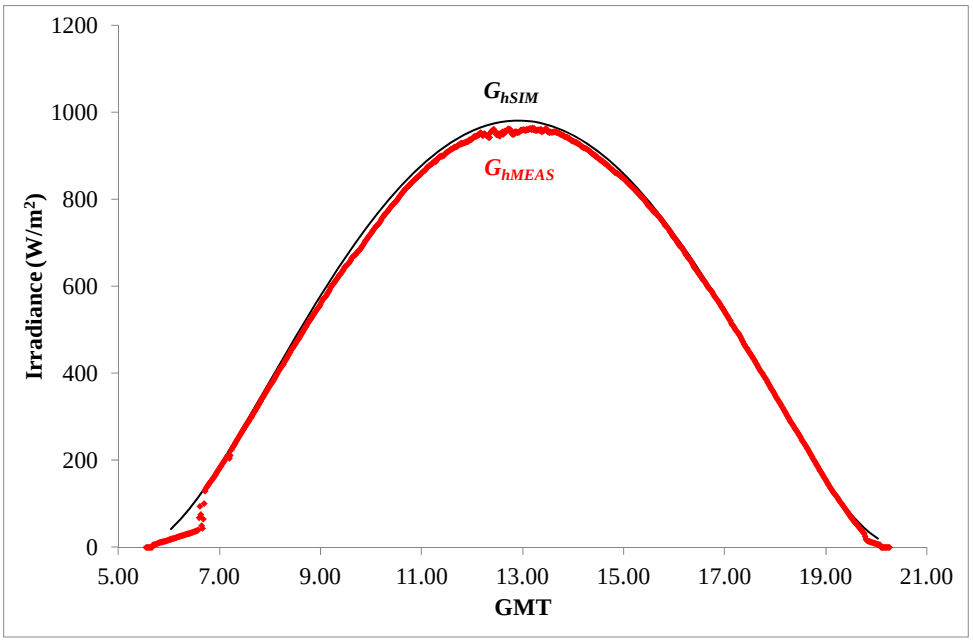

Fig. 3.12 − A comparison between measurements and simulation of horizontal irradiance in a clear day.

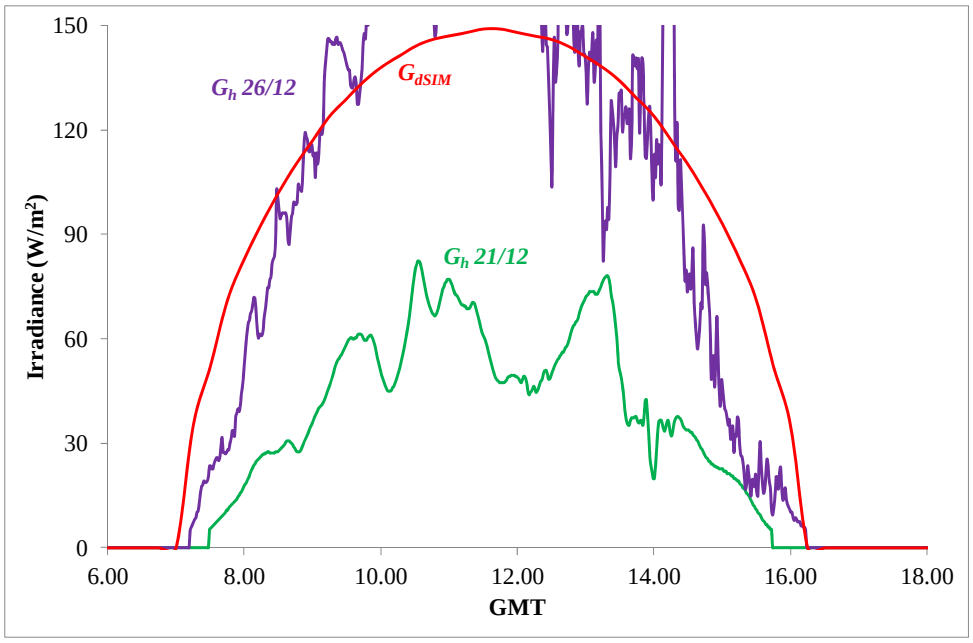

Fig. 3.13 − A comparison between measurements and simulation of horizontal irradiance in cloudy days.

3.5. Summary

This chapter has shown the setup of five meteorological stations and the concerning experimental results of short-term global irradiance on the horizontal plane and on the best tilted plane. These findings on yearly basis can be easily linked with the power profiles of PV plants installed at ground level typically without shading.

It is evident that the knowledge of “broken clouds” phenomenon and its prediction can be very useful to the Transmission System Operator for the management of the peak generation. Rapid variations of more than 500 W/m^2 can occur upward and downward in a few minutes. Therefore, in case of impressive derivatives of irradiance, positive or negative, a smoothing effect of the average values of multiple sites has been proved.

The information on the sunlight evolution of relative humidity could somehow substitute the direct measurement of the global irradiance. That is important, due to the frequent lack of the irradiance sensor in the usual meteorological stations.

Simple models for global irradiance in clear sky and completely cloudy sky situations can be used as a first approximation tool to predict the photovoltaic power profiles for the electricity market.

Chapter 4

Prediction of irradiance vs. experimental results

Introduction

The strong increase of power production by RES involves a substantial change in the system management for the generation, transmission and distribution of electricity. The hierarchical structure, in which a few centralized power plants deliver the energy required, becomes a distributed structure, in which many small production units are located in the territory. The advantage in terms of versatility and reliability is considerable, in fact, the subdivision of the production in many distributed power plants permits to deal with failure or maintenance situations, which involve the temporary shutdown of some units, as well as to respond more effectively to changes in energy demand.

The prediction of the power profiles with intermittent RES is essential to formulate saving and dispatching plans. Due to the lack of information and communication systems between the parts, the current forecasting of power plants' production does not take into account the contributions of DG systems. For an optimal management of the whole power system, it is needed to get the data of the power allocation and the corresponding forecasting in real time.

One of the main challenges for the future energy supply will be to integrate RES with the existing structures. To achieve this result, the important issue about the prediction of power flows must be treated [84]. This goal is not easy to be achieved, because the available power depends on the time-varying performance of RES, some of which are subject to considerable fluctuations during the day, as e.g. wind speed or solar irradiance. Here, only the latter source will be treated, analyzing an approach to predict PV power output based on forecasts up to three days ahead provided by the "Servei Meteorològic de Catalunya"(Meteo.cat).

4.1. State of the art

About the state of the art of the solar irradiance forecasting, early research was conducted more than twenty years ago in [85], using the Model Output Statistics (MOS) technique [86], which allows the prediction of a daily average value with one or two days ahead.

Remaining in the field of very short period (time horizon of a few hours), [87] has demonstrated the effectiveness of a statistical approach based on the prediction of the motion of the clouds through images provided by satellites of the Meteosat constellation; this method, however, requires a computational effort far from negligible.

Reference [88] has used a multi-resolution decomposition technique applied to satellite images to obtain information on the local mean value and the gradient of irradiance in different spatial scales. Other studies on short and very short time scales are available in literature, which make use of the information provided by satellites.

Concerning the current weather forecasting tools, they are based on numerical techniques, which provide good results when applied on extended spatial scales, but they are not able to collect the local variability.

The problem can be addressed using the most powerful analysis tools, especially the Artificial Intelligence techniques, which are able to achieve better results than traditional methods in many areas. The term Artificial Intelligence (AI) is a set of mathematical paradigms that address complex engineering problems replicating cognitive mode of humans. In the last few years, several researches for forecasting the solar irradiance in different timescales have been based on *Artificial Neural Networks* (ANNs), *Fuzzy Logic* (FL), *Adaptive Network based Fuzzy Inference System*(ANFIS) and *Genetic Algorithm* (GA) (for more information see Glossary).

4.2. Irradiance model on horizontal surface

Solar radiation, which affects the Earth's surface, is the result of complex interactions between the light radiation from the sun, the atmosphere and the Earth's surface. In general terms, it is subject to changes determined by the geometry of the Earth, its rotation and its revolution around the sun.

Otherwise, on a local scale, the main factor is the topography, especially the altitude, the slope, the exposure, and the shading effect caused by mountains or other natural obstacles. Some of these terms cannot be determined a priori, because they depend on the particular environmental conditions of a place, other, however, lend themselves to be represented by a mathematical model.

4.2.1 Reference coordinates for the position of the radiation source

During the year the Sun sends to Earth a certain amount of energy in the form of light radiation. An amount is reflected by clouds and atmospheric gases, another more modest part is absorbed by the atmosphere, while the remaining part, about 45 % of the total, crosses the gaseous layer surrounding the Earth without alterations. It is possible to

determine by means of appropriate geometric relationships how much of this radiation reaches locally a plane parallel to the ground [89].

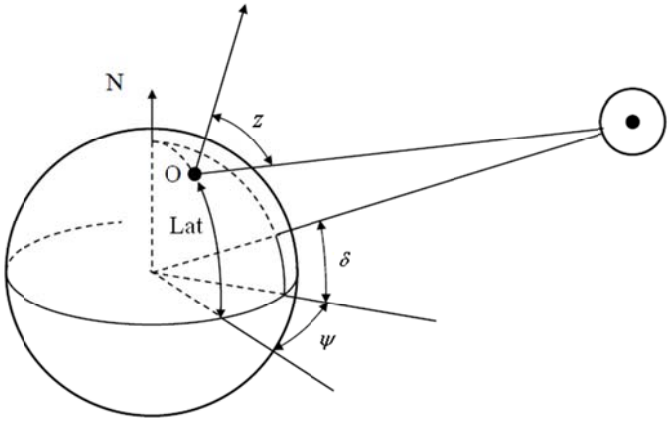

Fig. 4.1 − Hourly local coordinates of the Sun.

The first step is to determine the position of the Sun relative to an observer on the ground by using a suitable reference system, that is represented by the celestial coordinates. In this case, it is convenient to make use of hourly local coordinates (Fig. 4.1), because they depend on the position of the observer. They are:

ξ *latitude*, in radians, with respect to the equator (positive North);

ζ *longitude*, in radians, referred to the Greenwich line (positive East);

δ *solar declination angle*, that is the angle between the Sun-Earth line and the equator plane (positive North);

ψ *hour angle*, between the meridian plane passing through the observer and the meridian plane passing through the Sun (positive East);

φ *azimuth* angle between the projection of the Sun-Earth line and the plane at the horizon with South direction (positive West);

z *zenith angle* between the Sun-Earth line and the zenith direction;

α *solar height*, that is the angle between the Sun-Earth line and the horizon plane.

The *latitude* ξ and the *longitude* ζ are the only parameters that not require calculations, because are well-known at the moment in which the place of observation is fixed.

The *solar declination* δ can be found from the approximate equation of Cooper (1969):

$$\delta = \Delta_0 \frac{\pi}{180} \sin\left(\frac{2\pi(\omega_0 + g)}{g_{tot}} \right) \tag{4.1}$$

where, Δ_0=23.45°, ω_0=284, g is a progressive number that represents the day of the year, and g_{tot} is the total number of days in the year.

The *hour angle* ψ of the Sun is a more complex parameter, because it depends on the position of the observer and on the measurement of the local time.

During the course of the year, the time indicated from a meridian deviates periodically a few minutes than the time indicated by a clock, which in Italy it is normally referred to the Central European Time (CET).

This difference, neglecting the presence of the daylight savings time, is called “time equation”, τ, and it is due to the combined effect of the inclination of the ecliptic plane than the Earth's equator and the eccentricity of the orbit of the Earth around the Sun. In other words, the “time equation” component represents the conditions according to which the Sun is lagging with respect to the clock (sign +) or leading (sign -) [90].

The effects of the longitude and the time equation lead to obtain the maximum solar irradiance at a time instant different with respect to the hour 12:00. Considering the meridian line passing through the Etna volcano, with ζ_{ref}=15°, and using the value of τ taken from the time equation, the *tip hour* (i.e., the hour of maximum solar irradiance) is defined as:

$$h_t = 12 - (\zeta - \zeta_{ref})/15 + \tau \tag{4.2}$$

The *hour angle*, in radians, corresponding to the hour *h* is then defined by the following expression:

$$\psi = (h - h_t)\, 15\, \frac{\pi}{180} \tag{4.3}$$

The *azimuth angle* φ is:

$$\sin\varphi = \frac{\cos\delta\ \sin\psi}{\cos\alpha} \tag{4.4}$$

The *zenith angle z* corresponds to the expression:

$$\cos z = \sin\alpha = \cos\xi\ \cos\delta\ \cos\psi + \sin\xi\ \sin\delta \tag{4.5}$$

The *solar height* at the sunset and at the sunrise (tilt angle $\beta = 0$) is expressed as:

$$\kappa_s = \arccos(-\mathrm{tg}\xi\ \mathrm{tg}\delta) \tag{4.6}$$

The previous variables allow to identify the position of the Sun with respect to any point on the Earth's surface. However, to complete the mathematical model, it is necessary to define the intensity of irradiation.

4.2.2 Extraterrestrial radiation on a horizontal surface

From the point of view of an observer, the energy flow, which comes from the Sun, passed through the Earth's atmosphere and reached the surface of the planet, is not constant, but varies during the day and throughout the year.

It is important to note that the total radiation emitted by the Sun, that falls on a hypothetical perpendicular plane to the rays, placed at the top of the Earth's atmosphere, is almost constant in time. It is the solar constant G_{sc} and it is equal to 1360 W/m^2.

More precisely, this value is not perfectly constant, because it varies by about ± 3.3 % during the year, due to the revolution of the Earth.

At any point in time, the solar radiation incident on a horizontal plane outside of the atmosphere is the normal incident solar radiation given by [91]:

$$G_0 = G_{sc}\left(1 + 0.033\cos\frac{360n}{365}\right)\cos z \tag{4.7}$$

where n is the day of the year.

Combining the equation (4.5) with equation (4.7), it is possible to obtain G_0 for a horizontal surface at any time between sunrise and sunset:

$$G_0 = G_{sc}\left(1 + 0.033\cos\frac{360n}{365}\right)(\cos\xi\ \cos\delta\ \cos\psi + \sin\xi\ \sin\delta) \tag{4.8}$$

Integrating the equation (4.8) for a period between hour angles ψ_1 and ψ_2, which define an hour (where ψ_2 is the larger), G_0 in [MJ/m^2] is obtained, as:

$$G_0 = \frac{12\cdot 3600}{\pi} G_{sc}\left(1 + 0.033\cos\frac{360n}{365}\right)\left[\cos\xi\ \cos\delta\ (\sin\psi_2 - \sin\psi_1) + (\psi_2 - \psi_1)\sin\xi\ \sin\delta\right] \tag{4.9}$$

4.2.3 Estimation of clear-sky radiation

It is noteworthy that the solar radiation, during its travel though the atmosphere toward the earth surface, meets various phenomena, including scatter, absorption, reflection, diffusion, meteorological conditions and air mass, which change with time [92].

It is useful to define a standard “clear” sky and calculate the hourly and daily radiation which would be received on a horizontal surface under these standard conditions [93].

In order to calculate the clear sky solar radiation, several methods have been developed [94], [95]. Among these methods, the *Moon-Spencer* model provides the theoretical instantaneous values of the solar irradiance at clear sky on a surface orientated in any direction [96].

In the *Moon-Spencer* model, the contributions to the solar irradiance are partitioned into total horizontal irradiance G_{th}, beam normal irradiance G_{bn}, and horizontal diffuse irradiance G_{dh}.

The input data include the month and day of the year, converted into a progressive number g representing the day, the total number of days in the year g_{tot}, the hour of the day h, the latitude ξ and longitude ζ of the site, the tilt β and azimuth φ of the surface, and the *albedo* ρ, namely, the portion of irradiance reflected at the surface.

From the previous values, the sky-surface view factor is defined as:

$$F_{sc} = \frac{1+\cos\beta}{2} \tag{4.10}$$

The parameters of the *Moon-Spencer* model ,in Table 4.1, are used to define, in function of the day, the following constants:

- apparent solar constant A, expressed in [W/m^2]

$$A = \mu_A + \Delta_A \sin\left(\frac{2\pi(\varpi_A + g)}{g_{tot}}\right) \tag{4.11}$$

- coefficient of atmospheric extinction B

$$B = \mu_B + \Delta_B \sin\left(\frac{2\pi(\varpi_B + g)}{g_{tot}}\right) \tag{4.12}$$

- coefficient of diffuse irradiance C

$$C = \mu_C + \Delta_C \sin\left(\frac{2\pi(\varpi_C + g)}{g_{tot}}\right) \tag{4.13}$$

- solar declination as expressed in equation (4.1).

Table 4.1 − Parameters of the Moon-Spencer model.

average value	---	μ_A = 1158	μ_B = 0.17	μ_C = 0.095
deviation (amplitude)	Δ_0= 23.45	Δ_A = -73	Δ_B = 0.035	Δ_C = 0.04
deviation (phase)	ϖ_0 = 284	ϖ_A = 268	ϖ_B = 268	ϖ_C = 268

The value of the time equation, τ, is further added. At hour h, the hour angle ψ and the cosine of the zenith angle $\cos z$ are computed.

For $\cos z > 0$, the following irradiance values are obtained:

- normal beam irradiance

$$G_{bn} = A\, e^{-B/\cos z} \tag{4.14}$$

- diffuse horizontal irradiance

$$G_{dh} = C\, G_{bn} \tag{4.15}$$

- total horizontal irradiance

$$G_{th} = (C + \cos z) G_{bn} = G_{bn} \cos z + G_{dh} \tag{4.16}$$

The total irradiance is then computed in function of the auxiliary variable θ (i.e., the angle between the solar beam and the direction orthogonal to the tilt plane) evaluated in the cases with $\cos z > 0$ as:

$$\cos\theta = \sin\delta\sin\xi\cos\beta - \sin\delta\cos\xi\sin\beta\cos\Phi + \cos\delta\cos\xi\cos\beta\cos\psi + \\ + \cos\delta\sin\xi\sin\beta\cos\Phi\cos\psi + \cos\delta\sin\beta\sin\Phi\sin\psi \quad (4.17)$$

thus obtaining, for $\cos\theta > 0$, the total irradiance

$$G_t(\theta) = G_{bn}\cos\theta + G_{dh}F_{sc} + \rho G_{th}(1 - F_{sc}) \quad (4.18)$$

The irradiance values obtained from the *Moon-Spencer* model refer to free view with respect to the horizon. The results may differ in case of obstacles hiding the visual landscape, for some parts of the day, in the directions in which the Sun should impact on the surface (e.g., presence of mountains or adjacent buildings). In these cases, the results of the *Moon-Spencer* model have to be adjusted in order to take into account the actual skyline seen from the surface.

In order to compare the measured solar irradiance data with reference data set up, a dedicated variable space is created, in which the time axis is normalized in such a way to map the time interval between the sunrise and the sunset in the [0,1] interval. In the same way, the solar irradiance values are normalized in such a way that the unity value corresponds with the conditions at clear-sky taken from the *Moon-Spencer* model.

Fig. 4.2, Fig. 4.3, Fig. 4.4 and Fig. 4.5 show the comparison between the measured irradiance from the pyranometer, G_{pyr}, and the total horizontal irradiance extracted from the Moon-Spencer model, G_{th}, for the site “Gi” for the 01 July 2012, for the first week of July 2012, for the first week of January 2012 and for the whole year 2012.

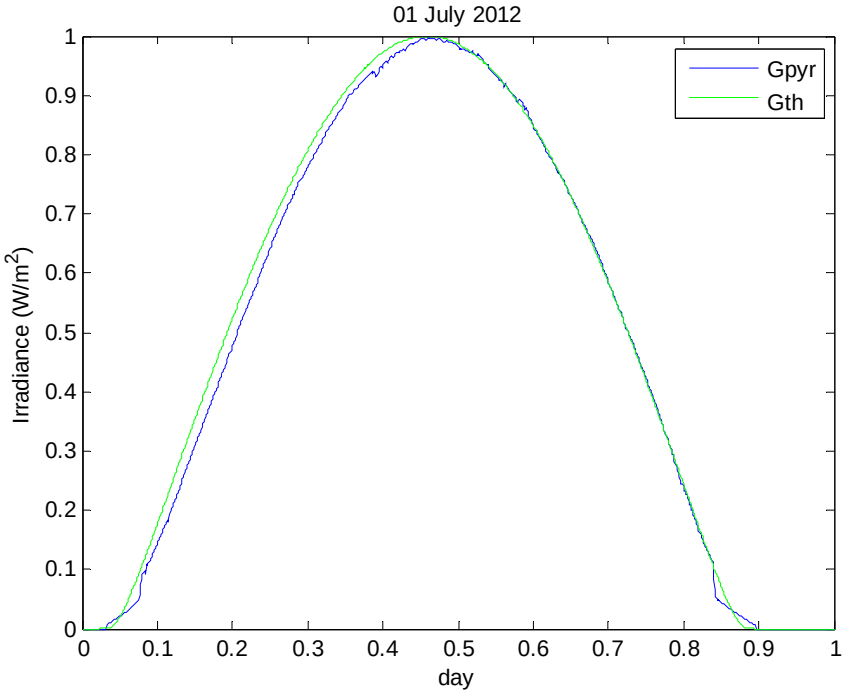

Fig. 4.2 – Irradiance values from the Moon-Spencer model (green line) vs. measured irradiance values (blue line) for 01 July 2012 in the site "Gi".

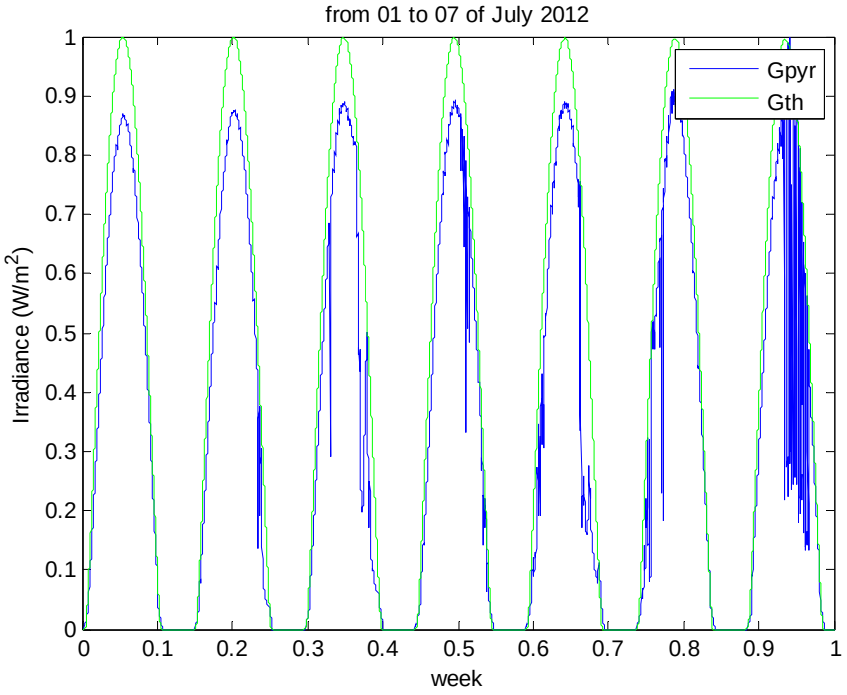

Fig. 4.3 – Irradiance values from the Moon-Spencer model (green line) vs. measured irradiance values (blue line) for the first week of July 2012 in the site "Gi".

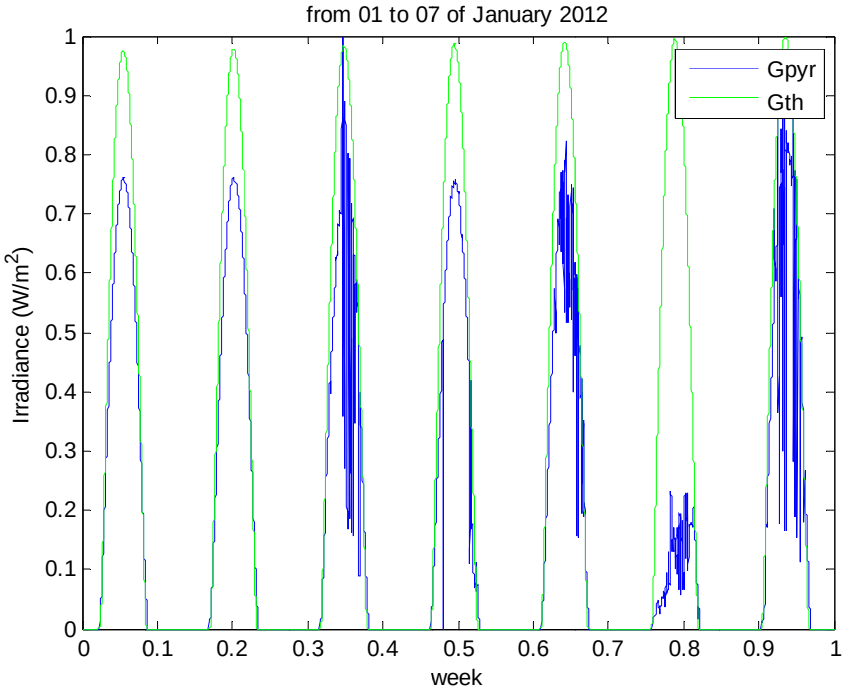

Fig. 4.4 – Irradiance values from the Moon-Spencer model (green line) vs. measured irradiance values (blue line) for the first week of January 2012 in the site "Gi".

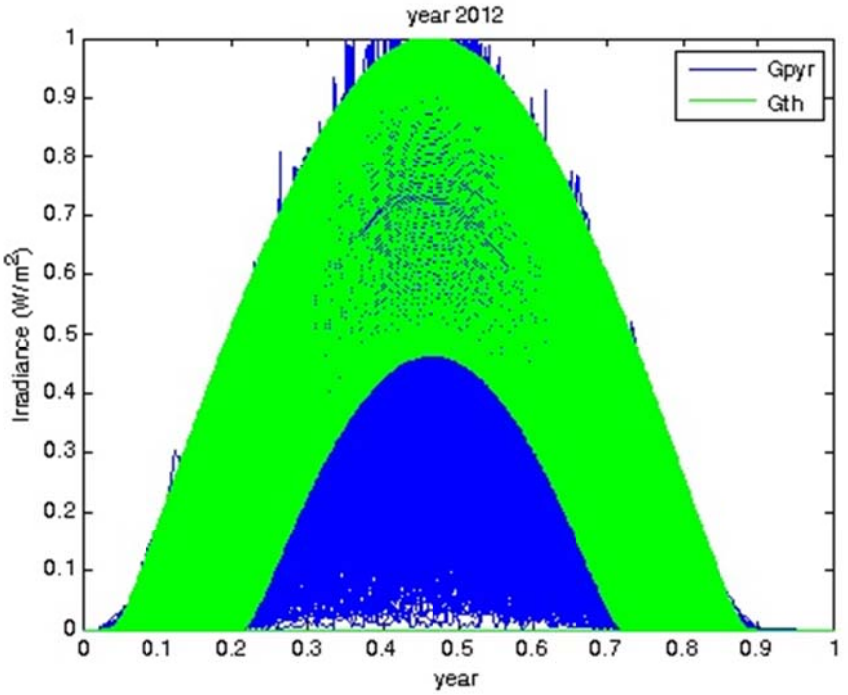

Fig. 4.5 – Irradiance values from the Moon-Spencer model (green line) vs. measured irradiance values (blue line) for the year 2012 in the site "Gi".

4.3 Beam and Diffuse Components of hourly irradiation

The amount of solar radiation that reaches the ground, besides the daily and yearly apparent motion of the sun, depends on the geographical location (latitude and longitude) and on the climatic conditions (e.g. cloud cover). Many studies have proved that cloudiness is the main factor affecting the difference between the values of solar irradiation measured outside the atmosphere and on the Earth surface.

The split of total solar irradiation on a horizontal surface into its diffuse and beam components is of paramount interest. The main reason is that calculation methods of total irradiation on surfaces of different tilt orientation from data on a horizontal surface require separate treatments of beams and diffuse radiation [97].

In order to give an hourly classification of sky conditions, it is possible to correlate k_d, defined as the fraction of the hourly irradiation on a horizontal plane which is diffuse, with the *hourly clearness index* $k_t = G_{th} / G_0$, defined as the ratio of the irradiance on the horizontal plane G_{th} [kW/m^2], that is the commonly available pyranometer measurement, to the extra-atmospheric total solar irradiance G_0 [kW/m^2].

For this purpose, several correlations have been proposed to establish a relationship between diffuse and total global horizontal irradiance. As explained in De Miguel et al. [98], some of the existing models [99], [100] have been developed for northern latitudes with high albedos and air masses. This is the reason for differences in diffuse radiation values and an error source in modelling diffuse solar irradiation [101], [102].

Only in most recent years, the development of models to calculate daily/hourly diffuse irradiation from the respective daily/hourly global value for the European Mediterranean area occurred.

Therefore, the hourly correlations taken into account in this context are represented by the following expressions:

$$k_d = \begin{cases} 0.995 - 0.081 k_t & for \quad k_t \le 0.21 \\ 0.724 + 2.738 k_t - 8.32 k_t^{\,2} + 4.967 k_t^{\,3} & for \quad 0.21 < k_t \le 0.76 \\ 0.180 & for \quad k_t > 0.76 \end{cases} \tag{4.19}$$

The correlations, above mentioned, permit to give an hourly classification of the sky conditions. In particular, it is possible to note that for k_t greater than 0.76 a linear expression is presented, with the meaning that the sun is not obscured by clouds, i.e. a clear-sky condition occurs, on the contrary for $k_t \le 0.21$ a constant value is presented, with the meaning that a total cloudy (i.e. overcast) sky condition occurs, while for the range $0.21 < k_t \le 0.76$, the correlation is represented by a cubic polynomial expression, with the meaning that a variable (i.e. partly-cloudy) sky condition occurs, in which the sun is partially obscured by clouds.

4.4 Forecast data

As it is known, meteorological data can be considered as widely variable sources and for this reason, it is important to forecast models of these meteorological data. In this chapter, forecast weather data, provided by the meteorological service of Catalonia (*Meteo.cat* [103]) have been used.

The available data are based on the *Weather Research and Forecasting* (WRF) [104] model: a next-generation mesoscale numerical weather prediction system designed to serve both atmospheric research and operational forecasting needs. It features two dynamical cores, a data assimilation system, and a software architecture allowing for parallel computation and system extensibility. The model serves a wide range of meteorological applications across scales ranging from meters to thousands of kilometers.

As regards the available irradiance prediction data, the forecast length is 72 hours, with an output sampling rate of three hours. Therefore, in order to compare with the measured data, the forecast data have been first interpolated (polynomial splines) [105] and the daily evolution of irradiance is classified into three categories: clear, variable and cloudy sky.

The data set provided by *Meteo.cat* consists of the solar radiation forecasts for only two of the five meteorological stations, “Gi” and “Ma”, during the whole year 2012. The other three sites are outside the boundary limits of *Meteo.cat* provider.

4.5 Hourly classification in clear, variable and cloudy sky according to the clearness index values

On the basis of the hourly correlations (eq. 4.19) presented in the work of De Miguel et al., it has been developed an algorithm, which permits to classify each hour of a day as clear, cloudy or variable. This algorithm essentially consists of two parts.

In the first part, the hourly classification procedure has been developed examining the value of the *hourly clearness index* k_t calculated as the ratio of the solar irradiance of the pyranometer to the extra-atmospheric total solar irradiance G_0.

In the second part, the classification procedure has also been developed taking into account the hourly clearness index value (called synthetically k_{tf}) calculated as the ratio between the 1-day ahead prediction data, considered as more accurate measurement, and G_0.

Moreover, in order to estimate the number of occurrences of "broken clouds" in a day, an additional control was performed. As previously said (Chapter 3 section 3.2), the presence of "broken clouds" appear when the sky is mainly clear, but the passage of clouds affects the irradiance evolution. For this purpose, it has been considered as clear-sky model, the one provided by the PVGIS online software [73].

So, establishing a threshold value, equal to the maximum clear-sky irradiance value on a fixed plane, G_{max_PVGIS}, (e.g. for the month of July in the site "Gi" it is equal to 1020 W/m^2), if the global irradiance of one of the 30° tilted solar cells, G_{tcell}, exceeds this threshold, then the presence of broken clouds can be considered.

In section 4.5.1 and 4.5.2, the measurements from the pyranometer (G_{pyr}), the three-hour predictions from *Meteo.cat* by satellite (represented with circles in the following figures) and the interpolated predictions (polynomial splines) are shown for the sites "Gi" and

"Ma" for the month of July 2012, when the irradiation is at maximum. Moreover, only the daylight hours (from 5 a.m. to 7 p.m.) were considered.

As per the three days ahead forecast data, the red line corresponds to the 1-day ahead prediction, the blue line corresponds to the 2-day ahead prediction and the green line corresponds to the 3-day ahead prediction.

4.5.1 Experimental results for the site "Gi"

In Fig. 4.6, the first week of the month of July 2012 is shown for the site "Gi". The hourly algorithm related to the measurements from the pyranometer classifies all the hours of these days as variable. On the other hand, concerning the hourly algorithm for the prediction of the 1-day before, all the hours of only the first 3 days of July are classified as variable.

More precisely, only the first day follows perfectly the predictions and the hourly clearness index k_t is between 0.27 and 0.69, while the hourly clearness index for the 1-day ahead prediction k_{tf} is between 0.67 and 0.75: maybe white clouds can have filtered radiations. The second day is different from the predictions in the hours from 4 p.m. to 6 p.m., and in particular at 6 p.m. it is considered as cloudy with k_t=0.18, on the contrary k_{tf}= 0.68 in the same hour, in all other hours the values of k_t is in the range0.26 − 0.69, on the contrary k_{tf} is between 0.66 and 0.74.

On 3 July k_t is between 0.39 and 0.72 until 2 p.m., while k_{tf} is in the range 0.68 − 0.75. At 3 p.m., the solar irradiance value of the pyranometer goes down to 200 W/m^2 (k_t=0.31, while k_{tf}=0.75), then this value decreases much more at 5 p.m. and the situation is cloudy with k_t=0.20, while k_{tf}=0.71.

A similar situation occurs on 5 July, in which k_t is in the range0.33 − 0.75 until 2 p.m., then from 3 p.m. to 6 p.m. k_t is within 0.37 and 0.24.The simulation related to the 1-day

ahead prediction classifies the hours from 9 a.m. to 4 p.m. as clear-sky, with k_{tf} in the range 0.77 − 0.78, and the remaining hours as variable, with k_{tf} in the range 0.72 − 0.74.

On 4 July k_t is between 0.38 and 0.74 until 12 a.m., then the forecast data are different from the pyranometer measurements in the second part of the day, i.e. from 1 p.m. to 3 p.m. and from 5 p.m. to 6 p.m., in which k_t is 0.50 and 0.27, respectively. As per the 1-day ahead prediction, the situation is similar to day 5, in which the hours from 10 a.m. to 4 p.m. are classified as clear-sky, with k_{tf} in the range 0.77−0.78, and the remaining hours as variable, with k_{tf} in the range 0.70−0.75.

An opposite situation takes place on 6 July, when the measurements are different respect to the predictions in the first part of the day, i.e. from 6 a.m. to 10 a.m. and from 11 a.m. to 6 p.m., in which k_t is in the range0.32−0.75.Also in this case, the situation for the 1-day ahead prediction is analogous to days 4 and 5, in which the hours from 10 a.m. to 4 p.m. as clear-sky, with k_{tf} in the range 0.76−0.78, and the remaining hours as variable, with k_{tf} in the range 0.69−0.75.

On day 7, the hourly variability is enhanced in the hours from 12 a.m. to 4 p.m. and from 11 a.m. to 5 p.m., in which k_t is in the range 0.38−0.72, on the contrary the simulation related to the 1-day ahead prediction classifies these hours as clear-sky, with k_{tf} within 0.77. Moreover, the presence of broken clouds on this day is verified for 39 minutes.

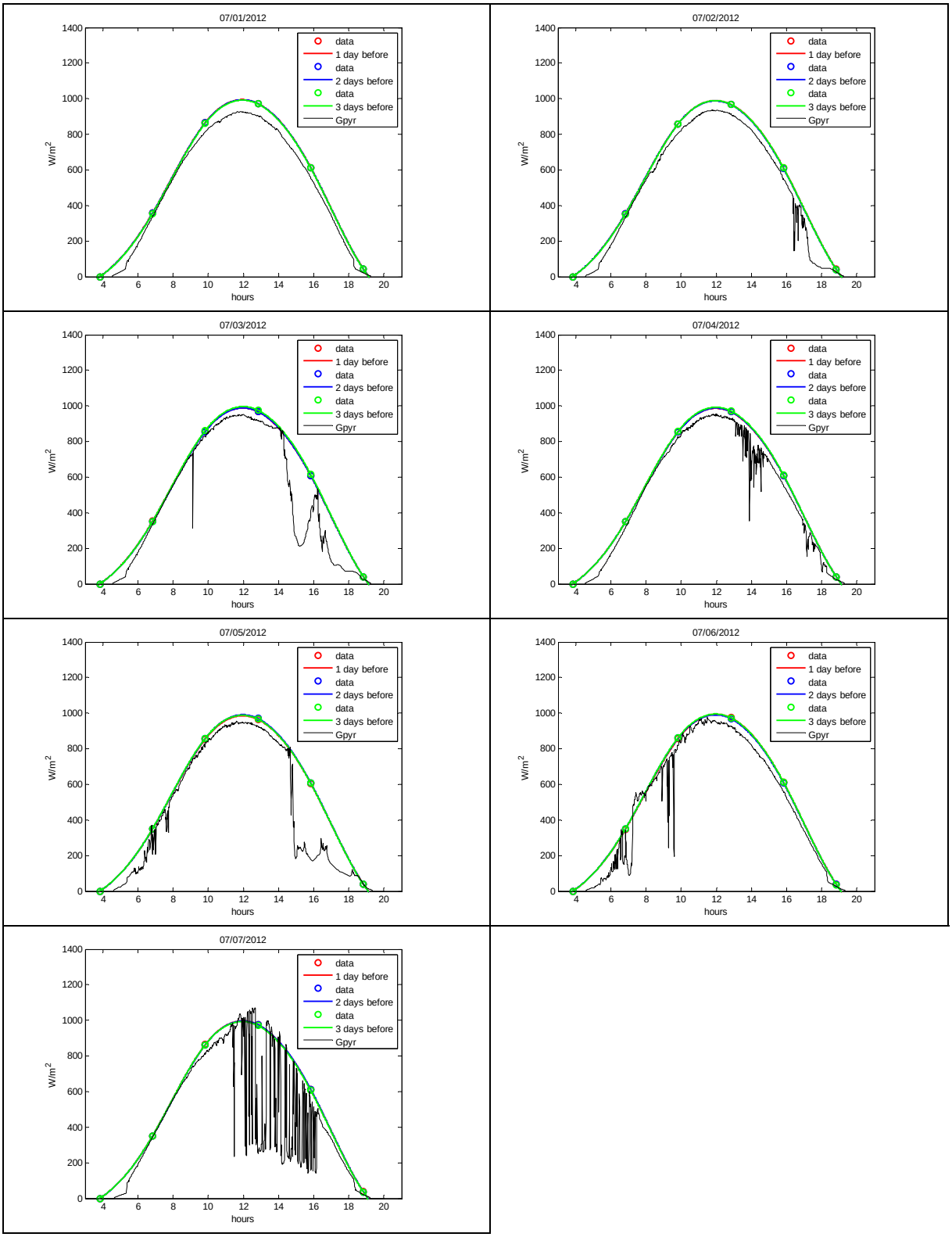

Fig. 4.6 − Measurements from the pyranometer, the three-hour predictions from Meteo.cat and the interpolated predictions from 01 July 2012 to 07 July 2012 for the site “Gi”.

In Fig. 4.7 the second week of the month of July 2012 is shown. The trends that follows well the predictions are related to day 09 and day 11.The latter day follows well only to the prediction of 1-day before and 3-day before. As per day 9, both the clearness index from the pyranometer and the same index for the 1-day ahead prediction classify all hours as variable, with k_t in the range 0.31 − 0.70 and k_{tf} in the range 0.68 − 0.75. Days 08 and 10 have a greater cloud cover in the hours from 1 p.m. to 2 p.m., considering the pyranometer measurements, in which k_t is about 0.65−0.68, on the contrary for all other hours of these days k_t is between 0.31 and 0.71.

As per day 08, the simulation related to the 1-day ahead prediction classifies all the hours as variable, with k_{tf} in the range0.67 − 0.74.On the other hand, the simulation related to the 1-day ahead prediction on day 10 classifies the hours from 9 a.m. to 3 p.m. as clear-sky, with k_{tf} between 0.76 and 0.77, and the remaining hours as variable, with k_{tf} in the range 0.70 − 0.75.

As mentioned before, unlike the previous days, in which the three days predictions are almost overlapped, for day 11 the prediction of 2-day before is closer to the pyranometer measurements and k_t is between 0.34 and 0.75. For this day, the simulation related to the prediction of 1-day before classifies the hours from 9 a.m. to 4 p.m. as clear-sky, with k_{tf} between 0.72 and 0.80, and the remaining hours as variable, with k_{tf} in the range 0.72 − 0.75.

On 12 July, the hourly algorithm related to the measurements from the pyranometer classifies all the hours of this day as variable. The hourly variability is enhanced in the hours from 12 a.m. to 4 p.m. and from 11 a.m. to 5 p.m., in which k_t is in the range 0.30 − 0.60. Moreover, the presence of broken clouds is verified for 31 minutes. As per the simulation related to the 1-day ahead prediction on day 12, it classifies the hours from 9 a.m. to 4 p.m. as clear-sky, with k_{tf} between 0.77 and 0.78, and the remaining hours as variable, with k_{tf} in the range 0.71 − 0.75.

Days 13 and 14 follow quite well the forecast trends, and k_t is in the range 0.32 – 0.75. For day 13, the simulation related to the 1-day ahead prediction classifies the hours from

10 a.m. to 3 p.m. as clear-sky, with k_{tf} within 0.77, and the remaining hours are classified as variable, with k_{tf} in the range $0.69 - 0.75$. For day 14, the simulation related to the 1-day ahead prediction classifies all the hours as variable, with k_{tf} in the range $0.68 - 0.74$.

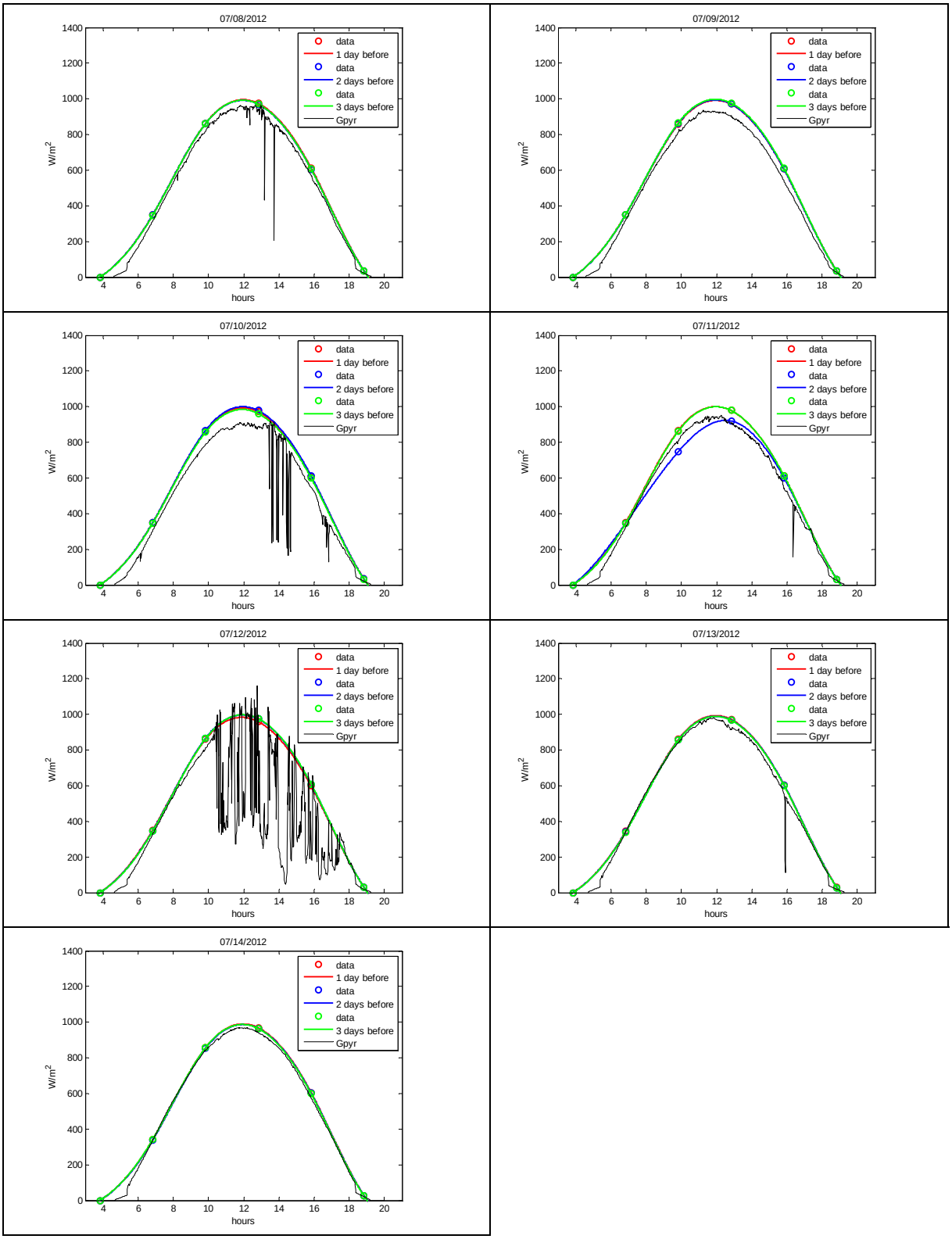

Fig. 4.7 − Measurements from the pyranometer, the three-hour predictions from Meteo.cat and the interpolated predictions from 08 July 2012 to 14 July 2012 for the site “Gi”.

With respect to Fig. 4.8, the hourly classification algorithm, related to the pyranometer measurements, considers all the hours of the days from 15 to 21 July as variable.

In fact, this variability is very pronounced on day 16 in the hours from 1 p.m. to 4 p.m., in which k_t is between 0.64 and 0.70, and the presence of broken clouds is verified for 6 minutes. For this day, the simulation related to the 1-day ahead prediction classifies the hours from 10 a.m. to 3 p.m. as clear-sky, with $k_{tf} > 0.76$, and the remaining hours as variable, with k_{tf} in the range $0.70 - 0.75$.

Day 15 has a similar trend to that of days 13 and 14, with k_t in the range 0.32 – 0.75 and k_{tf} in the range$0.68 - 0.74$.

As for days 17 and 18, the algorithm related to the pyranometer measurements classifies five hours in the morning as clear, i.e. from 9 a.m. to 1 p.m. and from 10 a.m. to 2 p.m. respectively, with k_t in the range from 0.77 and 0.78. The remaining hours of the day are considered variable, with k_t between 0.32 and 0.75.

The simulation related to the 1-day ahead prediction on day 17 and day 18 classifies the hours from 8 a.m. to 5 p.m. as clear-sky, with k_{tf} between 0.77 and 0.80, and the remaining hours as variable, with k_{tf} between 0.73 and 0.75. As per days 19, 20 and 21, the algorithm related to the pyranometer measurements considers all hours of these days as variable, with k_t in the range 0.31 – 0.75.

As per the simulation related to the 1-day ahead prediction on day 19, it classifies the hours from 9 a.m. to 4 p.m. as clear-sky, with k_{tf} between 0.77 and 0.78, and the remaining hours as variable, with k_{tf} in the range $0.71 - 0.74$. Similarly for day 20, the 1-day ahead prediction simulation classifies the hours from 11 a.m. to 13 p.m., as clear-sky, with $k_{tf} > 0.76$, and the remaining hours as variable, with k_{tf} in the range $0.69 - 0.75$.

Unlike the other days, for day 21 the mismatch between the pyranometer measurement and 3 days prediction is observed. The simulation related to the 1-day ahead prediction classifies all the hours as variable, with k_{tf} in the range$0.67 - 0.74$.

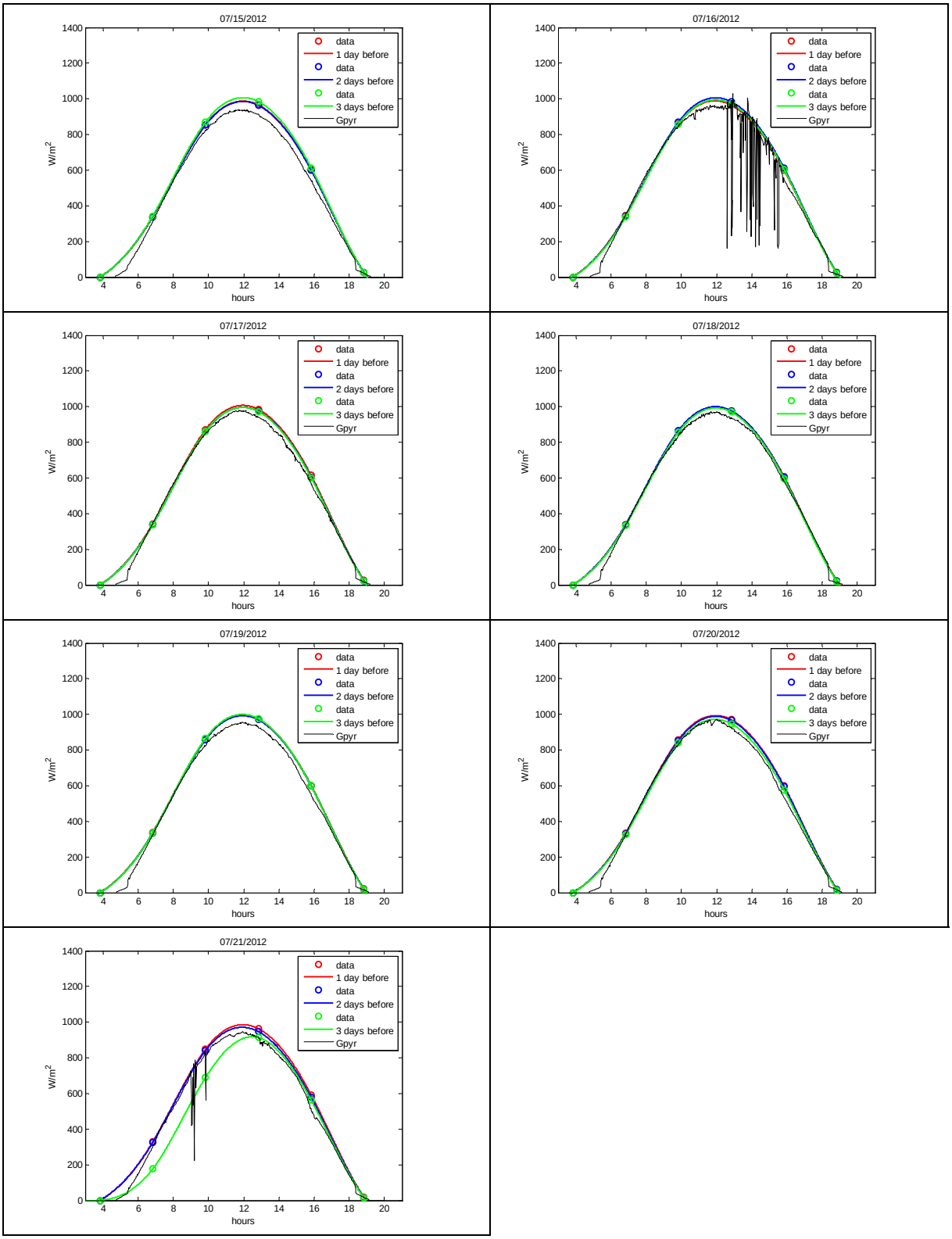

Fig. 4.8 − Measurements from the pyranometer, the three-hour predictions from Meteo.cat and the interpolated predictions from 15 July 2012 to 21 July 2012 for the site “Gi”.

In Fig. 4.9 the trends from day 22 to day 28 are shown. In particular, on day 22 the sky variability is very pronounced, especially from 12 a.m. to 2 p.m., in which the presence of broken clouds occurs for 20 minutes and k_t is 0.48 – 0.70. For this day, the prediction of 2-day before is deviated on the performance measured by the pyranometer. The simulation related to the 1-day ahead prediction on day 22 classifies all the hours as variable, with k_{tf} in the range 0.68 − 0.75.

The hours from 5 a.m. to 8 a.m. of days 23 and 24 are classified by the algorithm related to the pyranometer measurements as cloudy, in which k_t is between 0.04 and 0.16, and the value of the pyranometer irradiance does not reach 200 W/m^2. This situation is also repeated at 3 p.m. for day 23 in which k_t = 0.20, and at 6 p.m. for day 24 in which k_t = 0.13. Furthermore, for day 24 the presence of broken clouds occurs for 103 minutes, and at 10 a.m. the algorithm classifies this hour as clear, with k_t= 0.83. The simulation related to the 1-day ahead prediction of day 23 classifies all the hours as variable, with k_{tf} in the range 0.36 − 0.67.

For day 24, the forecast simulation of 1-day before classifies the hours from 9 a.m. to 4 p.m. as clear-sky, with k_{tf} between 0.77 and 0.78, and the remaining hours as variable, with k_{tf} between 0.70 and 0.73. As per the days from 25 to 28 July 2012, the hourly algorithm related to the measurements from the pyranometer classifies all the hours as variable. Of these days, the greater variability of the sky is for days 25 and 26. In particular, for day 25 the algorithm indicates the situation of cloudy sky with k_t= 0.18 at 4 p.m.. Moreover, in this day the presence of broken clouds occurs for 1 h and the hourly values of k_t (between 0.22 and 0.68) are lower than the ones of day 26 (between 0.31 and 0.72), in which the presence of broken clouds occurs for 32 min only. As per the simulation related to the 1-day ahead prediction of day 25, the hours from 10 a.m. to 3 p.m. as clear-sky, with k_{tf} within 0.77, and the remaining hours as variable, with k_{tf} in the range 0.71 − 0.74. For day 26, the simulation related to the 1-day ahead prediction classifies all the hours as variable, with k_{tf} in the range0.67 − 0.75. Days 27 and 28 have hourly values of k_t within the range from 0.33 and 0.72 and k_{tf} between0.67 − 0.75.

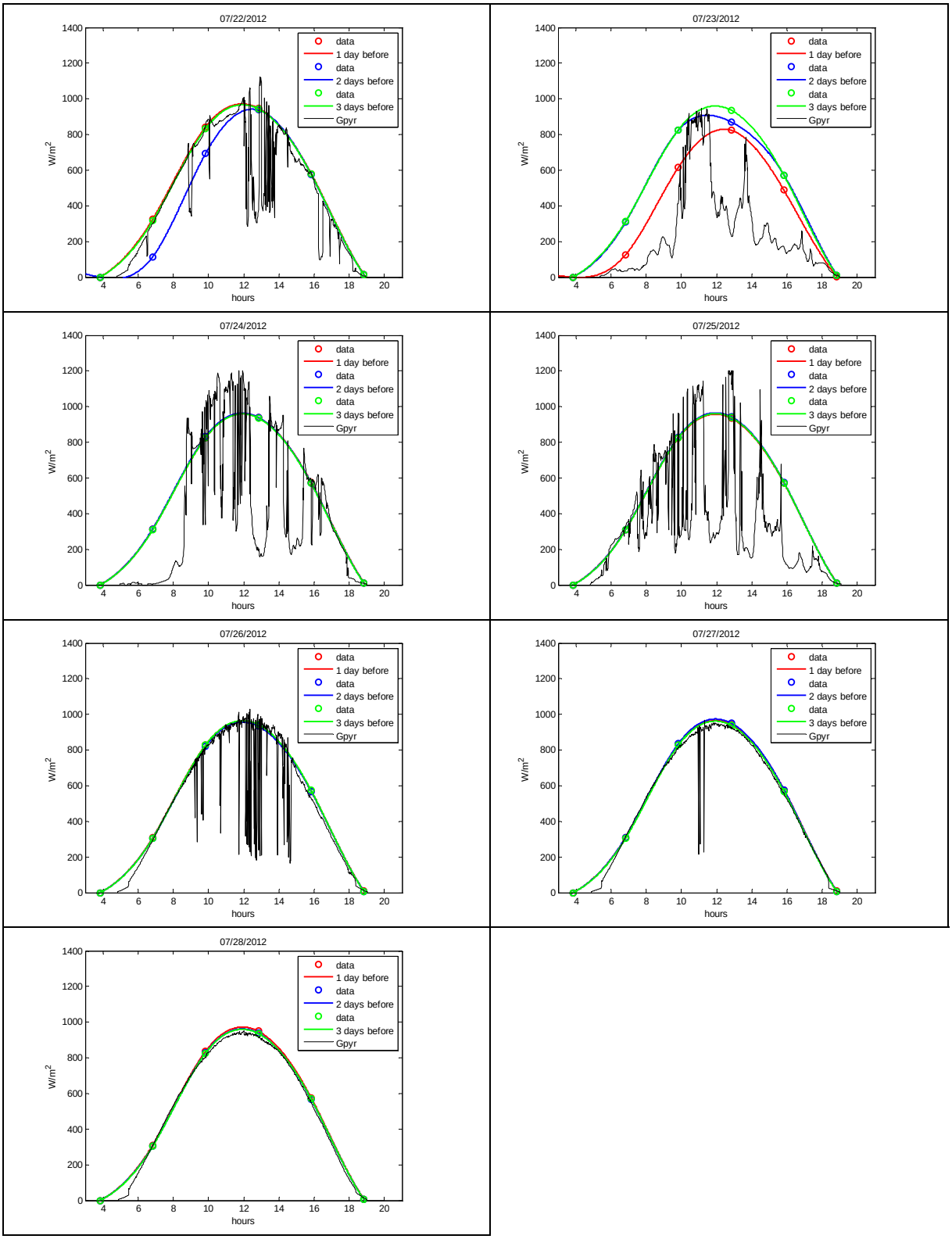

Fig. 4.9 − Measurements from the pyranometer, the three-hour predictions from Meteo.cat and the interpolated predictions from 22 July 2012 to 28 July 2012 for the site “Gi”.

In Fig. 4.10 the trends from day 29 to day 31are shown. As per day 29, the hourly algorithm related to the measurements from the pyranometer classifies all the hours as variable, with k_t within the range from 0.27 and 0.70. The simulation related to the 1-day ahead prediction on day 29 considers the hours from 10 a.m. to 2 p.m. as clear-sky, with $k_{tf} > 0.76$, and the remaining hours as variable, with k_{tf} in the range $0.72 - 0.75$.

Day 30 is classified as variable by the hourly algorithm related to the measurements from the pyranometer and the values of k_t are in the range between 0.37 and 0.75, with the exception at hour 11 a.m., in which k_t is >0.76 and it is considered as clear-sky. For this day the presence of broken clouds is estimated for only 8 minutes.

Day 31 is considered as clear-sky at 11 a.m. and 12 a.m. by the hourly algorithm with $k_t>0.76$, while in the other hours of the day it is considered as variable with k_t between 0.38 and 0.75.

The simulation related to the 1-day ahead prediction on days 30 and 31 classifies the hours from 9 a.m. to 4 p.m. as clear-sky, with k_{tf} between 0.77 and 0.79, and the remaining hours as variable, with k_{tf} between 0.71 and 0.75.

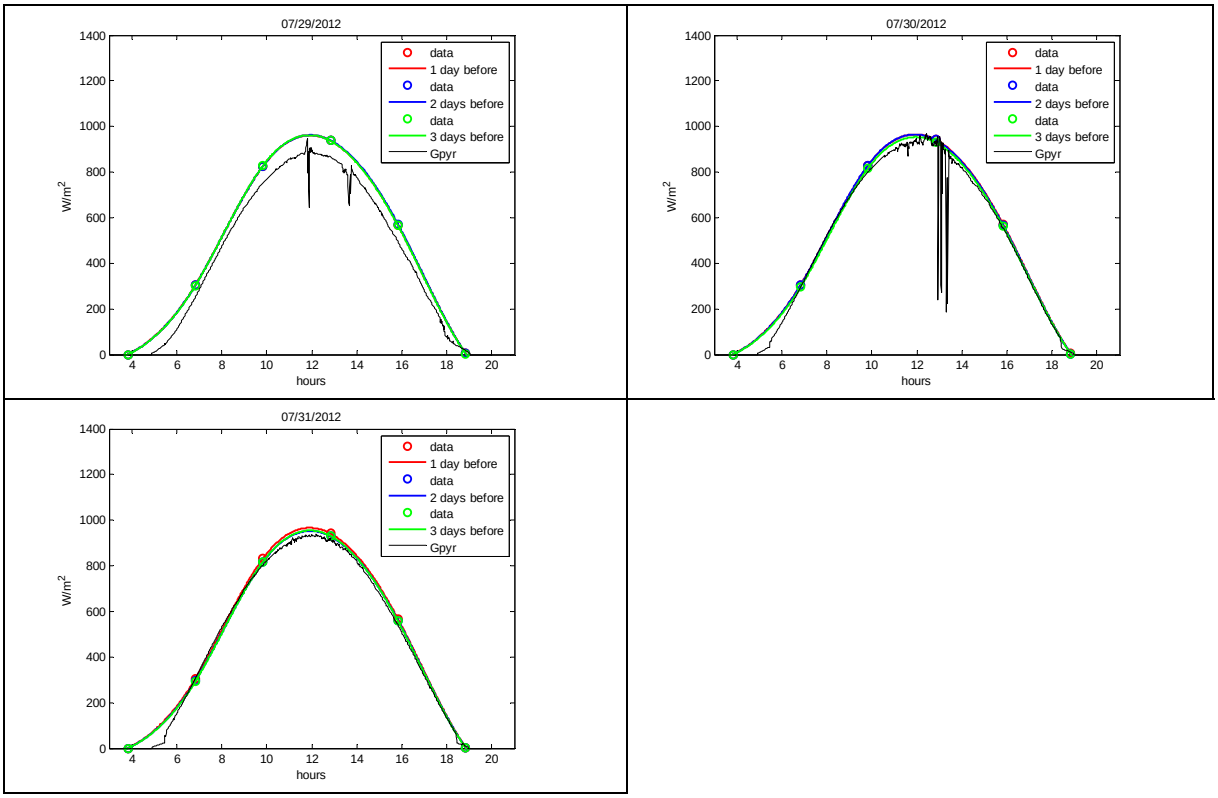

Fig. 4.10 − Measurements from the pyranometer, the three-hour predictions from Meteo.cat and the interpolated predictions from 29 July 2012 to 31 July 2012 for the site “Gi”.

In Table 4.2, Table 4.3, Table 4.4, Table 4.5, Table 4.6 and Table 4.7 the number of passes/fails (in hour) recorded by the hourly classifications from pyranometer measurements with respect to the hourly classifications from 1-day before forecast are summarized for all the month of the year 2012 for the site “Gi”.

As can be seen, for summer months, in particular for July, the highest number of hourly passes in which the prediction coincides with the measurement data of the pyranometer occurs for the variable − variable condition.

Moreover, it is noteworthy that the condition in which the hourly classification related to the pyranometer measurements is variable and that related to the 1-day ahead prediction is clear, occurs mainly in the middle hours of the day, from 10 a.m. to 3p.m., in those days with greater occurrence of “broken clouds”.

For winter months, the highest number of hourly passes occurs for the cloudy – cloudy condition. On the other hand, in spring months a great number of hourly fails for the variable – clear condition is recorded. The low number of clear days, especially in spring and summer months, can be explained by the actual turbidity in air, higher than the predicted turbidity: the pollution can play a fundamental role. It was also seen from the comparison with the clear-sky Moon-Spencer model (see Section 4.2.3).

Table 4.2 – Number of passes/fails by the hourly classification for the months of January and February 2012 for the site "Gi".

January			February		
Hourly classification from pyranometer measurements	Hourly classification from the day before prediction	N° of pass/fail (hour)	Hourly classification from pyranometer measurements	Hourly classification from the day before prediction	N° of pass/fail (hour)
Variable	Variable	114	Variable	Variable	64
Clear	Clear	39	Clear	Clear	31
Cloudy	Cloudy	160	Cloudy	Cloudy	149
Variable	Clear	21	Variable	Clear	50
Variable	Cloudy	4	Variable	Cloudy	2
Clear	Variable	50	Clear	Variable	21
Clear	Cloudy	0	Clear	Cloudy	0
Cloudy	Variable	49	Cloudy	Variable	88
Cloudy	Clear	28	Cloudy	Clear	30
Tot. Passes		313	Tot. Passes		244
Tot. Fails		152	Tot. Fails		191

Table 4.3 – Number of passes/fails by the hourly classification for the months of March and April 2012 for the site "Gi".

March			April		
Hourly classification from pyranometer measurements	Hourly classification from the day before prediction	N° of pass/fail (hour)	Hourly classification from pyranometer measurements	Hourly classification from the day before prediction	N° of pass/fail (hour)
Variable	Variable	104	Variable	Variable	106
Clear	Clear	35	Clear	Clear	44
Cloudy	Cloudy	89	Cloudy	Cloudy	59
Variable	Clear	99	Variable	Clear	146
Variable	Cloudy	4	Variable	Cloudy	0
Clear	Variable	52	Clear	Variable	6
Clear	Cloudy	1	Clear	Cloudy	0
Cloudy	Variable	35	Cloudy	Variable	58
Cloudy	Clear	46	Cloudy	Clear	31
Tot. Passes		228	Tot. Passes		209
Tot. Fails		237	Tot. Fails		241

Table 4.4 – Number of passes/fails by the hourly classification for the months of May and June 2012 for the site "Gi".

May			June		
Hourly classification from pyranometer measurements	Hourly classification from the day before prediction	N° of pass/fail (hour)	Hourly classification from pyranometer measurements	Hourly classification from the day before prediction	N° of pass/fail (hour)
Variable	Variable	147	Variable	Variable	186
Clear	Clear	25	Clear	Clear	15
Cloudy	Cloudy	12	Cloudy	Cloudy	29
Variable	Clear	213	Variable	Clear	212
Variable	Cloudy	0	Variable	Cloudy	0
Clear	Variable	2	Clear	Variable	0
Clear	Cloudy	0	Clear	Cloudy	0
Cloudy	Variable	43	Cloudy	Variable	5
Cloudy	Clear	23	Cloudy	Clear	3
Tot. Passes		184	Tot. Passes		230
Tot. Fails		281	Tot. Fails		220

Table 4.5 – Number of passes/fails by the hourly classification for the months of July and August 2012 for the site "Gi".

July			August		
Hourly classification from pyranometer measurements	Hourly classification from the day before prediction	N° of pass/fail (hour)	Hourly classification from pyranometer measurements	Hourly classification from the day before prediction	N° of pass/fail (hour)
Variable	Variable	266	Variable	Variable	221
Clear	Clear	14	Clear	Clear	11
Cloudy	Cloudy	9	Cloudy	Cloudy	25
Variable	Clear	142	Variable	Clear	191
Variable	Cloudy	0	Variable	Cloudy	0
Clear	Variable	0	Clear	Variable	0
Clear	Cloudy	0	Clear	Cloudy	0
Cloudy	Variable	33	Cloudy	Variable	16
Cloudy	Clear	1	Cloudy	Clear	1
Tot. Passes		289	Tot. Passes		257
Tot. Fails		176	Tot. Fails		208

Table 4.6 – Number of passes/fails by the hourly classification for the months of September and October 2012 for the site "Gi".

September			October		
Hourly classification from pyranometer measurements	Hourly classification from the day before prediction	N° of pass/fail (hour)	Hourly classification from pyranometer measurements	Hourly classification from the day before prediction	N° of pass/fail (hour)
Variable	Variable	199	Variable	Variable	156
Clear	Clear	27	Clear	Clear	12
Cloudy	Cloudy	86	Cloudy	Cloudy	105
Variable	Clear	101	Variable	Clear	99
Variable	Cloudy	1	Variable	Cloudy	16
Clear	Variable	10	Clear	Variable	19
Clear	Cloudy	0	Clear	Cloudy	8
Cloudy	Variable	16	Cloudy	Variable	39
Cloudy	Clear	10	Cloudy	Clear	11
Tot. Passes		312	Tot. Passes		273
Tot. Fails		138	Tot. Fails		192

Table 4.7 – Number of passes/fails by the hourly classification for the months of November and December 2012 for the site "Gi".

November			December		
Hourly classification from pyranometer measurements	Hourly classification from the day before prediction	N° of pass/fail (hour)	Hourly classification from pyranometer measurements	Hourly classification from the day before prediction	N° of pass/fail (hour)
Variable	Variable	116	Variable	Variable	104
Clear	Clear	0	Clear	Clear	20
Cloudy	Cloudy	172	Cloudy	Cloudy	192
Variable	Clear	5	Variable	Clear	14
Variable	Cloudy	4	Variable	Cloudy	4
Clear	Variable	51	Clear	Variable	66
Clear	Cloudy	0	Clear	Cloudy	0
Cloudy	Variable	76	Cloudy	Variable	64
Cloudy	Clear	26	Cloudy	Clear	1
Tot. Passes		288	Tot. Passes		316
Tot. Fails		162	Tot. Fails		149

It is useful to calculate the deviations of 2-day ahead prediction with respect to the 1-day ahead prediction, considered as the most accurate, and the deviations of 3-day ahead prediction with respect to the 1-day ahead prediction as follows:

$$\Delta G_{21} = G_{2\text{-}day} - G_{1\text{-}day} \tag{4.20}$$

$$\Delta G_{31} = G_{3\text{-}day} - G_{1\text{-}day} \tag{4.21}$$

The mean value is calculated for an output cadence of 3 hours. In the following figures (Fig. 4.11 – Fig. 4.22) positive and negative deviations are shown for the site "Gi". Positive deviations occur when the 2-day ahead forecast and 3-day ahead forecast are higher than the 1-day ahead forecast. On the contrary, negative deviations occur when the 1-day ahead prediction is higher than the other two forecasts.

In summer months, positive and negative deviations are quite negligible (< 20 W/m^2), with the exception of a few days of July (i.e. 21, 22 and 23), in which deviations are > 70 W/m^2.

Major deviations occur in winter, spring and autumn months. In particular, in March, April and May, the deviations are higher than 160 W/m^2.

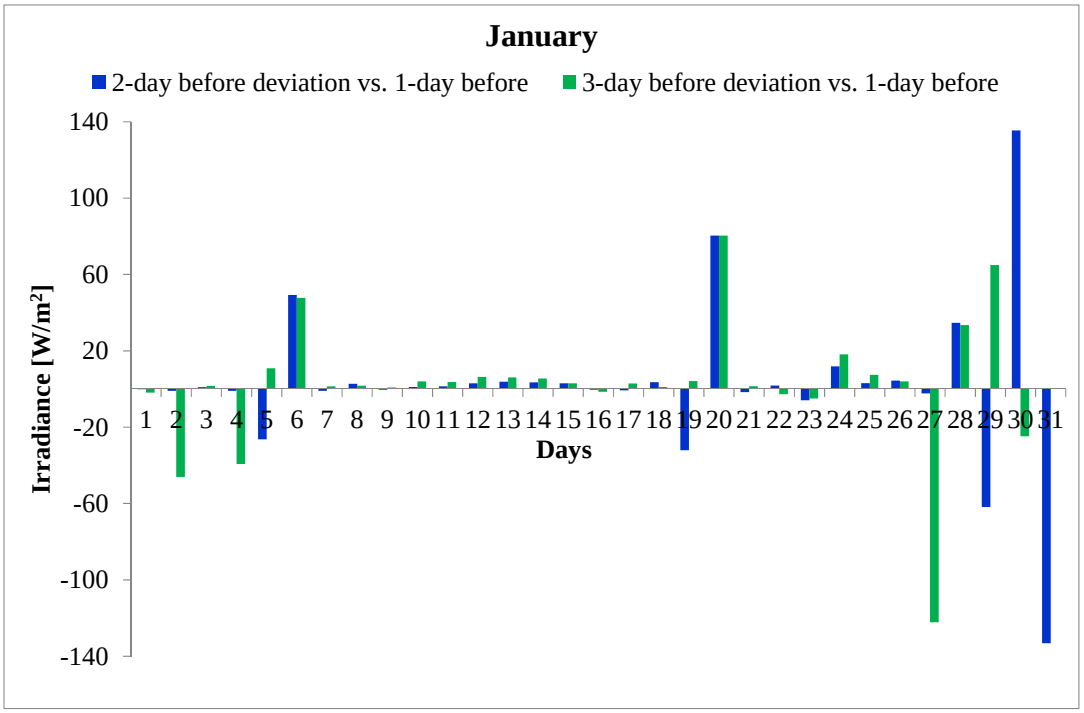

Fig. 4.11 – Deviations of 2, 3-day ahead forecasts vs. 1-day ahead forecasts for the month of January 2012 for the site “Gi”.

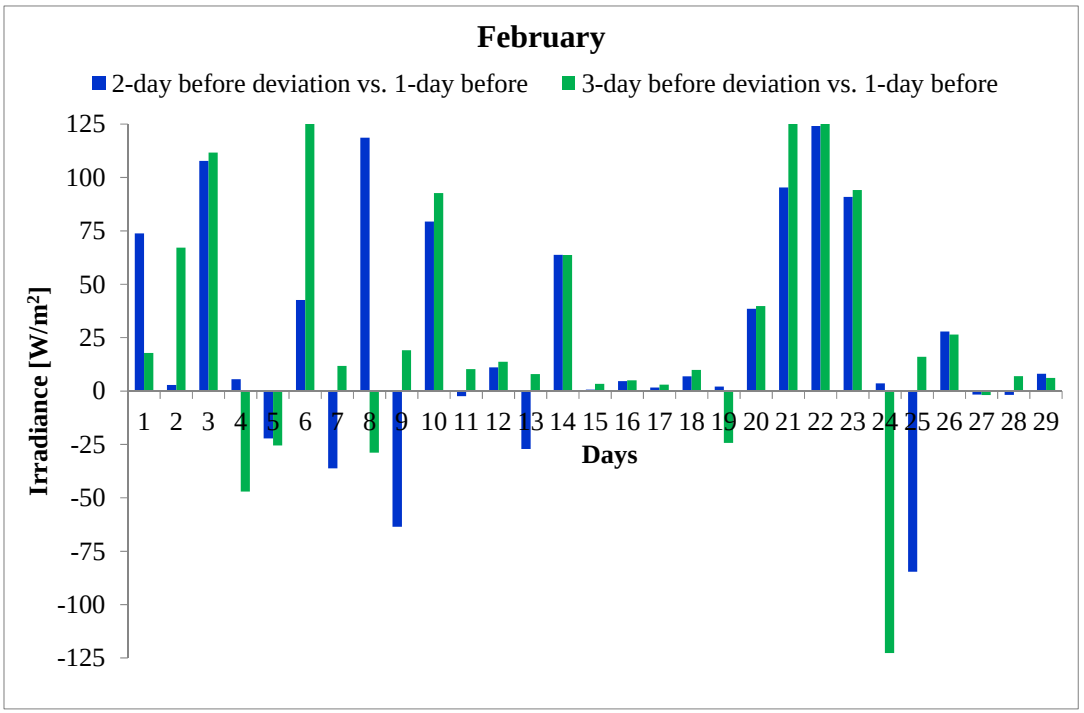

Fig. 4.12 – Deviations of 2, 3-day ahead forecasts vs. 1-day ahead forecasts for the month of February 2012 for the site “Gi”.

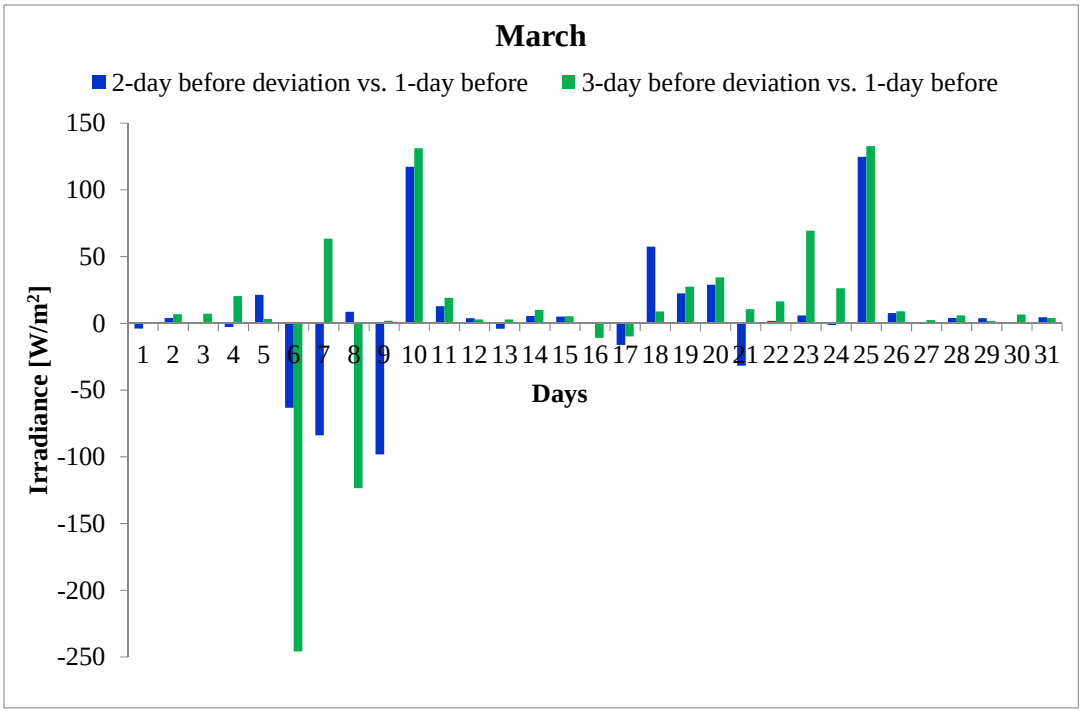

Fig. 4.13 – Deviations of 2, 3-day ahead forecasts vs. 1-day ahead forecasts for the month of March 2012 for the site "Gi".

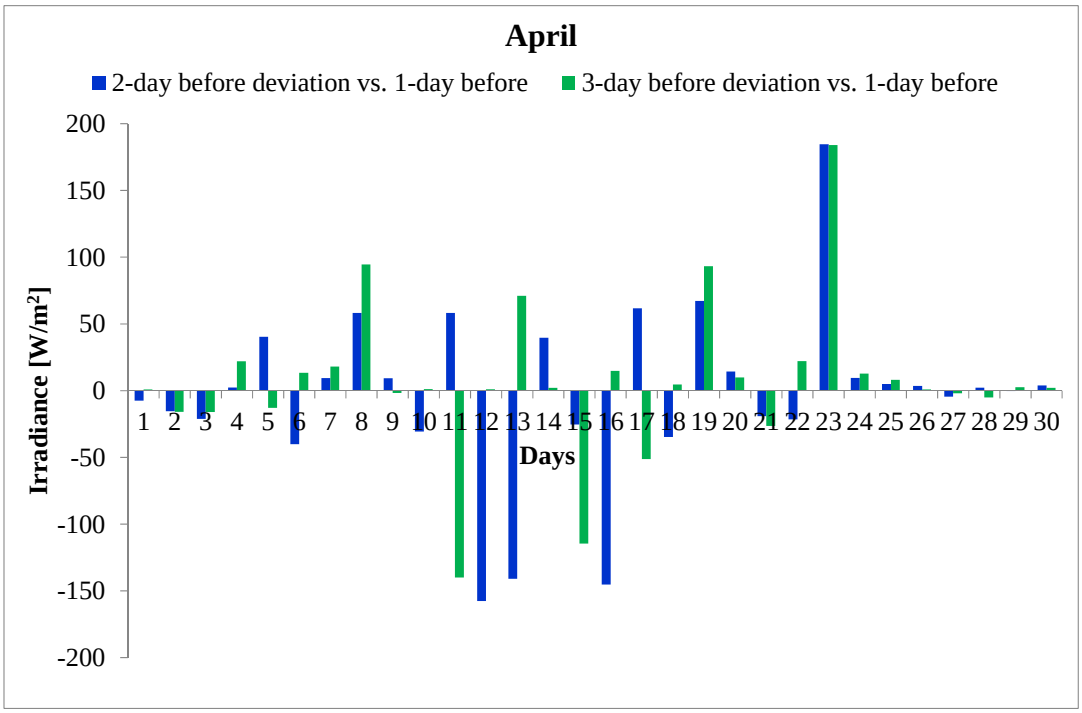

Fig. 4.14 – Deviations of 2, 3-day ahead forecasts vs. 1-day ahead forecasts for the month of April 2012 for the site "Gi".

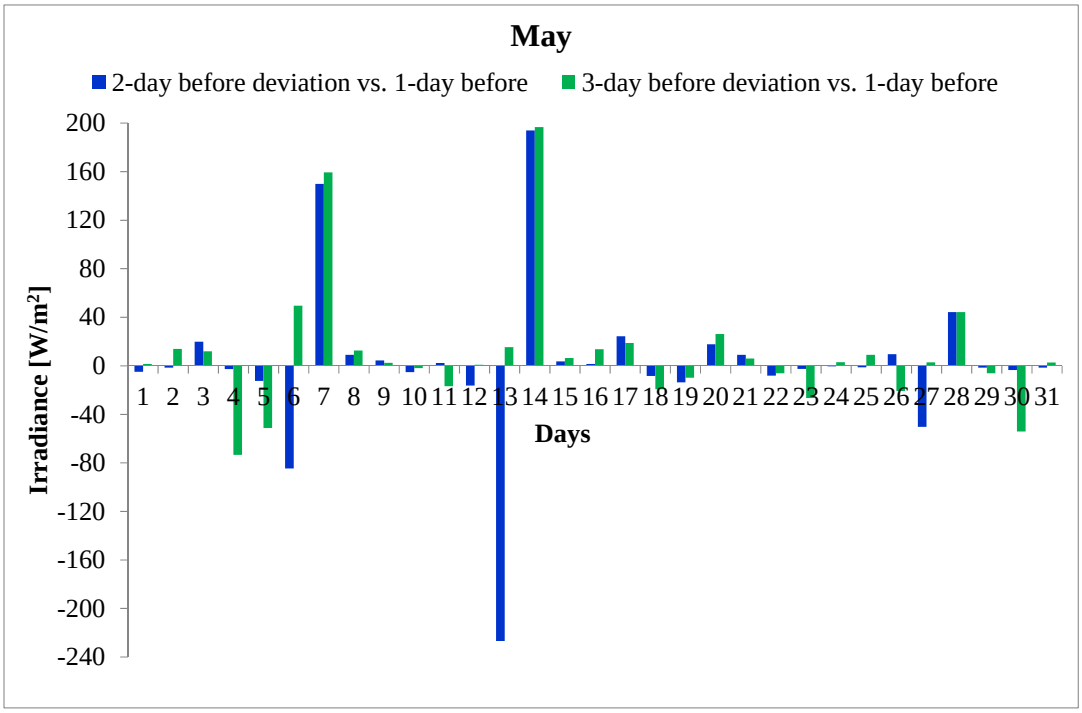

Fig. 4.15 – Deviations of 2, 3-day ahead forecasts vs. 1-day ahead forecasts for the month of May 2012 for the site "Gi".

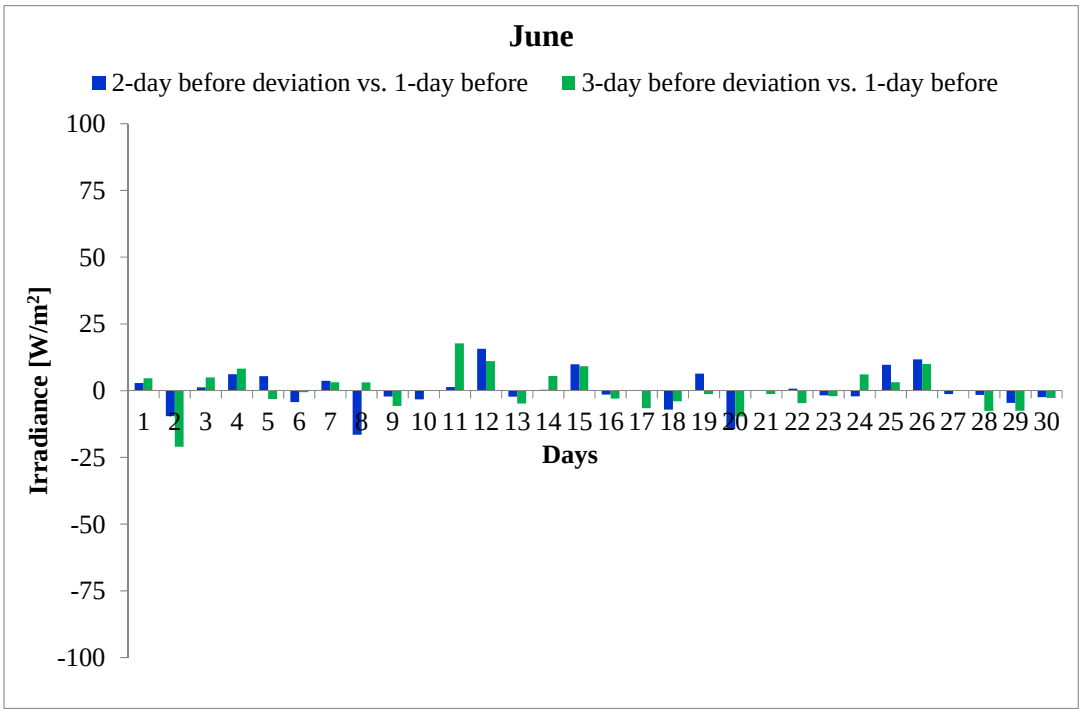

Fig. 4.16 – Deviations of 2, 3-day ahead forecasts vs. 1-day ahead forecasts for the month of June 2012 for the site "Gi".

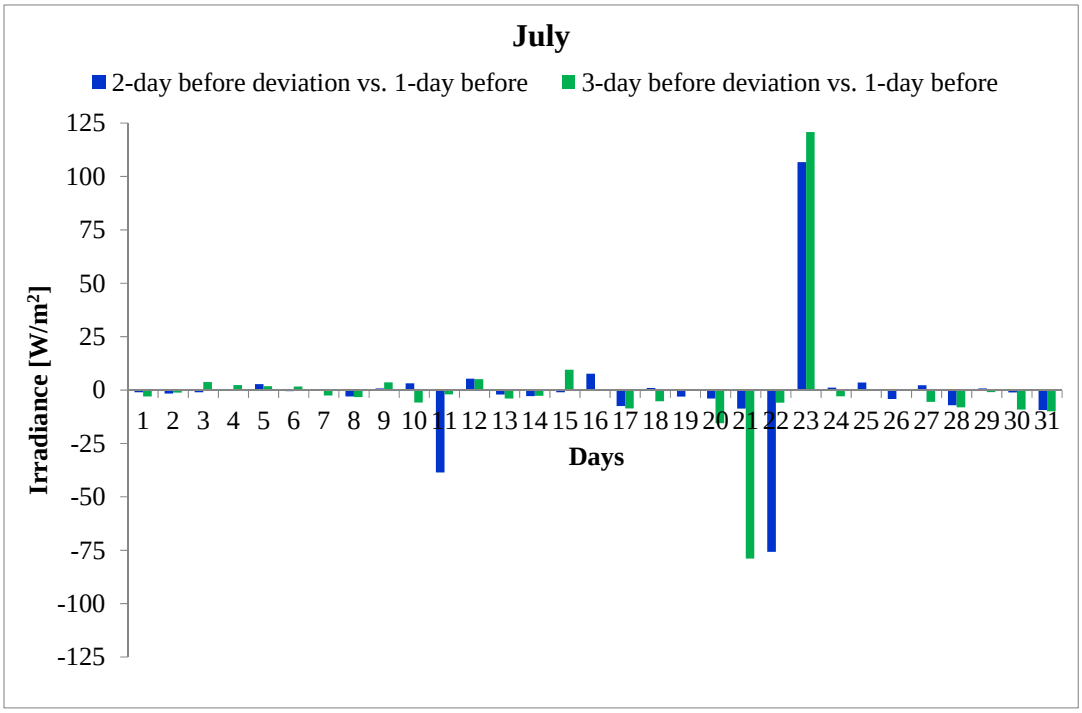

Fig. 4.17 – Deviations of 2, 3-day ahead forecasts vs. 1-day ahead forecasts for the month of July 2012 for the site "Gi".

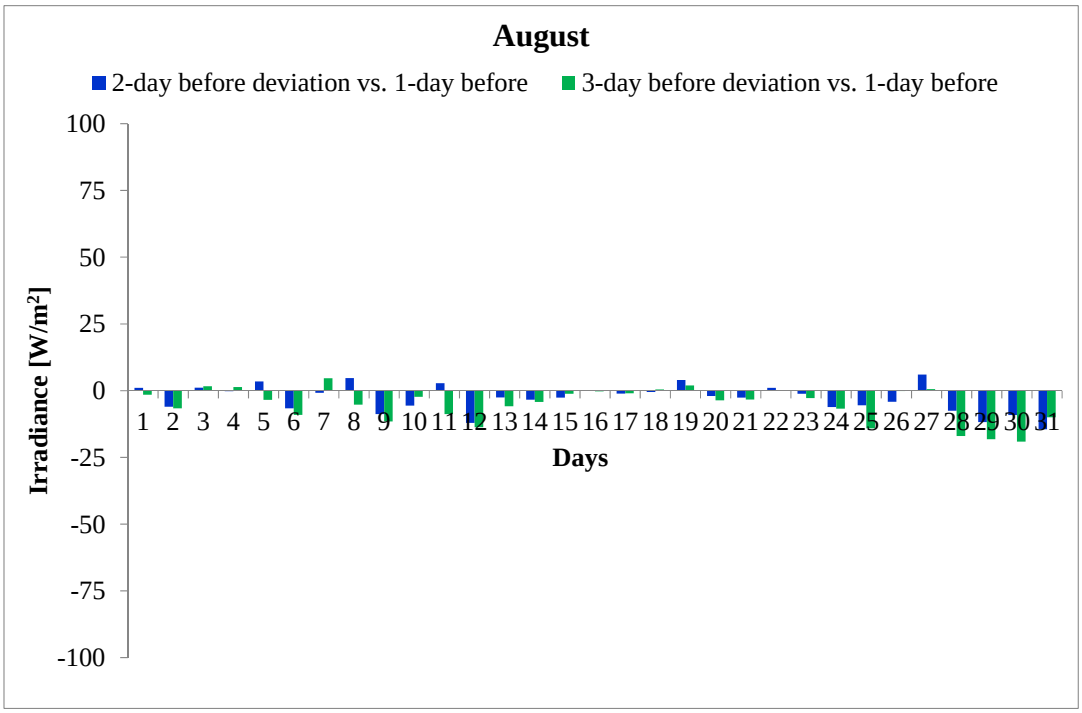

Fig. 4.18 – Deviations of 2, 3-day ahead forecasts vs. 1-day ahead forecasts for the month of August 2012 for the site "Gi".

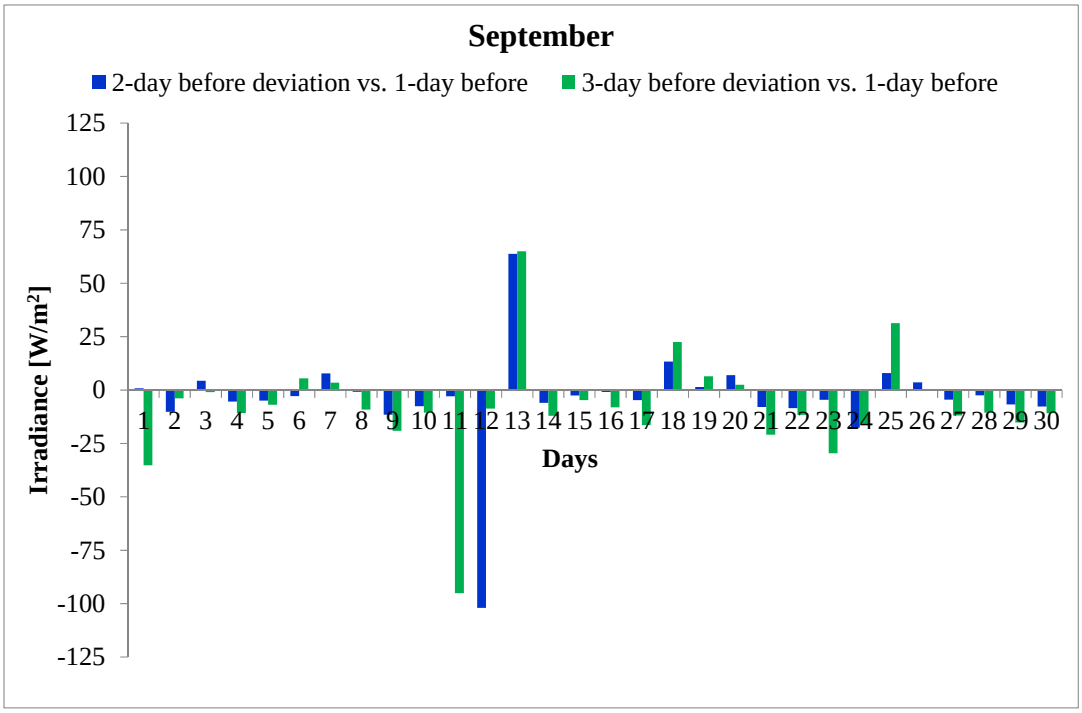

Fig. 4.19 – Deviations of 2, 3-day ahead forecasts vs. 1-day ahead forecasts for the month of September 2012 for the site "Gi".

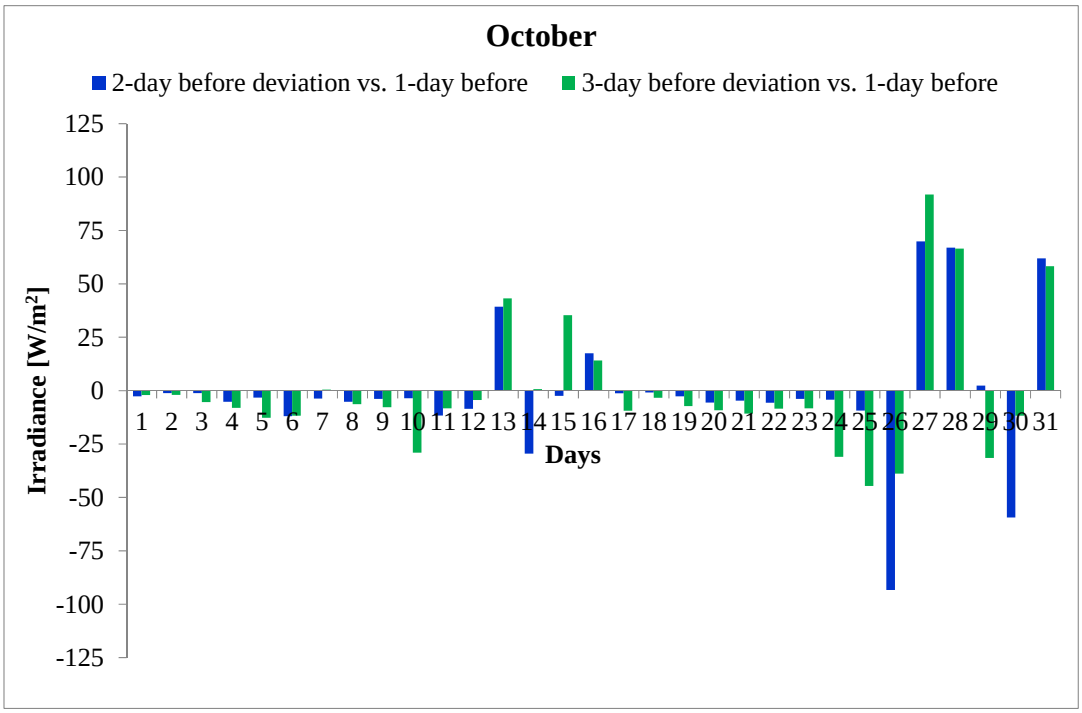

Fig. 4.20 – Deviations of 2, 3-day ahead forecasts vs. 1-day ahead forecasts for the month of October 2012 for the site "Gi".

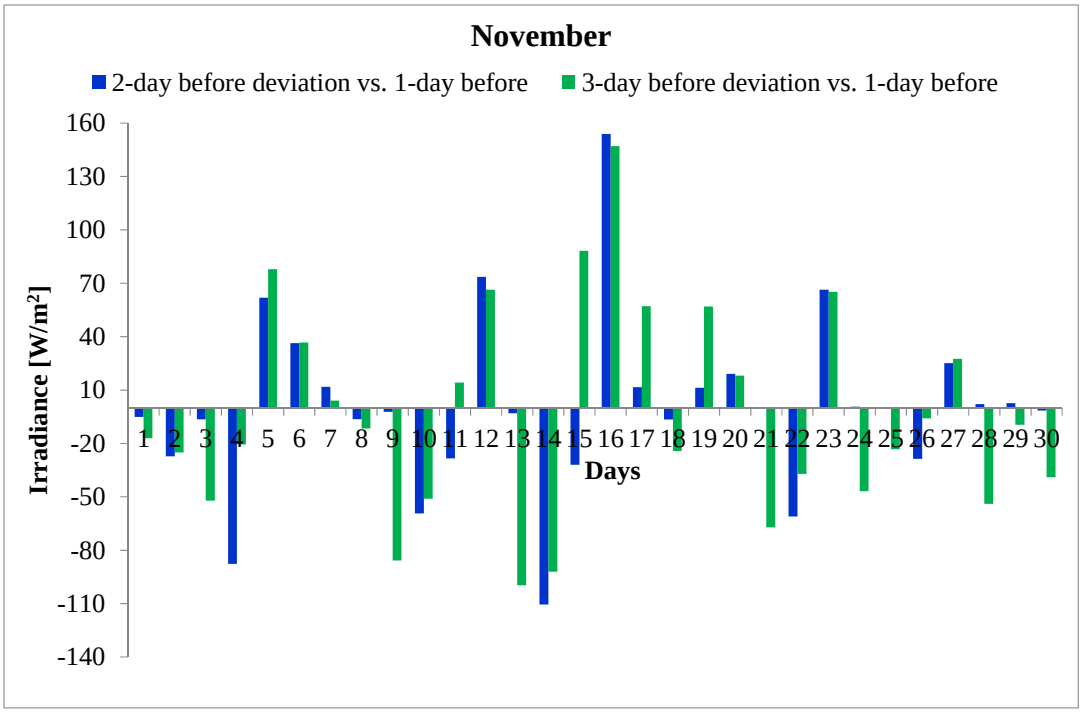

Fig. 4.21 – Deviations of 2, 3-day ahead forecasts vs. 1-day ahead forecasts for the month of November 2012 for the site "Gi".

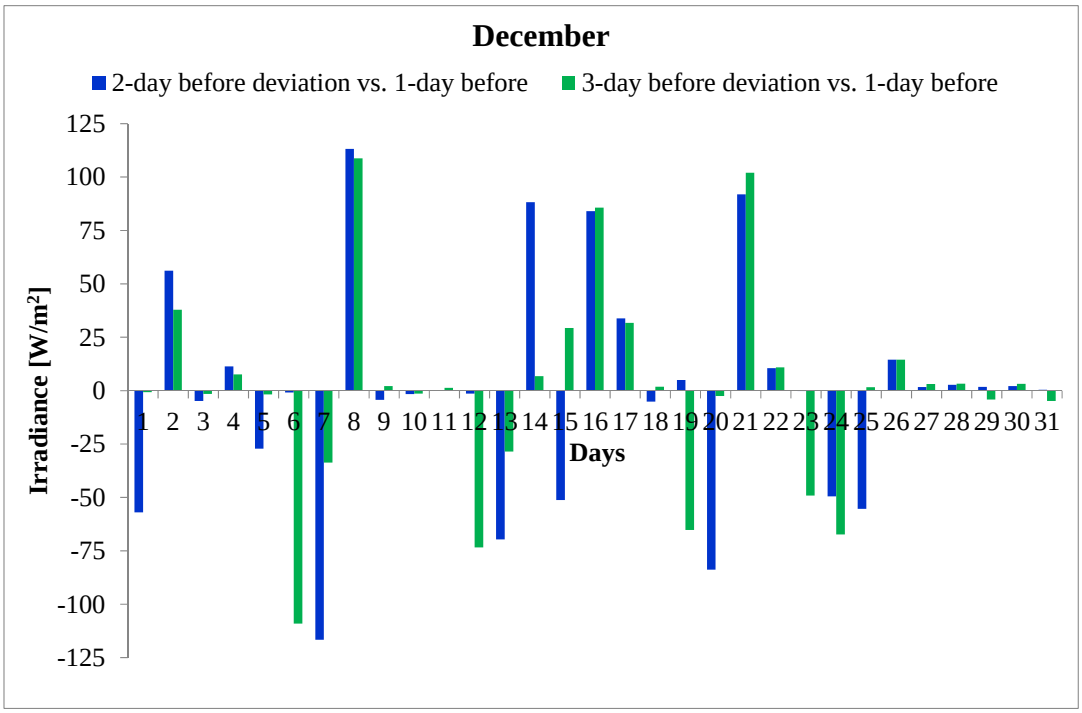

Fig. 4.22 – Deviations of 2, 3-day ahead forecasts vs. 1-day ahead forecasts for the month of December 2012 for the site "Gi".

By performing this analysis for all the months of the year 2012, it is possible to note that the broken clouds can be considered as a subset of the variable sky condition. In addition, the maximum value of clear-sky irradiance taken from PVGIS changes month by month, as shown in Table 4.8.

Thus, considering the global irradiance of one of the tilted solar cells G_{tcell} with sampling time of one minute, an occurrence of broken clouds equal to 76.97 hours is verified or the whole year 2012, that corresponds to 3 days 4 hours and 58 minutes, as shown in Table 4.9.

It is noteworthy that the months with a higher occurrence of broken clouds are in winter (January and February) and in spring (April and May).

Furthermore, with the perspective of the day-ahead market (MGP, Mercato Giorno Prima), it is useful to consider the occurrence of broken clouds for the quarter-hour averaged values. In this way, it has been considered the global irradiance of the same tilted solar cell G_{tcell} with sampling time averaged each 15 minutes. As it was desirable, in this situation, the presence of broken clouds is much more attenuated. In fact, an occurrence of broken clouds equal to 28.25 hours, that corresponds to 1 day 4 hours and 15 minutes, is considered for the year 2012, as shown in Table 4.9.

Table 4.8 – Maximum clear-sky irradiance values with tilted angle of 30° for the site "Gi" for each month, taken from PVGIS.

PVGIS	
Month	Max clear-sky irradiance on a fixed plane (30°) (W/m^2)
January	852
February	971
March	1080
April	1100
May	1060
June	1060
July	1020
August	1080
September	1040
October	1000
November	906
December	856

Table 4.9 – The occurrence of broken clouds for the site "Gi" for each month, considering G_{tcell} with sampling time of one minute and with sampling time averaged each 15 minutes.

Year 2012		
Month	N° of BrokenClouds/min	N° of BrokenClouds/15 min
January	942	29
February	547	21
March	94	0
April	503	12
May	706	12
June	152	1
July	300	7
August	38	0
September	410	8
October	398	8
November	285	7
December	243	8
Tot. Year 2012	4618	113

4.5.2 Experimental results for the site “Ma”

In Fig. 4.23 the first week of the month of July 2012 is shown for the site “Ma”. The hourly algorithm related to the measurements from the pyranometer classifies all the hours of these days as variable, with k_t in the range $0.22 - 0.75$, with the exception of day 5, in which the hours from 10 a.m. to 1 p.m. are considered as clear, with k_t within 0.78.

Concerning the hourly algorithm for the prediction of the 1-day before, all the hours of days 1, 2, 3 and 7 of July are classified as variable.

For days 5 and 6, the simulation related to the prediction of 1-day before classifies the hours until 8 a.m. as variable, with k_{tf} in the range$0.71 - 0.75$, then from 9 a.m. to 3 p.m. as clear-sky, with k_{tf} between 0.77 and 0.78, and the remaining hours as variable, with k_{tf} in the range $0.67 - 0.75$.

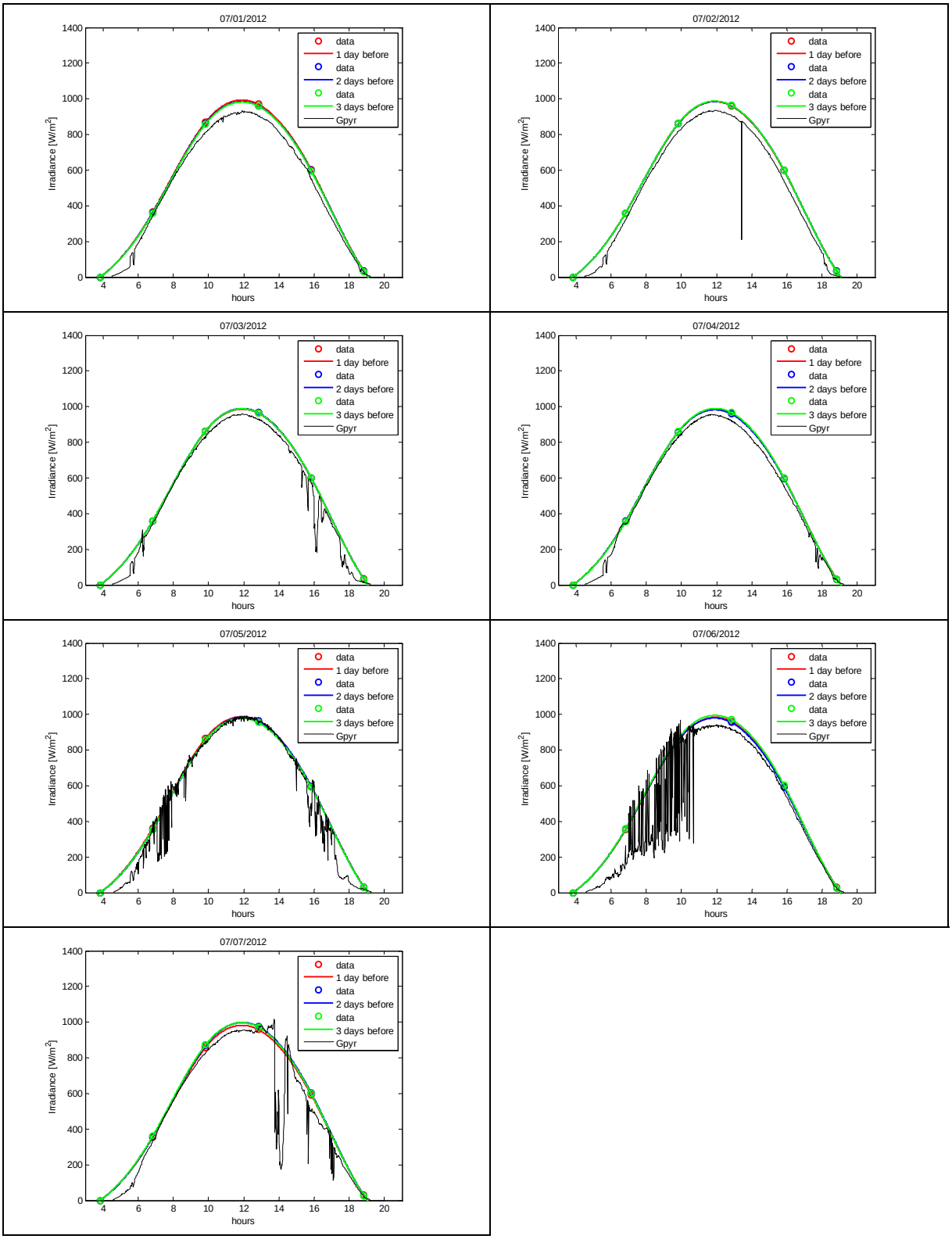

Fig. 4.23 − Measurements from the pyranometer, the three-hour predictions from Meteo.cat and the interpolated predictions from 01 July 2012 to 07 July 2012 for the site “Ma”.

In Fig. 4.24 the trends from day 8 to day 14 for the month of July are shown. The hourly algorithm for the pyranometer measurements classifies all the hours of these days as variable, with the exception of day 11, with k_t between 0.33 and 0.72 for day 8, 9, 10 and 14.For day 11, the hours from 11 a.m. to 12 p.m. are considered as clear, with k_t within 0.76.

The simulation related to the 1-day ahead prediction on days 8, 9 and 14classifies all the hours as variable with k_{tf} in the range $0.64 - 0.75$.

Moreover, unlike the previous days, in which the three days predictions are almost overlapped, for day 11 we note that the prediction of 2-day before is closer to the pyranometer measurements.

For day 10, 11, 12 and 13 the hours from 9 a.m. to 3 p.m. are considered as clear, with k_{tf} between 0.77 – 0.79, while the remaining hours are considered as variable with k_{tf} in the range 0.40 – 0.75.

In Fig. 4.25 the trends of the third week of July are shown. The hourly algorithm for the pyranometer measurements classifies all the hours of days 15, 16, 19, 20 and 21 as variable, with k_t between 0.34 and 0.75.

On the other hand, days 17 and 18 classify the hours from 9 a.m. to 2 p.m. as a clear with k_t between 0.77 and 0.78, and the remaining hours as variable with k_t between 0.36 and 0.77.

Concerning the simulation related to the 1-day ahead prediction on days 15, 20 and 21classifies all the hours as variable with k_{tf} in the range $0.42 - 0.75$. Days 16, 17, 18 and 19 classify the hours from 9 a.m. to 2 p.m.as clear with k_{tf} between 0.77 and 0.80,and the remaining hours as variable with k_t between 0.44 and 0.75.

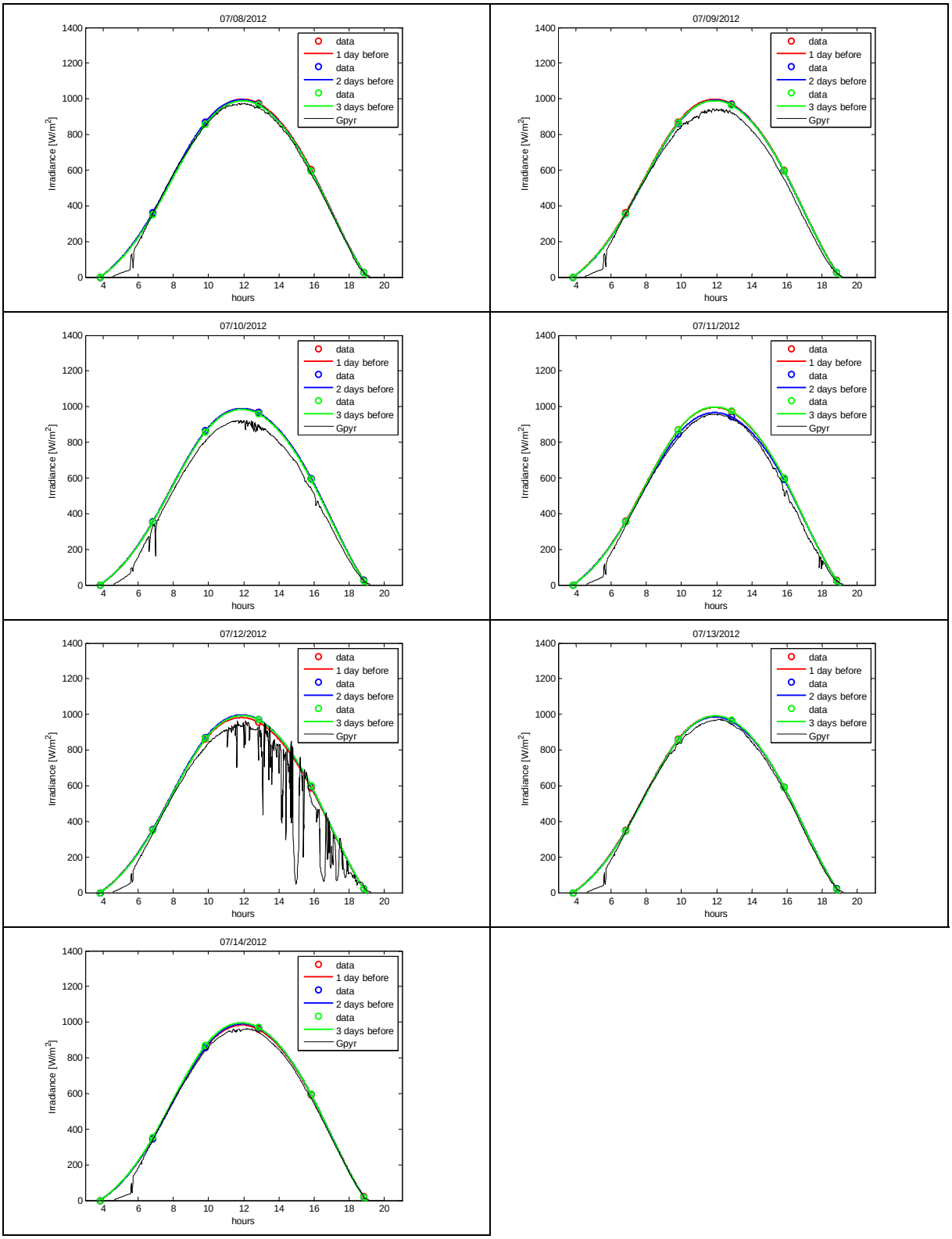

Fig. 4.24 − Measurements from the pyranometer, the three-hour predictions from Meteo.cat and the interpolated predictions from 08 July 2012 to 14 July 2012 for the site “Ma”.

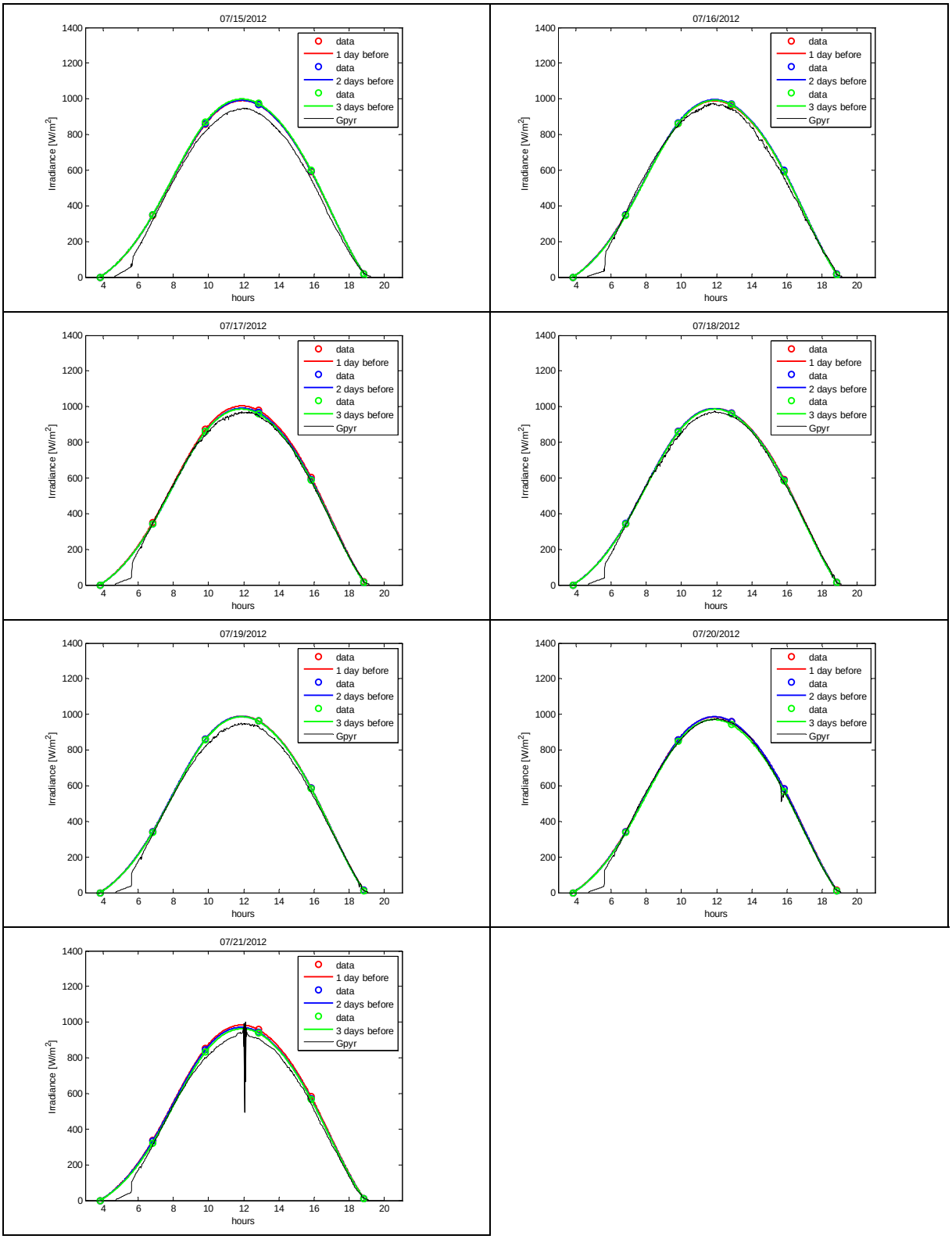

Fig. 4.25 − Measurements from the pyranometer, the three-hour predictions from Meteo.cat and the interpolated predictions from 15 July 2012 to 21 July 2012 for the site “Ma”.

In Fig. 4.26 the trends from day 22 to day 28 are shown. Unlike the other days, the 3-day predictions of days 22, 23 and 25 are not overlapped. In particular, the prediction of 2-day before on day 22 and 23 follow better the pyranometer measurement.

For day 25, the 1-day before prediction is less accurate than the other predictions, with respect to the pyranometer measurement.

Concerning the hourly algorithm for the pyranometer measurements, it classifies all the hours of days 22, 26, 27 and 28 as variables, with k_t between 0.31 and 0.72. Days 23 and 24 have some hours as variable.

In particular, for day 23 the hours from 4 p.m. to 5 p.m. are classified as cloudy with k_t within 0.13, and the remaining hours as variable with k_t between 0.21 and 0.61.

On the contrary, for day 24 the hours between 5 a.m. to 7 a.m. are classified as cloudy with k_t between 0.08 and 0.13, then the hours from 8 a.m. to 12 p.m. and from 3 p.m. to 6 p.m. are classified as variable with k_t between 0.24 and 0.71, and the hours from 1 p.m. to 2 p.m. are classified as clear with k_t within 0.78.

Concerning the simulation related to the 1-day ahead prediction, all the hours of days 21, 22, 26, 27, and 28 are classified as variable, with k_{tf} between 0.37 and 0.75. Days 23, 24 and 25 have some hours classified as clear and as variable.

In particular, for days 23 and 24 the hours between 10 a.m. to 1 p.m. are classified as clear with k_{tf} in the range $0.77 - 0.78$, and the remaining hours are variable with k_{tf} in the range $0.42 - 0.75$, for day 25 only the hours from 9 a.m. to 10 a.m. are classified as clear with k_{tf} within 0.77, and the remaining hours are variable with k_{tf} between 0.49 and 0.75.

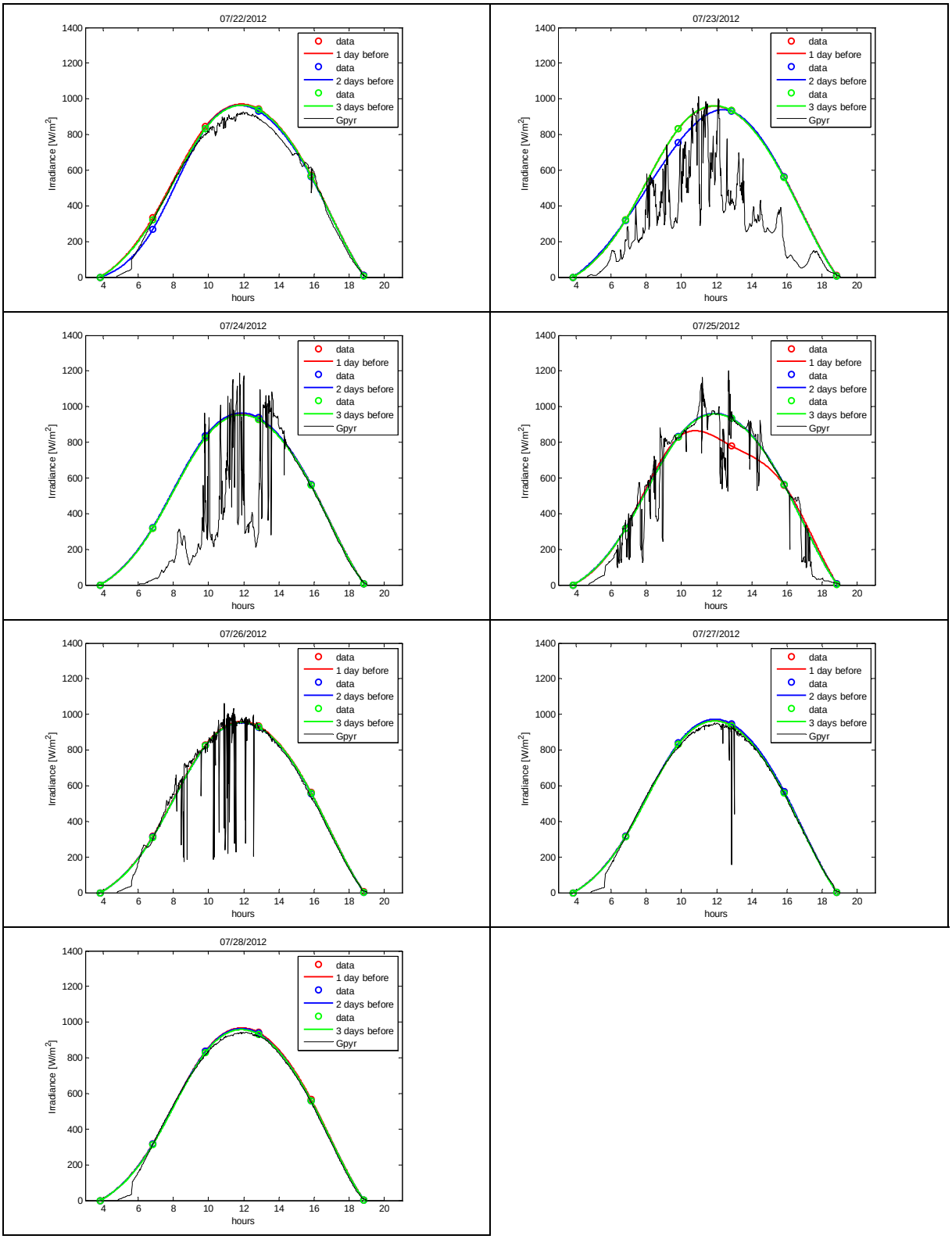

Fig. 4.26 − Measurements from the pyranometer, the three-hour predictions from Meteo.cat and the interpolated predictions from 22 July 2012 to 28 July 2012 for the site “Ma”.

In Fig. 4.27 the trends from day 29 to day 31 are shown. Concerning the simulation related to the pyranometer measurements all the hours of day 29 are classified as variable with k_t between 0.28 and 0.70. For days 30 and 31, the hours 10 a.m. to 1 p.m. are classified as clear with k_t within 0.77, and the remaining hours as variable with k_t between 0.37 and 0.75.

The hourly algorithm for the 1-day ahead prediction of day 29 classifies the hours from 10 a.m. to 1 p.m. as clear with k_{tf} within 0.77 and the remaining hours as variable with k_{tf} in the range 0.70 − 0.75.

The simulation related to the 1-day ahead prediction on days 30 and 31 classifies the hours from 9 a.m. to 4 p.m. as clear-sky, with k_{tf} in the range0.77 − 0.79, and the remaining hours as variable, with k_{tf} between 0.72 and 0.75.

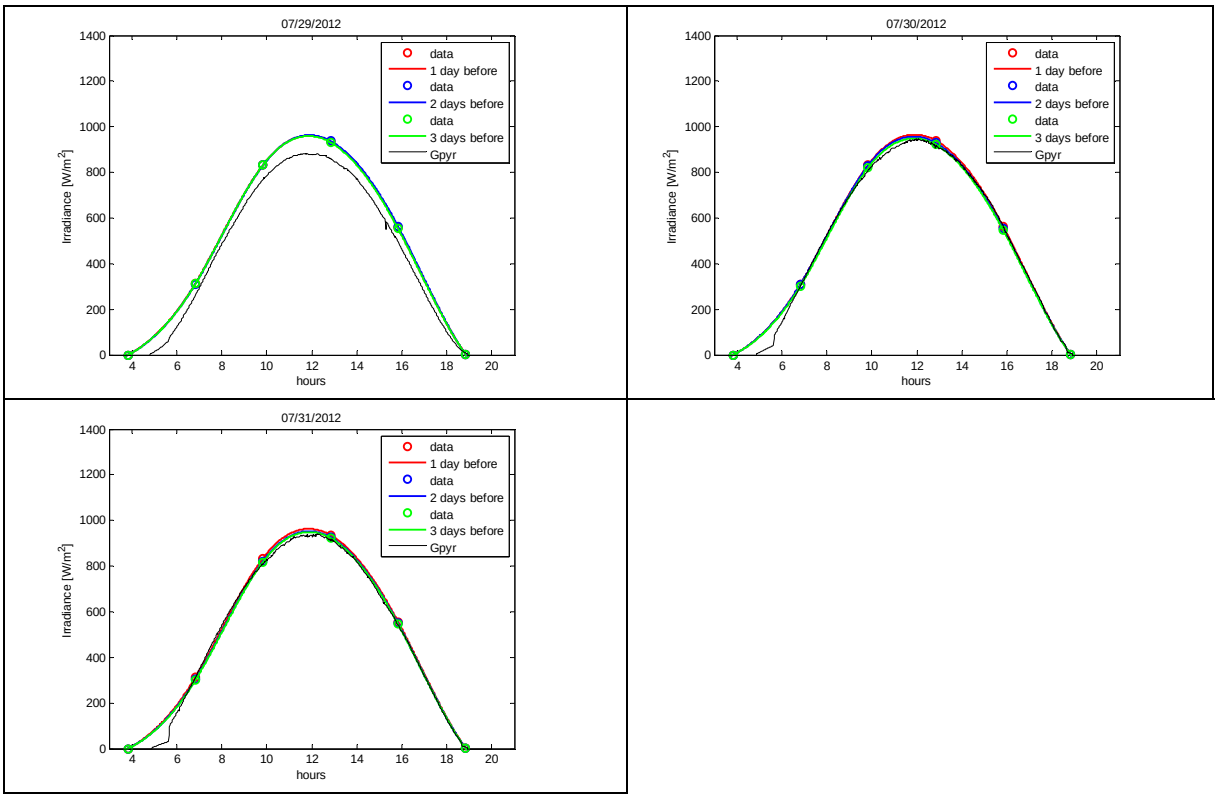

Fig. 4.27 − Measurements from the pyranometer, the three-hour predictions from Meteo.cat and the interpolated predictions from 29 July 2012 to 31 July 2012 for the site “Ma”.

In Table 4.10, Table 4.11, Table 4.12, Table 4.13, Table 4.14 and Table 4.15 the number of passes/fails (in hour) recorded by the hourly classifications from pyranometer measurements respect to the hourly classifications from 1-day before forecast are summarized for all the month of the year 2012 for the site “Ma”.

Examining the results month by month, it is possible to note that the number of hourly passes, in which the 1-day prediction coincides with the pyranometer measurements, is higher than for the site “Gi”.

In particular, in winter months an increase in the number of hours with the cloudy – cloudy condition occurs. On the contrary, in spring and autumn months, a greater number of hourly passes for the variable – variable condition is recorded.

Moreover, in summer months, as well as an increase in the number of hourly passes for the variable – variable condition, there is also a decrease in the number of hours with the variable – clear condition and clear – clear condition. In general, the number of clear-sky days is lower than for the site “Gi”. This can be explained by the proximity of the site “Ma” with high pollution areas, for example due to great quantity of fine dust in air from industrial steel mills.

Table 4.10 – Number of passes/fails, recorded by the hourly classification from pyranometer measurements vs. 1-day before forecast for the months of January and February 2012 for the site “Ma”.

January			February		
Hourly classification from pyranometer measurements	Hourly classification from the day before prediction	N° of pass/fail (hour)	Hourly classification from pyranometer measurements	Hourly classification from the day before prediction	N° of pass/fail (hour)
Variable	Variable	95	Variable	Variable	70
Clear	Clear	93	Clear	Clear	54
Cloudy	Cloudy	210	Cloudy	Cloudy	159
Variable	Clear	29	Variable	Clear	55
Variable	Cloudy	0	Variable	Cloudy	0
Clear	Variable	1	Clear	Variable	2
Clear	Cloudy	0	Clear	Cloudy	0
Cloudy	Variable	30	Cloudy	Variable	77
Cloudy	Clear	7	Cloudy	Clear	18
Tot. Passes		398	Tot. Passes		283
Tot. Fails		67	Tot. Fails		152

Table 4.11 – Number of passes/fails, recorded by the hourly classification from pyranometer measurements vs. 1-day before forecast for the months of March and April 2012 for the site "Ma".

March			April		
Hourly classification from pyranometer measurements	Hourly classification from the day before prediction	N° of pass/fail (hour)	Hourly classification from pyranometer measurements	Hourly classification from the day before prediction	N° of pass/fail (hour)
Variable	Variable	123	Variable	Variable	109
Clear	Clear	83	Clear	Clear	54
Cloudy	Cloudy	86	Cloudy	Cloudy	63
Variable	Clear	87	Variable	Clear	136
Variable	Cloudy	1	Variable	Cloudy	2
Clear	Variable	13	Clear	Variable	6
Clear	Cloudy	0	Clear	Cloudy	0
Cloudy	Variable	69	Cloudy	Variable	49
Cloudy	Clear	3	Cloudy	Clear	31
Tot. Passes		292	Tot. Passes		226
Tot. Fails		173	Tot. Fails		224

Table 4.12 – Number of passes/fails, recorded by the hourly classification from pyranometer measurements vs. 1-day before forecast for the months of May and June 2012 for the site "Ma".

May			June		
Hourly classification from pyranometer measurements	Hourly classification from the day before prediction	N° of pass/fail (hour)	Hourly classification from pyranometer measurements	Hourly classification from the day before prediction	N° of pass/fail (hour)
Variable	Variable	166	Variable	Variable	219
Clear	Clear	37	Clear	Clear	34
Cloudy	Cloudy	2	Cloudy	Cloudy	24
Variable	Clear	183	Variable	Clear	162
Variable	Cloudy	0	Variable	Cloudy	0
Clear	Variable	1	Clear	Variable	0
Clear	Cloudy	0	Clear	Cloudy	0
Cloudy	Variable	54	Cloudy	Variable	8
Cloudy	Clear	22	Cloudy	Clear	3
Tot. Passes		205	Tot. Passes		277
Tot. Fails		260	Tot. Fails		173

Table 4.13 – Number of passes/fails, recorded by the hourly classification from pyranometer measurements vs. 1-day before forecast for the months of July and August 2012 for the site "Ma".

July			August		
Hourly classification from pyranometer measurements	Hourly classification from the day before prediction	N° of pass/fail (hour)	Hourly classification from pyranometer measurements	Hourly classification from the day before prediction	N° of pass/fail (hour)
Variable	Variable	284	Variable	Variable	244
Clear	Clear	26	Clear	Clear	3
Cloudy	Cloudy	0	Cloudy	Cloudy	26
Variable	Clear	113	Variable	Clear	171
Variable	Cloudy	0	Variable	Cloudy	0
Clear	Variable	3	Clear	Variable	0
Clear	Cloudy	0	Clear	Cloudy	0
Cloudy	Variable	38	Cloudy	Variable	16
Cloudy	Clear	1	Cloudy	Clear	5
Tot. Passes		310	Tot. Passes		273
Tot. Fails		155	Tot. Fails		192

Table 4.14 – Number of passes/fails, recorded by the hourly classification from pyranometer measurements vs. 1-day before forecast for the months of September and October 2012 for the site "Ma".

September			October		
Hourly classification from pyranometer measurements	Hourly classification from the day before prediction	N° of pass/fail (hour)	Hourly classification from pyranometer measurements	Hourly classification from the day before prediction	N° of pass/fail (hour)
Variable	Variable	214	Variable	Variable	181
Clear	Clear	32	Clear	Clear	21
Cloudy	Cloudy	86	Cloudy	Cloudy	109
Variable	Clear	92	Variable	Clear	82
Variable	Cloudy	1	Variable	Cloudy	9
Clear	Variable	4	Clear	Variable	20
Clear	Cloudy	0	Clear	Cloudy	13
Cloudy	Variable	12	Cloudy	Variable	26
Cloudy	Clear	9	Cloudy	Clear	4
Tot. Passes		332	Tot. Passes		311
Tot. Fails		118	Tot. Fails		154

Table 4.15 – Number of passes/fails, recorded by the hourly classification from pyranometer measurements vs. 1-day before forecast for the months of November and December 2012 for the site "Ma".

November			December		
Hourly classification from pyranometer measurements	Hourly classification from the day before prediction	N° of pass/fail (hour)	Hourly classification from pyranometer measurements	Hourly classification from the day before prediction	N° of pass/fail (hour)
Variable	Variable	194	Variable	Variable	141
Clear	Clear	7	Clear	Clear	21
Cloudy	Cloudy	162	Cloudy	Cloudy	193
Variable	Clear	10	Variable	Clear	13
Variable	Cloudy	2	Variable	Cloudy	1
Clear	Variable	12	Clear	Variable	41
Clear	Cloudy	0	Clear	Cloudy	0
Cloudy	Variable	61	Cloudy	Variable	54
Cloudy	Clear	2	Cloudy	Clear	1
Tot. Passes		363	Tot. Passes		355
Tot. Fails		87	Tot. Fails		110

In the following figures (Fig. 4.28 – Fig. 4.39) the deviations of the 2-day ahead predictions with respect to the 1-day ahead predictions, considered as the most accurate, and the deviations of the 3-day ahead predictions with respect to the 1-day ahead predictions are calculated for the site "Ma", according to eq. (4.20) and (4.21). According to the site "Gi", major deviations occur in winter, spring and autumn months, on the other hand in summer months, positive and negative deviations are quite negligible ($\leq$ 30 W/m^2). In general, for each of the two site, the deviations between the 3-day before predictions vs. the 1-day before predictions are greater than the 2-day before predictions vs. the 1-day before predictions. In particular, the site "Gi" presents major deviations than the site "Ma".

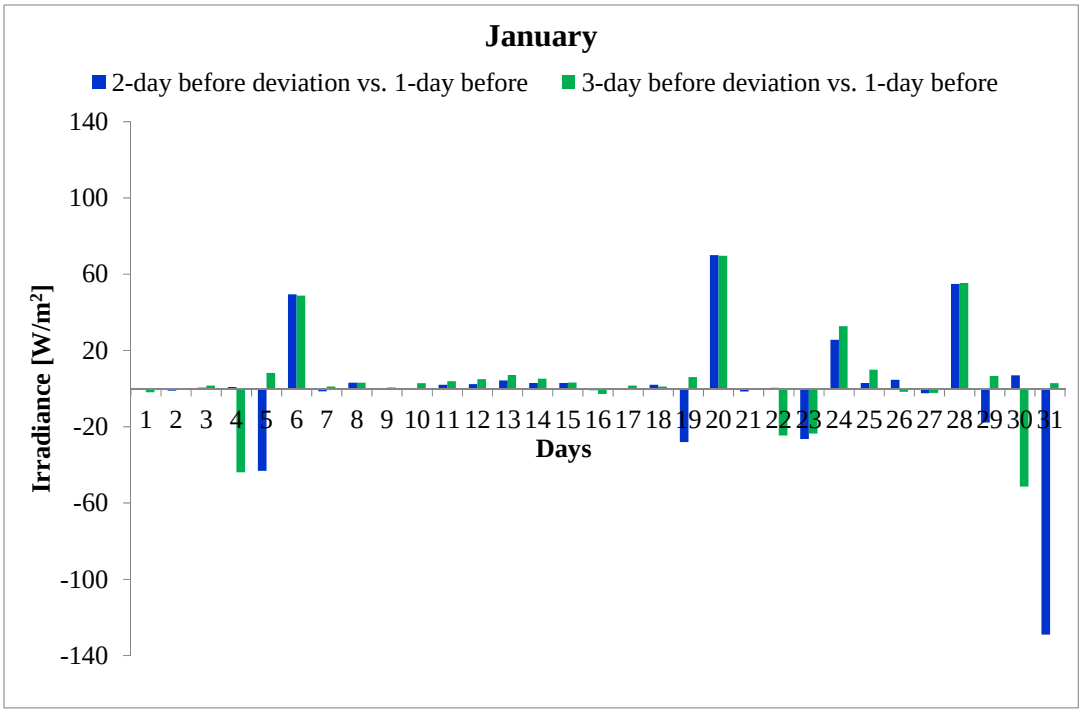

Fig. 4.28 – Deviations of 2, 3-day ahead forecasts vs. 1-day ahead forecasts for the month of January 2012 for the site "Ma".

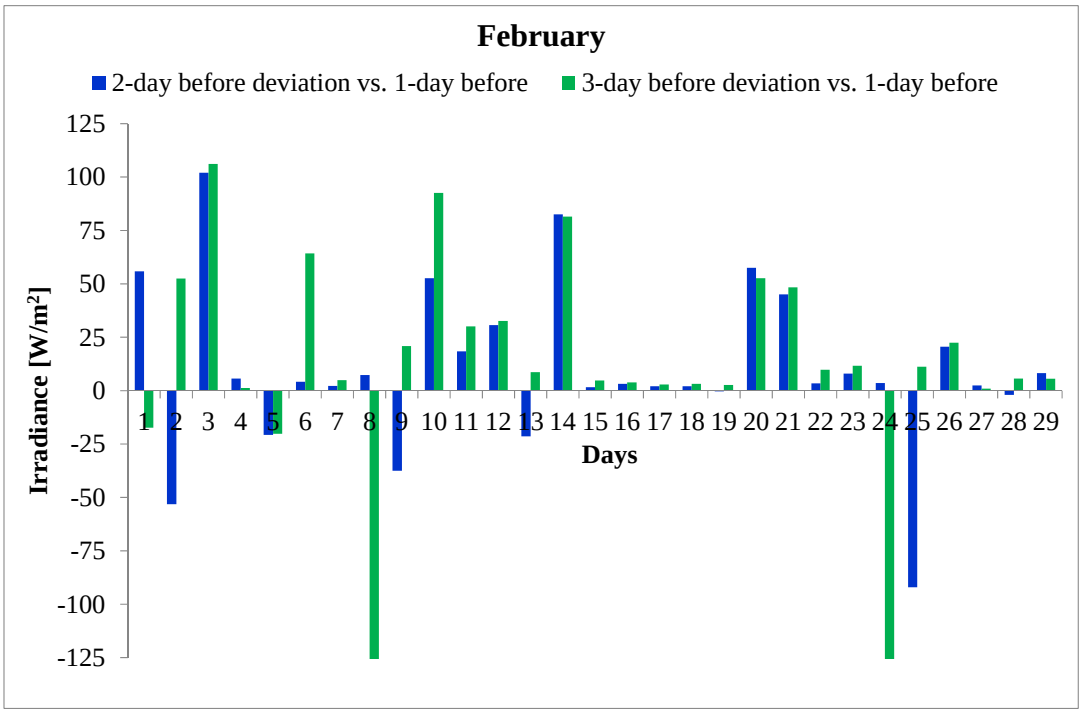

Fig. 4.29 – Deviations of 2, 3-day ahead forecasts vs. 1-day ahead forecasts for the month of February 2012 for the site "Ma".

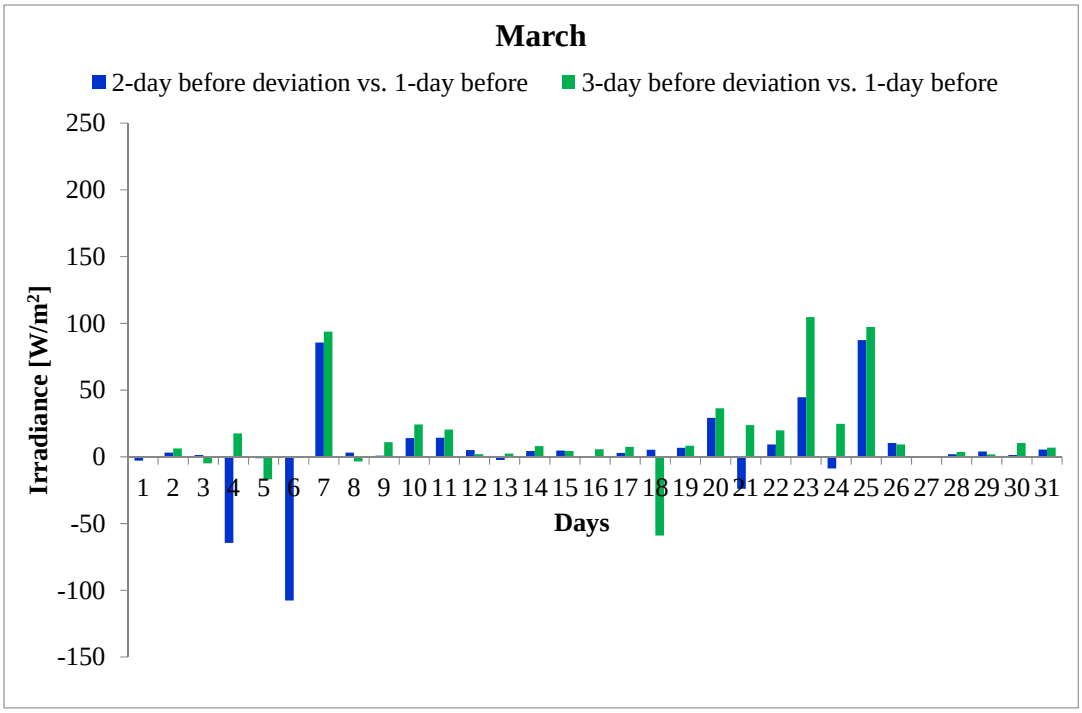

Fig. 4.30 – Deviations of 2, 3-day ahead forecasts vs. 1-day ahead forecasts for the month of March 2012 for the site “Ma”.

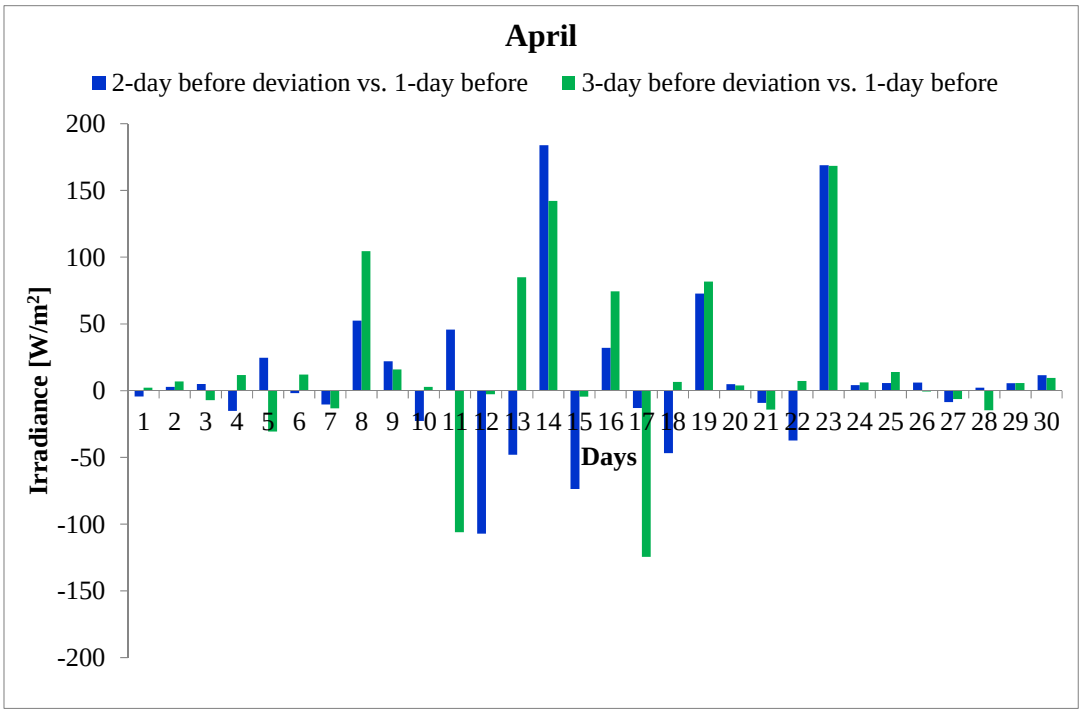

Fig. 4.31 – Deviations of 2, 3-day ahead forecasts vs. 1-day ahead forecasts for the month of April 2012 for the site “Ma”.

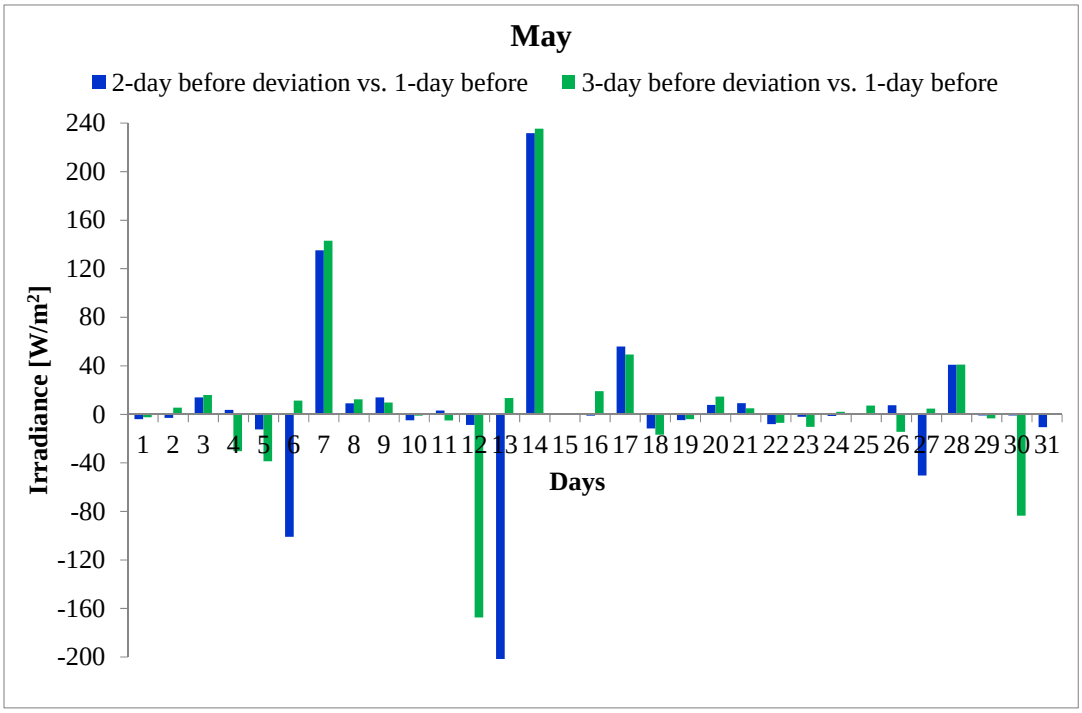

Fig. 4.32 – Deviations of 2, 3-day ahead forecasts vs. 1-day ahead forecasts for the month of May 2012 for the site “Ma”.

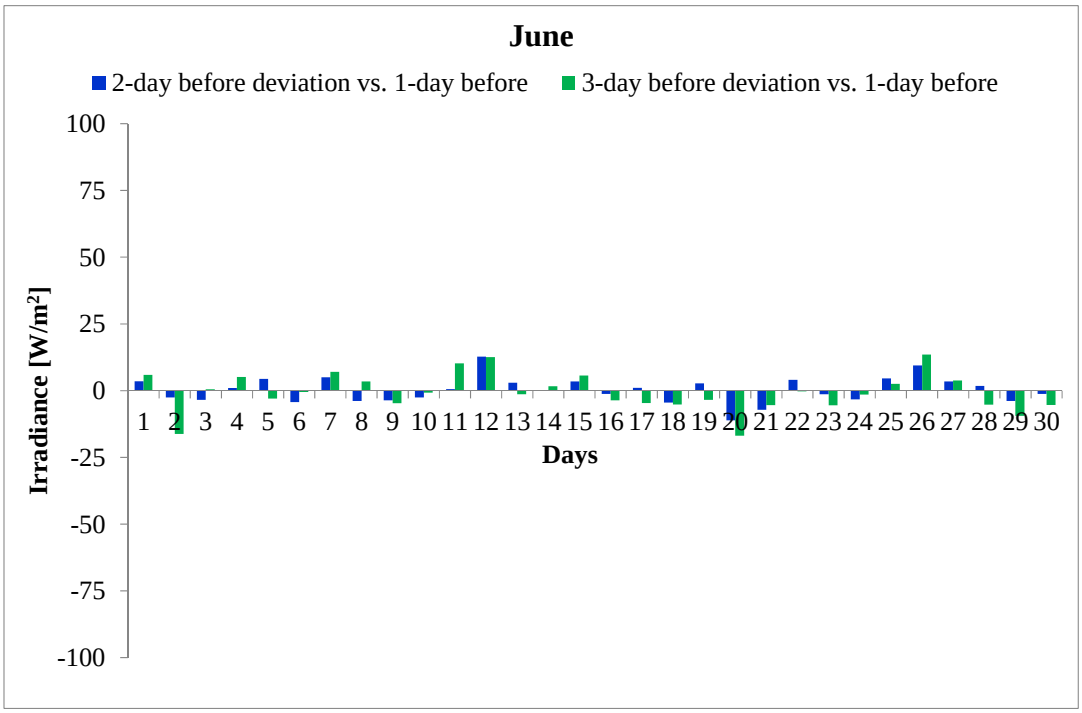

Fig. 4.33 – Deviations of 2, 3-day ahead forecasts vs. 1-day ahead forecasts for the month of June 2012 for the site “Ma”.

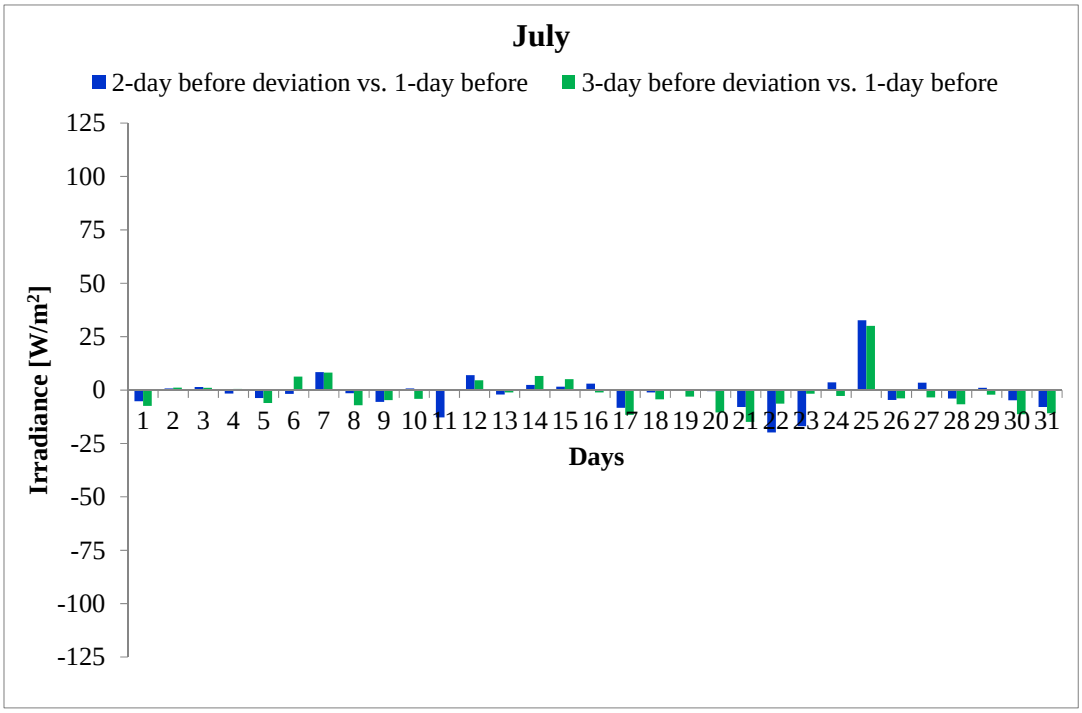

Fig. 4.34 – Deviations of 2, 3-day ahead forecasts vs. 1-day ahead forecasts for the month of July 2012 for the site “Ma”.

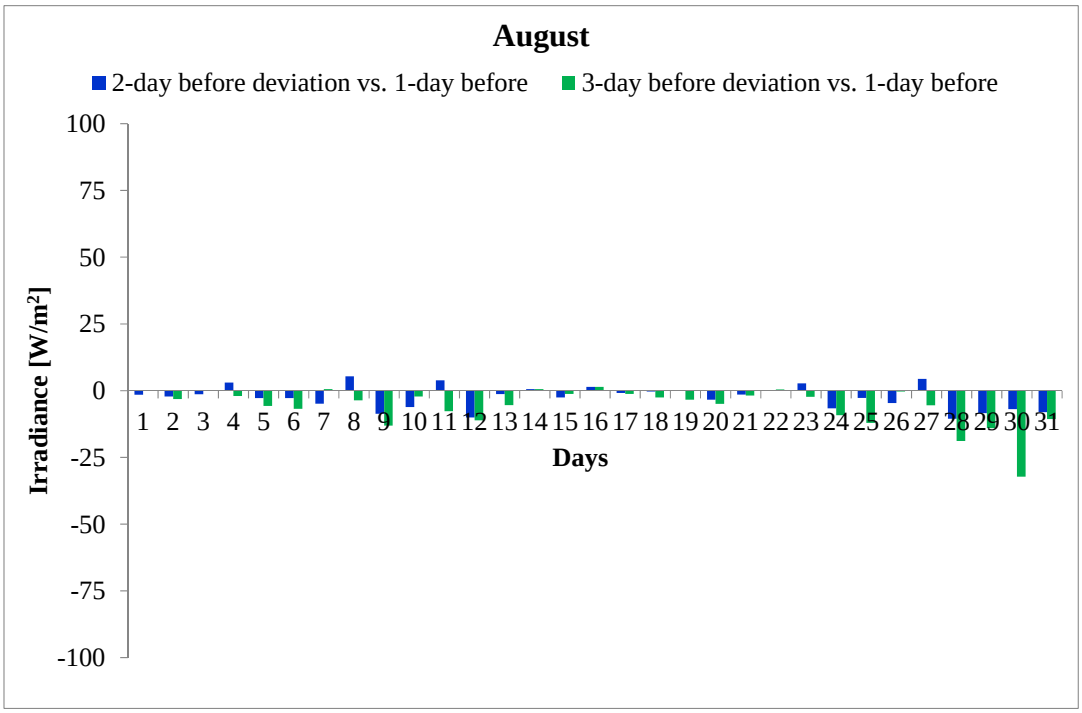

Fig. 4.35 – Deviations of 2, 3-day ahead forecasts vs. 1-day ahead forecasts for the month of August 2012 for the site “Ma”.

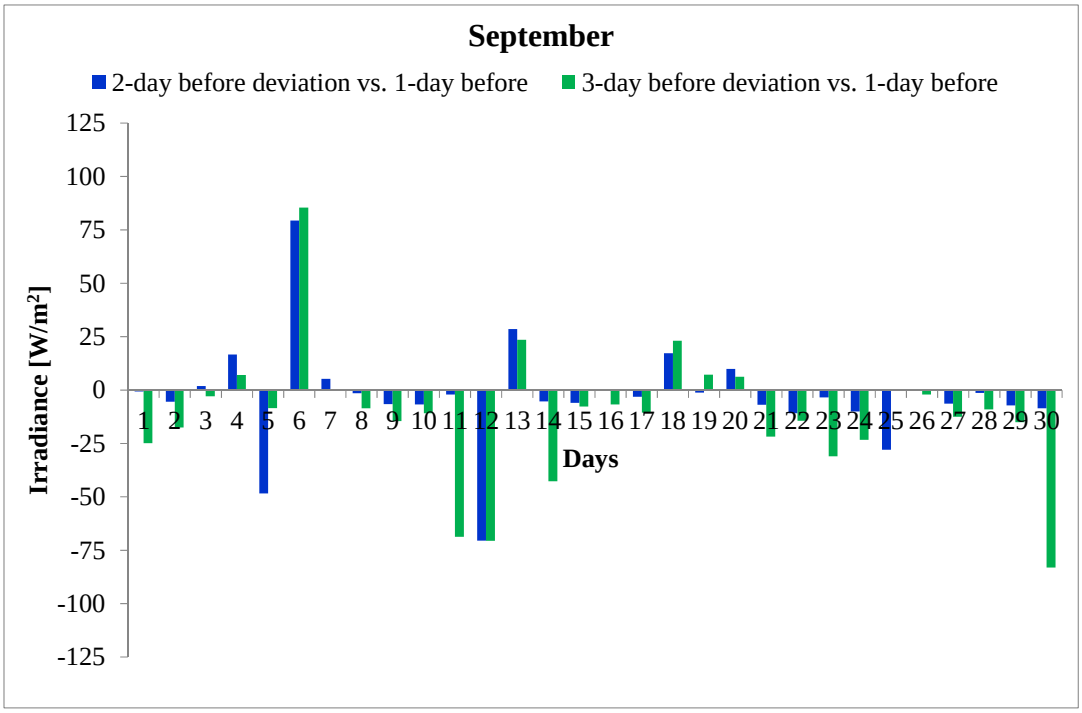

Fig. 4.36 – Deviations of 2, 3-day ahead forecasts vs. 1-day ahead forecasts for the month of September 2012 for the site “Ma”.

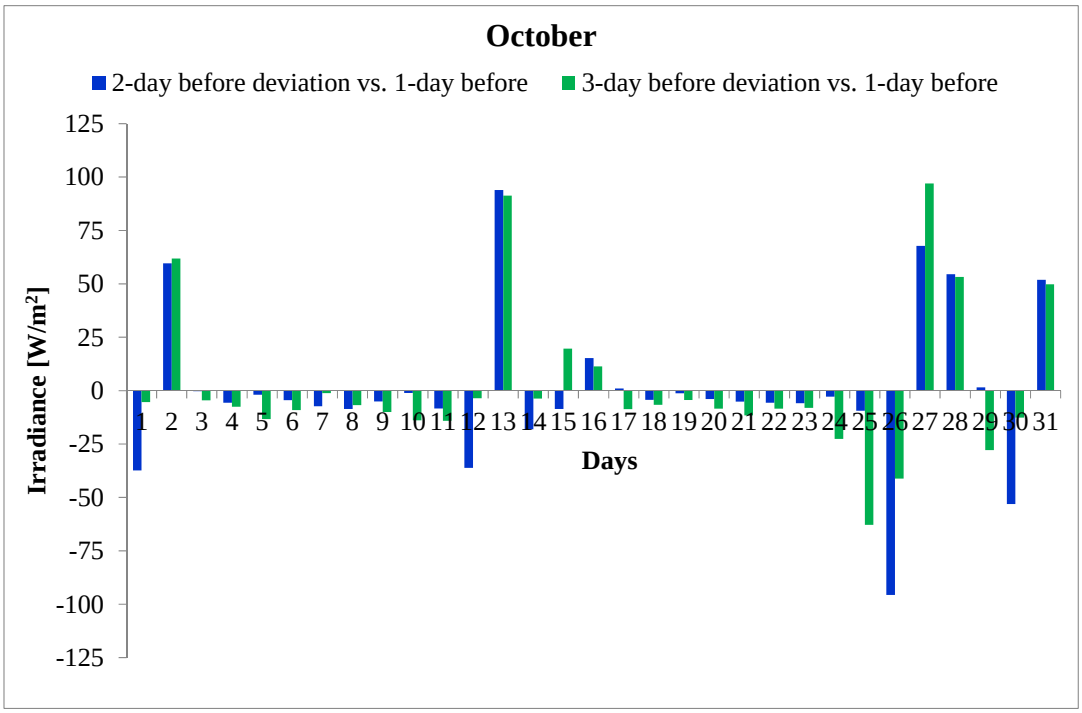

Fig. 4.37 – Deviations of 2, 3-day ahead forecasts vs. 1-day ahead forecasts for the month of October 2012 for the site “Ma”.

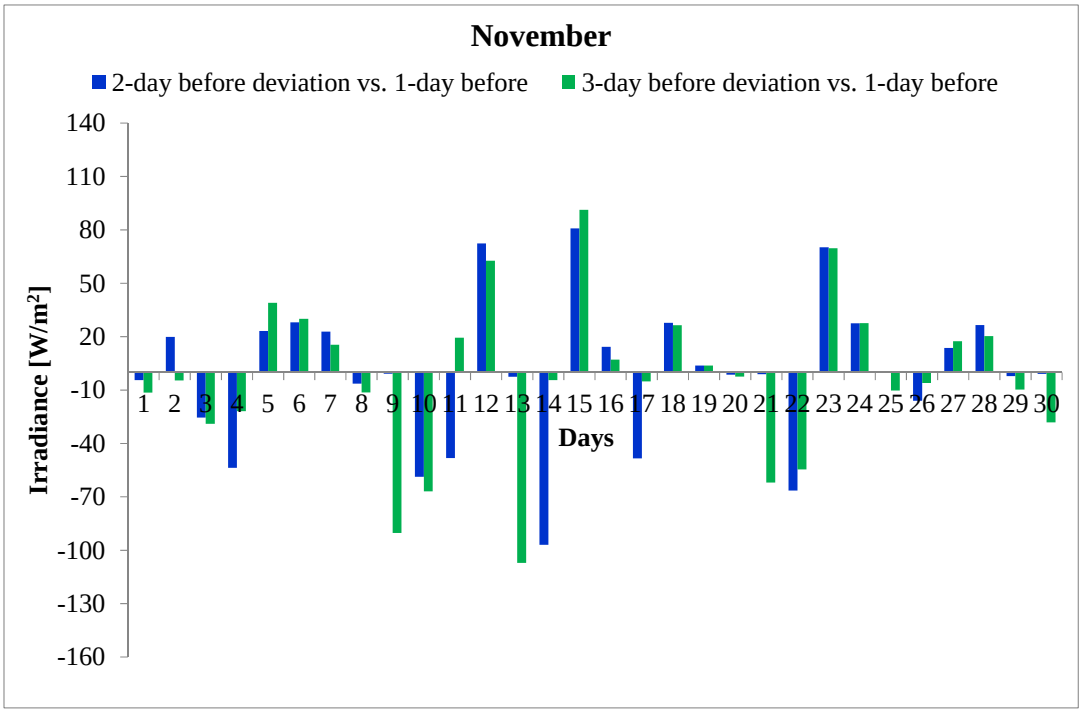

Fig. 4.38 – Deviations of 2, 3-day ahead forecasts vs. 1-day ahead forecasts for the month of November 2012 for the site "Ma".

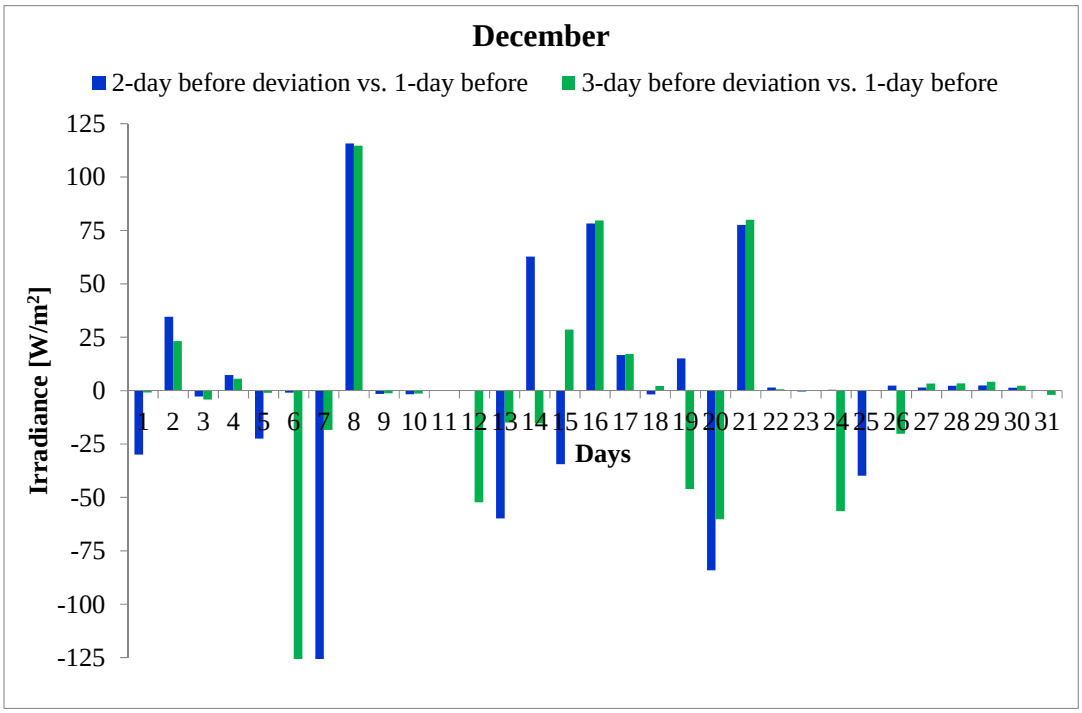

Fig. 4.39 – Deviations of 2, 3-day ahead forecasts vs. 1-day ahead forecasts for the month of December 2012 for the site "Ma".

In Table 4.16 and Table 4.17 the maximum value of clear-sky irradiance taken from PVGIS [73] for each month and the occurrence of broken clouds are shown for the site “Ma”.

As well as the site “Gi”, for the calculation of the occurrence of broken clouds, it has been considered the global irradiance of one of the tilted solar cells G_{tcell} with sampling time, respectively, of one minute and the average value every 15 minutes.

The occurrence of broken clouds for the whole year 2012 for the site “Ma” is lower than for the site “Gi”, in particular 67.92 hours of broken clouds per minute are verified, that corresponds to 2 days 19 hours and 55 minutes.

It is noteworthy that the months with a higher occurrence of broken clouds are in winter (January) and in autumn (September). On the contrary, in spring and summer the number of broken clouds per minute is lower than for the site “Gi”.

Also in this case, with the perspective of the day-ahead market , the occurrence of broken clouds for the quarter-hour averaged values is much more attenuated. In particular, for the whole year 2012 only 20.25 hours of broken clouds/15 min occur.

Table 4.16 – Maximum clear-sky irradiance values with tilted angle of 30° for the site "Ma" for each month, taken from PVGIS.

PVGIS	
Month	Max clear-sky irradiance on a fixed plane (30°) (W/m^2)
January	856
February	977
March	1100
April	1110
May	1070
June	1060
July	1030
August	1080
September	1040
October	1020
November	905
December	853

Table 4.17 – The occurrence of broken clouds for the site "Ma" for each month, considering G_{tcell} with sampling time of one minute and with sampling time averaged each 15 minutes.

Year 2012		
Month	N° of BrokenClouds/min	N° of BrokenClouds/15 min
January	1155	33
February	367	8
March	210	0
April	279	1
May	338	6
June	138	1
July	106	2
August	17	0
September	640	9
October	183	4
November	282	10
December	360	7
Tot. Year 2012	4075	81

4.6 Accuracy of predictions

The data obtained with a forecasting model contain uncertainties: the only way to judge whether a forecast is good or not is to compare the estimated quantities with those measured. The result of this comparison is a representation of the estimation error, that represents the quality of the forecast compared to the historical measured data [84], [106], [107], [108], [109], [110], [111]. In other words, the uncertainties are quantities associated with future variables, but estimated according to historical evaluations [112].

Generally, the quantitative evaluation of the errors requires the use of some statistic methods. It is very important that such instruments give a representation of accuracy which is comparable to that obtained by other measurements.

For this purpose, it is possible to define ε, the prediction error, as the difference between the forecast and the measured irradiance:

$$\varepsilon_x = x_{fore} - x_{meas} \tag{4.22}$$

In this way, positive errors stand for the prediction overestimates the actual value. In literature [84], [106]-[112], the most popular index is the *root mean square error* (*RMSE*), nevertheless the electric power generated by PV devices is not a square function of irradiance. It is defined as follows:

$$RMSE = \sqrt{\frac{1}{N}\sum_{i=1}^{N}\varepsilon_i^2} \tag{4.23}$$

where N is the number of available data.

The *RMSE* is a parameter that has the same measurement unit of the examining quantities. In order to compare different phenomena with different units is often convenient to normalize it, obtaining a relative value in percentage, the *normalized root mean square error* (*nRMSE*). For this purpose, the *RMSE* is conventionally divided by

the average value of the measured data on the same interval and then converted in percentage, that is:

$$nRMSE = \frac{RMSE}{\sqrt{\frac{1}{N}\sum_{i=1}^{N} x_{meas,i}^2}} \tag{4.24}$$

The *RMSE* measures the difference between the desired distribution and that obtained from numerical simulation and calculates a weighted average error.

It is shown that this index can be expressed as a linear combination of two terms:

$$RMSE^2 = MBE^2 + STDERR^2 \tag{4.25}$$

The two terms in the previous formula are respectively:

- the *mean bias error* (*MBE*), defined as the mean difference between the prediction and the measurement and it represents the systematic part (bias) of the error, defined as:

$$MBE = \bar{\varepsilon} = \frac{1}{N}\sum_{i=1}^{N} \varepsilon_i \tag{4.26}$$

- the *standard deviation of errors* (*STDERR*), which indicates the dispersion level of errors around their arithmetic mean value, it corresponds to the statistical error:

$$STDERR = \sigma = \sqrt{\frac{1}{N}\sum_{i=1}^{N}\left(\varepsilon_i - \bar{\varepsilon}\right)^2} \tag{4.27}$$

From equation (4.25), it is worth noted that the standard deviation captures the part of the *RMSE* that is not due to systematic error, and provides an indication of the *RMSE* that can be achieved once the *MBE* is essentially eliminated [112]. The *RMSE* is only a relative indicator of the quality of the model, therefore, a difference of 20 – 30 % between a prediction model and another is significant and should be taken into account. However, a difference less than 10 % is meaningless, while a difference of a few percent is totally negligible. This means that to earn only 2 % or 5 % in terms of *RMSE*,

increasing the complexity of the model, does not give any significant improvement in the results, but only a greater computational effort.

Another useful parameter to evaluate the accuracy of forecasts is the *mean absolute error* (*MAE*), defined as follows:

$$MAE = \frac{1}{N}\sum_{i=1}^{N}\left|\varepsilon_i\right| \tag{4.28}$$

This parameter is more sensitive to high-value errors, so it is a statistical measure, useful in those applications insensitive to minor error. The *MAE* provides a more appropriate measurement of the amplitude of the mean error than the *RMSE*, because the latter parameter also includes a part of error related to the dispersion of data. For this reason the values of *MAE* are never higher than those of *RMSE* (*MAE* ≤ *RMSE*). It should be noted that the *MAE* is inversely proportional to the number of available data N, while the *RMSE* is inversely proportional to $\sqrt{N}$, therefore when the number of data increases, their difference increases.

As explained in [112], forecast evaluation and accuracy metrics provide a way to generate prediction intervals (or confidence intervals) for forecasting. These prediction intervals indicate the range in which the actual value is expected to appear with a quantified probability [84]. Therefore, adding prediction intervals to the forecasts, builds an indicator of its expected accuracy: single deterministic forecast values are replaced by distributions or ranges of values that can be expected.

4.7 Error calculation of the prediction with respect to irradiance measurements

One of the main reasons of the importance of the solar irradiance forecast is the management of electrical grids in order to minimize the costs of energy imbalance.

From eq. (4.22), the prediction error, ε, is defined as the difference between the 1-day ahead forecast and the measured irradiance from pyranometer:

$$\varepsilon_G = G_{fore} - G_{meas} \tag{4.29}$$

Tables 4.18, 4.19, 4.20, 4.21 and 4.22 show the errors calculation results between the 1, 2, and 3-day ahead irradiance forecasts and the pyranometer measurements for the days of July 2012 in the site "Gi". It is noteworthy that the *RMSE* and *STDERR* errors are in W/m^2. On the contrary, the *nRMSE, MBE* and *MAE* errors are reported in per unit with respect to 1 kW/m^2 for all the types of forecast.

Examining the results, the 1-day ahead forecast is the most accurate, with low errors compared to the 2-day and 3-day ahead forecasts. In particular, considering the *RMSE* errors in Table 4.18, the average value of the 1-day ahead forecasts give figures around 119 W/m^2, whereas the maximum value is around 266 W/m^2 and the minimum value is around 81 W/m^2. As per the *nRMSE* errors in Table 4.19, the average value of the 1-day ahead forecasts is around 27 W/m^2, the maximum value is around 81 W/m^2, whereas the minimum value is around 16 W/m^2. As shown in Table 4.20, the *STDERR* errors for the 1-day ahead forecasts give figures around 108 W/m^2 in average, whereas the maximum value is around 240 W/m^2 and the minimum value is around 77 W/m^2.

Considering the *MBE* errors in Table 4.21, it can be pointed out that, in average, the 1-day ahead forecasts give figures around 0.05. In the best results the *MBE* index decreases down to 0.02 and in the worst results they rise up to 0.14. As per the *MAE* errors show in

Table 4.22, the average value for the 1-day ahead forecasts is 0.09, the minimum value is 0.06 and the maximum value is 0.18.

Table 4.18 – The Root Mean Square Errors in July in the site "Gi".

Date	***RMSE* 1-day**	***RMSE* 2-day**	***RMSE* 3-day**
01/07/2012	88.50	124.81	152.06
02/07/2012	93.14	131.47	160.79
03/07/2012	124.98	176.37	217.65
04/07/2012	91.06	128.64	158.47
05/07/2012	138.21	196.59	241.15
06/07/2012	106.64	151.71	186.64
07/07/2012	187.72	265.60	324.53
08/07/2012	91.54	129.25	158.02
09/07/2012	90.06	127.96	157.86
10/07/2012	115.65	165.01	200.00
11/07/2012	90.10	119.08	148.58
12/07/2012	217.54	311.00	382.51
13/07/2012	82.02	115.34	140.77
14/07/2012	81.44	114.54	140.99
15/07/2012	86.81	123.07	154.13
16/07/2012	108.59	155.48	189.54
17/07/2012	83.22	115.68	141.03
18/07/2012	84.68	120.82	146.94
19/07/2012	86.23	121.04	148.92
20/07/2012	82.90	116.06	139.52
21/07/2012	93.81	130.77	143.52
22/07/2012	147.87	196.77	244.51
23/07/2012	219.18	373.12	486.69
24/07/2012	262.97	372.57	455.33
25/07/2012	266.33	378.85	463.78
26/07/2012	135.56	190.59	233.91
27/07/2012	88.01	125.35	152.41
28/07/2012	82.14	114.48	139.34
29/07/2012	98.71	140.02	171.38
30/07/2012	96.49	136.48	165.05
31/07/2012	81.50	112.22	135.96

Table 4.19 – The Normalized Root Mean Square Errors in July in the site “Gi”.

Date	***nRMSE* 1-day**	***nRMSE* 2-day**	***nRMSE* 3-day**
01/07/2012	18.20	18.15	18.06
02/07/2012	19.24	19.20	19.18
03/07/2012	26.56	26.51	26.71
04/07/2012	18.79	18.78	18.89
05/07/2012	29.70	29.87	29.92
06/07/2012	21.76	21.89	21.99
07/07/2012	42.25	42.27	42.17
08/07/2012	18.52	18.49	18.46
09/07/2012	18.64	18.73	18.87
10/07/2012	24.70	24.92	24.66
11/07/2012	18.40	17.20	17.52
12/07/2012	53.71	54.29	54.52
13/07/2012	16.28	16.19	16.13
14/07/2012	16.11	16.02	16.10
15/07/2012	17.83	17.87	18.28
16/07/2012	21.89	22.16	22.06
17/07/2012	16.43	16.15	16.08
18/07/2012	16.75	16.90	16.78
19/07/2012	17.41	17.28	17.36
20/07/2012	16.72	16.55	16.24
21/07/2012	19.48	19.20	17.20
22/07/2012	32.81	30.88	31.33
23/07/2012	81.48	98.08	104.46
24/07/2012	61.22	61.33	61.20
25/07/2012	75.46	75.90	75.87
26/07/2012	29.09	28.92	28.98
27/07/2012	18.09	18.21	18.08
28/07/2012	16.86	16.61	16.51
29/07/2012	21.98	22.05	22.03
30/07/2012	20.16	20.16	19.91
31/07/2012	16.90	16.46	16.28

Table 4.20 – The Standard Deviation of Errors in July in the site “Gi”.

Date	*STDERR* 1-day	*STDERR* 2-day	*STDERR* 3-day
01/07/2012	77.30	117.36	164.16
02/07/2012	79.61	122.67	174.64
03/07/2012	106.23	163.87	235.84
04/07/2012	80.71	121.61	168.88
05/07/2012	117.84	182.11	262.06
06/07/2012	97.34	145.43	196.21
07/07/2012	168.37	252.37	345.44
08/07/2012	83.66	124.37	166.55
09/07/2012	79.29	120.43	168.53
10/07/2012	101.38	154.56	216.41
11/07/2012	80.74	118.20	152.76
12/07/2012	188.82	290.31	411.90
13/07/2012	77.31	112.36	146.20
14/07/2012	77.68	112.28	145.15
15/07/2012	78.63	117.64	160.98
16/07/2012	103.50	150.79	195.94
17/07/2012	78.07	113.16	146.85
18/07/2012	81.05	118.17	151.59
19/07/2012	80.08	117.26	155.28
20/07/2012	76.96	112.57	147.40
21/07/2012	85.96	126.84	155.66
22/07/2012	135.70	196.48	247.96
23/07/2012	180.53	319.13	509.40
24/07/2012	239.83	356.38	480.80
25/07/2012	228.02	352.05	503.53
26/07/2012	129.02	186.56	240.78
27/07/2012	84.83	122.84	156.70
28/07/2012	78.19	112.62	143.83
29/07/2012	86.10	131.23	184.78
30/07/2012	92.43	133.79	170.38
31/07/2012	77.83	110.75	140.11

Table 4.21 – The Mean Bias Errors in July in the site “Gi”.

Date	***MBE* 1-day**	***MBE* 2-day**	***MBE* 3-day**
01/07/2012	0.043	0.086	0.127
02/07/2012	0.048	0.096	0.143
03/07/2012	0.066	0.131	0.199
04/07/2012	0.042	0.084	0.128
05/07/2012	0.072	0.146	0.220
06/07/2012	0.044	0.087	0.131
07/07/2012	0.083	0.166	0.247
08/07/2012	0.037	0.072	0.107
09/07/2012	0.043	0.086	0.131
10/07/2012	0.056	0.113	0.165
11/07/2012	0.040	0.054	0.093
12/07/2012	0.108	0.220	0.331
13/07/2012	0.027	0.053	0.078
14/07/2012	0.024	0.047	0.070
15/07/2012	0.037	0.073	0.116
16/07/2012	0.033	0.071	0.104
17/07/2012	0.029	0.053	0.076
18/07/2012	0.025	0.050	0.071
19/07/2012	0.032	0.062	0.094
20/07/2012	0.031	0.059	0.080
21/07/2012	0.038	0.069	0.056
22/07/2012	0.059	0.069	0.124
23/07/2012	0.124	0.318	0.520
24/07/2012	0.108	0.217	0.323
25/07/2012	0.138	0.278	0.416
26/07/2012	0.042	0.081	0.122
27/07/2012	0.023	0.048	0.068
28/07/2012	0.025	0.046	0.066
29/07/2012	0.048	0.097	0.145
30/07/2012	0.028	0.055	0.077
31/07/2012	0.024	0.042	0.060

Table 4.22 – The Mean Absolute Errors in July in the site “Gi”.

Date	***MAE* 1-day**	***MAE* 2-day**	***MAE* 3-day**
01/07/2012	0.069	0.138	0.205
02/07/2012	0.073	0.146	0.219
03/07/2012	0.093	0.185	0.280
04/07/2012	0.069	0.138	0.208
05/07/2012	0.099	0.201	0.302
06/07/2012	0.071	0.142	0.215
07/07/2012	0.116	0.232	0.348
08/07/2012	0.068	0.137	0.205
09/07/2012	0.069	0.138	0.210
10/07/2012	0.083	0.169	0.250
11/07/2012	0.070	0.124	0.192
12/07/2012	0.146	0.294	0.441
13/07/2012	0.062	0.122	0.182
14/07/2012	0.063	0.125	0.189
15/07/2012	0.066	0.132	0.205
16/07/2012	0.074	0.149	0.221
17/07/2012	0.063	0.124	0.186
18/07/2012	0.067	0.135	0.202
19/07/2012	0.066	0.130	0.197
20/07/2012	0.061	0.121	0.179
21/07/2012	0.068	0.134	0.172
22/07/2012	0.096	0.167	0.261
23/07/2012	0.153	0.374	0.602
24/07/2012	0.179	0.358	0.536
25/07/2012	0.181	0.363	0.544
26/07/2012	0.084	0.166	0.250
27/07/2012	0.064	0.130	0.194
28/07/2012	0.063	0.124	0.184
29/07/2012	0.076	0.152	0.228
30/07/2012	0.069	0.138	0.205
31/07/2012	0.063	0.122	0.181

Tables 4.23, 4.24, 4.25, 4.26 and 4.27 show the errors calculation results between the 1, 2, and 3-day ahead irradiance forecasts and the pyranometer measurements for the days of July 2012 in the site “Ma”.

By analyzing the results, for the *RMSE* errors in Table 4.23 the average value of the 1-day ahead forecasts give figures around 107 W/m^2, whereas the maximum value is around 280 W/m^2 and the minimum value is around 82 W/m^2. Considering the *nRMSE* errors in Table 4.24, the average value of the 1-day ahead forecasts is around 23 W/m^2, the maximum value is around 82 W/m^2, whereas the minimum value is around 16 W/m^2. As shown in Table 4.25, the *STDERR* errors for the 1-day ahead forecasts give figures around 98 W/m^2 in average, whereas the maximum value is around 248 W/m^2 and the minimum value is around 79 W/m^2.

As per the *MBE* errors in Table 4.26, it can be pointed out that, in average, the 1-day ahead forecasts give figures around 0.04. In the best results the *MBE* index decreases down to 0.01 and in the worst results they rise up to 0.16. Considering the *MAE* errors show in Table 4.27, the average value for the 1-day ahead forecasts is 0.08, the minimum value is 0.06 and the maximum value is 0.19.

Table 4.23 – The Root Mean Square Errors in July in the site “Ma”.

Date	***RMSE* 1-day**	***RMSE* 2-day**	***RMSE* 3-day**
01/07/2012	91.20	127.12	154.25
02/07/2012	92.01	130.40	160.08
03/07/2012	89.07	126.44	155.14
04/07/2012	84.97	120.23	147.35
05/07/2012	99.15	137.85	168.40
06/07/2012	157.58	223.53	275.71
07/07/2012	116.01	166.57	205.47
08/07/2012	83.67	119.47	144.69
09/07/2012	89.06	123.47	151.05
10/07/2012	95.65	136.01	165.47
11/07/2012	89.68	124.04	152.78
12/07/2012	126.50	181.64	222.98
13/07/2012	86.11	120.95	147.64
14/07/2012	85.01	120.45	149.85
15/07/2012	89.73	128.03	158.47
16/07/2012	82.39	117.06	142.63
17/07/2012	87.81	122.17	148.97
18/07/2012	87.61	124.42	151.78
19/07/2012	89.40	126.96	154.76
20/07/2012	84.32	119.03	145.01
21/07/2012	92.79	129.13	154.61
22/07/2012	90.67	117.73	146.23
23/07/2012	251.97	347.56	428.62
24/07/2012	280.46	399.24	487.39
25/07/2012	132.72	177.48	212.55
26/07/2012	112.16	157.71	192.83
27/07/2012	86.21	122.67	149.58
28/07/2012	83.60	117.74	143.29
29/07/2012	96.36	136.36	166.48
30/07/2012	85.54	120.91	146.53
31/07/2012	82.38	113.91	137.79

Table 4.24 – The Normalized Root Mean Square Errors in July in the site “Ma”.

Date	***nRMSE* 1-day**	***nRMSE* 2-day**	***nRMSE* 3-day**
01/07/2012	18.72	18.45	18.28
02/07/2012	18.96	19.00	19.04
03/07/2012	17.94	18.01	18.05
04/07/2012	17.16	17.16	17.18
05/07/2012	19.62	19.29	19.24
06/07/2012	33.48	33.59	33.82
07/07/2012	23.73	24.10	24.27
08/07/2012	16.36	16.52	16.33
09/07/2012	18.09	17.73	17.71
10/07/2012	20.02	20.12	19.99
11/07/2012	18.08	17.68	17.78
12/07/2012	27.08	27.50	27.56
13/07/2012	17.09	16.97	16.92
14/07/2012	16.88	16.91	17.18
15/07/2012	18.33	18.50	18.69
16/07/2012	16.27	16.35	16.26
17/07/2012	17.30	17.02	16.94
18/07/2012	17.35	17.42	17.35
19/07/2012	18.08	18.15	18.06
20/07/2012	16.63	16.60	16.51
21/07/2012	19.30	18.99	18.57
22/07/2012	19.00	17.44	17.69
23/07/2012	81.90	79.88	80.43
24/07/2012	75.31	75.80	75.56
25/07/2012	27.29	25.80	25.23
26/07/2012	23.19	23.06	23.02
27/07/2012	17.62	17.73	17.65
28/07/2012	17.11	17.04	16.93
29/07/2012	21.28	21.29	21.22
30/07/2012	17.53	17.53	17.34
31/07/2012	16.97	16.59	16.38

Table 4.25 – The Standard Deviation of Errors in July in the site “Ma”.

Date	*STDERR* 1-day	*STDERR* 2-day	*STDERR* 3-day
01/07/2012	81.42	121.40	165.11
02/07/2012	82.08	123.42	170.48
03/07/2012	81.31	120.81	163.49
04/07/2012	78.64	116.13	153.92
05/07/2012	92.65	133.85	175.91
06/07/2012	145.30	215.37	287.74
07/07/2012	108.83	160.17	213.16
08/07/2012	80.15	117.24	149.13
09/07/2012	80.89	118.79	159.81
10/07/2012	84.55	128.26	177.92
11/07/2012	82.24	120.98	159.12
12/07/2012	112.55	170.61	237.80
13/07/2012	82.39	118.61	151.71
14/07/2012	81.95	117.99	152.75
15/07/2012	82.62	122.85	165.49
16/07/2012	79.32	114.52	146.47
17/07/2012	83.83	120.40	153.68
18/07/2012	84.69	122.51	155.34
19/07/2012	84.71	123.77	160.23
20/07/2012	82.06	117.49	148.28
21/07/2012	85.51	125.39	163.49
22/07/2012	84.63	115.99	151.48
23/07/2012	193.15	313.31	482.46
24/07/2012	248.40	376.59	522.05
25/07/2012	132.14	174.36	212.52
26/07/2012	109.32	156.16	195.98
27/07/2012	83.82	120.61	152.84
28/07/2012	80.52	116.06	146.96
29/07/2012	85.11	128.40	178.85
30/07/2012	83.19	119.74	149.60
31/07/2012	79.74	112.84	140.97

Table 4.26 – The Mean Bias Errors in July in the site “Ma”.

Date	***MBE* 1-day**	***MBE* 2-day**	***MBE* 3-day**
01/07/2012	0.041	0.079	0.115
02/07/2012	0.042	0.084	0.126
03/07/2012	0.036	0.074	0.111
04/07/2012	0.032	0.063	0.096
05/07/2012	0.035	0.068	0.100
06/07/2012	0.061	0.121	0.186
07/07/2012	0.040	0.086	0.131
08/07/2012	0.024	0.047	0.066
09/07/2012	0.037	0.071	0.105
10/07/2012	0.045	0.090	0.132
11/07/2012	0.036	0.063	0.099
12/07/2012	0.058	0.120	0.181
13/07/2012	0.025	0.049	0.073
14/07/2012	0.023	0.047	0.074
15/07/2012	0.035	0.071	0.109
16/07/2012	0.022	0.046	0.068
17/07/2012	0.026	0.047	0.065
18/07/2012	0.022	0.044	0.064
19/07/2012	0.029	0.057	0.083
20/07/2012	0.019	0.038	0.051
21/07/2012	0.036	0.067	0.093
22/07/2012	0.033	0.053	0.081
23/07/2012	0.162	0.312	0.473
24/07/2012	0.130	0.263	0.391
25/07/2012	0.012	0.046	0.077
26/07/2012	0.025	0.047	0.070
27/07/2012	0.020	0.043	0.060
28/07/2012	0.022	0.042	0.060
29/07/2012	0.045	0.091	0.135
30/07/2012	0.020	0.037	0.049
31/07/2012	0.021	0.036	0.050

Table 4.27 – The Mean Absolute Errors in July in the site “Ma”.

Date	***MAE* 1-day**	***MAE* 2-day**	***MAE* 3-day**
01/07/2012	0.070	0.138	0.205
02/07/2012	0.068	0.136	0.205
03/07/2012	0.068	0.137	0.207
04/07/2012	0.064	0.128	0.193
05/07/2012	0.075	0.147	0.221
06/07/2012	0.097	0.194	0.294
07/07/2012	0.079	0.162	0.246
08/07/2012	0.065	0.131	0.195
09/07/2012	0.068	0.133	0.199
10/07/2012	0.074	0.148	0.220
11/07/2012	0.067	0.130	0.196
12/07/2012	0.092	0.187	0.281
13/07/2012	0.067	0.133	0.199
14/07/2012	0.066	0.133	0.203
15/07/2012	0.068	0.137	0.208
16/07/2012	0.062	0.125	0.187
17/07/2012	0.069	0.136	0.204
18/07/2012	0.069	0.139	0.208
19/07/2012	0.070	0.141	0.211
20/07/2012	0.066	0.132	0.199
21/07/2012	0.071	0.140	0.205
22/07/2012	0.072	0.128	0.197
23/07/2012	0.189	0.370	0.558
24/07/2012	0.188	0.378	0.566
25/07/2012	0.100	0.186	0.271
26/07/2012	0.070	0.141	0.211
27/07/2012	0.066	0.133	0.199
28/07/2012	0.065	0.130	0.193
29/07/2012	0.073	0.147	0.219
30/07/2012	0.068	0.137	0.204
31/07/2012	0.064	0.126	0.187

In the following figures, the error duration curve, calculated both for *MBE* and *MAE*, of the 1-day ahead predictions with respect to the irradiance measurements with sampling time of quarter-hours and on an annual basis are represented for the sites “Gi” and “Ma”.

In Fig. 4.40 the error duration curves of positive and negative *MBE* are shown for the site “Gi”. In this case, the prediction error is within a range of 10 − 80 %. To consider the maximum errors (here equal to 80 %) corresponding to 100 % of the time for *MBE* parameter is not a practical choice. In this regard, a good compromise is represented by the 95 % threshold for which the previous parameters are highlighted in the following duration curves. Therefore, for the 95 % of the time, considering positive *MBE* errors (prediction > measurement), *MBE* is less than 25 %; on the contrary, for negative *MBE* errors (prediction < measurement), *MBE* is less than 20 %. Similar considerations are made for *MAE*. In Fig. 4.41 the *MAE* error duration curve is shown for the site “Gi”. Also in this case, to consider the maximum errors corresponding to 100 % of the time for *MAE* parameter is not a practical choice. Therefore, for 95 % of time, *MAE* is less than 28 %.

In Fig. 4.42 the error duration curves of positive and negative *MBE* are shown for the site “Ma”. In this case, the prediction error is within the 80 % and 10 %. For 95 % of the time, considering positive *MBE* errors, *MBE* is less than 22 %; on the contrary, for negative *MBE* errors, *MBE* is less than 20 %. Considering the *MAE* error duration curve for the site “Ma” in Fig. 4.43, for 95 % of time, *MAE* is less than 25 %.

Actually, from the given definitions of the different errors, the *MAE* figures are intrinsically higher than the corresponding ones in *MBE*.

In Fig. 4.44 the zoom of duration curves for positive *MBE* errors are shown in the same graph for the site “Gi” and “Ma”. For 95 % of the time, positive *MBE* is less than 50 % for the site “Gi” and around 45 % for the site “Ma”. On the contrary, in Fig. 4.45 the zoom of duration curves for negative *MBE* errors are shown in the same graph for the site “Gi” and “Ma”. For 95 % of the time, negative *MBE* is around 27 % for the site “Gi” and less than 25 % for the site “Ma”. In Fig. 4.46 the zoom of duration curves for *MAE* errors

are shown in the same graph for the site “Gi” and “Ma”. For 95 % of the time, *MAE* is around 42 % for the site “Gi” and less than 38 % for the site “Ma”.

It is noteworthy that the two locations are closed to the correctness boundary limits of *Meteo.cat* provider. Therefore, considering more locations the errors may decrease.

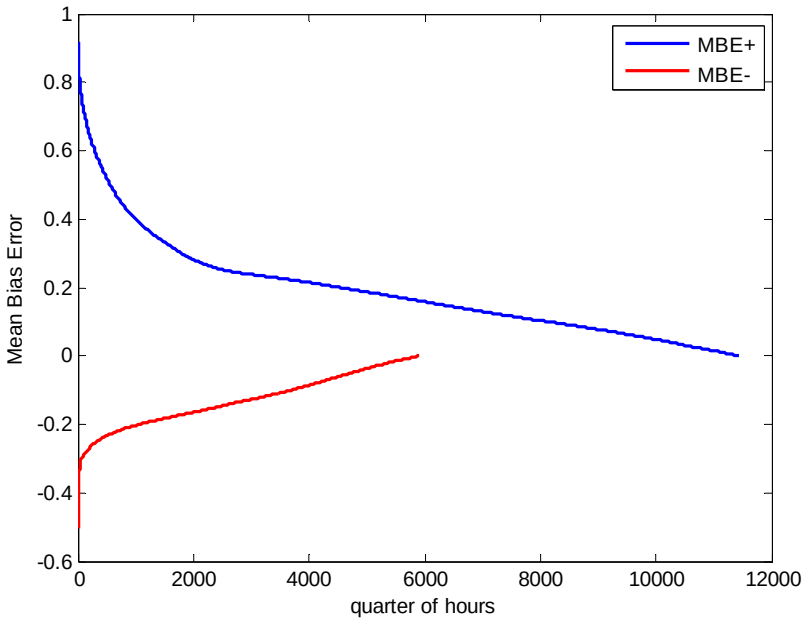

Fig. 4.40 − Error duration curve of positive and negative *MBE* errors for the prediction wrt irradiance measurements for the year 2012 for the site “Gi”.

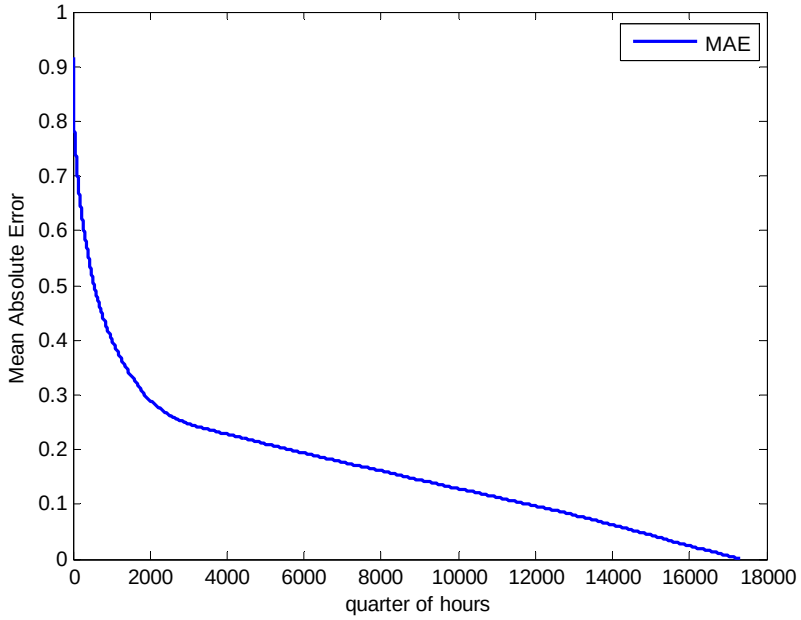

Fig. 4.41 − Error duration curve of *MAE* error for the prediction wrt irradiance measurements for the year 2012 for the site “Gi”.

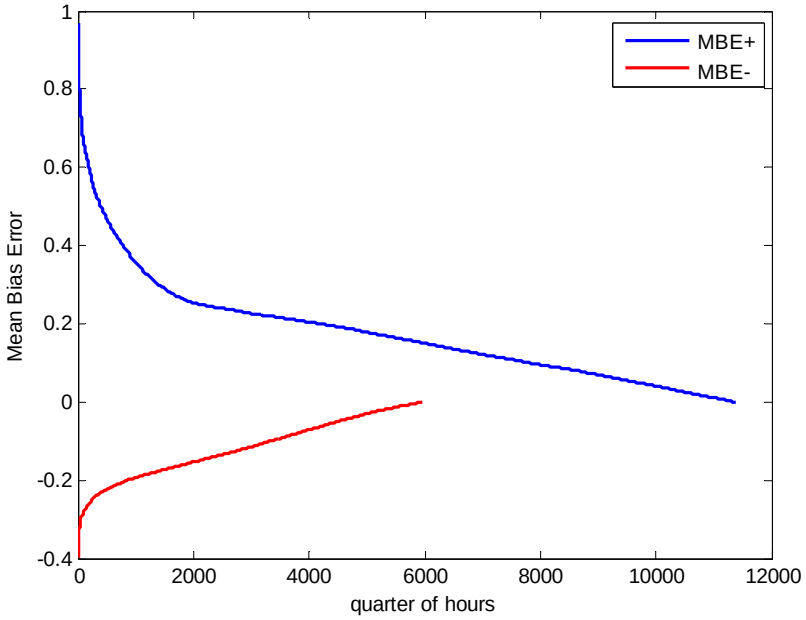

Fig. 4.42 − Error duration curve of positive and negative *MBE* errors for the prediction wrt irradiance measurements for the year 2012 for the site “Ma”.

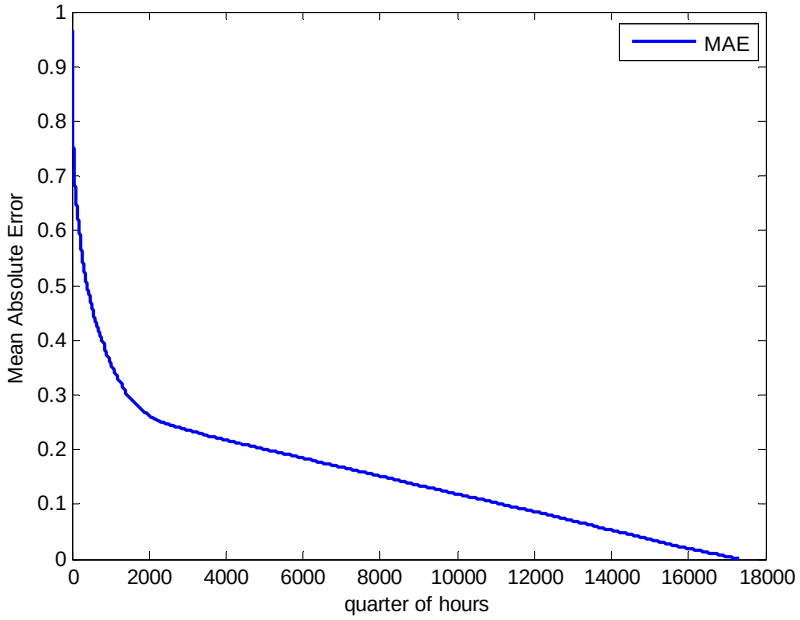

Fig. 4.43 − Error duration curve of *MAE* error for the prediction wrt irradiance measurements for the year 2012 for the site “Ma”.

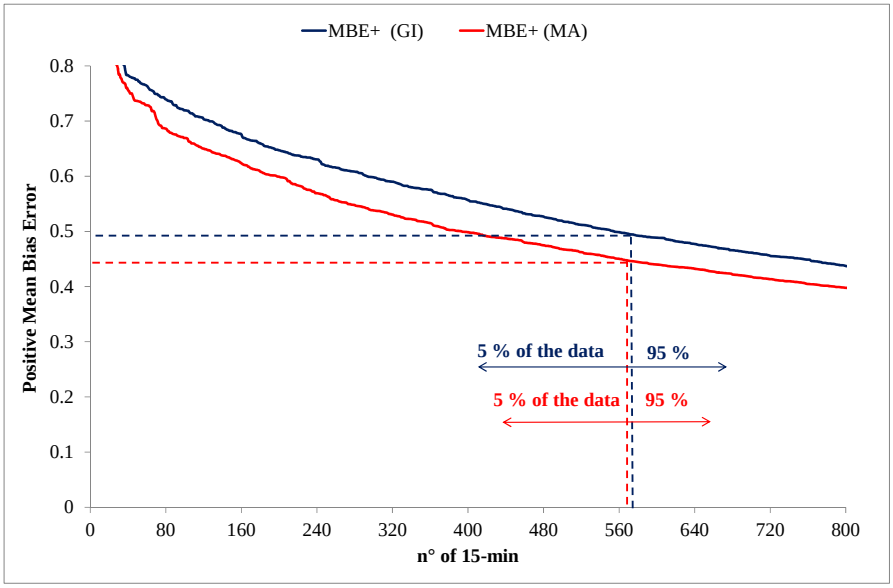

Fig. 4.44 – Zoom of the error duration curves of positive *MBE* errors for the prediction wrt irradiance measurements for the year 2012 for the sites “Gi” and “Ma”.

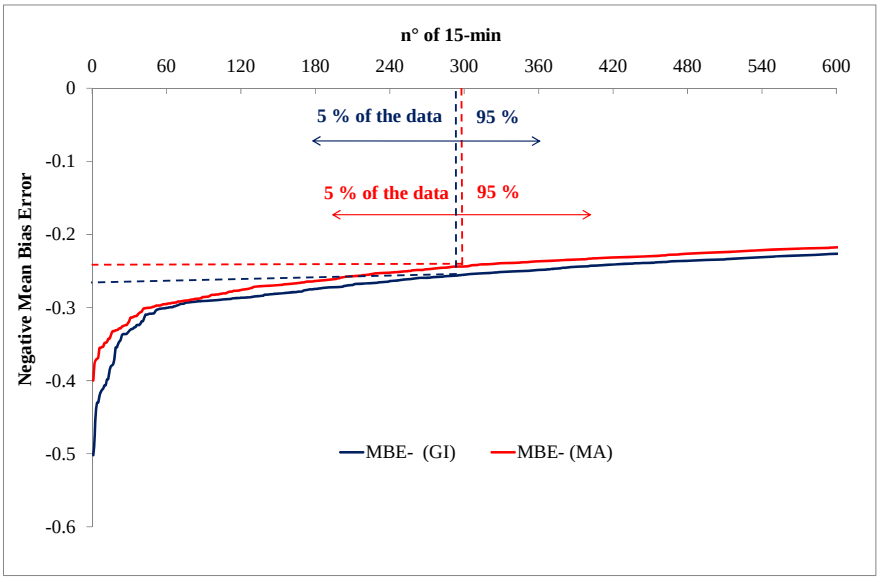

Fig. 4.45 – Zoom of the error duration curves of negative *MBE* errors for the prediction wrt irradiance measurements for the year 2012 for the sites "Gi" and "Ma".

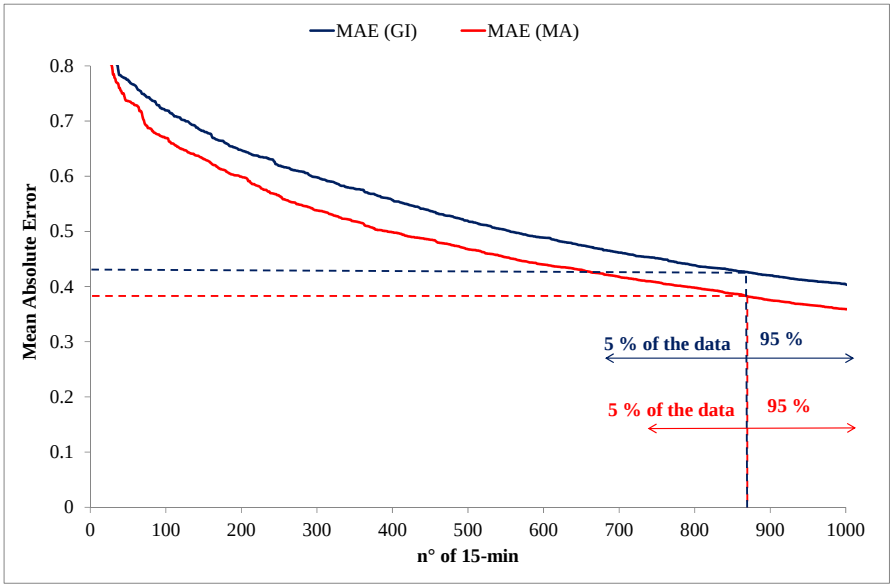

Fig. 4.46 – Zoom of the error duration curves of *MAE* errors for the prediction wrt irradiance measurements for the year 2012 for the sites "Gi" and "Ma".

4.8 Summary

Due to the intermittent nature of the solar irradiance, the ability to predict, with low error, the 1-day ahead PV production permits to reduce the unbalance between provisional budget and final budget in the electricity market. In this chapter, the comparison between irradiance measurements and 3-day ahead forecasts, properly interpolated, is presented for two sites ("Gi" and "Ma") placed in South of Italy.

A method to classify each hour of a day in three categories (variable, cloudy, or clear) is implemented on annual basis. In this way, the number of passes/fails recorded by the hourly classification method from pyranometer measurements with respect to the hourly classification method from 1-day before forecast is analyzed. As results, in summer the highest number of hourly passes occurs for the variable − variable condition; on the contrary, in winter it occurs for the cloudy – cloudy condition. The low number of clear-sky days in spring and summer months, can be explained by the turbidity in air, e.g. due to pollution. In the site "Ma" the number of clear-sky days is lower than in the site "Gi", e.g. due to its proximity with high pollution areas (industrial steel mills).

From the comparison of the 2-day ahead and 3-day ahead predictions vs. the 1-day ahead prediction, considered as the most accurate, the deviations show that positive and negative deviations are quite negligible in summer months (< 20 W/m^2 in the site "Gi" and ≤ 30 W/m^2 in the site "Ma"). Major deviations occur in winter, spring and autumn months. In particular, the deviations between the 3-day ahead predictions vs. the 1-day ahead predictions are greater than the 2-day ahead predictions vs. the 1-day ahead predictions. The site "Gi" presents major deviations than the site "Ma". Moreover, the analysis of the "broken clouds" phenomenon, considered as a subset of the variable sky condition, even if noticeable on 1-min scale, loses importance on 15-min scale.

Finally, the accuracy between the predicted and measured data is carried out through the use of statistical indicators: the Mean Absolute Error (*MAE*) and the Mean Bias Error (*MBE*). Considering, positive and negative *MBE* errors, the error duration curves are

presented for 15-min averaged solar irradiance values and on annual basis. As results, for 95 % of the time, in case of positive errors (prediction > measurement), the *MBE* is < 25 % in the site “Gi” and ≈ 22 % in the site “Ma”, on the contrary for negative errors, *MBE* is < 20 % in the site “Gi” and ≈ 20 % in the site “Ma”.

Chapter 5

Prediction of AC power profiles vs. experimental results

Introduction

A dedicated PV conversion model is the tool to link the irradiance and cell temperature data with the AC power delivered to the grid.

In this chapter, for the definition of the PV conversion model [113], many loss factors that influence the PV system behavior, are firstly taken into account. Moreover, the error parameters are determined with respect to the real grid-connected PV systems in the sites “Gi” and “Ma” 1 MW_p per each.

5.1. Loss Factors in PV systems

In Ref. [114] the authors give a list of energy losses, that covers losses in PV systems under normal operation and excludes energy losses due to defects and breakdowns of the system. It is possible to classify these losses in irradiation losses and system losses, as follows.

[1] Irradiation losses:

- *Tilt conversion effect*

The tilt conversion effect includes the gain or loss of global irradiation in a tilted plane with respect to the horizontally received global irradiation in the same period.

- *Spectral losses*

The spectral loss covers the losses of useful irradiation due to the selective spectral response of PV modules in case of deviations between the available irradiation's spectrum and the standard spectrum at AM 1.5.

- *Reflection losses*

The reflection loss is the loss of irradiation at the surface of the PV modules where a part of the incident light is reflected before being absorbed by the PV modules.

- *Irradiation losses caused by shading*

The irradiation loss caused by shading is the difference between the irradiation of the unshaded PV array and the irradiation of the shadowed array.

- *Soiling losses*

For the evaluation of the PV soiling losses, two environments, in which the PV system can be located, are considered.

In the first case, i.e. clean environment, no maintenance is required because the losses are limited to 1 – 5 % (mean value 3 %). In the second case, i.e. dirty (polluted) environment, due to surrounding landfill, mine, construction site, agricultural land, quarries, etc., suitable cleaning should be carried out.

In particular, in order to decide the interval between two cleanings, it is possible to follow a conventional procedure taking into account the months from April to September (about 70 % of the yearly production) and assuming that in a clear-sky day after a rainy day the solar cell is considered clean.

Thus, the losses due to soiling can be determined according to the values of daily irradiation of the solar cell in two clear-sky days, before rain (G_{b_rain}) and after rain (G_{a_rain}) as:

$$\eta_{dirt} = \frac{\left(G_{a\_rain} - G_{b\_rain}\right)}{G_{a\_rain}} \cdot 100 \tag{5.1}$$

Taking into account the data collected from the meteorological station in the site “Gi”, with time step of 1 minute, and considering that between 2 clear-sky days (July 20th and 28th 2012) with the same weather conditions , after a long period without rain (about 1 month and a half), there were moderate (2 − 6 mm/h) and strong (> 6 mm/h) rain, the losses due to soiling are equal to 2.4 % for one of the solar cells placed on the horizontal plane and 2.3 % for the pyranometer.

Therefore, generally in case of suitable cleaning, the soiling losses are in the range 1 – 5 % (mean value 3 %) and three washes in the spring/summer months are necessary. If no maintenance of the dirty environment is carried out, the soiling losses are in the range from 10 – 20 %.

[2] System losses:

- *Module deviation from power specifications*

Module deviation from power specifications comprise the difference between the rated name-plate value of the PV modules and the mean installed nominal power per PV module under STC conditions.

- *Low irradiance losses*

Low irradiance losses are the energy losses in the PV modules at irradiance levels other than the STC irradiance of 1000 W/m^2, at the STC temperature of 25°C and assuming ideal maximum power-point tracking.

- *Temperature effect*

The temperature effect covers both the energy gain and the energy loss due to module temperatures being lower than or exceeding the STC temperature of 25°C, on the assumption of ideal maximum power-point tracking.

- *DC-cable losses*

DC-cable losses are defined by the ohmic losses in the wiring, on the assumption that parts of the PV array are uncoupled and that maximum power-point tracking is ideal.

- *Losses in string diodes*

String diodes bring about a small voltage drop in the DC-cables, which leads to an energy loss.

- *$I-V$ mismatch losses*

Mismatch losses are caused by deviations between the shapes of the I-V curves of coupled PV modules or larger sub-parts of the PV system. For this reason, the maximum power-point decreases with respect to its optimum under the corresponding meteorological conditions.

Several sources of variations in the I-V curves of modules can be distinguished:

- Variations between PV modules due to the manufacturing process.
- Spatially varying array temperatures.

- Mismatch losses due to inhomogeneous irradiance on the array plane: A PV array can be irradiated inhomogeneously because of shading resulting from surrounding objects, or because of differences in the orientation of portions of the array.
- Different DC-cables.
- Different types of PV modules.

- *Losses due to non-ideal maximum power-point tracking*

These losses, called MPPT-losses, occur when the power produced by PV array deviates from the expected value, given the actual meteorological and system conditions which cover all losses mentioned before. These losses can be subdivided into:

- Static MPPT-losses that are determined by the efficiency of the MPP-tracker under stable irradiance conditions.
- Dynamic MPPT-losses that include the energy effect of two causes, i.e. firstly the searching algorithm of the MPP-tracker, which sweeps through the voltage domain of the tracker, and secondly, fast fluctuating irradiance levels which result in a varying array power which may not be detected correctly by a relatively slow tracker.

- *Inverter-losses*

Energy effects occurring in the inverter can be divided into two sources:

- Losses caused by DC/AC energy conversion. These losses are determined by the inverter's efficiency curve which should include the standby energy consumption of inverter.
- Effects caused by inverter control. Effects resulting from inverter control are, firstly, the energy loss resulting from the protective cut-off procedure at high input powers and increased inverter temperatures, and, secondly, the effect of the cascade coupling of a number of inverters.

5.2. Description of the grid-connected PV systems

The real grid-connected PV system has a power rating of 993.6 kW_p for the site "Gi" and of 997.285 kW_p for the site "Ma" in Standard Test Conditions (STC: global irradiance G_{STC} = 1 kW/m^2 and cell temperature T_{STC} = 25 °C).

The PV system in the site "Gi" is equipped with polycrystalline silicon modules of 230 W_p each, tilted at 30° with South orientation (mod. SLK60P6L).

On the contrary, the PV system in the site "Ma" is equipped with monocrystalline silicon modules of 230 W_p, 235 W_p and 240 W_p (mod. SLK60M6L) and with polycrystalline silicon modules of 230 W_p, 235 W_p and 240 W_p (mod. SLK60P6L), tilted at 30° with South orientation.

The PV arrays of each site, placed on a metallic structure which permit the natural air circulation, feed two centralized inverters with high efficiency (transformerless option).

These power conditioning units are slightly undersized, given that the 500-kVA inverter (mod. 500 HE) is supplied by a 552 kW_p array for the site "Gi" and by a 541.956 kW_p array for the site "Ma"; and the 400-kVA inverter (mod. 400 HE), is supplied by a 441.6 kW_p array for the site "Gi" and by a 455.329 kW_p array for the site "Ma", respectively.

5.3. Comparison between predicted power profiles and experimental results

As previously mentioned, for the definition of the PV conversion model [113], many loss factors that influence the PV system behavior, must be taken into account. In the case under study, the main sources are reported in the following:

- losses for soiling and dirt (l_{dirt}), due to pollution, with the assumption that the plant is located in a clean environment, away from mines, landfills, etc.
- losses due to reflection of the PV module glass (l_{refl}): the amount has been taken from PVGIS website [73];
- thermal losses (l_{th}) with respect to STC, they are calculated by the following formula:

$$l_{th} = \gamma_{th} \cdot \left(T_C - T_{STC}\right) \tag{5.2}$$

where γ_{th} is the thermal coefficient of maximum power of the modules, dependent on the PV technology (for crystalline silicon $\gamma_{th} \approx$ -0.5 %/°C); T_C is the cell temperature, calculated, in a first analysis, by (5.3), in which *NOCT* (Normal Operating Cell Temperature: 42−50 °C) is a mean temperature in outdoor operation:

$$T_C = T_{amb} + \left(NOCT - 20°C\right) \cdot G_{tcell} \Big/ 0.8\,kW/m^2 \tag{5.3}$$

- electrical mismatch losses (l_{mis}), assumed equal to the manufacturing tolerance with typical values of ±3 %;
- DC-cable losses (l_{cable}) around 1 − 2 %, according to a good design criteria.

On the basis of the previous parameters in terms of efficiencies, the available power at maximum power point is achieved by:

$$P_{mpp} = P_{rated} \cdot \left(G_{tcell} - G_{\lim}\right) \cdot \eta_{dirt} \cdot \eta_{refl} \cdot \eta_{th} \cdot \eta_{mis} \cdot \eta_{cable} \tag{5.4}$$

where G_{lim} is the irradiance limit below which the output is vanishing.

Finally, thanks to the conversion model of power conditioning unit, the AC power injected into the grid is calculated:

$$P_{DC} = \eta_{MPPT} \cdot P_{mpp} \tag{5.5}$$

$$P_{DC} = P_{AC} + P_0 + c_L \cdot P_{AC} + c_s \cdot P_{AC}^2 \tag{5.6}$$

where: η_{MPPT} is the efficiency of the tracker; P_0 are the no-load power losses along the operation; c_L is the linear loss coefficient; c_S is the square loss coefficient.

Thus, by using the solving formula of the 2nd order equation, P_{AC} is calculated from the input power and the loss parameters of the inverter model as follows:

$$P_{AC} = \frac{-\left(1+c_L\right)+\sqrt{\left(1+c_L\right)^2+4\cdot c_S\cdot\left(P_{DC}-P_0\right)}}{2\cdot c_S} \tag{5.7}$$

Therefore, if the reference-cell data G_{tcell}, averaged on 15-min basis, are used as inputs of the above-described model, the outputs in terms of delivered power to the grid, P_{fore}, can be compared with the energy meters of the PV plant, P_{meas}.

Figures 5.1, 5.2, 5.3, 5.4 and 5.5 show the application of the PV conversion model to the reference-cell data in the best month for the irradiation (July) in the site “Gi”.

For example, in Fig. 5.2, day 10 shows that the 15-min averaging, typical for electricity tariff, smooth the power variations around 2 p.m. (at 35−40 quarters of hour) from the viewpoint of the utility grid. In Fig. 5.4, day 23 exhibits low deviations in this extremely variable day: that means the model is able to follow also huge irradiance variations. Moreover, thanks to the days with clear sky, since the deviations are proportional to the irradiance, it is possible to detect the failure of a portion in the PV arrays: the model is useful for fault diagnosis. More precisely, from day 04 to day 19 of July the failure of a portion in the PV arrays is detected.

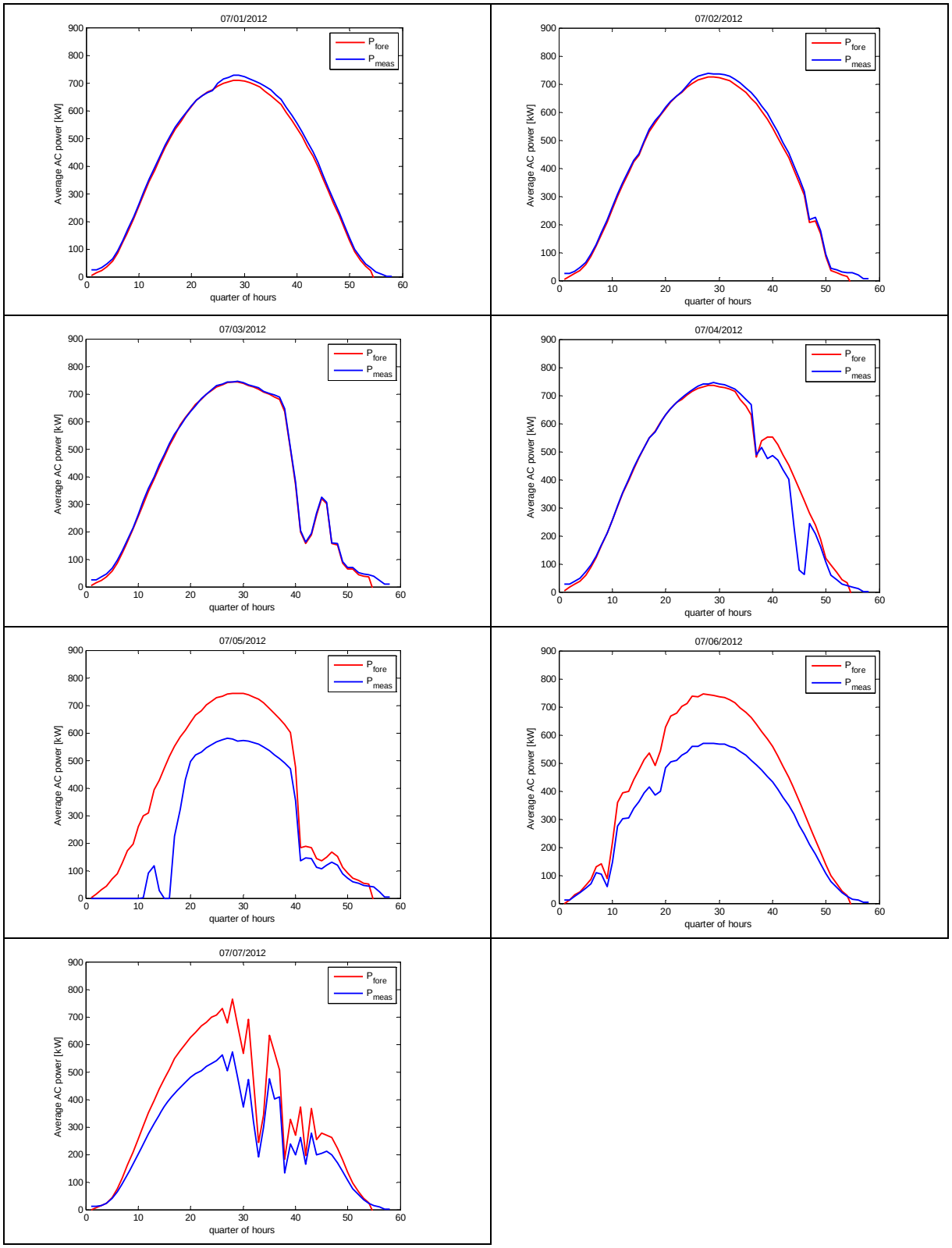

Fig. 5.1 − PV power measurements vs. simulations from 01 to 07 of July 2012 in the site “Gi”.

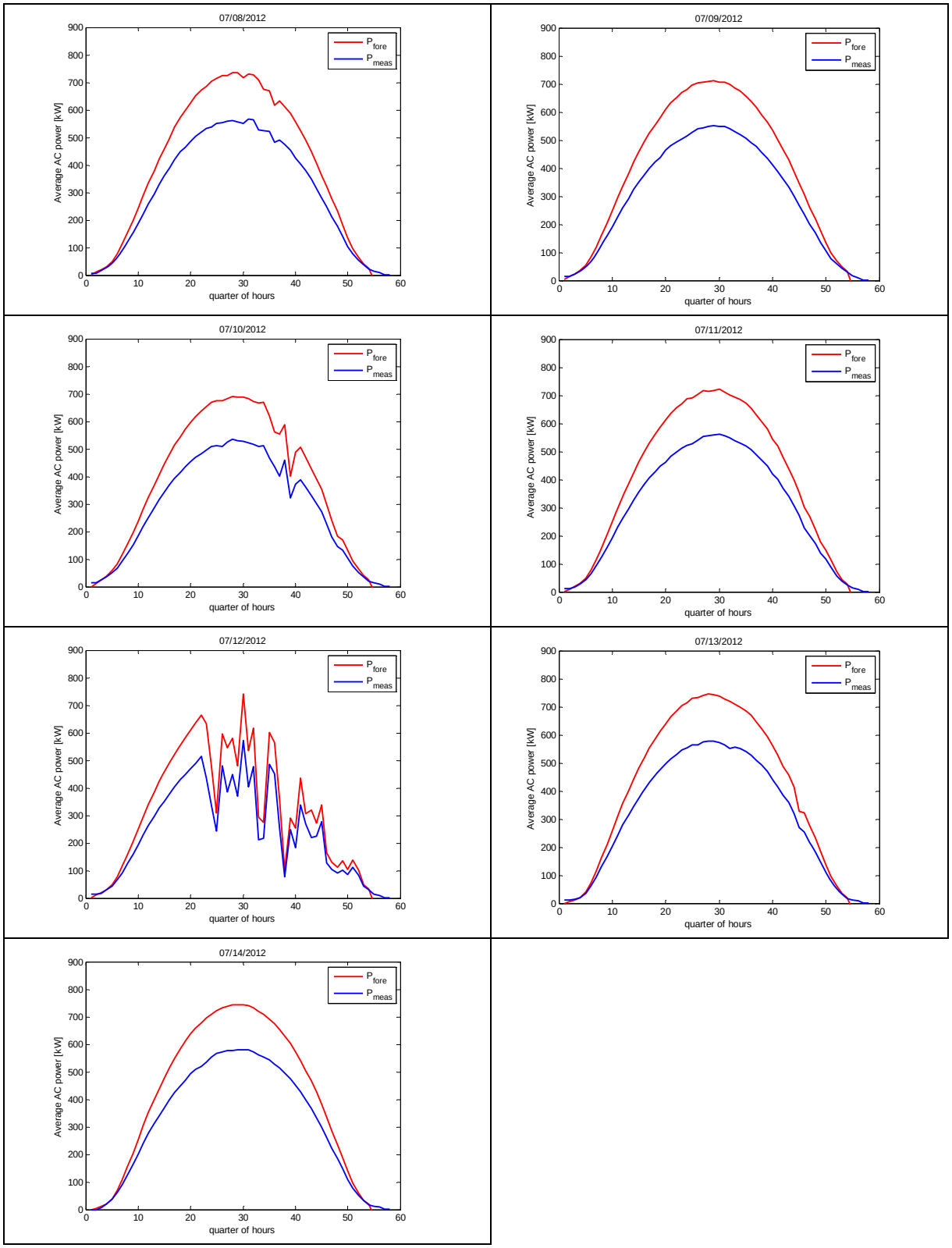

Fig. 5.2 − PV power measurements vs. simulations from 08 to 14 of July 2012 in the site “Gi”.

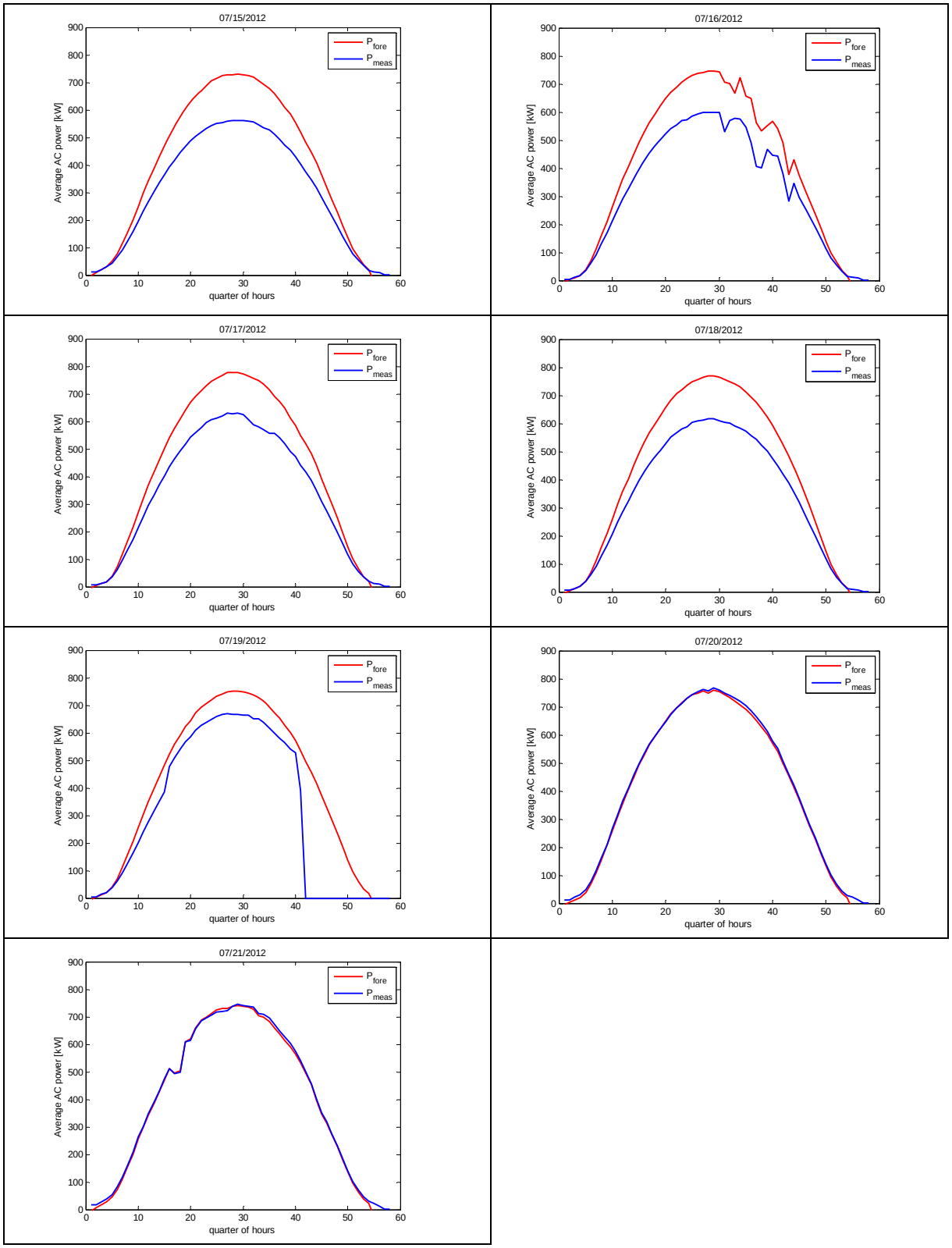

Fig. 5.3 − PV power measurements vs. simulations from 15 to 21 of July 2012 in the site “Gi”.

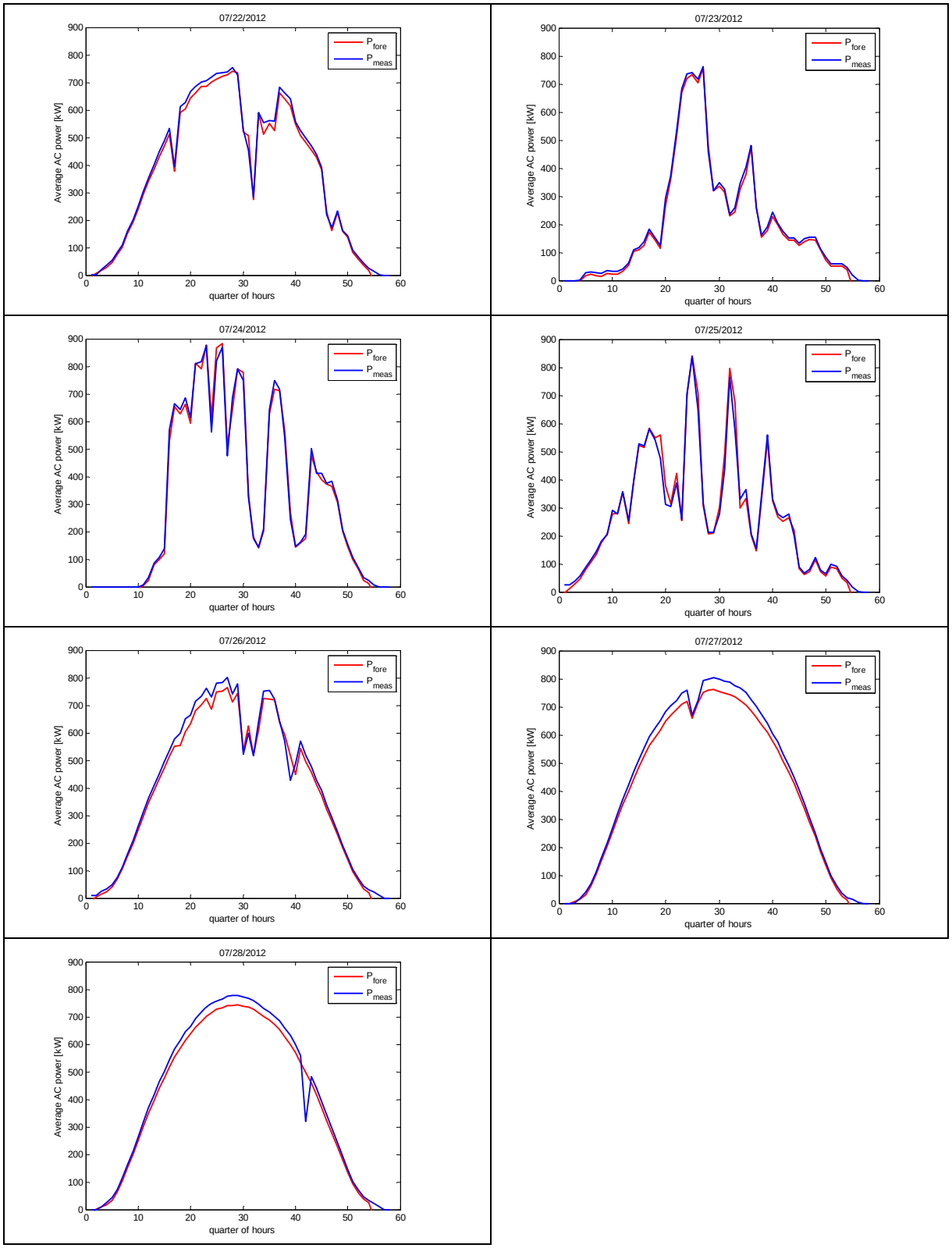

Fig. 5.4 − PV power measurements vs. simulations from 22 to 28 of July 2012 in the site “Gi”.

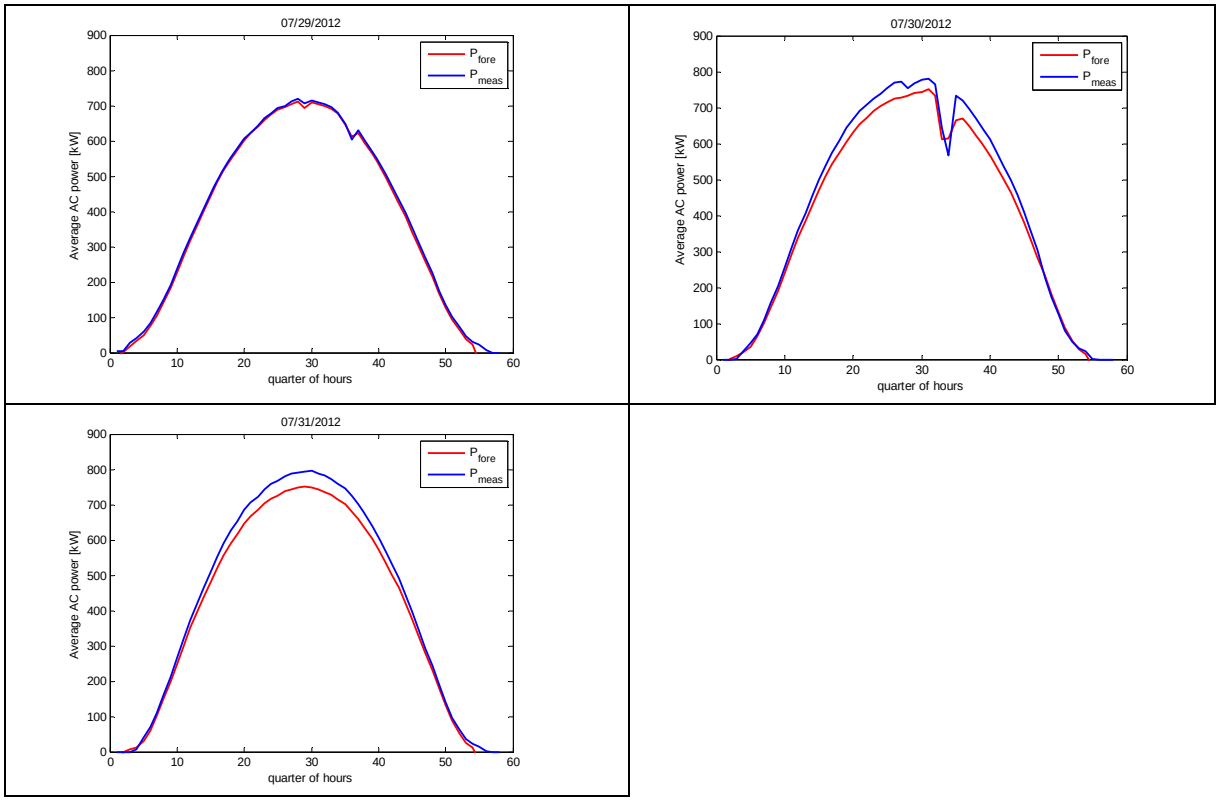

Fig. 5.5 − PV power measurements vs. simulations from 29 to 31 of July 2012 in the site “Gi”.

Moreover, it has been proven that better results, in which $P_{fore} > P_{meas}$, as shown in Fig. 5.6, Fig. 5.7, Fig. 5.8, Fig. 5.9, Fig. 5.10, in comparison, respectively, with Fig. 5.1, Fig. 5.2, Fig. 5.3, Fig. 5.4 and Fig. 5.5, are obtained by calculating the solar cell temperature T_C (°C) as a function of ambient temperature T_a, total irradiance G and wind speed v_w, through the following formula [115]:

$$T_C = 0.943 \cdot T_{amb} + 0.028 \cdot G_{tcell} - 1.528 \cdot v_w + 4.3 \quad (5.8)$$

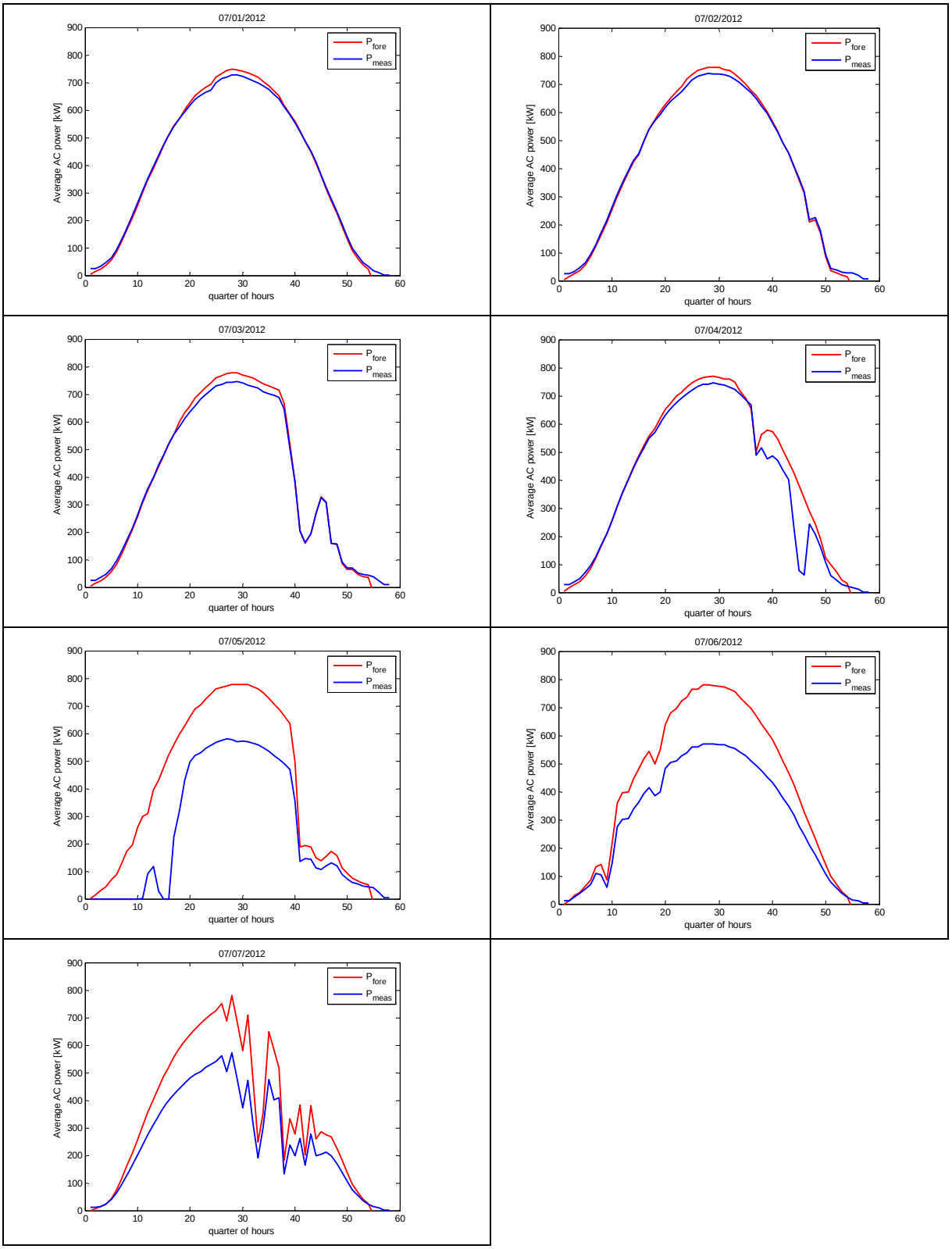

Fig. 5.6 – Improvement in the T_c formula due to wind speed, from 01 to 07 of July in the site "Gi".

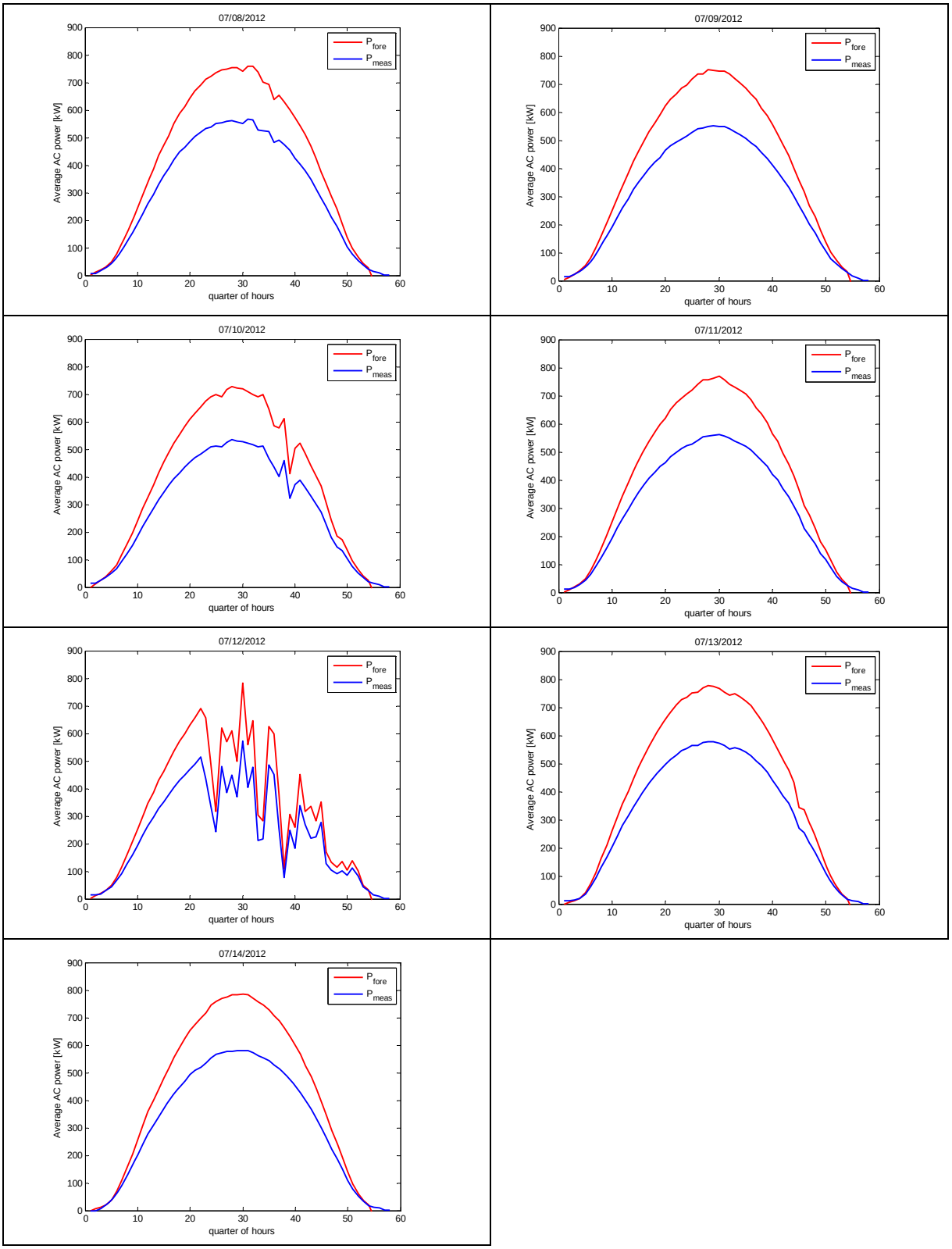

Fig. 5.7 – Improvement in the T_c formula due to wind speed, from 08 to 14 of July in the site "Gi".

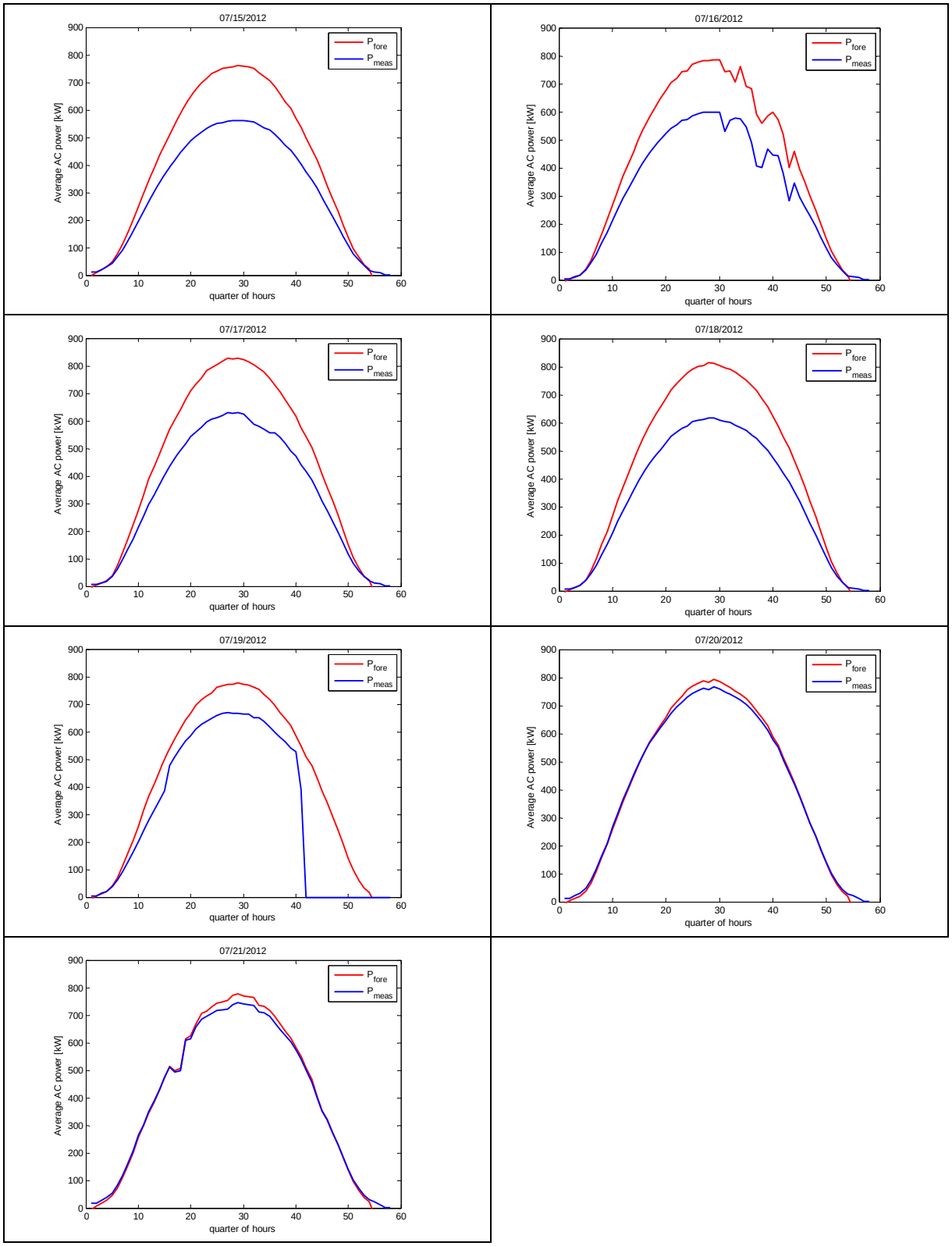

Fig. 5.8 – Improvement in the T_c formula due to wind speed, from 15 to 21 of July in the site "Gi".

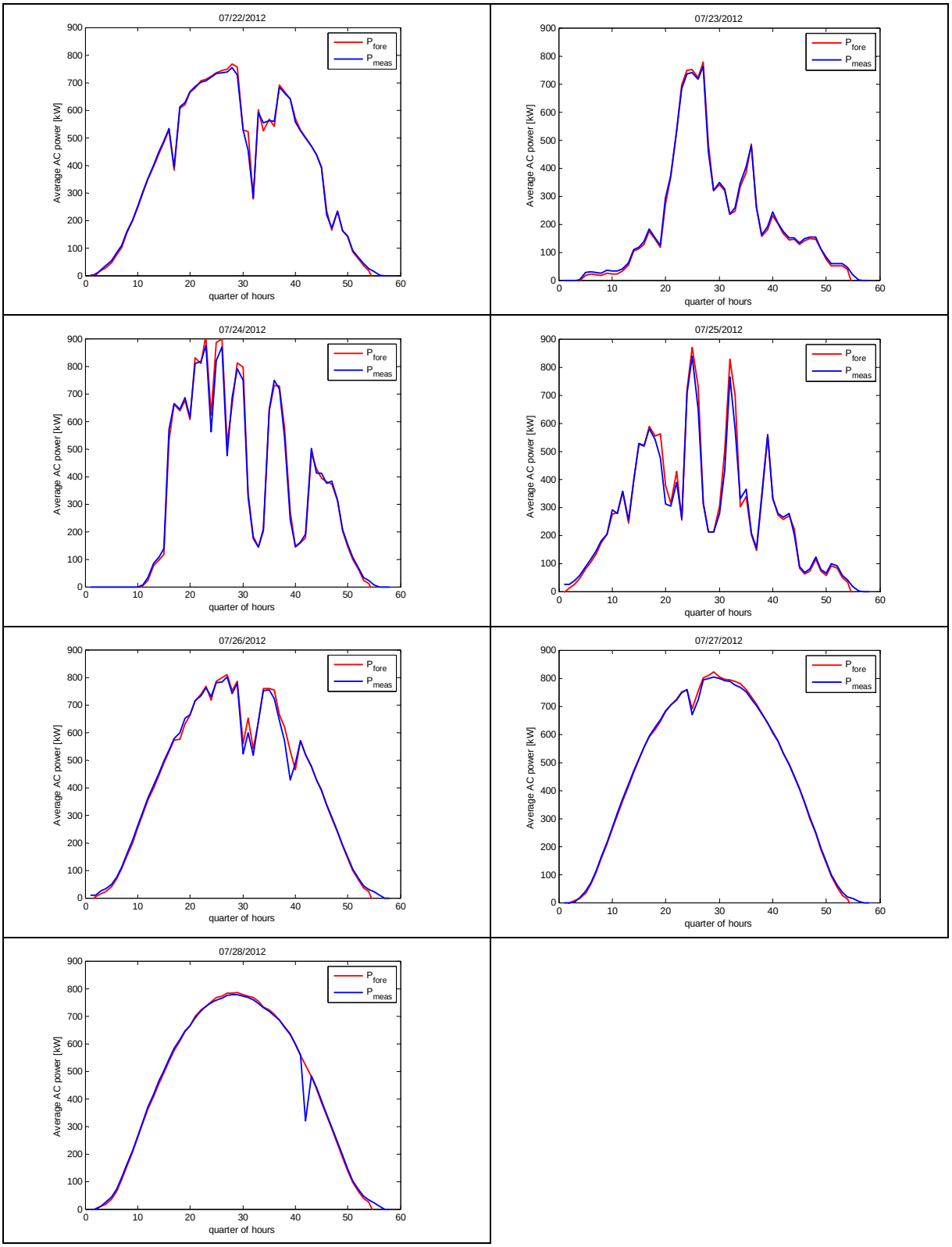

Fig. 5.9 – Improvement in the T_c formula due to wind speed, from 22 to 28 of July in the site "Gi".

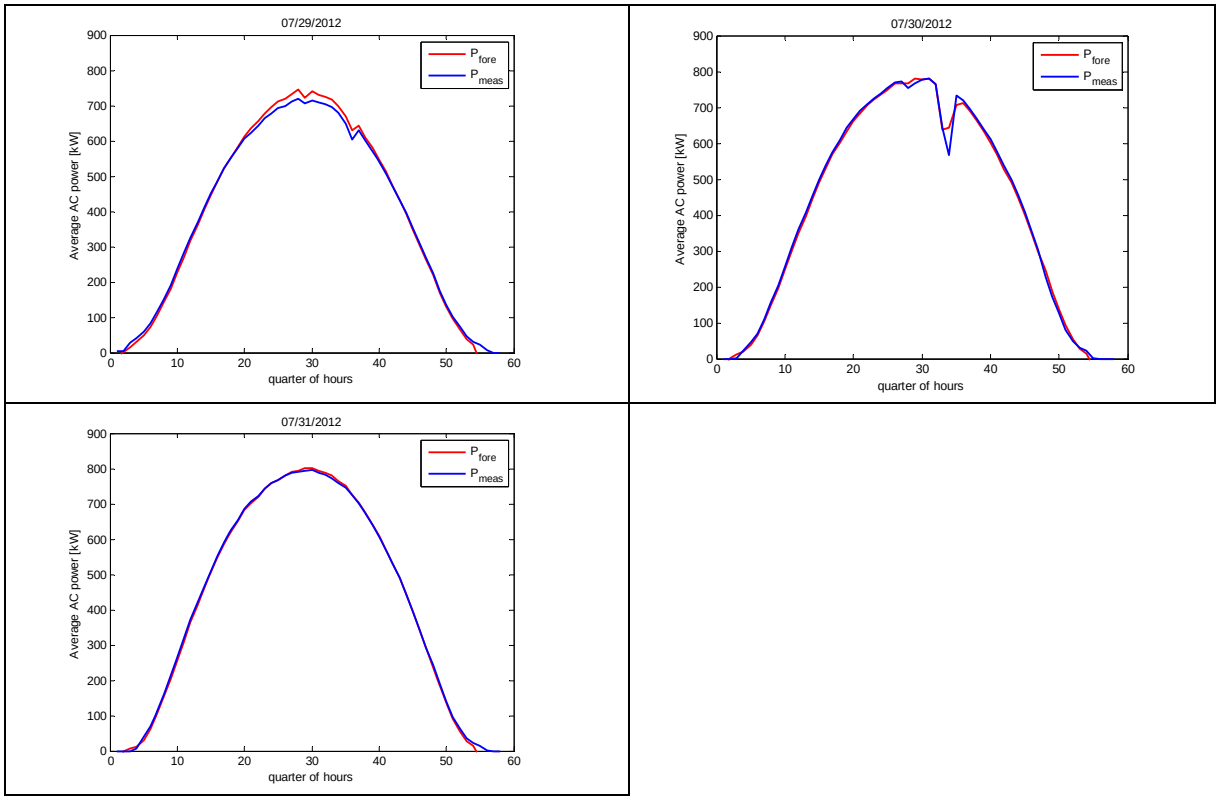

Fig. 5.10 – Improvement in the T_c formula due to wind speed, from 29 to 31 of July in the site "Gi".

5.4. Error calculation for the predicted power profiles with respect to the experimental results

For the error calculation of the AC power profiles compared to the experimental results of each PV plant in the sites "Gi" and "Ma", it is useful to normalize the *MBE* and *MAE* errors with the rated power of each plant. Therefore, a relative value in per-unit is obtained. In this case, from eq. (4.22), the prediction error ε is defined as the difference between the predicted power to be delivered to the grid, P_{fore}, and the AC power measured by the energy-meter of each PV plant:

$$\varepsilon_P = P_{fore} - P_{meas} \tag{5.9}$$

For the calculation of P_{fore}, the reference-cell data on tilt plane G_{tcell}, averaged on 15-min basis, are used as inputs of the model previously described.

As discussed in section 5.2., the real grid-connected PV system has a power rating of 993.6 kW_p for the site "Gi" and of 997.285 kW_p for the site "Ma" in STC.

In the following figures, the error duration curves, calculated for both *MBE* and *MAE*, are represented with sampling time of quarter-hours and on an annual basis. The 95 % threshold, i.e. the exclusion of the worst 5 % of the time, is a suitable choice for representing the maximum errors of the predictions, as already done in section 4.7.

In Fig. 5.11 the error duration curves of positive and negative *MBE* errors are shown for the site "Gi". For 95 % of the time, considering positive *MBE* errors (prediction > measurement), *MBE* is around 13 %; on the contrary, for negative *MBE* errors (prediction < measurement), *MBE* is around 5.5 %. Considering *MAE* error duration curve for the site "Gi" in Fig. 5.12, for 95 % of time, *MAE* is less than 10 %.

In Fig. 5.13 the error duration curve for the site "Ma" is shown. For 95 % of the time, considering positive *MBE* errors, *MBE* is around 12 %; on the contrary, for negative *MBE* errors, *MBE* is around 10 %. Considering the *MAE* error duration curve for the site "Ma" in Fig. 5.14, for 95 % of time, *MAE* is less than 10 %.

Considering the geographical proximity between the two sites of about 70 km, it is useful to plot the positive and negative *MBE* errors for the sites "Gi" and "Ma" in the same graph (Fig. 5.15 and Fig. 5.17). In Fig. 5.16 is shown the zoom of these curves. For the 95 % of the data, positive *MBE* error is about 12 % for the site "Ma" and 13 % for the site "Gi". On the contrary, in Fig. 5.17 the negative errors *MBE* for the sites "Gi" and "Ma" are plotted. In Fig. 5.18 the zoom of these curves shows that for the 95 % of the data, negative *MBE* error is about 10 % for the site "Ma" and about 5.5 % for the site "Gi".

Finally, for the calculation of P_{fore} in eq. (5.9), the 1-day ahead forecast data reported to the tilt plane, averaged on 15-min basis, are used as inputs of the model previously described. In Fig. 5.19 and Fig. 5.20 the error duration curves of positive and negative *MBE* errors are shown for the sites of "Gi" and "Ma". It is noteworthy that the errors in

these situations are higher than in the case with G_{tcell} as input of the model. In Fig. 5.21 the zoom of the duration curves for positive *MBE* errors is shown for the site “Gi” and “Ma”. For the 95 % of the data, positive *MBE* error is about 55 % for the site “Gi” and 50 % for the site “Ma”. In Fig. 5.22 the zoom of duration curves for negative *MBE* errors is shown for the site “Gi” and “Ma”. For the 95 % of the data, negative *MBE* error is about 13 % for the site “Ma” and about 17 % for the site “Gi”.

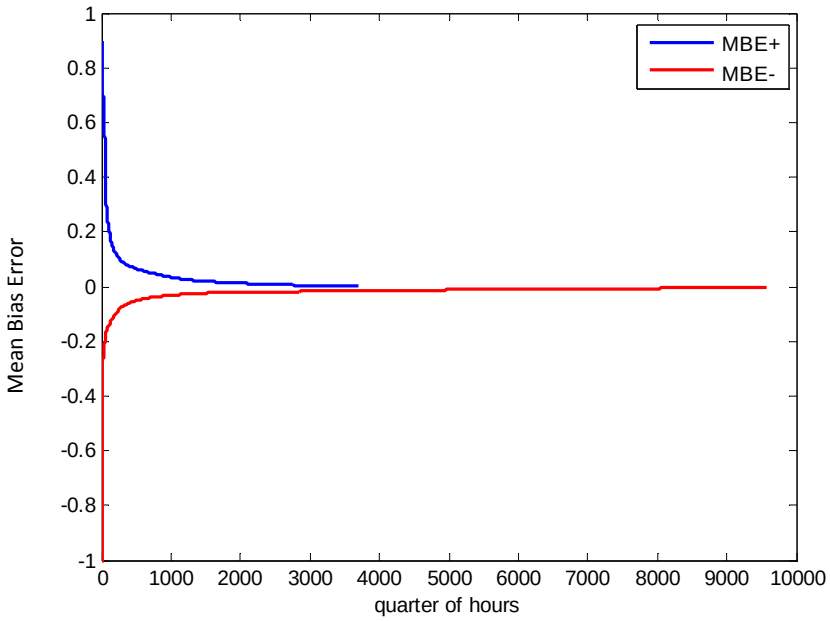

Fig. 5.11 − Error duration curve of positive and negative *MBE* errors of the AC power profiles wrt experimental results for the year 2012 for the site “Gi”.

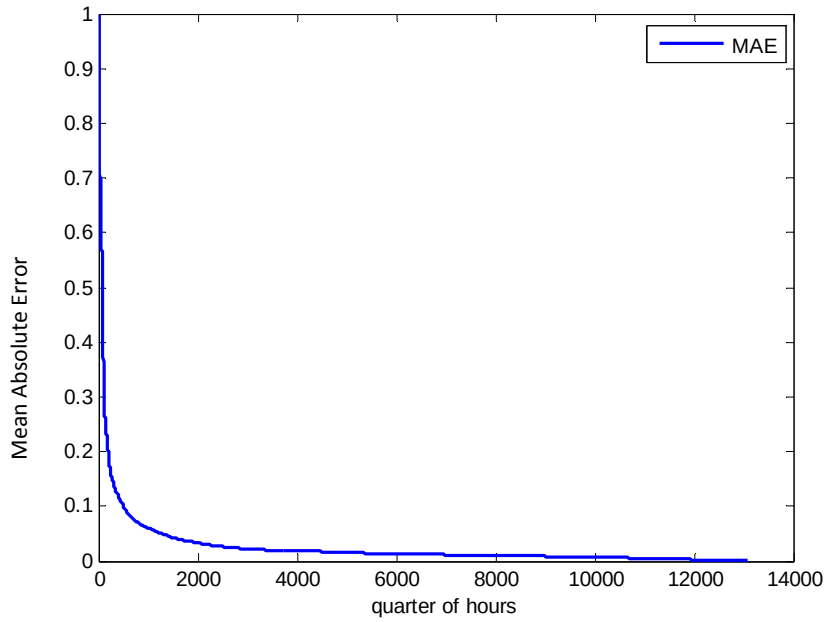

Fig. 5.12 − Error duration curve of *MAE* error of the AC power profiles wrt experimental results for the year 2012 for the site “Gi”.

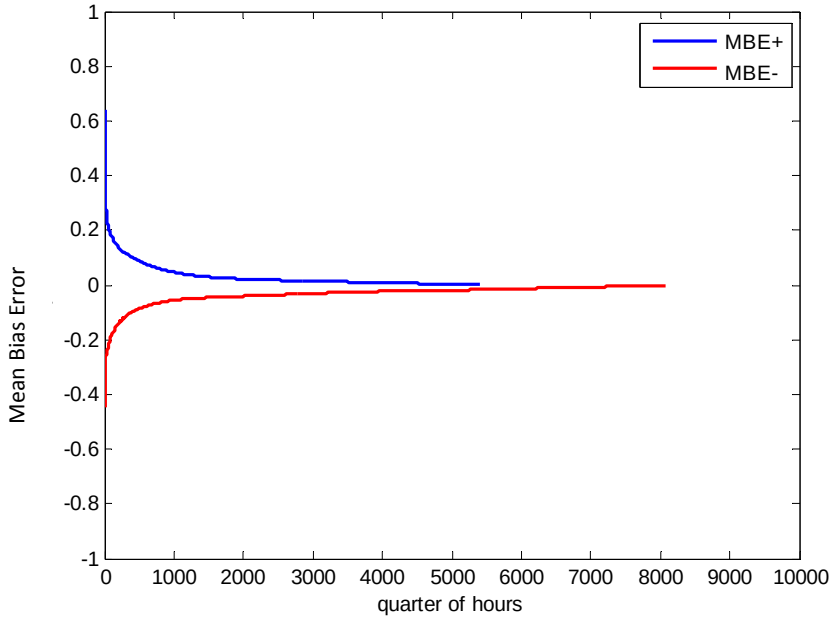

Fig. 5.13 − Error duration curve of positive and negative *MBE* errors of the AC power profiles wrt experimental results for the year 2012 for the site “Ma”.

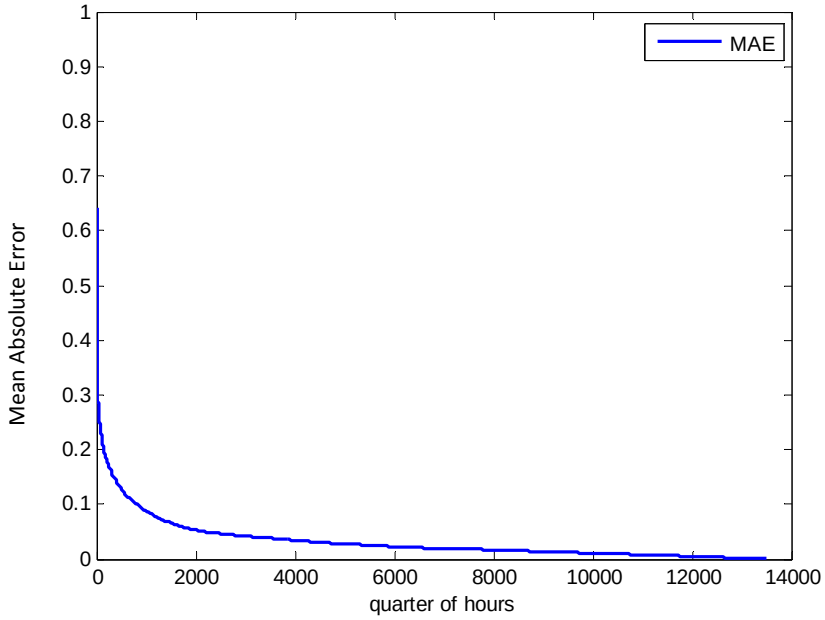

Fig. 5.14 − Error duration curve of *MAE* error of the AC power profiles wrt experimental results for the year 2012 for the site “Ma”.

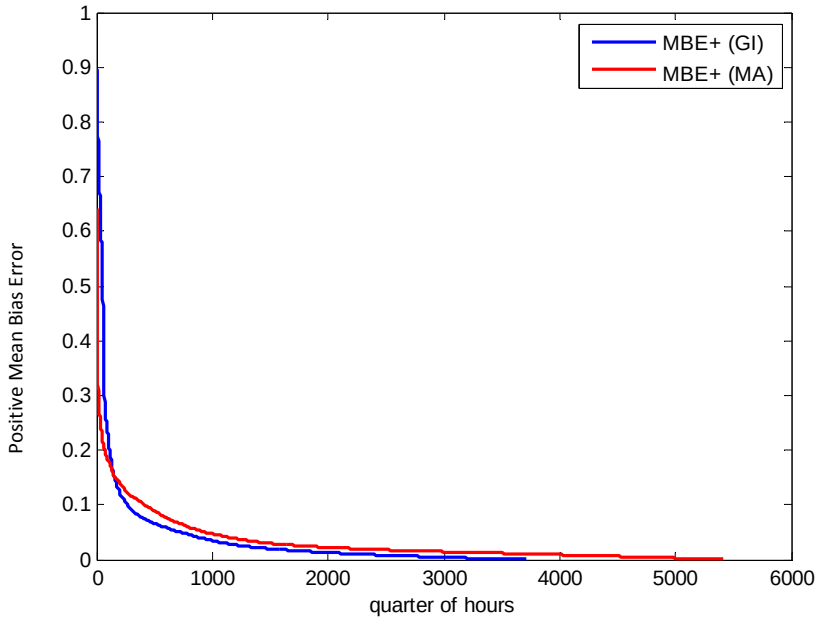

Fig. 5.15 − Error duration curves of positive *MBE* errors of the AC power profiles wrt experimental results for the year 2012 for the sites “Gi” and “Ma”.

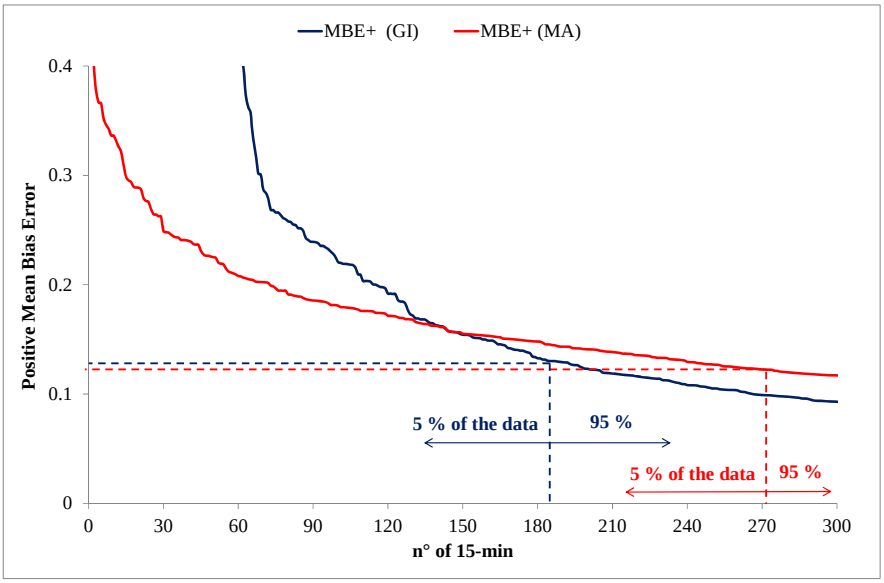

Fig. 5.16 – Zoom of the error duration curves of positive *MBE* errors of the AC power profiles wrt experimental results for the year 2012 for the sites “Gi” and “Ma”.

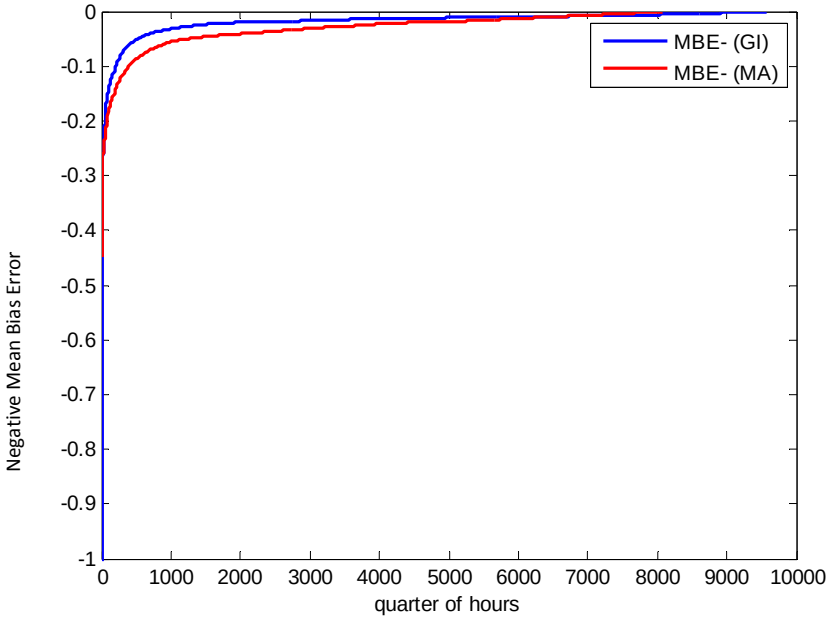

Fig. 5.17 − Error duration curves of negative *MBE* errors of the AC power profiles wrt experimental results for the year 2012 for the sites “Gi” and “Ma”.

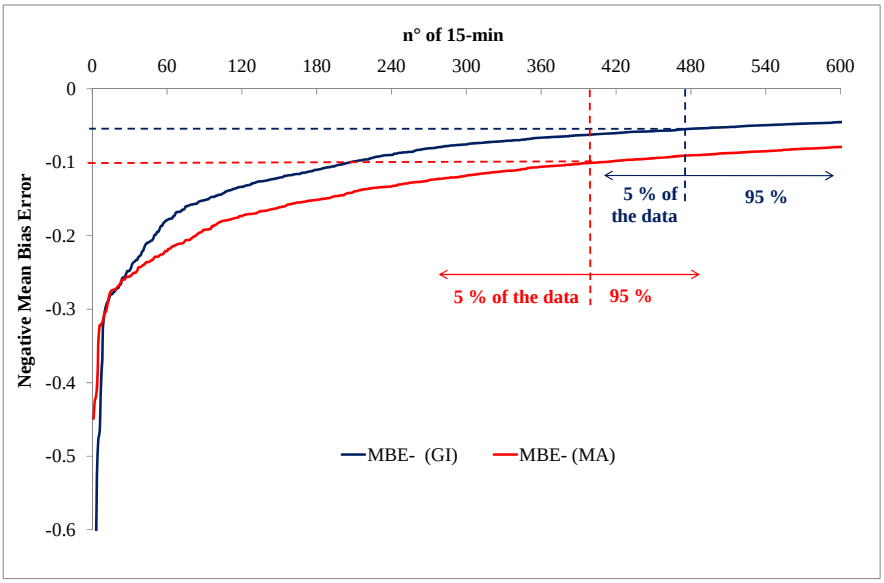

Fig. 5.18 – Zoom of the error duration curves of negative *MBE* errors of the AC power profiles wrt experimental results for the year 2012 for the sites “Gi” and “Ma”.

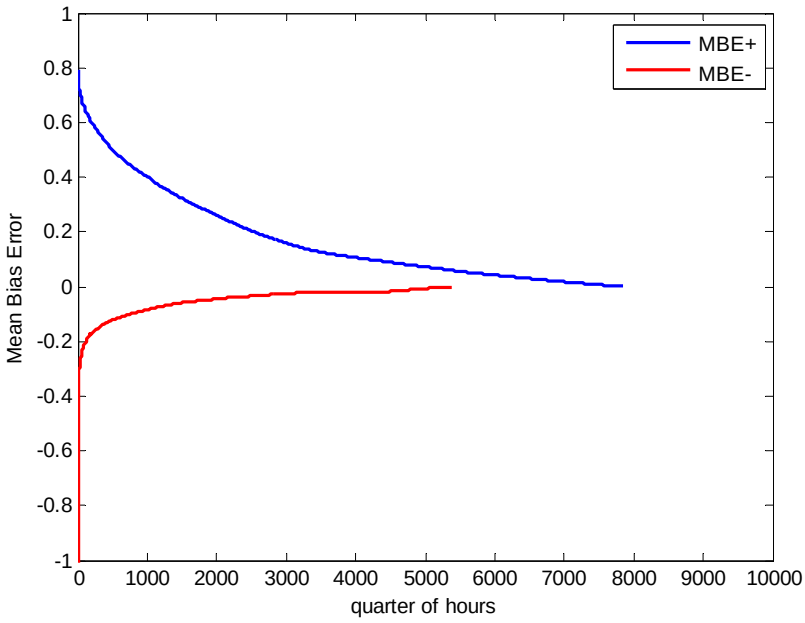

Fig. 5.19 − Error duration curve of positive and negative *MBE* errors of the AC power profiles with the 1-day ahead prediction as input for the year 2012 in the site “Gi”.

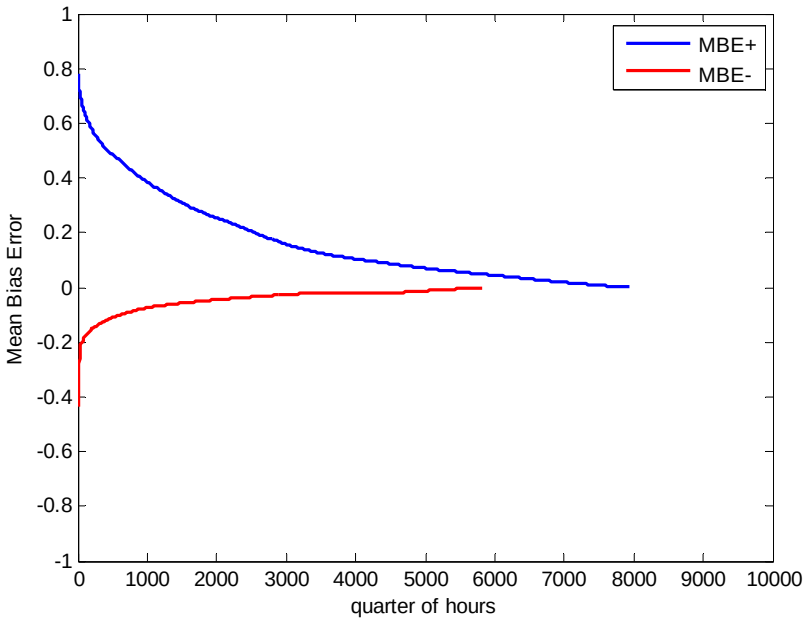

Fig. 5.20 − Error duration curve of positive and negative *MBE* errors of the AC power profiles with the 1-day ahead prediction as input wrt experimental results for the year 2012 in the site “Ma”.

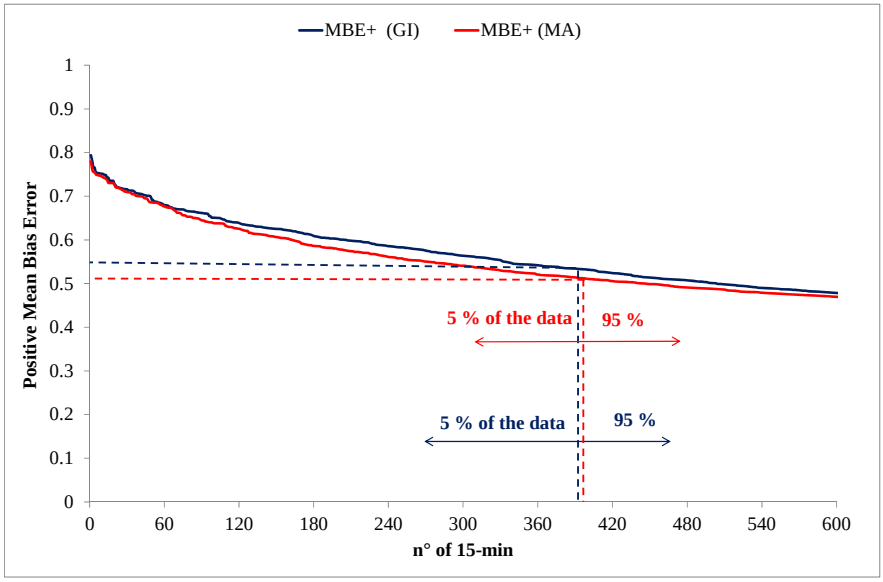

Fig. 5.21 – Zoom of the error duration curves of positive *MBE* errors of the AC power profiles with the 1-day ahead prediction as input wrt experimental results for the year 2012 for the sites “Gi” and “Ma”.

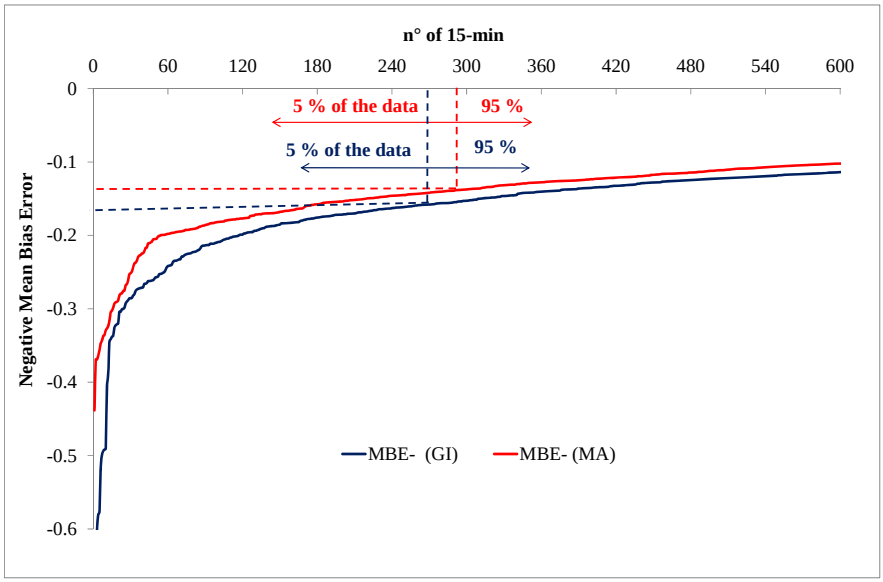

Fig. 5.22 – Zoom of the error duration curves of negative *MBE* errors of the AC power profiles with the 1-day ahead prediction as input wrt experimental results for the year 2012 for the sites "Gi" and "Ma".

5.5. Summary

In this chapter the comparison between PV power measurements and simulations is presented. For the definition of the PV conversion model, many loss factors that influence the PV system behavior are taken into account. The case studies are the real grid-connected PV systems with remarkable size (≈ 1 MW_p), installed in the site "Gi" and "Ma" in South of Italy. In these systems, analyzed on annual basis, the errors of the PV conversion model for AC power with respect to the energy meter used for the feed-in tariff calculation are within the range 12 − 13 % in case of positive errors and within 10 % in case of negative errors.

Conclusions

In this thesis, the economic aspects of grid-connected PV systems and the comparison of irradiance/electric power predictions with respect to experimental results have been presented.

The work has been structured in two parts. First of all, the profitability of investments in the rooftop grid-connected PV systems subjected to incentive and the grid-parity analysis in the two main European PV markets have been discussed.

The economic analysis pointed out the variable profit margins of four different investments in rooftop PV systems subjected to feed-in tariff in Italy and Germany. The results have shown that in Italy, since 2010, the feed-in tariffs framework is affected by a stop-and-go mode. Due to the slow political intervention, the incentive rates had a little decay in the period 2007 − 2010, when the worldwide economies of scale in PV module capacity achieved an impressive decrement in the global costs, boosting the investment profitability ("gold rush" effect). The huge profits in the commercial/industrial PV systems have almost saturated the global funds in the Italian electricity bill. On the contrary, the situation is different in Germany, where the feed-in tariff maturity is substantially maintained in the last 7 years. In this case, the Net Present Value is subjected to limited fluctuations, thanks to timely legislator regulations after the decline of the installation costs.

Then, a new concept of photovoltaic grid-parity has been presented, regarding three typical case studies (dwelling houses, common users of apartment-blocks and tertiary-sector users), by including the distribution-network limits and the fixed costs of the electricity bills. The results have shown that for dwelling houses the grid-parity is

reached in Germany and Central/Southern Italy, whereas it is almost achieved in Northern Italy. For the common users of apartment-blocks, the grid-parity is reached in Germany, while it is unrealistic in Italy with the current economic/regulatory situation. For the tertiary-sector users, the grid-parity is reached in Germany and in Italy.

In the second part of the thesis, the comparison of irradiance and electric power predictions with respect to the experimental results of meteorological stations and grid-connected PV systems in Southern Italy has been analyzed. The main goals of the PV power forecasting are to reduce problems of grid integration, to facilitate energy trading and to minimize the costs of energy imbalance in the Italian electricity market.

With the aim of improving the PV power injection into the grid, the short-term global radiation data on annual basis from solar cells on the horizontal and tilted plane (five meteorological stations) have been measured as accurately as possible, through the comparison with secondary standard pyranometer, taken as reference. The results have shown that in spring and summer months, measurements of solar cells are generally within the pyranometer uncertainty ($\pm$ 2 $-$ 5 %). By considering the linearity and the correlation between the pyranometer and the solar cells, it has been possible to use the solar cell measurements as inputs for the PV production model.

In order to make a comparison with the measured data for two of the five meteorological stations, called synthetically “Gi” and “Ma”, as a sample, the irradiance forecasts of 3-days ahead on the horizontal plane are available from a weather forecast provider at the same geographic coordinates of the PV plants. Since the forecast length is 72 hours, with an output cadence of 3 hours, an interpolation through polynomial splines has been first carried out.

Then, to understand if a strong correlation between the irradiance from measured data and from forecasts exists, a method to classify each hour of a day in three categories (variable, cloudy, or clear) has been implemented. Examining the results month by month, it has been possible to determine the number of passes/fails recorded by the hourly classification method from pyranometer measurements with respect to the hourly

classification method from 1-day before forecast. In particular, in summer months the highest number of hourly passes, in which the 1-day ahead prediction coincides with the measurement data from the pyranometer, occurs for the variable − variable condition. In winter months, the highest number of hourly passes occurs for the cloudy – cloudy condition. On the other hand, in spring months a great number of hourly fails for the variable – clear condition has been recorded. The low number of clear-sky days, especially in spring and summer months, can be explained by the turbidity in air, e.g. due to pollution deriving from human activities. In general, the number of clear-sky days in the site "Ma" is lower than the site "Gi". The reason can be explained by the proximity of the site "Ma" with high pollution areas, e.g. due to great quantity of fine dust in air from industrial steel mills.

Comparing the 2-day ahead and 3-day ahead predictions with respect to the 1-day ahead prediction, considered as the most accurate, the deviations have shown that in summer months, positive and negative deviations are quite negligible (< 20 W/m^2 in the site "Gi" and ≤ 30 W/m^2 in the site "Ma"). Major deviations occur in winter, spring and autumn months. In general, for each site, the deviations between the 3-day ahead predictions and the 1-day ahead predictions are greater than the 2-day ahead predictions with respect to the 1-day ahead predictions. In particular, the site "Gi" has presented major deviations than the site "Ma". The results obtained for the "broken clouds" have shown that this particular phenomenon can be considered as a subset of the variable sky condition, and the months with a higher occurrence are in winter and in spring. Moreover, the "broken clouds" phenomenon, even if noticeable on 1-min scale, is smoothed on 15-min scale and considering more locations (e.g. 3 sites).

The accuracy between the predicted and measured data has been assessed through the use of statistical indicators: the Mean Absolute Error (*MAE*) and the Mean Bias Error (*MBE*). Considering positive and negative *MBE* errors, it has been possible to obtain the error duration curves for 15-min averaged solar irradiance values and on annual basis. As a result, for 95 % of the time, in case of positive errors, in which the prediction is highest of the measurement, the *MBE* is less than 25 % in the site "Gi" and around 22 %

in the site “Ma”, on the contrary for negative errors, *MBE* is less than 20 % in the site “Gi” and around 20 % in the site “Ma”.

Finally, the combination of irradiance prediction and PV conversion model provides interesting results to boost the PV penetration into the grid. Analyzing the error duration curve between the power measured by the meters of the real grid-connected PV systems and the AC power calculated from the model, it has been obtained that for 95 % of the time, in case of positive errors, *MBE* is around 13 % in the site “Gi” and around 12 % in the site “Ma”, on the contrary for negative errors *MBE* is around 5.5 % in the site “Gi” and around 10 % in the site “Ma”.

Glossary

- **Artificial Neural Networks (ANNs)** are mathematical tools originally inspired by the way the human brain processes information. Their basic unit is the artificial neuron that receives (numerical) information through a number of input nodes, processes it internally and puts out a response [116],[117]. The most important achievements that ANN enables are:

- The functions approximation, in which the ANN is able to reconstruct the link between a set of dependent variables (response variables) and a set of independent variables (explanatory variables), approximating with an appropriate function.
- The pattern recognition, in which the ANN processes a number of input/output reference schemes and extracts from them the characteristic data that compares with unknown cases, in order to search any matches. The advantage of this approach is to solve engineering problems without any a priori knowledge of the mathematical model underlying the phenomenon.
- The associative memories, in which the ANN stores a large number of input/output learning schemes to respond with a known output for each input, similar to one acquired during learning.

ANNs are used to solve problems based on input data that are not always well defined or contain a certain degree of uncertainty, for which the exact procedures to determine the solution are not known. Therefore, the most interesting feature of a neural network is its learning ability, that consists in developing a set of observations in order to find the relationships that are able to solve the problem optimally. The learning is achieved providing the largest possible number of input/output relationships to the system, so that each new signal can be classified identifying the path that it take within the network.

This process involves the definition of a cost function, whose purpose is to establish how the prediction of the model is far from the experimental value. This function must be constructed in order to minimize the error between the generated output and the desired value, in order to proceed with the adjustment of weight coefficients associated to the connections of each neuron.

ANNs can be classified in two main types: "*Feed-forward*" and "*Vector quantization*" networks. The first type contains the *Multilayer Perceptron* (MLP) and the *Recurrent Neural Networks* (RNN) as distributed knowledge, and the *Radial Basis Function* network (RBF) as Kernel-based. The second type contains the *Kohonen's Self-Organizing Map* (SOM). As per the Feed-forward network architecture, the flow of information moves forward, that is the outputs of one layer are used as the inputs of the following layer. If a feedback line is also considered, the algorithm is called "*back-propagation*", which uses the error between the real and the desired output to adjust the weights of the connections and make more effective the minimization of the cost function. In order to reduce the learning time, that the back-propagation algorithm requires to reach the global minimum, the *Levenberg-Marquardt* (LM) algorithm can be utilized. The difference between these two algorithms is that for the back-propagation algorithm the weights are updated for each input, each epoch denotes a pass from all inputs. In comparison, for the LM all inputs are presented to the network at the same time on each epoch. For each epoch, the LM requires more computational time and memory.

In the MLP type, the neurons are organized in layers. In particular, each neuron is connected to the following ones, forming a set, that can be divided into 3 layers. The first layer operates directly on the inputs and it is used to adjust the signals in order to be processed by the subsequent levels. The second layer is called "*hidden*" because it is not directly knowable from the outside, only observing the network behavior, it is responsible for processing and can be also composed of more arrays of neurons. The third level corresponds to the output stage, that collects the results and adapts them to the particular characteristics that must have to interface with what is downstream.

In the RNN type, the neurons are also organized in layers. Because the information is no longer transmitted only in one direction but it is also transmitted backwards, this fact creates an internal state of the network which allows it to exhibit dynamic temporal behavior. So, in the basic topology of RNN, the artificial neuron is directly connected to every other neuron in all direction.

The Kernel-based networks are supervised networks with three layers, that allow knowledge removal and incremental learning. In particular, the RBF is composed of: an input layer that computes the Euclidean distance amongst the input vector and the weight vectors of the hidden layer; a hidden layer composed by units with Gaussian transfer function (radial bases), whose weight vectors form a vectorial quantization of the input space; and a linear output layer. This type of ANN performs a linear combination of non-linear functions of the input values; and concerning the learning process, it is divided in two parts: first, the weight vectors of the hidden layer (centroids of the radial bases) are found by clustering techniques or randomly assigned in the input space, or alternatively employing an optimal method; afterwards, the weights of the output layer are computed by linear regression.

As per the Vector quantization type, it concerns the unsupervised/supervised networks that project data from a high dimensional space in a bi-dimensional map, preserving as much as possible the original topology In this context, the Kohonen's SOM is a rectangular grid of competitive units, in which each unit has a fixed position in the grid and is associated to a weight vector of N components, where N is the dimension of the input space. Concerning the learning procedure, the weights are randomly initialized; the units compete and the unit closest to the input vector is the winning unit; the weights of the winning unit and those of the adjacent units (neighborhood) are adjusted to get closer to the input vector; the procedure is repeated until the map becomes stable [118].

- **Fuzzy logic (FL)** is based on the fuzzy theory, first introduced in 1965 by Zadeh [119]. Its peculiarity lies in the being a logic that does not apply the non-contradiction principle and is, therefore, an extension of classical set theory. Fuzzy logic, in fact, does

not attach to a proposition a degree of absolute truth, that is totally true (value 1) or totally false (value 0), but gives it a degree of truth between the extremes of true (1) and false (0). Therefore, according to this theory, it does not exist a set of true propositions distinct from that of false propositions, because the two sets have boundaries that may overlap, for this reason it is interesting to speak of membership degree of an element to a certain set. Typically, a model of fuzzy logic is a functional relationship between two multidimensional spaces.

The *Fuzzy Associative Memories* (FAM) are the relationships between the known input and the fuzzy output, in which are referred both the linguistic variables and the attributes, applying the association rules between the different sets. Therefore, fuzzy logic allows to solve mathematical problems, applying rules based on natural language, without addressing the difficulty of building a mathematical model that defines the mathematical relationships between the input and the output variables. However, its main disadvantage is the lack of self-learning ability, i.e. it is not able to extract useful information from data, only partially valid, or to deal with unknown events.

- **Adaptive Network based Fuzzy Inference System (ANFIS)** is a mathematical model that combines the fuzzy logic with the neural networks, first introduced in 1993 by Jang [120]. The architecture of this system provides for the acquisition of the knowledge by typical operation algorithms of neural networks, while their representation is via fuzzy logic rules. ANFIS combines the learning ability of a neural network with the reasoning ability of fuzzy logic, creating a very complex information processing system. The ANFIS strategy is widely used in cases that involve considerable uncertainty or imprecision in the variables definitions, that constitute the behavior of the system. In fact, ANFIS has the ability to shape qualitatively a phenomenon without knowing it; it is also able to identify linear systems and predict the chaotic behavior of time-dependent systems.

- **Genetic Algorithms (GA)** are research and optimization heuristic methods, inspired by the principle of natural selection, that regulates the biological evolution. The idea of

mathematically mimic the evolution process of populations by selecting only individuals most suitable for the survival has proven very efficient in resolution of a wide variety of optimization problems, not suitable for classical algorithms, in particular if the objective function is discontinuous, derivable or not strongly nonlinear [121]. Generally, a genetic algorithm starts from a number of possible solutions, referred to as “population”, which are made to evolve during the program execution. For each iteration, it makes a selection among individuals (or chromosomes) of the population according to a fitness function, that is a measure of how the solution is able to respond to the problem. If the result is not satisfactory, it is used to generate new elements of the population, that will replace an equal number of individuals already present and thus constitute a new population for the next iteration, that is a new generation. This succession of generations evolves towards an optimal solution of the assigned problem. As in nature, the evolution is obtained by the partial recombination of solutions. It is assumed that each individual transmits a portion of its gene to its offspring, but during this process it happens that random mutations in the starting population can be introduced. Occasionally, individuals with not included features among those present in the genetic of the original species are born. This mutation is used to explore new solutions avoiding to trapped in a local optimum. At the end of the evolution, the population of solutions is analyzed and the best solutions to solve the problem are chosen. In biological terms, it means that only individuals who have the most suited qualities to the environment in which they are and have a better chance of surviving and reproducing, are preserved. These solutions will undergo a new stage of development and so on. The algorithm stops when one of the stopping criteria is satisfied, or after a certain number of iterations. The characteristic of this method is that there is no way to know in advance whether it will actually able to find an acceptable solution.

References

[1] Hax C., Majluf N. S., Competitive cost dynamics: the experience curve. Interfaces, Vol. 12 (N. 5), pp. 50–61, 1982.

[2] EPIA, European Photovoltaics Industry Association, Market Report 2011, pp. 1-7, 2011[document available also on the Internet at: http://www.epia.org].

[3] IEA, International Energy Agency, Annual Report 2010. Photovoltaic Power Systems Programme (PVPS), pp. 1-143, 2010 [document available also on the Internet at: http://www.iea-pvps.org].

[4] IEA, International Energy Agency, Annual Report 2011. Photovoltaic Power Systems Programme (PVPS), pp. 1-129, 2010 [document available also on the Internet at: http://www.iea-pvps.org].

[5] Politecnico di Milano, Dipartimento di Ingegneria Gestionale, Scool of Managment, Solar Energy Report – Il sistema industriale italiano nel business dell'energia solare, pp. 1-219, 2011.

[6] GSE, Gestore Servizi Energetici, Rapporto Statistico 2010. Solare Fotovoltaico, pp. 1-48, 2010 [document available also on the Internet at: http://www.gse.it].

[7] GSE, Gestore Servizi Energetici, Application Rules for Italian feed-in tariff, Regole applicative per il riconoscimento delle tariffe incentivanti previste dal D.M. 5 May 2011 (quarto conto energia per il fotovoltaico) – Revisione 2 (in Italian language), pp. 1-120, 2011 [document available also on the Internet at: http://www.gse.it].

[8] Ministerial Decree for Italian feed-in tariff, D.M. 5 May 2011, Incentivazione della produzione di energia elettrica da impianti solari fotovoltaici. Gazzetta Ufficiale Della Repubblica Italiana, Serie generale – n.109, pp. 103-122, 2011.

[9] Bruns E., Ohlhorst D., Wenzel B., A success Story: Twenty Years of Support for Electricity from Renewable Energies in Germany. Renewable Energies Agency, Renews Special Issue 41/September 2010, pp. 33-40, 2010.

[10] Kohler S., Altevogt J., German Energy Agency (Deutsche Energie-Agentur GmbH - DENA), PV Policy Group, Designing Photovoltaic Policies in Europe, Joint Position Paper and Action Plan of the PV Policy Group on Photovoltaic Policies in Europe, pp. 1-52, 2007.

[11] Wissing L., PV Market in Germany. Joint International Workshop, 21st International Science and Engineering Conference 2011 PVSEC-21, Fukuoka, Japan, Federal Ministry for the Environment, Nature Conservation and Nuclear Safety, pp. 2-23, 2011.

[12] IEA-PVPS, International Energy Agency Co-Operative Programme On Photovoltaic Power Systems, Exchange and dissemination of information on PV power systems, Task 1. National Survey Report of PV Power Applications in Germany 2010, by L. Wissing, pp. 1-39, 2011.

[13] Danchev S., Maniatis G., Tsakanikas A., Returns on investment in electricity producing photovoltaic systems under de-escalating feed-in tariffs: The case of Greece. Renewable and Sustainable Energy Reviews 14, pp. 500-505, 2010.

[14] Hüsser P., Trends of European PV market: investors perspective, PVSEC 2011 - 21st International Photovoltaic Science and Engineering Conference (PVSEC-21), 1 Dec 2011, Fukuoka, Japan, pp. 1-17.

[15] Masters G. M., 2004. Renewable and Efficient Electric Power Systems. IEEE Wiley-Interscience, New Jersey (USA), pp. 242-246, 2011.

[16] Focacci A., Residential plants investment appraisal subsequent to the new supporting photovoltaic economic mechanism in Italy. Renewable and Sustainable Energy Reviews 13, pp. 2710-2715, 2009.

[17] Grau T., Huo M., Neuhoff K., Survey of photovoltaic industry and policy in Germany and China. Energy policy 51, pp. 20-37, 2012.

[18] IEA, International Energy Agency, Trends in Photovoltaic Applications, Survey report of selected IEA countries between 1992 and 2010. Photovoltaic Power Systems Programme (PVPS), pp. 1-48, 2011. [document available also on the Internet at: http://www.iea-pvps.org].

[19] IEA, International Energy Agency, Trends in Photovoltaic Applications, Survey report of selected IEA countries between 1992 and 2010. Photovoltaic Power Systems Programme (PVPS), pp. 1-48, 2010. [document available also on the Internet at: http://www.iea-pvps.org].

[20] IEA, International Energy Agency, Trends in Photovoltaic Applications, Survey report of selected IEA countries between 1992 and 2010. Photovoltaic Power Systems Programme (PVPS), pp. 1-43, 2009. [document available also on the Internet at: http://www.iea-pvps.org].

[21] IEA, International Energy Agency, Trends in Photovoltaic Applications, Survey report of selected IEA countries between 1992 and 2010. Photovoltaic Power Systems Programme (PVPS), pp. 1-44, 2008. [document available also on the Internet at: http://www.iea-pvps.org].

[22] IEA, International Energy Agency, Trends in Photovoltaic Applications, Survey report of selected IEA countries between 1992 and 2010. Photovoltaic Power Systems Programme (PVPS), pp. 1-40, 2007. [document available also on the Internet at: http://www.iea-pvps.org].

[23] IEA, International Energy Agency, Trends in Photovoltaic Applications, Survey report of selected IEA countries between 1992 and 2010. Photovoltaic Power Systems Programme (PVPS), pp. 1-37, 2006. [document available also on the Internet at: http://www.iea-pvps.org].

[24] Klein A., Merkel E., Pfluger B., Held A., Ragwitz M., Resch G. , Busch , S. Evaluation of different feed-in tariff design options – Best practice paper for the International Feed-In Cooperation. Fraunhofer ISI - Energy Economics Group (EEG), 3rd edition updated by Dec. 2010, pp. 10-61, 2010.

[25] Fulton M., Mellquist N., The German feed-in tariff for PV: managing volume success with price response. Deutsche Bank Group, DB Climate Change Advisors, May 2011, pp. 1-33, 2011.

[26] Inflation.eu: Worldwide inflation data, 2013. [available on the website: http://www.inflation.eu/inflation-rates/cpi-inflation-2002.aspx].

[27] EUROSTAT, European Commission, Gas and electricity market statistics. Statistical book, 2007 edition, pp. 60-72, 2007.

[28] EUROSTAT, European Commission, Energy Prices Statistics, 2012. [available on the website: http://epp.eurostat.ec.europa.eu/statistics_explained/index.php/Energy_price_statistics].

[29] EUROSTAT, European Commission, Electricity prices for domestic consumers, from 2007 onwards - bi-annual data, 2013. [available on the website: http://appsso.eurostat.ec.europa.eu/nui/show.do?dataset=nrg_pc_204&lang=en].

[30] EUROSTAT, European Commission, Electricity prices for industrial consumers, from 2007 onwards - bi-annual data, 2013. [available on the website: http://appsso.eurostat.ec.europa.eu/nui/show.do?dataset=nrg_pc_205&lang=en].

[31] Kaldellis J.K., Vlachou D.S., Korbakis G., Techno-economic evaluation of small hydro power plants in Greece: a complete sensitivity analysis. Energy Policy, vol. 33, Issue 15, pp. 1969-1985, 2005.

[32] Esen H., Inalli M., Esen M., Technoeconomic appraisal of a ground source heat pump system for a heating season in eastern Turkey. Energy Conversion and Management, vol. 47, Issues 9–10, pp. 1281-1297, 2006.

[33] Esen H., Inalli M., Esen M., A techno-economic comparison of ground-coupled and air-coupled heat pump system for space cooling. Building and Environment, vol. 42, Issue 5, pp. 1955-1965, 2007.

[34] Talavera D.L., Nofuentes G., Aguilera J., The internal rate of return of photovoltaic grid-connected systems: A comprehensive sensitivity analysis. Renewable Energy, vol. 35, Issue 1, pp. 101-111, 2010.

[35] IEC Standard 61724, Photovoltaic system performance monitoring, Guidelines for measurement, data exchange and analysis, 1998.

[36] Italian Ministry of Economy and Finance, Revenue Agency, 2009. Document web link: http://www.agenziaentrate.gov.it/wps/file/nsilib/nsi/documentazione/provvedimenti+circolari+e+risoluzioni/risoluzioni/archivio+risoluzioni/risoluzioni+2009/maggio+2009/risoluzione+n+127+2009/ris+127e+del+25+maggio+2009.pdf

[37] Urmet Group S.p.A., owner of a rooftop PV system (about 350 kW_p), web site: http://www.urmet.it/urmet_web/en/Company0.html

[38] European Photovoltaic Technology Platform, A Strategic Research Agenda for Photovoltaic Solar Energy Technology. Edition 2, pp. 1-84, 2011.

[39] Breyer, C. and Gerlach, A., Global overview on grid-parity. Prog. Photovolt: Res. Appl., 21, pp. 121–136, 2013.

[40] P. Welter, J. Siemer, G. Hering, Searching for the Holy Grail: the short path to a self-supporting PV market, *Photon International*, The Photovoltaic Magazine, pp. 160-163, 2006.

[41] Bloomberg, Data about 10-year Government bond yields, 2013. [available on the website: http://www.bloomberg.com/markets/rates-bonds/]

[42] UniCredit [documents available on the Internet at: https://www.unicredit.it].

[43] Intesa San Paolo[documents available on the Internet at: http://www.intesasanpaolo.com].

[44] UmweltBank [documents available on the Internet at: http://www.umweltbank.de/kreditkonditionen/solarkonditionen.html#Konditionen].

[45] SwkBank[documents available on the Internet at: https://www.mein-solarkredit.de/index.php?partnerId=dynamicdrive_pv].

[46] Bhandari R., Stadler I., Grid parity analysis of solar photovoltaic systems in Germany using experience curves. Solar Energy, vol. 83, issue 9, pp. 1634–1644, 2009.

[47] Breyer C., Gerlach A., Global Overview On Grid-Parity. Progress In Photovoltaics: Research and Applications, vol. 21, pp. 121–136, 2013.

[48] Reichelstein S., Yorston M., The prospects for cost competitive solar PV power. Energy Policy, vol. 55, pp.117–127, 2013.

[49] Branker K., Pathak M.J.M., Pearce J.M., A review of solar photovoltaic levelized cost of electricity. Renewable and Sustainable Energy Reviews, vol. 15, Issue 9, December 2011, pp. 4470-4482, 2011.

[50] Hernández-Moro J., Martínez-Duart J.M., Analytical Model For Solar PV And CSP Electricity Costs: Present LCOE Values And Their Future Evolution. Renewable and Sustainable Energy Reviews, vol. 20, pp. 119–132, 2013.

[51] Short W., Packey D.J., Holt T., A Manual For The Economic Evaluation Of Energy Efficiency And Renewable Energy Technologies. National Renewable Energy Laboratory (NREL), NREL/TP-462–5173, Golden, 1995. Documents available on the Internet from: [www.nrel.gov/csp/troughnet/pdfs/5173.pdf]

[52] Lin C.H., Hsieh W.L., Chen C.S., Hsu C.T., Ku T.T., Optimization of Photovoltaic Penetration in Distribution Systems Considering Annual Duration Curve of Solar Irradiation. Power Systems, IEEE Transactions, vol. 27, no.2, pp. 1090–1097, 2012.

[53] Povlsen F., Impacts of Power Penetration From Photovoltaic Power System in Distribution Network. IEA, Paris, France, Rep. IEA-PVPS Task, 2002.

[54] Baumgartner F.P., Achtnich T., Remund J., Gnos S., Nowak S., Steps Towards Integration of PV-Electricity Into The Grid. Progress in Photovoltaics: Research and Applications, vol. 19, pp. 834–843, 2011.

[55] Shayani RA, Gonçalves de Oliveira MA. Photovoltaic Generation Penetration Limits in Radial Distribution Systems. IEEE Transactions on Power Systems, vol. 26, no. 3, 2011, pp. 1625–1631.

[56] Canova A., Giaccone L., Spertino F., Tartaglia M., Electrical Impact of Photovoltaic Plant in Distributed Network.IEEE Transactions on Industry Applications, vol. 45, pp. 341–347, 2009.

[57] European Commission. Eurostat, Environment and Energy. documents available on the Internet from: [http://epp.eurostat.ec.europa.eu]

[58] Spertino F., Corona F., Di Leo P., Limits of Advisability for Master–Slave Configuration of DC–AC Converters in Photovoltaic Systems. IEEE Journal ofPhotovoltaics, vol. 2, no.4, Oct. 2012, pp. 547–554, 2012.

[59] International Energy Agency (IEA), World Energy Outlook 2012, 2012.

[60] Autorità per l'energia elettrica e il gas (AEEG). La Bolletta Spiegata, document available on the Internet from: [http://www.autorita.energia.it/it/consumatori/bollettatrasp_ele.htm]

[61] Drewag (German electricity company), documents available on the Internet from: [http://www.drewag.de/de/privatkunden/drewag_produkte/allgemein/pk_dp_strom_preise_zusammensetzung.php]

[62] Flextrom (German electricity company), documents available on the Internet from: [http://www.flexstrom.de/]

[63] Stadwerke Bamberg (German electricity company), documents available on the Internet from: [http://www.stadtwerke-bamberg.de/cms/Strom/Strom.html]

[64] European Photovoltaic Technology Platform, A Strategic Research Agenda for Photovoltaic Solar Energy Technology. Edition 2, pp. 1–84, 2011.

[65] Aste N., Del Pero C., Technical and economic performance analysis of large-scale ground-mounted PV plants in Italian context. Progress In Photovoltaics: Research and Applications, vol. 18, pp. 371–384, 2010.

[66] IEA, International Energy Agency. Trends in Photovoltaic Applications, Survey report of selected IEA countries between 1992 and 2012. Photovoltaic Power Systems Programme (PVPS), pp. 1–80, 2013. Document available also on the Internet from: [http://www.iea-pvps.org].

[67] Bloomberg, Data about 10-year Government bond yields, 2013. Available on the website: [http://www.bloomberg.com/markets/rates-bonds/]

[68] Patel M. R., Wind and solar power systems; design, analysis and operation, Taylor & Francis Group, CRC Press, Boca Raton, FL, USA, 2006.

[69] IEC Standard 61724. Photovoltaic system performance monitoring, Guidelines for measurement, data exchange and analysis, 1998.

[70] Spertino F., Di Leo P., Cocina V., Economic analysis of investment in the rooftop photovoltaic systems: A long-term research in the two main markets, Renewable and Sustainable Energy Reviews, vol. 28, pp. 531-540, 2013.

[71] Swift K. D., A comparison of the cost and financial returns for solar photovoltaic systems installed by businesses in different locations across the United States, Renewable Energy, vol. 57, pp. 137–143, 2013.

[72] Lacchini C., Dos Santos J. C. V., Photovoltaic energy generation in Brazil – Cost analysis using coal-fired power plants as comparison, Renewable Energy, vol. 52, pp. 183–189, 2013.

[73] PVGIS website [http://re.jrc.ec.europa.eu/pvgis/apps4/pvest.php#]

[74] Eclareon, Photovoltaic Grid Parity Monitor (GPM), 2013. Available on the Internet from: [http://www.eclareon.com/en/gpm]

[75] Papaioannou I.T., Alexiadis M.C., Demoulias C.S., Labridis D.P., Dokopoulos P.S., Modeling and Field Measurements of Photovoltaic Units Connected to LV Grid. Study of Penetration Scenarios, *IEEE Transactions on Power Delivery*, vol. 26, no. 2, pp. 979-987, 2011.

[76] Sauer K. J., Roessler T., Systematic Approaches to Ensure Correct Representation of Measured Multi-Irradiance Module Performance in PV System Energy Production Forecasting Software Programs, *IEEE Journal of Photovoltaics*, pp.1-7, 2012.

[77] Huan-Liang Tsai, Insolation-oriented model of photovoltaic module using Matlab/Simulink, *Solar Energy*, vol. 84, pp. 1318-1326, 2010.

[78] Donovan M., Bourne B., Roche J., Efficiency vs. irradiance characterization of PV modules requires angle-of-incidence and spectral corrections, *35th IEEE Photovoltaic Specialists Conference (PVSC),* pp. 2301-2305, 2010.

[79] Marcos J., Marroyo L., Lorenzo E., From irradiance to output power fluctuations: the PV plant as a low pass filter, *Prog. Photovolt: Res. Appl.*, vol. 19, pp. 505-510, 2011.

[80] Lave M., Kleissl J., Stein J. S., A Wavelet-Based Variability Model (WVM) for Solar PV Power Plants, *IEEE Transactions on Sustainable Energy*, vol. PP, no. 99, pp.1-9, 2012.

[81] Whitfield K., Osterwald C. R., Procedure for determining the uncertainty of photovoltaic module outdoor electrical performance, *Prog. Photovolt: Res. Appl.*, vol. 9, pp. 87-102, 2001.

[82] Kumar R., Umanand L., Estimation of global radiation using clearness index model for sizing photovoltaic system, *Renewable Energy*, vol. 30, pp. 2221–2233, 2005.

[83] Liu B. Y. H., Jordan R. C., The interrelationship and characteristic distribution of direct, diffuse and total solar radiation, *Solar Energy*, vol. 4 (3), pp. 1-19, 1960.

[84] Lorenz E., Hurka J., Heinemann D., Beyer H. G., Irradiance forecasting for the power prediction of grid-connected photovoltaic systems, IEEE Journal of Selected Topics in Applied Earth Observations and Remote Sensing, Vol. 2, No. 1, pp. 2-10, 2009.

[85] Jensenius J. S., Insolation Forecasting. Solar Resources, MIT Press Cambridge, pp. 335-349, 1989.

[86] Glahn H. R., Lowry D. A., The Use of Model Output Statistics (MOS) in Objective Weather Forecasting, Journal of Applied Meteorology, 11, pp. 1203-1211, 1972.

[87] Kaifel A. K., Jesemann P., An Adaptive Filtering Algorithm for Very Short-range Forecast of Cloudiness Applied to Meteosat Data, Proceedings 9th Meteosat Scientific Users Meeting, Locarno,1992.

[88] Beyer H. G., Costanzo C., Heinemann D., Reise, C., Short Range Forecast of PV Energy Production Using Satellite Image Analysis, Proceedings 12th European Photovoltaic Solar Energy Conference, Amsterdam, pp. 1718-1721, 1994.

[89] Iqbal M., An introduction to solar radiation, Academic press, Toronto, 1983.

[90] Foresta Martin F., Lanciano N., Lanciano P., From Earth to galaxies, Quaderni ENEA-MUSIS, pp. 1-64, 1993.

[91] Duffie J. A., Beckman W. A., Solar Engineering of Thermal Processes (second ed.), Wiley Interscience, New York, pp. 37-41, 1991

[92] Şen Z., Solar energy fundamentals and modeling techniques, Springer, pp. 70-71, 2008.

[93] Duffie J. A., Beckman W. A., Solar Engineering of Thermal Processes (second ed.), Wiley Interscience, New York, pp. 85-95, 1991.

[94] ASHRAE, Handbook of Fundamentals, American Society of Heating, Refrigeration and Air-Conditioning Engineers, Atlanta, 1993.

[95] Iqbal M., An introduction to solar radiation, Academic Press, London, 1983.

[96] Batrinu F., Carpaneto E., Chicco G., Gagliano S., Spertino F., Tina G.M., Assessing the performance of photovoltaic sites and grid-connected systems: a study case, PV WESC, 2009.

[97] Duffie J. A., Beckman W. A., Solar Engineering of Thermal Processes (second ed.), Wiley Interscience, New York, pp. 75-77, 1991.

[98] De Miguel A., Bilbao J., Aguiar R., Kambezidis H., Negro E., Diffuse solar irradiation model evaluation in the North Mediterranean Belt area, Solar Energy, Vol. 70, Issue 2, pp. 143-153, 2001.

[99] Erbs D. G., Kein S. A., Duffie J. A., Estimation of the diffuse radiation fraction for hourly, daily and monthly-average global radiation, Solar Energy, Vol. 28, No. 4, pp.293-302, 1982.

[100] Orgill J. F., Hollands K. G. T., Correlation equation for hourly diffuse radiation on a horizontal surface, Solar Energy, Vol. 19, pp. 357, 1977.

[101] Iqbal M., Prediction of hourly diffuse solar radiation from measured hourly global radiation on a horizontal surface, Solar Energy, Vol. 24, pp. 491, 1980.

[102] Bilbao J., Miguel A., Medina J. A., Lo´pez J. J., Task II CLIMED Project: Model Performance Tests, Report, UVA, Valladolid, pp. 248, 1997.

[103] Meteo.Cat website: http://www.meteo.cat

[104] The Weather Research & Forecasting Model website: http://www.wrf-model.org

[105] Sluiter R., Interpolation methods for climate data. Literature review, KNMI, R&D Information and Observation Technology, De Bilt, pp. 1-24, 2008.

[106] Lorenz E., Hurka J., Karampela G., Hei D., Beyer H. G., Schneider M., Qualified Forecast of Ensemble Power Production by Spatially Dispersed Grid-Connected PV Systems, in Proceedings of the 23rd European Photovoltaic Solar Energy Conference and Exhibition, Valencia, pp. 3285-3291, 2008.

[107] Lorenz E., Remund J., Müller S. C., Traunmüller W., Steinmaurer G., Pozo D., Ruiz-Arias J. A., Lara Fanego V., Ramirez L., Romeo M. G., Kurz C., Pomares L. M., Guerrero C. G., Benchmarking of Different Approaches to Forecast Solar Irradiance, Proceedings of the 24th European Photovoltaic Solar 35 Energy Conference, Hamburg, Germany, pp. 4199-4208, 2009.

[108] Lorenz E., Scheidsteger T., Hurka J., Heinemann D., Kurz C., Regional PV power prediction for improved grid integration, Progress in Photovoltaics Research and Applications, Vol. 19, No. 7, pp. 757-771, 2011.

[109] Lorenz E., Hammer A., Heinemann D., Short term forecasting of solar radiation based on satellite data, EUROSUN2004 (ISES Europe Solar Congress), Freiburg, Germany, 2004.

[110] Lorenz E., Heinemann D., Kurz C., Local and regional photovoltaic power prediction for large scale grid integration: Assessment of a new algorithm for snow detection, Progress in Photovoltaics Research and Applications, Vol. 20, No. 6, pp. 760-769, 2012.

[111] Lorenz E., Heinemann D., Wickramarathne H., Beyer H. G. and Bofinger S., Forecast of Ensemble Power Production by Grid-Connected PV Systems, in Proceedings of the 20th European PV Conference, Milan, Italy, pp. 3-7, 2007.

[112] IEA, International Energy Agency, Photovoltaic and solar forecasting: state of the art, Report IEA Photovoltaic Power Systems Programme (PVPS) 2013, pp. 1-36, 2013.

[113] Spertino F., Corona F., Di Leo P., Limits of Advisability for Master–Slave Configuration of DC–AC Converters in Photovoltaic Systems, , IEEE Journal of Photovoltaics, vol.2, no.4, pp.547-554, 2012.

[114] Reinders A. H. M. E., Van Dijk V. A. P., Wiemken E. and Turkenburg W. C., Technical and Economic Analysis of Grid-connected PV Systems by Means of Simulation, Progress In Photovoltaics: Research And Applications Vol. 7, pp. 71-82, 1999.

[115] Chenni R., Makhlouf M., Kerbache T., Bouzidì A., A detailed modeling method for photovoltaic cells, Energy, Vol. 32, Issue 9, pp. 1724-1730, 2007.

[116] Hippert H. S., Pedreira C. E., Souza R. C., Neural Networks for Short-Term Load Forecasting: A Review and Evaluation, IEEE Transactions On Power Systems, Vol 16, No.1, pp. 44-55, 2001.

[117] Krenker A., Bešter J., Kos A., Introduction to the Artificial Neural Networks, Artificial Neural Networks - Methodological Advances and Biomedical Applications, InTech, pp. 1-18, 2011.

[118] Chicco G., Napoli R., Piglione F., Neural networks for fast voltage prediction in power systems, Power Tech Proceedings, 2001 IEEE Porto, Vol 2, pp. 1-5, 2001.

[119] Zadeh L.A., Fuzzy sets, Information and Control, Elsevier, Vol 8, Issue 3, pp. 338-353, 1965.

[120] Jang, J. S. R., ANFIS: adaptive-network-based fuzzy inference system, IEEE Transactions on Systems, Man and Cybernetics, Vol 23, no.3, pp.665-685, 1993.

[121] Winter G., Genetic Algorithms in Engineering and Computer Science, JOHN WILEY & SON Ltd., 1995.